Investigation of the mitochondrial functions of proteins genetically associated with Parkinson's disease

Victoria Suzanne Burchell

UCL Institute of Neurology

Thesis submitted in fulfilment of the degree of Doctor of Philosophy (UCL)

Declaration

I, Victoria Suzanne Burchell, confirm that the work presented in this thesis is my own. Where information has been derived from other sources, I confirm that this has been indicated in the thesis.

Acknowledgments

My deepest thanks go to all the individuals without whom this thesis would not have been possible. I would especially like to thank my supervisor, Hélène Plun-Favreau, for giving me this opportunity and for offering her continued support whilst allowing me the independence to grow as a researcher. Thanks also to Andrey Abramov, whose knowledge and guidance regarding all things mitochondrial shaped much of this thesis. Both have also contributed data to this thesis, and this can be seen in chapters 3 and 5 where indicated. I am grateful to Michelangelo Campanella for his help with the ATP production assay in chapter 3, to Gyuri Szabadkai and Greg Keen for their help in setting up the ROS assay on the Cellomics in chapter 4, to Heike Laman and Dave Nelson for the contribution of reagents and data in chapter 5, to Marta Delgado-Camprubi for her help in chapter 5, and to Henry Houlden and Selina Wray for obtaining and culturing the patient cells.

On a personal level, I must also say a huge thank you to all the postdocs and PhD students, past and present, who made the lab an enjoyable place to work. Special thanks go to Zhi Yao and Kira Holmström, both great scientists and great friends: I'll always be grateful that our desks were allocated as they were! To Laura Dunn, Selina Wray, Kate Duberley, Sybille Dihanich, Claudia Manzoni, Marc Soutar, Serena Wu, Marta Delgado-Camprubi, Fernando Bartoleme-Robledo and many more – I'll miss you all. Thanks especially to Kira and to Tim Funnell for reading this thesis even when neither of you really had the time: your comments have been invaluable and this thesis is much the better for them.

Finally, I would like to thank my family and friends for their support through the highs and lows of the last four years: my parents, whose love and support have always meant the world to me; Kira and Marc, for the afternoon coffees that kept me going both physically and emotionally; and Peter Dawson, who now knows more about mitochondria than any Maths teacher before him. Thank you for always listening, even if you weren't always sure what I was talking about!

Abstract

Parkinson's disease (PD) is a common neurodegenerative disorder which usually occurs sporadically, but in 5-10% of cases is genetically inherited. Many of the causative mutations underlying these familial forms have been identified, and studying the functions of the proteins encoded by these genes has highlighted several common pathogenic mechanisms. In particular, mitochondrial dysfunction has been shown to play a major role in the pathogenesis of both familial and sporadic forms of the disease.

This thesis investigates the importance of the proteins encoded by these PD-associated genes in mitochondrial function, focusing on two proteins in detail. Firstly, live cell imaging techniques were used to investigate the mitochondrial physiology of cells derived from HtrA2 knockout mice, an animal model in which the loss of a mitochondrial protein gives rise to severe neurodegenerative phenotype. Similar approaches were then applied to an RNAi screen to investigate the effects of other PD-associated genes on mitochondrial function, while a separate study specifically investigated the putative mitochondrial localisation and function of the PD-associated protein Fbxo7.

Results from these studies revealed that HtrA2 has an important role in maintaining the function of the ATP synthase, as HtrA2 deficient cells exhibited a severe uncoupling combined with an increase in proton translocation through the ATP synthase but a reduction in ATP synthesis. Furthermore, Fbxo7, a protein with no reported link to the mitochondria, was found to partially localise to the mitochondria under basal conditions and to further accumulate on depolarised mitochondria. Further work indicated that this protein interacts with two other PD proteins, PINK1 and Parkin, and together with these proteins functions in a previously described pathway to mediate the selective autophagic clearance of damaged mitochondria. These results contribute to our understanding of the functions of these proteins and further emphasise the relevance of mitochondrial dysfunction in PD pathogenesis.

Table of Contents

Table of Figures

Table of Tables

Abbreviations

$\Delta\Psi_m$	Mitochondrial membrane potential
3-MA	3-methyl adenine; an inhibitor of type III PI3Ks (used to block autophagy)
6-OHDA	6-hydroxydopamine
AD	Alzheimer's disease
ADP	Adenosine diphosphate
ALS	Amyotrophic lateral sclerosis
Apaf-1	Apoptotic protease activating factor 1
Atg	Autophagy; the prefix given to genes identified as mediators of autophagy in yeast
ATP	Adenosine triphosphate
BSA	Bovine serum albumin
Bcl2	B-cell lymphoma 2; a family of proteins that regulate apoptosis
BH3	Bcl2-homology domain 3
$[Ca^{2+}]_m$	Mitochondrial calcium
CBD	Corticobasal degeneration
CBP	Calmodulin binding peptide
CCCP	Carbonyl cyanide 3-chlorophenylhydrazone; a mitochondrial uncoupler
cDNA	complementary DNA
CDS	Coding sequence
CHAPS	3-[(3-Cholamidopropyl)dimethylammonio]-1-propanesulfonate; a detergent
cIAP	Cellular inhibitor of apoptosis protein
CxVα/β	Complex V (ATP synthase) subunit α/β
Cyto	Cytosol
DAPI	4′,6-Diamidino-2-phenylindole; a nuclear stain
DDM	n-dodecyl β-D-maltopyranoside; a detergent
DHE	Dihydroethidium; an indicator of ROS

DLB	Dementia with Lewy bodies
DMEM	Dulbecco's modified Eagle medium
DMSO	Dimethyl sulfoxide
DNA	Deoxyribonucleic acid
Drp1	Dynamin-related protein 1
DTT	Dithiothreitol; a reducing agent
EB virus	Epstein-Barr virus; used for immortalisation of primary lymphoblasts
ECACC	European collection of cell cultures
ECL	Enhanced chemiluminescence substrate
EDTA	Ethylenediaminetetraacetic acid; a chelator of both calcium and magnesium
EGFP	Enhanced green fluorescent protein
EGTA	Ethylene glycol tetraacetic acid; a selective calcium chelator
ETC	Electron transport chain
$FADH_2$	Reduced form of flavin adenine dinucleotide (FAD^{++})
FBS	Foetal bovine serum
FCCP	Carbonyl cyanide 4-(trifluoromethoxy)phenylhydrazone; a mitochondrial uncoupler
FBP	F-box protein
Fbxo7	F-box only protein 7
GBA	Glucocerebrosidase
GIGYF2	Grb10-Interacting GYF Protein 2
GFP	Green fluorescent protein
GTP	Guanosine triphosphate
GWAS	Genome-wide association study
HBS	HEPES buffered saline
HBSS	Hanks buffered salt solution
HD	Huntington's disease
HIV	Human immunodeficiency virus
HEPES	4-(2-hydroxyethyl)-1-piperazineethanesulfonic acid; a buffering agent

HSE	Health and Safety Executive
HtrA2	High temperature requirement protein A2
HURP	Hepatoma upregulated protein; a substrate of Fbxo7
IAP	Inhibitor of apoptosis protein
IBM	IAP binding motif
IMM	Inner mitochondrial membrane
IMS	Intermembrane space
IP	Immunoprecipitation
iPS cells	Induced pluripotent stem cells
KD	Knockdown
KO	Knockout
LAMP2	Lysosomal-associated membrane protein 2
LB	Luria broth (also called lysogeny broth)
LC3	Microtubule-associated protein light chain 3
L-DOPA	levo-3,4-dihydroxyphenylalanine; a treatment for PD
LDS	Lithium dodecyl sulfate
LRRK2	Leucine-rich repeat kinase 2
MAC	Mitochondrial apoptosis-induced channel
MAPT	*Microtubule-associated protein tau*; the gene encoding tau
MEF	Mouse embryonic fibroblast
MES	2-(*N*-morpholino)ethanesulfonic acid; a buffering agent
Mfn1/Mfn2	Mitofusin 1/mitofusin 2
Mito	Mitochondria
MOI	Multiplicity of infection; the number of infectious virus particles added per cell plated during transduction
MPP^+	1-methyl-4-phenylpyridium; a potent inhibitor of complex I
MPPP	1-methyl-4-phenyl-4-propionoxypiperidine
MPTP	1-methyl-4-phenyl-1,2,3,6-tetrahydropyridine; metabolised in dopaminergic neurons to MPP^+ causing acute parkinsonism
mRNA	messenger RNA

miRNA	micro RNA
MSA	Multiple system atrophy
mtDNA	mitochondrial DNA
mTOR	Mammalian target of rapamycin; a regulator of autophagy
MTS	Mitochondrial targeting sequence
MW	Molecular weight
NADH	Reduced form of nicotinamide adenine dinucleotide (NAD^+)
NADPH	Reduced form nicotinamide adenine dinucleotide phosphate ($NADP^+$)
NGS	Normal goat serum
NO	Nitric oxide
$O_2^{\cdot}$	Superoxide
OMM	Outer mitochondrial membrane
OPA1	Optic atrophy 1
PBS	Phosphate buffered saline
PCR	Polymerase chain reaction
PD	Parkinson's disease
PDHE1α	Pyruvate dehydrogenase E1α; an enzyme of the TCA cycle
PDL	Poly-D-lysine
PDZ	A protein interaction domain shared by post synaptic density protein (PSD95), Drosophila disc large tumour suppressor (Dlg1), and zonula occludens-1 protein (zo-1)
PI3K	Phosphatidylinositol 3-kinase; class III PI3Ks are essential in autophagosome formation
PINK1	PTEN-induced putative kinase 1
PK	Protease K
PLA2G6	Phospholipase A2, group VI
PSP	Progressive supranuclear palsy
PTP	Permeability transition pore
PVDF	Polyvinylidene fluoride
qPCR	Quantitative PCR

RNA	Ribonucleic acid
RNAi	RNA interference
RPMI-1640	Roswell Park Memorial Institute medium
ROS	Reactive oxygen species
SERCA	Sarcoplasmic/endoplasmic reticulum calcium ATPase
siRNA	small interfering RNA
shRNA	short hairpin RNA
SNCA	Gene encoding α-synuclein
SNP	Single-nucleotide polymorphism
TAP	Tandem-affinity purification
TBE	Tris-borate-EDTA solution
TCA cycle	Tricarboxylic acid cycle (also called the Kreb cycle or citric acid cycle)
TEV	Tobacco etch virus
TMRM	Tetramethylrhodamine methyl ester; an indicator of $\Delta\Psi_m$
TRAP1	Tumour necrosis factor (TNF) receptor-activated protein 1; a mitochondrial chaperone
TOM	Translocase of the outer membrane
UBL	Ubiquitin-like domain
UCHL-1	Ubiquitin carboxy-terminal hydrolase 1
UV	Ultraviolet
VDAC	Voltage-dependent anion channel
VSV	Vesicular stomatitis virus
WB	Western blot
WT	Wild-type
XIAP	X-linked inhibitor of apoptosis protein
YFP	Yellow fluorescent protein

Publications arising from this thesis

Burchell VS*, Nelson DE*, Sanchez-Martinez A, Delgado-Camprubi M, Wray S, Lewis PA, Houlden H, Abramov AY, Hardy J, Whitworth AJ, Wood NW, Laman H, Plun-Favreau H. *The Parkinson's disease genes Fbxo7 and Parkin interact to mediate mitophagy.* (Manuscript in submission)

Plun-Favreau H*, **Burchell VS***, Holmstrom KH, Yao Z, Deas E, Cain K, Fedele V, Campanella M, Martins LM, Wood NW, Gourine AV, Abramov AY. *HtrA2 deficiency causes mitochondrial uncoupling through the F_1F_0-ATP synthase and consequent ATP depletion*. Cell Death and Disease 2012; 3:e335

Burchell VS, Gandhi S, Deas E, Wood NW, Abramov AY, Plun-Favreau H. *Targeting mitochondrial dysfunction in neurodegenerative disease: Part I.* Expert Opinion on Therapeutic Targets 2010; 14(4):369-85

Burchell VS, Gandhi S, Deas E, Wood NW, Abramov AY, Plun-Favreau H. *Targeting mitochondrial dysfunction in neurodegenerative disease: Part II*. Expert Opinion on Therapeutic Targets 2010; 14(5):497-511

* indicates joint authorship

Presentations

Burchell VS, Abramov AY, Wood NW, Plun-Favreau H. *Identification of new components in PINK1 pathways by shRNA screen.* (Poster presentation)

- Gordon Research Conference in Bioenergetics, New Hampshire, USA 2009

Burchell VS, Yao Z, Vaarman A, Plun-Favreau H, Abramov AY. *HtrA2 deficiency causes neuronal death via mitochondrial uncoupling.* (Platform presentation)

- Biochemical Society Christmas Bioenergetics Meeting, London, 2009

Burchell VS, Wood NW, Abramov AY, Plun-Favreau H. *Investigation of the mitochondrial function of the Parkinson's disease-associated genes PINK1 and HtrA2.*

- Brain Energy Metabolism, Budapest, Hungary, 2010 (Platform presentation)

Chapter 1

Introduction

1.1. Parkinson's disease

Parkinson's disease (PD) is an incurable neurodegenerative disease affecting approximately 1% of the population over 65, making it the second most common neurodegenerative disorder after Alzheimer's disease (Hirtz et al., 2007). With an ageing population worldwide, this represents a substantial social and economic problem and novel therapeutic strategies are urgently needed. A great deal has already been learnt about the pathology and pathogenesis of the disease, but there are still a number of gaps in our knowledge and these remain important areas for current and future research.

1.1.1. Clinical features

PD is characterised clinically by four motor symptoms, first described by James Parkinson in his 'Essay on the Shaking Palsy' in 1817. These are: bradykinesia (slowness of movement); muscular rigidity; resting tremor; and postural instability, which often arises a few years after first presentation. The disease frequently presents asymmetrically, although symptoms become bilateral in later stages (Fernandez, 2012).

In addition to the cardinal motor symptoms , PD patients may experience a range of non-motor symptoms (table 1.1) which may be more disabling (Poletti et al., 2012). In particular, dementia is common in PD patients, with an incidence up to six times that in age-matched controls (Emre, 2003). This is a particular problem as it limits treatment options, as many PD treatments exacerbate the dementia. Psychosis and mood disturbances such as depression, anxiety or apathy are also very common. The four motor

MOTOR SYMPTOMS	NON-MOTOR SYMPTOMS
Bradykinesia	**Craniofacial features**
Muscular rigidity	Masked facies (reduced facial expression)
Resting tremor	Sialorrhea (drooling)
Postural instability	Anosmia (loss of sense of smell)
	Hypophonia (soft speech)
	Dysarthria (difficulty pronouncing words)
	Dysphagia (trouble swallowing)
	Sensory features
	Paresthesia (sensations of tingling, prickling or numbness)
	Pain
	Neuropyschiatric features
	Depression
	Anxiety
	Apathy
	Dementia
	Psychosis
	Other
	Fatigue
	Sleep disturbance
	Seborrheic dermatitis
	Eye abnormalities

Table 1.1 List of motor and non-motor symptoms of PD. Table adapted from (Fernandez, 2012).

symptoms of PD are grouped into an umbrella term, 'parkinsonism' (Fahn, 2003). While idiopathic PD (IPD) is by far the most common cause of parkinsonism, secondary parkinsonism (in which the symptoms are not due to disease) and atypical parkinsonism (in which the symptoms are due to a disease other than PD) must also be discounted. Secondary parkinsonism may have a number of causes including dopamine receptor-blocking agents such as the anti-psychotic haloperidol, or strokes in the basal ganglia (Lees, 2007). Atypical parkinsonism includes the 'Parkinson-plus' syndromes: progressive supranuclear palsy (PSP); multiple system atrophy (MSA); corticobasal degeneration (CBD); and dementia with Lewy bodies (DLB) (Stacy and Jankovic, 1992). Each of these syndromes is characterised by parkinsonism with additional clinical features, such as vertical gaze palsy (an inability to look downwards without moving the head) in the case of PSP (Stacy and Jankovic, 1992), and each has distinct pathological hallmarks (Halliday et al., 2011).

1.1.2. Pathology

The primary pathological hallmark of PD, and the underlying cause of the symptoms, is the death of dopaminergic neurons projecting from the substantia nigra pars compacta to the striatum (Greenfield and Bosanquet, 1953). This degeneration is clearly visible upon post-mortem as a pallor of the substantia nigra (figure 1.1), which is usually pigmented due to high levels of neuromelanin (Carstam et al., 1991). It is estimated that in most cases nigral loss reaches approximately 70% before symptoms emerge (Dauer and Przedborski, 2003; Weintraub et al., 2008).

In addition to nigral degeneration, for a diagnosis of PD to be upheld ubiquitinated proteinaceous cytoplasmic inclusions termed Lewy bodies must be identified in the surviving neurons of the substantia nigra and locus coeruleus (Hughes et al., 1992). Lewy body pathology has been shown to spread in a defined manner over the course of disease, originating in the brainstem and progressing upwards, eventually reaching into the cerebral cortex in the latter stages of disease (Braak et al., 2002).

The primary constituent of Lewy bodies is α-synuclein (α-syn), a largely presynaptic protein whose normal physiological function is not entirely clear. Duplications and triplications of the gene encoding α-syn cause an autosomal dominant form of PD (Chartier-Harlin et al., 2004; Singleton et al., 2003), suggesting that α-syn aggregation may play a role in disease pathogenesis. Aggregation of α-syn is observed in a number of

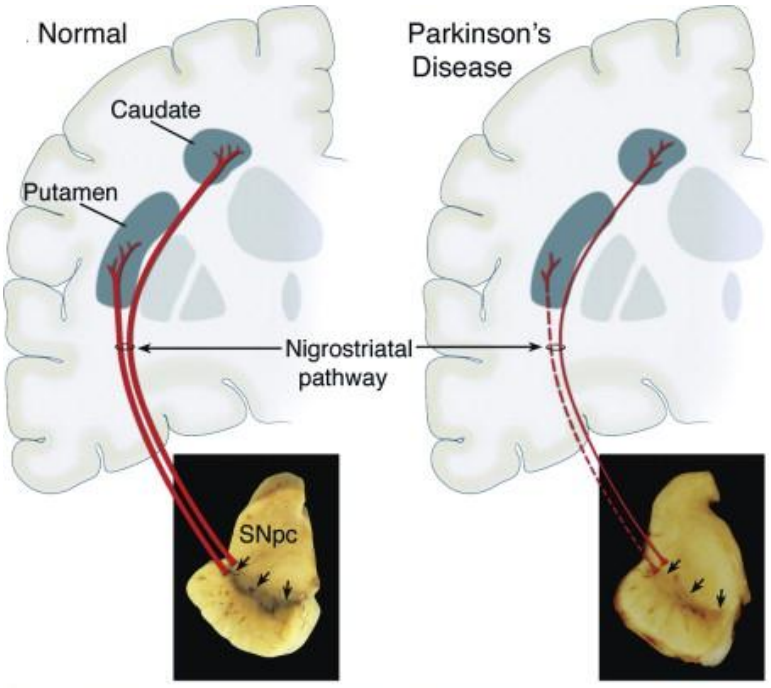

Figure 1.1 Degeneration of the nigrostriatal pathway in PD. Pallor of the substantia nigra is indicated by arrows on slices of fixed post mortem brain from a control (left) and a patient with PD (right). Projection of these neurons to the two regions of the striatum, the caudate and putamen, is shown. Figure reproduced from (Dauer and Przedborski, 2003).

disorders in addition to PD, including DLB and MSA (Halliday et al., 2011), and is sometimes observed *post mortem* in individuals with no symptoms of neurological disease. These cases are termed incidental Lewy body disease (ILBD) and are usually assumed to represent presymptomatic PD (DelleDonne et al., 2008). Figure 1.2 shows immunohistochemical staining of a Lewy body for both ubiquitin and α-syn.

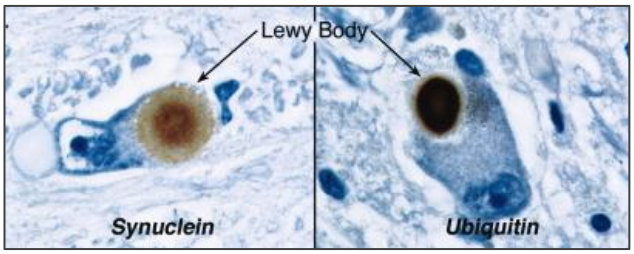

Figure 1.2 Lewy body staining in PD. Lewy bodies in the substantia nigra are stained for α-synuclein (left) and ubiquitin (right). Image from (Dauer and Przedborski, 2003).

The finding that Lewy body pathology progresses through adjacent brain regions (Braak et al., 2002) led some to suggest that the disease may spread through cell-to-cell transmission (Brundin et al., 2008). This idea has gained momentum due to the observation of Lewy bodies in foetal mesencephalic stem cell grafts which had been transplanted into the striatum of PD patients ten years previously, suggesting that the disease had spread from the surrounding neurons to the grafted cells (Kordower et al., 2008; Li et al., 2008). Evidence that α-syn is secreted into biological fluids *in vivo* and extracellular media in cultured neurons (Borghi et al., 2000; El-Agnaf et al., 2003), combined with the finding that introduction of exogenous α-syn fibrils into cultured cells prompts aggregation of endogenous α-syn (Luk et al., 2009), points to α-syn as the probable culprit. It should be pointed out, however, that the study by Luk and colleagues used cationic liposomes to deliver exogenous α-syn into the cytoplasm and the uptake of cell-secreted α-syn by neurons has not been demonstrated (Emmanouilidou et al., 2010). It remains possible, therefore, that secreted α-syn mediates disease spread via a mechanism other than endocytosis, perhaps at the level of the plasma membrane of the recipient neuron (Vekrellis et al., 2011).

1.1.3. Treatment

The death of dopaminergic neurons and the consequent depletion of dopamine in the striatum provides the rationale for all current drug therapies for PD (reviewed by Fernandez, 2012). Of these, the most effective and the cheapest is the dopamine precursor

levo-3,4-dihydroxyphenylalanine (L-DOPA), which has been a mainstay therapy since its discovery in the 1960s (Birkmayer and Hornykiewicz, 1962; Cotzias et al., 1968). It is usually given in combination with carbidopa to prevent its conversion to dopamine in the periphery, reducing side effects such as nausea and vomiting.

Although L-DOPA therapy is effective in alleviating the symptoms, its major disadvantage is that after four to six years of treatment patients begin to develop side effects such as motor fluctuations or choreiform dyskinesias (Mones et al., 1970). For this reason L-DOPA is often not prescribed in the early stages of disease, particularly in younger patients. The next most effective class of drugs is the dopamine agonists, which have consistently been shown in clinical trials to be less effective than L-DOPA but to involve less wearing-off effects and dyskinesia (Parkinson Study Group, 2003; Rascol et al., 2000). Monoamine oxidase B (MAO-B) inhibitors reduce the degradation of dopamine in the brain and may also be effective, either as monotherapy or in addition to L-DOPA to extend the 'on' time (Elmer and Bertoni, 2008). Finally, deep brain stimulation (DBS) may be beneficial, particularly in patients with advanced parkinsonism (Benabid et al., 2009). DBS involves the implantation of electrodes into the subthalamic nucleus (Benazzouz et al., 1993) or globus pallidus (Siegfried and Lippitz, 1994), which can be stimulated at regular intervals by a unit implanted under the skin of the patient's chest. High frequency stimulation mimics the effects of surgical lesioning of the area, but is reversible and therefore safer (Benabid et al., 2009). Subthalamic stimulation is more commonly used as it is thought to have a wider range of beneficial effects, improving both motor and non-motor features of PD (Fasano et al., 2012). By contrast, pallidal stimulation is primarily effective in reducing the effects of DOPA-dyskinesia (Krause et al., 2001).

1.1.4. Aetiology

PD was originally considered a purely sporadic disorder, with one of the exclusion criteria for diagnosis being a family history of the disease (Hughes et al., 1992). Since then, however the boundaries between the familial and sporadic forms of the disease have blurred, with some inherited mutations found to induce a form of the disease clinically almost indistinguishable from sporadic forms (Aasly et al., 2005; Chartier-Harlin et al., 2004), while other mutations have been identified in a proportion of sporadic as well as familial cases (Gilks et al., 2005). Very recently, large scale genome-wide association studies (GWAS) have identified common genetic variants which significantly increase susceptibility to PD (Lesage and Brice, 2012), contributing to a view of the disease in

which genetic susceptibility factors interact with poorly understood environmental variables to determine onset. As is the case for most neurodegenerative disorders, age is the primary environmental factor, with the mean age of diagnosis in the seventh decade of life (Weintraub et al., 2008). Exposure to certain pesticides and herbicides can also significantly increase susceptibility (Tanner, 1992), while other factors such as cigarette smoking and caffeine consumption appear to correlate inversely with the disease (Hernan et al., 2002). Improving understanding of both genetic and environmental factors is crucial as it will have a direct bearing on our understanding of disease pathogenesis and potential therapeutic strategies.

1.1.5. Disease pathogenesis: lessons from genetics

In the past two decades it has been recognised that 5-10% of all PD cases are either dominantly or recessively inherited, and linkage analysis in these pedigrees has led to the identification of a number of genetic loci, named 'PARK' loci (see **Error! Reference source ot found.**). Of these, genes have been identified which correspond to 11 loci: *SNCA* (*PARK1/4*); *Parkin* (*PARK2*); *UCHL-1* (*PARK5*); *PINK1* (*PARK6*); *DJ-1* (*PARK7*); *LRRK2* (*PARK8*); *ATP13A2* (*PARK9*); *GIGYF2* (*PARK11*); *HtrA2* (*PARK13*); *PLA2G6* (*PARK14*); and *FBXO7* (*PARK15*), although the genetic evidence for three of these genes, *HtrA2*, *UCHL-1* and *GIGYF2*, has been disputed (Healy et al., 2006; Nichols et al., 2009; Ross et al., 2008; Simon-Sanchez and Singleton, 2008; Vilarino-Guell et al., 2009). Although not assigned a PARK locus, heterozygous mutations in *GBA*, which encodes a lysosomal lipid hydrolase, have also been shown to associate with PD (Lwin et al., 2004). *GBA* is one of several genes involved in ceramide metabolism which have been found to result in Lewy body pathology, possibly highlighting a novel pathway in PD pathogenesis (Bras et al., 2008).

In addition to these rare disease-causing mutations, GWAS analysis has revealed common single nucleotide polymorphisms (SNPs) with more subtle effects on PD risk. Several studies have identified SNPs in *SNCA* and *MAPT,* the genes encoding α-synuclein and tau respectively, in conferring risk for PD (Edwards et al., 2010; Satake et al., 2009; Simon-Sanchez et al., 2009), and larger studies have subsequently identified five new risk loci: a locus on 12q24 (Saad et al., 2011); the *BST1* locus on 4p15 (Satake et al., 2009); the *GAK* locus on4p16 (Hamza et al., 2010); and the *HLA* region on chromosome 6p (Hamza et al., 2010). A very large meta-analysis of over 12,000 cases and21,000 controls has recently identified eight further loci (*ACMSD, STK39, MCCC1/LAMP3, SYT11, CCDC62/HIP1R, STX1B*

Locus	Location	Gene	Functions	Parkinsonism	Pathology	Reference
PARK1/4	4q21	SNCA	Synaptic protein	EOPD (AD) and sporadic	LB	(Chartier-Harlin et al., 2004; Ibanez et al., 2004; Polymeropoulos et al., 1997)
PARK2	6q25-27	Parkin	E3 ubiquitin ligase	Juvenile/EOPD (AR) and sporadic	No LB	(Kitada et al., 1998)
PARK3	2p13	Unknown	Unknown	LOPD (AD)	Unknown	(Gasser et al., 1998)
PARK5	4p14	UCHL-1	Ubiquitin C-terminal hydrolase	LOPD (AD)	LB	(Leroy et al., 1998)
PARK6	1p35-36	PINK1	Mitochondrial kinase	EOPD (AR)	LB	(Valente et al., 2004)
PARK7	1p36	DJ-1	Redox sensor	EOPD (AR)	Unknown	(Bonifati et al., 2003)
PARK8	12q12	LRRK2	Kinase/GTPase	LOPD (AD) and sporadic	LB (usually)	(Zimprich et al., 2004) (Paisan-Ruiz et al., 2004)
PARK9	1p36	ATP13A2	Lysosomal ATPase	Juvenile Kufor-Rakeb syndrome and EOPD (AR)	Unknown	(Ramirez et al., 2006)
PARK10	1p32	Unknown	Unknown	Unknown	Unknown	(Li et al., 2002b)
PARK11	2q36-37	GIGYF2	Regulation of tyrosine receptor kinase signalling?	LOPD (AD)	Unknown	(Lautier et al., 2008)
PARK12	Xq21-25	Unknown	Unknown	Unknown	Unknown	(Pankratz et al., 2002)
PARK13	2p13	HtrA2	Mitochondrial protease	Unknown	Unknown	(Bogaerts et al., 2008; Strauss et al., 2005)
PARK14	22q13.1	PLA2G6	A2 phospholipase	Juvenile levodopa-reponsive parkinsonism(AR)	LB and tau pathology	(Paisan-Ruiz et al., 2009)
PARK15	22q12-13	FBXO7	E3 ubiquitin ligase adaptor protein	EO parkinsonian-pyramidal syndrome (AR)	Unknown	(Di Fonzo et al., 2009b; Shojaee et al., 2008)
PARK16	1q32	Unknown	Unknown	Unknown	Unknown	(Satake et al., 2009)

Table 1.2 Genetic loci associated with PD. Table adapted from (Seol, 2010). Abbreviations: AR, autosomal recessive; AD, autosomal dominant; EO, early onset; LO, late onset; LB, Lewy body.

and *GPNMB*) as having small but significant effects on disease odds ratio (International Parkinson's Disease Genomics Consortium and Wellcome Trust Case Control Consortium 2, 2011).

Although familial forms of PD represent only a small percentage of total PD worldwide, the effort that has gone into genetic characterisation of these families has paid dividends in our understanding of the disease. Investigating the physiological functions of the proteins encoded by these genes has revealed a number of common pathways: for example, mutations have been identified in components of the ubiquitin proteasome system (UPS), in the form of Parkin, UCHL-1 and Fbxo7 (Kitada et al., 1998; Leroy et al., 1998; Shojaee et al., 2008), and in the lysosomal proteins ATP13A2 and GBA (Lwin et al., 2004; Ramirez et al., 2006), linking dysfunction of both proteolytic systems to PD pathogenesis. Figure 1.3 (overleaf) highlights some of the implicated pathways such as proteasomal and lysosomal dysfunction, α-syn aggregation, mitochondrial dysfunction and altered signal transduction, all of which can impact on numerous cellular processes. This thesis will focus on mitochondrial dysfunction in PD pathogenesis, by investigating the roles of proteins genetically associated with the disease in mitochondrial function. The existing evidence linking these proteins to the mitochondria will be discussed in section 1.3; before this, however, it is worth discussing the physiological functions of the mitochondria and their cellular importance in the context of neurodegeneration.

Figure 1.3 Pathways to pathogenesis. Figure adapted from (Farrer, 2006).

1.2. Mitochondria: from physiology to pathology

Mitochondria are often described as 'the powerhouse of the cell', but they are more than simple ATP producers: mitochondrial function is essential in processes from cell division to cell death (Scheffler, 1999). In a healthy cell, these functions are highly regulated by mechanisms that control mitochondrial polarisation, morphology, distribution and degradation, to list but a few. Failure of those mechanisms is disastrous for neuronal physiology, with mitochondrial dysfunction playing a role in the pathogenesis not only of PD but also of Alzheimer's disease (AD), Huntington's disease (HD), amyotropic lateral sclerosis (ALS) and numerous rarer neurodegenerative disorders (for review, see Burchell et al., 2010a, b). This section aims to introduce some of the major mitochondrial functions and dysfunctions implicated in neurodegeneration.

Mitochondria are composed of two membranes: the outer mitochondrial membrane (OMM) is permeable to solutes and proteins up to 5 kDa, while the inner mitochondrial membrane (IMM) is highly impermeable, enabling the generation of ionic gradients across the membrane (section 1.2.1). The IMM has a much greater surface area than the OMM which surrounds it, resulting in the formation of invaginations termed cristae (see figure 1.4). Crista junctions are formed by dimerisation of OPA1 at the neck of the crista (Frezza et al., 2006), and function partly to keep cytochrome c contained until its release during apoptosis (Cipolat et al., 2006). Other important mediators of apoptosis such as SMAC/Diablo and HtrA2 also localise to the intermembrane space (IMS; see section 1.2.5).

Figure 1.4 Mitochondrial structure

The area enclosed by the IMM, termed the mitochondrial matrix, is the location for most of the metabolic enzymes of the mitochondria and the mitochondrial DNA (mtDNA), a 16 kDa circle of DNA containing genes encoding 37 of the mitochondrial proteins (the remainder being encoded by the nuclear DNA). These proteins include components of the NADH dehydrogenase complex (complex I) and the ATP synthase, which are translated in the mitochondrial matrix and inserted into the IMM in a co-translational manner (Szyrach et al., 2003).

1.2.1. Mitochondrial respiration and ATP production

One of the reasons that neurons are so dependent on mitochondrial function is because of their high demand for ATP, which is produced most efficiently by mitochondrial respiration (Vander Heiden et al., 2009). High ATP levels are needed primarily for the control of cytosolic calcium levels by plasmalemmal and endoplasmic reticulum (ER) ATPases following synaptic transmission (DiPolo, 1974), without which the cell floods with calcium causing necrotic cell death (see section 1.2.5). Defects in mitochondrial respiration appear to be a key factor in the pathogenesis of PD, since inhibitors of respiratory complex I induce PD symptoms in both humans and mice (Betarbet et al., 2000; Langston et al., 1984; Mizuno et al., 1988), and complex I deficiency is observed in PD patients (Schapira, 1993; see section 1.3).

Mitochondrial respiration describes the transfer of high energy electrons between the four IMM protein complexes of the electron transport chain (ETC), culminating in the reduction of molecular oxygen to water at complex IV (see Alberts et al., 2002; figure 1.5). Free energy released as the electrons are transferred to lower energy acceptors is used to pump protons out of the mitochondrial matrix through complexes I, III and IV, generating a potential across the IMM ($\Delta\Psi_m$, figure 1.5). This proton gradient is harnessed by the F_1F_0-ATP synthase (complex V), which produces ATP by coupling the re-entry of protons into the mitochondria to conformational changes that catalyse the addition of inorganic phosphate (P_i) to ADP (Senior et al., 2002; discussed further in chapter 3). In addition to generating ATP, maintenance of the $\Delta\Psi_m$ is essential for mitochondrial protein import (Schleyer et al., 1982), calcium uptake (see section 1.2.3) and to prevent opening of the mitochondrial permeability transition pore (see section 1.2.5). $\Delta\Psi_m$ is thus commonly used as an indicator of mitochondrial function (see chapters 3, 4 and 5).

The ETC is fed by electrons from either NADH, the electron donor for complex I, or $FADH_2$, which is produced as an intermediate at complex II. Both NADH and $FADH_2$ are generated in the mitochondria either by the tricarboxylic acid (TCA) cycle, which is fed by the products of carbohydrate, protein or lipid catabolism, or by β-oxidation of lipids (for further detail, see Alberts et al., 2002). The major source of energy in the cell is carbohydrate, which is metabolised by glycolysis in the cytosol to pyruvate. Pyruvate then enters the mitochondria and is converted to acyl-CoA which feeds into the TCA cycle (see Alberts et al., 2002; figure 1.5). Defects in any of the components of the TCA cycle or the ETC can result in low $\Delta\Psi_m$ and a lack of ATP, but because of their proximity to a major site of reactive oxygen species (ROS) production (discussed in the next section) the respiratory complexes are particularly prone to damage and this has been implicated in the pathogenesis of several neurodegenerative disorders including PD, AD and HD (Gu et al., 1996; Keeney et al., 2006; Parker et al., 1990).

Figure 1.5 Mitochondrial production of ATP. Abbreviations: OMM, outer mitochondrial membrane; IMM, inner mitochondrial membrane; TCA, tricarboxylic acid; I, complex I; II, complex II; Q, ubiquinone; III, complex III; cyt c, cytochrome c; IV, complex IV; V, complex V (ATP synthase)

1.2.2. Reactive oxygen species production

Oxidative stress is one of the key routes to cell death, either through redox activation of the intrinsic apoptosis pathway, or by widespread damage leading to loss of cell integrity and necrotic cell death (see section 1.2.5). The mitochondria are major producers of both reactive oxygen species (ROS; reviewed by Balaban et al., 2005) and antioxidants (Rabilloud et al., 2001), placing them in a unique position to regulate oxidant levels under basal conditions, but also making them highly vulnerable to oxidative damage at pathologically high ROS levels (reviewed by Van Remmen and Richardson, 2001). This damage impairs mitochondrial function and further increases mitochondrial ROS production (see below), resulting in a vicious cycle which is proposed to underlie natural aging (Harman, 1965).

Reactive oxygen and nitrogen species (ROS and RNS) are oxygen or nitrogen species which carry an unpaired electron, making them thermodynamically unstable and therefore highly reactive. Mitochondria are usually considered the single most important source of cellular ROS because, although other enzymes such as NADPH oxidase or xanthine oxidase produce higher levels when activated (Agarwal et al., 2011; Kennedy et al., 2012), the mitochondria generate oxidative radicals continually (see Balaban et al., 2005). Mitochondrial ROS production occurs primarily at the ETC, where it is estimated that between 1 and 4% oxygen consumed is reduced to superoxide ($O_2^{\cdot-}$) rather than water (reviewed by Zhang and Gutterman, 2007). $O_2^{\cdot-}$ is produced at both complex I, which releases it into the mitochondrial matrix (Kushnareva et al., 2002), and at complex III, where it is released into the intermembrane space (IMS) (Chen et al., 2003). This distinction is important since $O_2^{\cdot-}$ is unable to pass through membranes except via anion channels (Lynch and Fridovich, 1978), resulting in its potential accumulation in the mitochondrial matrix. Matrix $O_2^{\cdot-}$ is dismutated to hydrogen peroxide (H_2O_2) by the enzyme superoxide dismutase 2 (SOD2), while SOD1 in the cytosol catalyses the reduction of $O_2^{\cdot-}$ (Weisiger and Fridovich, 1973). H_2O_2 is freely diffusible across membranes and may be further reduced to water by catalase (Evans, 1907), or it can react with free iron in the Fenton reaction to produce the highly reactive hydroxyl radical ($OH^{\cdot-}$) (Fong et al., 1976). Other important antioxidant systems include glutathione (GSH), which acts as a scavenger of H_2O_2 (Mills, 1960), peroxidiredoxin, which catalyses the reduction of H_2O_2 and peroxinitrite (Kim et al., 1988), and thioredoxin, which acts as a potent reducing agent (Holmgren, 1979). Of these, it is particularly worth noting that the recycling of glutathione requires NADPH generated by the pentose phosphate pathway (Mann, 1932), which uses

glucose 6-phosphate as its starting substrate. This is important since glucose 6-phosphate is an intermediate of glycolysis, forcing the cell to choose between ATP production and antioxidant production (Cohen and Hochstein, 1961).

ROS are often considered no more than a toxic by-product of respiratory activity, but an increasing body of evidence suggests that basal ROS production from sources including mitochondria has an important signalling role (Zhang and Gutterman, 2007). Mitochondrial ROS production may be modulated by various factors including $\Delta\Psi_m$, intracellular calcium and nitric oxide (NO) (Zhang and Gutterman, 2007). $\Delta\Psi_m$-dependent modulation is of particular interest since it allows mitochondrial ROS to be modulated by mitochondrial uncoupling, discussed in further detail in chapter 3. Meanwhile a calcium-dependent increase in mitochondrial ROS production allows for a potential role of ROS as second messengers. These redox signalling pathways may be involved in basal cell function, in the production of antioxidants to keep free radical production under control, or even in the triggering of apoptosis when oxidant levels are dangerously high (Valko et al., 2007).

Although ROS and RNS have important physiological functions, it is essential that their production is tightly controlled. If allowed to reach pathological levels, free radicals damage both nuclear and mitochondrial DNA, causing mutations and double-stranded breaks (Demple and Harrison, 1994); they modify proteins, altering their function (Forster et al., 1996); and they peroxidise lipids, generating damaging reactive lipid species and altering membrane fluidity and permeability (Choe et al., 1995; Racay et al., 1997; Raess et al., 1997). The 'Free radical theory of ageing' (Harman, 1965) proposes that over time low levels of oxidative damage accumulate at the mitochondria, resulting in damage to mtDNA, the ETC and antioxidant systems which further increases ROS production, producing a vicious cycle. High levels of oxidative damage are consistently observed in patients with neurodegenerative disease including PD, AD and HD (Browne et al., 1997; Butterfield et al., 2006; Jenner, 2003), although it is difficult to say whether this is a primary cause of pathology or a symptom of prior mitochondrial dysfunction.

1.2.3. Mitochondrial calcium handling

Calcium ions are key intracellular signalling molecules in all cells and particularly in neurons, where synaptic transmission depends on calcium-mediated action potentials (Berridge et al., 2000). Calcium overload, however, is a major cause of neurotoxicity (Rang

et al., 2003). The mitochondrial network plays an essential role in protecting against this overload by acting as a buffer similar to the ER, taking up calcium in a $\Delta\Psi_m$-dependent manner through the calcium uniporter when cytosolic levels are high, then releasing it via ion exchangers when the wave has passed (Werth and Thayer, 1994). Calcium uptake into the mitochondria additionally stimulates ATP production by increasing activity of three critical rate-limiting enzymes of the TCA cycle: pyruvate dehydrogenase, isocitrate dehydrogenase and oxoglutarate dehydrogenase (Denton et al., 1980; McCormack et al., 1988), which enables the cell to meet the increased energy demands imposed by the calcium stimulus (Jouaville et al., 1999). On the other hand, excessive uptake of calcium into the mitochondria triggers opening of the permeability transition pore (see section 1.2.5), which releases calcium back into the cytosol and if prolonged, activates cell death mechanisms (Rasola and Bernardi, 2011). Thus any form of mitochondrial dysfunction can have severe consequences for calcium handling, impairing neuronal signalling and potentially causing neuronal death (Duchen et al., 2008). In the case of PD, one explanation proposed to account for the specific death of the nigrostriatal dopaminergic neurons is that these cells, unlike other dopaminergic neurons, express L-type calcium channels which regularly allow waves of calcium to enter the cell, producing a so-called 'pacemaker' signal (Chan et al., 2009). This type of signal places greater strain on the mitochondria, which were hypothesised to consequently produce more ROS and thus accumulate oxidative damage more rapidly. In agreement with this hypothesis, a mouse model expressing a genetically-encoded fluorescent mitochondrial redox probe under the expression of the tyrosine hydroxylase (TH) promoter revealed increased mitochondrial oxidant levels in dopaminergic neurons of the substantia nigra compared to those of the ventrotegmental area which do not exhibit pacemaking activity (Guzman et al., 2010). Furthermore, oxidation of the probe was inhibited by either L-type channel antagonists or inhibitors of mitochondrial calcium uptake (Guzman et al., 2010), indicating that this oxidative stress does result from elevated mitochondrial calcium levels. Mitochondrial calcium mishandling has also been implicated in disease pathogenesis: mutations in *SOD1*, the most common cause of familial ALS, appear to inhibit calcium buffering by the mitochondria (Jaiswal et al., 2009), while mutations in *PINK1*, the second most common cause of autosomal recessive parkinsonism, cause calcium dyshomeostasis by interfering with the action of the mitochondrial Na^+-Ca^{2+} exchanger (Gandhi et al., 2009).

1.2.4. Mitochondrial maintenance

Given the cellular importance of mitochondrial function, it is essential that damaged mitochondrial components can be effectively removed and the integrity of the mitochondrial network maintained. This is achieved through two pathways. Within the mitochondria, a system of chaperones, proteases and E3 ubiquitin ligases act to ensure the correct folding of mitochondrial proteins and the degradation of damaged or misfolded proteins (section 1.2.4.1). At the same time, repeated cycles of fusion, fission and mitophagy allow minor mitochondrial defects to be complemented by fusion while severely damaged mitochondria are degraded by the lysosome (section 1.2.4.2). Defects in either process can allow damaged mitochondria to accumulate, with deleterious consequences for the cell (Imai and Lu, 2011; Karbowski and Neutzner, 2012).

1.2.4.1. Protein quality control in the mitochondria

Degradation of mitochondrial proteins occurs through distinct mechanisms depending on their submitochondrial localisation (see figure 1.6). OMM proteins are accessible to the cytosol and can therefore be targeted for proteasomal degradation by ubiquitination, either by E3 ubiquitin ligases in the cytosol or in the OMM (Karbowski and Youle, 2011). By contrast, the mitochondrial matrix, IMM and IMS are believed to be devoid of ubiquitination machinery (Karbowski and Neutzner, 2012) and are thus reliant on alternative mechanisms of protein degradation. In these compartments proteolysis is mediated by a number of ATP-dependent proteases such as the AAA^+ metalloproteases *i*-AAA and *m*-AAA in the IMM or Lon in the matrix (Voos, 2012). At the same time, chaperone proteins function to mediate the folding of imported mitochondrial proteins (Voos, 2012) (figure 1.6).

Consistent with a key role for mitochondrial protein quality control in mitochondrial maintenance and thus neuronal health, several components of this system have been linked to neurodegenerative disease (Karbowski and Neutzner, 2012). One such protein is the mitochondrial chaperone mortalin, also called mitochondrial heat shock protein 70 (mtHSP70). Mortalin protein levels were found to be significantly reduced in the substantia nigra of patients with PD compared to controls (Jin et al., 2007), and genetic association studies have identified three mutations in the *mortalin* gene in PD patients and not in controls (Burbulla et al., 2010; De Mena et al., 2009). All three mutations were found to interfere with protein function, since mitochondrial dysfunction in mortalin

Figure 1.6 Mitochondrial protein quality control. A system of mitochondrial chaperones, proteases and E3 ubiquitin ligases co-operate to ensure mitochondrial proteins are correctly folded and damaged or misfolded proteins (indicated by a red star) are swiftly removed. Figure based on (Tatsuta and Langer, 2008).

deficient cells could be rescued by overexpression of wild-type (WT) but not mutant mortalin (Burbulla et al., 2010).

Genetic mutations in a number of mitochondrial proteases have also been identified. Mutations in AFG3L2 and paraplegin, the two subunits of the metalloprotease *m*-AAA, both result in neurodegeneration with AFG3L2 mutations causing spinocerebellar ataxia type 28 (Di Bella et al., 2010) and paraplagin mutations causing hereditary spastic paraplegia (Casari et al., 1998). Of particular interest to this thesis, the mitochondrial protease HtrA2 (see section 1.3.3.2) has been suggested to function in mitochondrial protein quality control (Moisoi et al., 2009; Papa and Germain, 2011; Radke et al., 2008) and loss of HtrA2 in mice causes striatal neurodegeneration and a parkinsonian behavioural phenotype (Martins et al., 2004). This putative role of HtrA2 will be discussed further in chapters 3 and 6.

1.2.4.2. Fusion, fission and mitophagy

Mitochondria are not static organelles: even their name stems from the Greek "mitos" meaning thread and "khondrion" meaning grain, highlighting the dual nature of their morphology. By balancing the processes of mitochondrial fusion and fission, the cell can rearrange its mitochondria according to local metabolic demand, creating a dynamic network of mitochondria. This is important for several reasons, but of particular relevance to this this thesis is the role of mitochondrial dynamics in mitochondrial maintenance, through its interaction with the process of selective mitochondrial autophagy, termed mitophagy. The mechanisms and importance of these processes will be addressed both in this section and in chapter 5, which describes the identification of a novel mediator of mitophagy.

Mitochondrial fusion and fission are controlled by a family of large dynamin-related GTPases. Fission is mediated by the cytosolic protein Drp1 (dynamin-related protein 1) (Smirnova et al., 2001), which oligomerises on the OMM at the point of scission and pinches the mitochondria apart in a GTP-dependent manner (Ingerman et al., 2005; Mears et al., 2011). Mitochondrial fusion, on the other hand, requires the OMM GTPases mitofusins 1 and 2 (Mfn1 and Mfn2; Legros et al., 2002) and the IMM GTPase OPA1 (optic atrophy 1; Misaka et al., 2002). GTP-dependent oligomerisation of mitofusins on the surface of the two mitochondria enables the tethering and fusion of the outer membranes (Ishihara et al., 2004; Koshiba et al., 2004), followed by inner membrane fusion mediated by membrane-bound OPA1 (Meeusen et al., 2006). Inherited mutations in the genes

encoding both OPA1 and Mfn2 result in degeneration of the optic nerve and the peripheral nerves respectively (Alexander et al., 2000; Zuchner et al., 2004), and a point mutation in the *Drp1* gene caused such a severe neurodegenerative disorder that the patient only survived 37 days (Waterham et al., 2007), highlighting the importance of both processes in neuronal function.

Unsurprisingly given the severe clinical phenotype of these patients, disruption of either mitochondrial fission or fusion can induce severe mitochondrial abnormalities including bioenergetic deficits, loss of mtDNA and ultrastructural alterations (reviewed by Burchell et al., 2010b; see figure 1.7 overleaf). These defects arise in part because both fusion and fission are essential for mitochondrial maintenance, in that mitochondrial damage may be partially ameliorated by fusion with healthy mitochondria (a process termed 'functional complementation'; Ono et al., 2001) while unequal mitochondrial fission followed by removal of the more depolarised daughter mitochondrion enables the quality of the overall mitochondrial network to be maintained (Twig et al., 2008). This removal of depolarised mitochondria occurs via a mitochondria-selective form of macroautophagy termed mitophagy (Twig et al., 2008).

Macroautophagy is a form of autophagy ('self-eating') in which a double-membraned vesicle forms around the substrate before fusing to the lysosome where it is degraded (Lee, 2012). It was originally considered a non-selective process for nutrient recycling, but over the years selective forms of macroautophagy have been identified for the removal of damaged cellular components including peroxisomes (pexophagy), endosomes (heterophagy) and mitochondria (mitophagy) (Klionsky, 2007). These processes share a requirement for many of the molecular components involved in starvation-induced autophagy, with 15 of the 35 Atg (autophagy) genes identified in yeast essential for all forms of macroautophagy. This core autophagic machinery mediates (i) formation of the pre-autophagosomal structure, requiring a complex of Beclin (Atg6 in yeast) with a class III phosphatidylinositol 3-kinase (PI3K) (He and Levine, 2010); (ii) expansion of the autophagosomal membrane by insertion of cleaved and lipidated LC3 (Kabeya et al., 2000; Tanida et al., 2004); and (iii) fusion of the autophagosome to the lysosome, mediated by Rab7 and the lysosomal transmembrane protein LAMP2 (Gutierrez et al., 2004; Jager et al., 2004; Saftig et al., 2008). Protein degradation is then mediated by enzymes in the mature autophagolysosome (Eskelinen, 2005). Figure 1.8 shows the stages of autophagy and the main proteins involved.

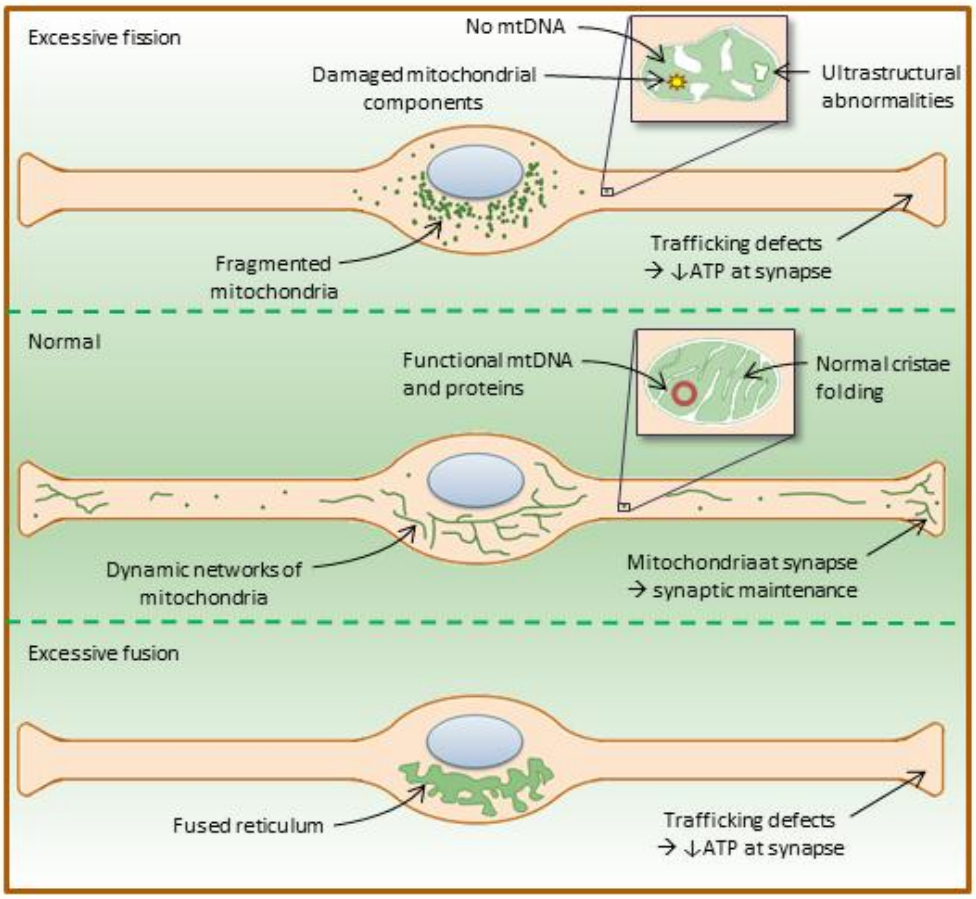

Figure 1.7 Importance of mitochondrial fusion and fission. Figure reproduced from (Burchell et al., 2010b).

Figure 1.8 The macroautophagy pathway. A simplified overview of the major stages in autophagy and the most important proteins involved. Adapted from (Yang and Klionsky, 2010).

In both yeast and mammalian systems mitophagy is selective for damaged or depolarised mitochondria (Campbell and Thorsness, 1998; Goldman et al., 2010; Lemasters et al., 1998). In yeast it is not clear how depolarised mitochondria are recognised, but in mammalian cells mounting evidence suggests that the PD-associated ubiquitin ligase Parkin is central to the process (Youle and Narendra, 2011).

Interest in mitophagy in the PD field began with the observation by Narendra and colleagues that overexpressed tagged Parkin relocates from the cytosol to the mitochondria following treatment with the mitochondrial uncoupler carbonyl cyanide 3-chlorophenylhydrazone (CCCP), and that prolonged mitochondrial depolarisation in Parkin overexpressing cells induces the complete removal of mitochondria (Narendra et al., 2008). Further studies have also shown that Parkin recruitment requires the mitochondrial accumulation of the kinase PINK1, another protein encoded by a PD-associated gene, and that PD-causing mutations in either protein interfere with mitophagy (Geisler et al., 2010a; Geisler et al., 2010b; Kawajiri et al., 2010; Narendra et al., 2010; Vives-Bauza et al., 2010). Although full length PINK1 contains an N-terminal mitochondrial targeting sequence (MTS), under basal conditions it is cleaved in the IMM by the protease PARL and the short form is released into the cytosol (Deas et al., 2011; Jin et al., 2010), with the result that under basal conditions it is largely cytosolic (Haque et al., 2008). However, loss of $\Delta\Psi_m$ interferes with mitochondrial import (Schleyer et al., 1982) and therefore prevents PINK1 from reaching the IMM to be cleaved, where it instead

accumulates at the OMM of depolarised mitochondria, associated with the translocase of the outer membrane (TOM) (Lazarou et al., 2012).

PINK1-dependent recruitment of Parkin has been shown to result in ubiquitination of several mitochondrial substrates, most notably the voltage-dependent anion channel VDAC1 (Geisler et al., 2010a) and the fusion proteins Mfn1 and Mfn2 (Gegg et al., 2010; discussed in further detail in chapter 5). Parkin is capable of mediating different types of ubiquitination (Imai et al., 2001; Joch et al., 2007; Lim et al., 2005; Shimura et al., 2001), which can perform different signalling functions (Trempe, 2011). VDAC1 was shown to undergo modification by the addition of chains of ubiquitin molecules (polyubiquitination) linked through lysine-27 (K27), resulting in recruitment of the adaptor protein p62 (Geisler et al., 2010a). p62 binds both ubiquitinated proteins and LC3, providing a mechanism by which the protophagophore may be recruited to the depolarised mitochondrion. Other studies have similarly found that p62 is recruited to depolarised mitochondria in a Parkin-dependent manner (Ding et al., 2010; Lee et al., 2010), but one report suggests that although p62 recruitment is essential for clustering of depolarised mitochondria in the perinuclear region, it is not essential for clearance of those mitochondria after 24 hr CCCP treatment (Narendra et al., 2010). Unlike VDAC1, Mfn1 and Mfn2 are modified by K48-linked polyubiquitination which results in their degradation by the proteasome, and this appears to be essential for the fragmentation of the mitochondrial network and subsequent mitophagy (Gegg et al., 2010; Tanaka et al., 2010; Ziviani et al., 2010). Inhibition of either Drp1-mediated mitochondrial fission or proteosomal degradation of Mfn1 or 2 inhibited mitophagy, indicating that this is an important stage in the mitophagy process (Tanaka et al., 2010).

In addition to these two proteins, a number of other mitochondrial proteins have been implicated in mitophagy. One study showed that Parkin monoubiquitinates and stabilises Bcl-2 at the mitochondria (Chen et al., 2010), while another suggested that Nix plays an essential role in initiating mitophagy (Ding et al., 2010). It seems likely that mitochondrial depolarisation results in the accumulation of numerous proteins on the OMM, and that Parkin has multiple substrates which mediate different aspects of the mitophagy process. Consistent with this hypothesis, one paper showed that ubiquitination and proteasomal degradation of multiple OMM substrates was required for mitophagy (Chan et al., 2011).

1.2.5. Mitochondria in cell death: apoptosis, necrosis and the permeability transition

Many of the mitochondrial defects described in the preceding sections have been found to cause neuronal cell death, highlighting the importance of mitochondrial function in cell survival. Cell death can most commonly occur through two major pathways: apoptosis, which is characterised by cell shrinkage and blebbing of the cell membrane (Kerr et al., 1972), or necrosis, in which the cell swells and ruptures, releasing its contents into the extracellular matrix (Golstein and Kroemer, 2007). Mitochondrial defects may result in cell death via either mechanism, either indirectly through redox signalling pathways (Azad et al., 2010; Franco et al., 2008) or failure of calcium homeostasis (Wrogemann and Pena, 1976), or directly by causing the opening of a high conductance pore in the IMM termed the mitochondrial permeability transition pore (PTP; Rasola and Bernardi, 2011). This pore was for some time thought to be composed of the adenine nucleotide transporter (ANT) in the IMM (Marzo et al., 1998) and the voltage dependent anion channel (VDAC) in the OMM (Szabo et al., 1993; Szabo and Zoratti, 1993), but subsequent evidence revealed that PTP opening could still occur in cells from WT from *ANT*$^{-/-}$ or *VDAC*$^{-/-}$ mice (Baines et al., 2007; Kokoszka et al., 2004), leaving the major structural components of the pore uncertain. A modulatory role has been attributed to the peptidyl prolyl isomerase protein cyclophilin D (CypD), encoded by the gene *Ppif*, as genetic ablation of *Ppif* or treatment with the CypD inhibitor cyclosporin A results in a two-fold increase in the concentration of mitochondrial calcium required to open the PTP (Basso et al., 2005). It is important to note that this opening can still occur, however, indicating that CypD is not an essential structural component of the pore; in fact, more recent work has revealed that CypD masks an inhibitory P_i binding site on the PTP which is revealed following treatment with cyclosporin (Basso et al., 2008). Intriguingly, CypD was found to associate with the F_1F_O-ATP synthase in a P_i dependent manner (Giorgio et al., 2009) and it has recently been proposed that the ATP synthase may either form part of the PTP or potentially have high sequence homology with a part of the PTP complex (Chinopoulos and Adam-Vizi, 2012).

Apoptotic cell death is controlled by two distinct pathways: intrinsic and extrinsic. In the extrinsic pathway, death receptors at the cell surface are activated by an external stimulus, resulting in the recruitment and activation of caspases which execute cell death (Green, 2000). This pathway occurs independently of the mitochondria. In the intrinsic pathway, on the other hand, apoptosis is triggered by pro-apoptotic members of the Bcl-2 family in

response to cellular stress such as DNA damage or oxidative stress (Adams and Cory, 2001). Initially, members of the 'BH3-only' subfamily such as Bid or Bim engage and activate another set of Bcl-2 proteins, members of the Bax subfamily (Kuwana et al., 2005). The latter oligomerise and insert into the OMM, mediating outer membrane permeabilisation by controlling formation of the mitochondrial apoptosis-induced channel (MAC) (Pavlov et al., 2001). This releases pro-apoptotic factors from the IMS, including cytochrome c, Smac/DIABLO and HtrA2. Smac/DIABLO and HtrA2 inhibit Inhibitor of Apoptosis Proteins (IAPs), a family of proteins which block apoptosis by binding to caspases (Du et al., 2000; Suzuki et al., 2001; Verhagen et al., 2002); meanwhile, released cytochrome c binds the cytosolic protein apoptotic protease activating factor 1 (Apaf-1), resulting in its oligomerisation and the recruitment and activation of caspases (Cain et al., 2000). Mitochondrial outer membrane permeabilisation is opposed by anti-apoptotic members of the Bcl-2 family such as Bcl-2 and Bcl-xL (Kluck et al., 1997).

Unlike apoptosis, which is a tightly controlled cell death pathway with minimal disruption to the surrounding cells, necrosis is usually considered uncontrolled and releases intracellular components into the extracellular space, causing inflammation and further cytotoxicity (Golstein and Kroemer, 2007). A major cause of necrotic cell death is excessive cytosolic calcium (Wrogemann and Pena, 1976), which may occur due to a lack of ATP for ionic homeostasis as previously described (section 1.2.1). This results in activation of enzymes that damage proteins, lipids and DNA, culminating in a disruption of organelle and cell integrity which leads to cell swelling and rupture (Rasola and Bernardi, 2011).

Opening of the PTP was originally considered part of the intrinsic apoptosis pathway, but more recent evidence has demonstrated that it occurs independently of this pathway (Baines et al., 2005; Nakagawa et al., 2005) and may lead to either apoptotic or necrotic cell death (Rasola and Bernardi, 2007). Pore opening is dependent primarily on mitochondrial calcium levels and may be modulated by factors including mitochondrial depolarisation (Rasola and Bernardi, 2007), providing a direct pathway by which mitochondrial dysfunction can cause cell death (Rasola and Bernardi, 2007). Opening may be transient, providing a mechanism for the rapid release of calcium from the mitochondrial matrix (Huser and Blatter, 1999; Petronilli et al., 1999), or prolonged, in which case cell death pathways are irreversibly initiated (Crompton, 1999). Prolonged opening of the PTP causes cell death by allowing solutes to freely enter the mitochondrial

matrix, opening the cristae junctions and rupturing the OMM (Feldmann et al., 2000). This releases pro-apoptotic factors such as cytochrome c and HtrA2 into the cytosol, triggering apoptosis if a relatively small population of mitochondria are involved (Marchetti et al., 1997). If the permeability transition occurs in a very large population of mitochondria simultaneously, however, the resultant mitochondrial depolarisation means that insufficient ATP can be produced to fulfil the energy requirements of the caspases and other components of the apoptotic machinery. In this case, ATP depletion results in failure of calcium homeostasis and necrotic cell death (Bernardi and Rasola, 2007).

While the death of a small number of cells may have no deleterious consequences to the organism, if the triggering mitochondrial defect occurs in many cells at the same time, for example if it arises from a systemic genetic defect, the result can be highly pathogenic. This and the preceding sections have highlighted the importance of mitochondria in cellular function, and the multiple ways in which failure of the mitochondria can lead to cell death. These mechanisms are summarised in figure 1.9.

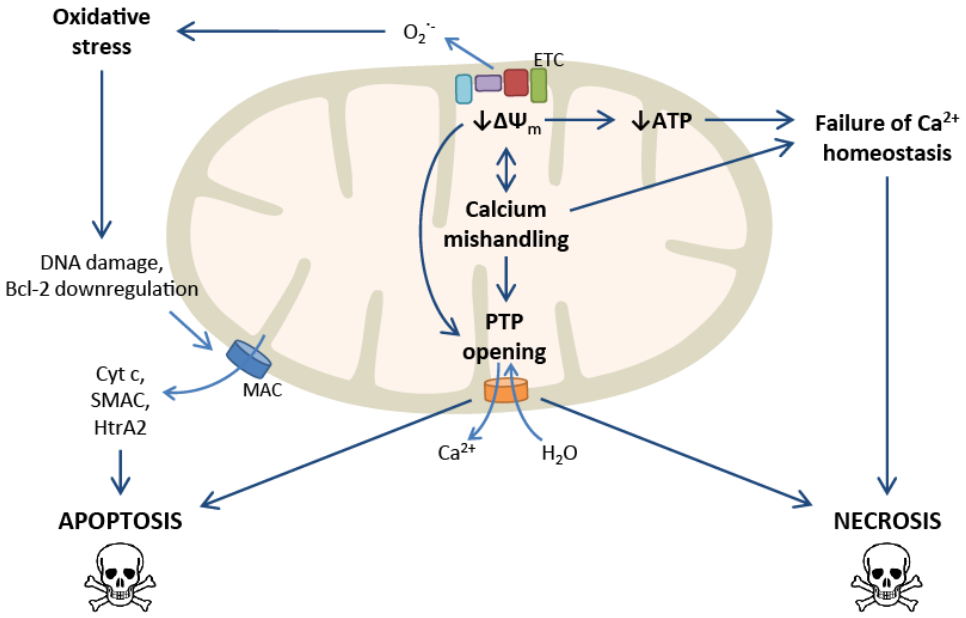

Figure 1.9 Mitochondrial dysfunction causes cell death. Abbreviations: $\Delta\Psi_m$, mitochondrial membrane potential; ETC, electron transport chain; PTP, permeability transition pore; MAC, mitochondrial apoptosis channel.

1.3. Mitochondrial dysfunction in PD

As discussed in the last section, mitochondrial function is essential to cell survival and mitochondrial defects are a major cause of neuronal death. This fact, coupled with their susceptibility to age-related oxidative damage, has implicated the mitochondria in the pathogenesis of every common neurodegenerative disease (Burchell et al., 2010a, b). In PD, three major strands of evidence link mitochondrial function to disease pathogenesis: first, mitochondrial toxins cause PD symptoms in both human and animal models (section 1.3.1); second, mitochondrial abnormalities are observed in cells and post-mortem tissue from patients with idiopathic PD (section 1.3.2); and third, many of the genetic mutations found to cause familial forms of PD also impact on mitochondrial function (section 1.3.3).

1.3.1. Mitochondrial toxins and animal models

The first suggestion that mitochondrial dysfunction could play a causal role in PD pathogenesis was provided over 25 years ago, when a group of intravenous drug users attempting to produce the synthetic drug 1-methyl-4-phenyl-4-propionoxypiperidine (MPPP) instead accidentally synthesised and self-administered the neurotoxin 1-methyl-4-phenyl-1,2,3,6-tetrahydropyridine (MPTP). MPTP is metabolised in the body to 1-methyl-4-phenylpyridinium (MPP^+), a potent inhibitor of complex I which is selectively taken up into dopaminergic neurons by the dopamine transporter and causes death of the substantia nigra and acute irreversible parkinsonism (Langston et al., 1983; Langston et al., 1984). This observation has since been refined in animal models and extended to other inhibitors of complex I, such as rotenone (Betarbet et al., 2000; Mizuno et al., 1988). These toxin models recapitulate not only the nigral death and behavioural symptoms of PD, but also the oxidative damage and Lewy body pathology observed *post mortem* in PD (Betarbet et al., 2000; Sherer et al., 2003), suggesting that complex I inhibition closely models the pathogenesis of the sporadic disease.

1.3.2. Mitochondrial dysfunction in idiopathic PD

The finding that complex I inhibition mimicked the symptoms of PD was soon given physiological relevance by the observation of complex I deficiency in the substantia nigra of patients with idiopathic PD (Schapira et al., 1989). Since then inhibition of complex I and sometimes II/III has also been observed in platelets and lymphocytes from patients, while results from skeletal muscle have varied (reviewed by Schapira, 1999). In addition

to these respiratory complex deficiencies, levels of coenzyme Q_{10} (CoQ_{10}), a key electron carrier and antioxidant in the ETC, and α-ketoglutarate dehydrogenase, an enzyme of the Krebs cycle, have been shown to be reduced in *post mortem* PD brains (Hargreaves et al., 2008; Mizuno et al., 1994).

Other signs of mitochondrial dysfunction are also apparent in PD patient tissue. Oxidative damage to mtDNA has been observed in the substantia nigra of PD patients (Zhang et al., 1999), which may underlie the complex I deficiency observed: in support of this hypothesis, transfer of mitochondria from PD patient platelets into rho-zero cells (cells lacking any mtDNA) recapitulates the complex I deficiency in the cybrid cells (Swerdlow et al., 1996). Mitochondrial depolarisation and ultrastructural abnormalities are also observed in these cells (Trimmer et al., 2000).

1.3.3. Mitochondrial function of PD-associated genes

Further evidence for a causative role for mitochondrial dysfunction in PD pathogenesis has derived from the identification of disease-causing mutations in a number of genes, several of which encode proteins that either localise to or have physiological functions at the mitochondria. This is particularly true for those mutations which are recessively inherited, suggesting a loss-of-function mechanism of pathogenesis, although dominantly inherited mutations in the genes encoding leucine-rich repeat kinase 2 (LRRK2) and α-synuclein have also been associated with mitochondrial dysfunction. In this section, the evidence linking some of the PD genes to the mitochondria will be briefly outlined.

1.3.3.1. PINK1

Mutations in the gene encoding the mitochondrial kinase PINK1 (PTEN-induced putative kinase 1) represented the first genetic evidence linking mitochondrial dysfunction to PD (Valente et al., 2004), and as such were critical in exciting interest in mitochondrial involvement in the disease. Although rare, approximately 100 different mutations or deletions have now been described, the majority of which occur in the kinase domain or otherwise impair kinase activity (Deas et al., 2009).

Numerous studies have shown that PINK1 is essential for healthy mitochondrial function: PINK1 deficiency in knockdown cell models leads to mitochondrial dysfunction and increased vulnerability to apoptosis (Deng et al., 2005; Valente et al., 2004; Wood-Kaczmar et al., 2008), and overexpression of WT but not mutant PINK1 protects cells

against apoptosis induced by mitochondrial toxins (Deng et al., 2005; Haque et al., 2008; Petit et al., 2005). PINK1 knockout (KO) flies display a severe mitochondrial defect leading to dopaminergic neurodegeneration, male sterility and apoptotic muscle degeneration (Clark et al., 2006; Park et al., 2006; Yang et al., 2006). Mice lacking PINK1 (like most other genetic models of PD) have not displayed an obvious parkinsonian phenotype, but closer analysis of cultured cells from these animals revealed that they too have a mitochondrial defect including respiratory chain deficits (Gautier et al., 2008; Morais et al., 2009), mitochondrial depolarisation and elevated mitochondrial calcium (Gandhi et al., 2009). The cause of the respiratory defect is not entirely clear: one study reported a reduction in activity of complex I (Morais et al., 2009), another in complexes I-III (Gautier et al., 2008), while a third found that the reduction in respiration was due to a lack of substrate supply to the mitochondria, which could be fully rescued by providing substrates for respiratory complexes I or II (Gandhi et al., 2009). Interestingly, a recent paper from the group of Gautier and colleagues showed that overexpression of the yeast homologue of complex I in *PINK1* mutant flies rescued the phenotype (Vilain et al., 2012), which they take to indicate that complex I defects are central to pathogenesis in the case of PINK1 deficiency. Further research will be required in order to resolve this discrepancy.

In addition to respiratory dysfunction, a number of studies have implicated mitochondrial calcium mishandling in PINK1 deficient cells. Marongiu *et al.* found that the effect of PINK1 knockdown or mutation could be reversed by blocking mitochondrial calcium uptake (Marongiu et al., 2009), while a recent paper has also observed an increase in vulnerability to mitochondrial calcium in PINK1 KO mice which preceded a reduction in striatal dopamine levels (Akundi et al., 2011). Using live cell imaging techniques to dissect the mitochondrial phenotype of PINK1 KO mouse neurons, Gandhi and colleagues suggested that the primary defect was in mitochondrial calcium homeostasis, resulting in an increase in basal mitochondrial calcium and an inability to adequately buffer physiological cytosolic calcium stimuli. The in turn resulted in calcium activation of the plasmalemmal superoxide producer NADPH oxidase, which damaged the glucose transporter and thus impaired mitochondrial substrate supply (Gandhi et al., 2009).

PINK1 has frequently been linked to mitochondrial morphology, but its role in the fusion/fission machinery remains unclear. In flies, PINK1 appears to have a pro-fission role, with several studies reporting genetic interactions between *PINK1* and the genes encoding either the fission protein Drp1 or the fusion proteins OPA1 or Mfn1/2 (Deng et

al., 2008; Poole et al., 2008; Yang et al., 2008). A recent study in primary neurons from PINK1 KO mice reported increased mitochondrial fusion which could be rescued by overexpression of Drp1 or knockdown of OPA1 (Yu et al., 2011), but overall the majority of studies in mammalian cells have reported mitochondrial fragmentation in PINK1 deficient cells (Exner et al., 2007; Wood-Kaczmar et al., 2008). It is unclear whether this fragmentation is a direct result of PINK1 deficiency or secondary to mitochondrial dysfunction: one study, for example, reported dephosphorylation and therefore activation of Drp1 in PINK1 deficient cells as a result of mitochondrial calcium mishandling leading to activation of the calcium dependent phosphatase calcineurin (Sandebring et al., 2009).

PINK1 has also been suggested to play a role in mitochondrial quality control as an upstream regulator of the mitochondrial protease HtrA2 (Plun-Favreau et al., 2007), the mitochondrial chaperone protein TRAP1 (Pridgeon et al., 2007), and the E3 ubiquitin ligase Parkin (Clark et al., 2006; Exner et al., 2007; Park et al., 2006; Yang et al., 2006). In particular, several recent studies have focused on the role of the PINK1/Parkin pathway in mitophagy, as previously discussed. The question of whether failure of mitochondrial maintenance is in itself sufficient to explain the phenotype of PINK1 deficient models will be revisited in chapter 6.

1.3.3.2. HtrA2

The second mitochondrial protein to be encoded by a PARK gene is HtrA2 (high temperature requirement protein A2), the mammalian homologue of a bacterial serine protease (HtrA/DegP) which functions as a chaperone as low temperatures but degrades misfolded proteins through its protease activity at high temperatures (Spiess et al., 1999). By contrast, the first function of HtrA2 to be discovered was in apoptosis, when several groups identified it in pulldown experiments with tagged X-linked inhibitor of apoptosis (XIAP) (Martins et al., 2002; Suzuki et al., 2001; Verhagen et al., 2002) or the BIR3 domain of XIAP (Hegde et al., 2002). HtrA2 is imported into mitochondria via its mitochondrial targeting sequence but is cleaved to reveal an N-terminal Reaper motif, the amino acid sequence AVPS. During apoptosis mature HtrA2 is released from the mitochondrial intermembrane space together with Smac and cytochrome c, where it binds IAPs including XIAP, cIAP-1 and opIAP (Verhagen et al., 2002), releasing their inhibitory effect on caspases and thus inducing cell death. In addition, HtrA2 appears to have an extramitochondrial death-inducing activity which is dependent on its protease activity but not its ability to bind IAPs (Suzuki et al., 2001; Verhagen et al., 2002).

Given the known function of HtrA2 in apoptosis, it was expected that a mouse lacking this gene would have a cancer phenotype. It was thus surprising when a KO mouse and a mouse carrying a loss-of-function mutation in the *HtrA2* gene were found instead to exhibit a severe neurodegenerative phenotype, with premature death resulting from loss of a population of striatal neurons (Jones et al., 2003; Martins et al., 2004). HtrA2 KO mice develop normally until day 18 after birth, but fail to gain weight after weaning and develop a progressive parkinsonian movement disorder including a pronounced tremor. HtrA2 was then linked to PD by the identification of a mutation and a polymorphism in the gene in a German PD cohort, both of which resulted in defective protease activity and mitochondrial dysfunction when transfected into cells (Strauss et al., 2005). These results were called into question, however, when a study in a large North American cohort identified these risk variants in both PD patients and neurologically normal controls (Simon-Sanchez and Singleton, 2008). Another novel mutation and six risk variants have additionally been identified in a Belgian cohort (Bogaerts et al., 2008), but these also failed to replicate in a North American population (Ross et al., 2008). Despite the controversy regarding the genetic evidence, the severe phenotype of the KO mice provides strong support for an important neuroprotective role for HtrA2 at the mitochondria. This neuroprotective function is poorly understood, although a number of studies have suggested a possible role for HtrA2 in mitochondrial protein quality control (Moisoi et al., 2009; Radke et al., 2008). This subject will be discussed in further detail in chapter 3.

1.3.3.3. Parkin and DJ-1

Although both the E3 ubiquitin ligase Parkin and the redox sensor DJ-1 localise predominantly to the cytosol, both can relocate to the mitochondria under certain conditions: Parkin in response to mitochondrial depolarisation and PINK1 accumulation, and DJ-1 due to oxidative stress. In both cases, loss of protein function results in mitochondrial dysfunction and can lead to cell death.

Parkin is known to act in a common pathway with PINK1, since Parkin KO flies were found to exhibit an identical phenotype to that of PINK1 KO flies and overexpression of Parkin completely rescued the effects of PINK1 KO (Clark et al., 2006; Park et al., 2006; Yang et al., 2006). This was confirmed in a mammalian system when overexpression of Parkin was found to rescue the mitochondrial defect in human cells lacking PINK1 (Exner et al., 2007). Recent work on Parkin function has focused heavily on its role in mitophagy, following the finding that Parkin is specifically recruited to depolarised mitochondria (Narendra et al.,

2008; see section 1.2.4.2). Two recent studies have also highlighted a role for Parkin in mitochondrial trafficking, showing that following mitochondrial depolarisation PINK1 phosphorylates the kinesin attachment protein Miro on the OMM, which results in its ubiquitination by Parkin and degradation (Liu et al., 2012; Wang et al., 2011b). This detaches the mitochondrion from the microtubular network, thereby 'quarantining' damaged mitochondria (Wang et al., 2011b) and promoting their clustering at the perinucleus (Liu et al., 2012) prior to mitophagy. These findings follow previous work showing that PINK1 forms a complex with Miro and the adaptor protein Milton on the OMM (Weihofen et al., 2009), and provide the first direct evidence that PINK1 phosphorylation of a specific substrate targets it for Parkin ubiquitination. It is important to note that not all ubiquitination events lead to proteasomal degradation: Parkin has also been shown to mediate non-degradative monoubiquitination (Joch et al., 2007) and K63-linked polyubiquitination (Geisler et al., 2010a; Lim et al., 2005) and may thus have additional roles in signal transduction.

Whereas Parkin recruitment to mitochondria appears to depend primarily on mitochondrial depolarisation (Narendra et al., 2008), DJ-1 relocation is triggered by oxidative modification of a conserved cysteine residue (Canet-Aviles et al., 2004). Mutations in *DJ-1* cause an early-onset autosomal recessive parkinsonism (Bonifati et al., 2003) similar to that described for *PINK1* and *Parkin* (Kitada et al., 1998; Valente et al., 2004), leading several groups to postulate that the three proteins could function in a common pathway. A number of studies have shown either that DJ-1 overexpression can rescue loss of PINK1 in flies or mammals (Hao et al., 2010; Haque et al., 2012) or that PINK1 or Parkin overexpression can rescue loss of DJ-1 (Irrcher et al., 2010; Thomas et al., 2011), but it there is little evidence of a single pathway: a more likely explanation seems that these findings represent two parallel pathways which protect mitochondrial function (Thomas et al., 2011). Loss of DJ-1 has been shown to result in oxidative damage, depolarisation and fragmentation of the mitochondria (Irrcher et al., 2010; Thomas et al., 2011), although its physiological function and the mechanism by which it exerts this protective effect remains unclear (Cookson, 2010). One recent study demonstrated a down-regulation of uncoupling proteins in DJ-1 KO mice which led to an increase in oxidative stress in the substantia nigra, suggesting a transcriptional effect (Guzman et al., 2010), while another has shown that lysosomal function and basal autophagy is impaired in cells from DJ-1 KO mice, suggesting that the mitochondrial dysfunction could arise from

an accumulation of damaged mitochondria due to impaired mitophagy (Krebiehl et al., 2010).

1.3.3.4. LRRK2 and α-synuclein

Point mutations in *LRRK2* and gene multiplications and mutations in *SNCA*, encoding the protein kinase/GTPase LRRK2 and the synaptic protein α-syn respectively, cause an autosomal dominant and later onset form of PD. Neither is generally considered a mitochondrial protein; however, both have been linked to the mitochondria, and in both cases mitochondrial dysfunction has been suggested to play a part in disease pathogenesis.

Although predominantly cytosolic, LRRK2 contains ankyrin repeats which are known to associate with glycosylphosphatidylinositol anchors, and has been shown to localise to several membranous structures in the brain including the mitochondrial outer membrane (Biskup et al., 2006). Its expression in *C. elegans* increases survival after treatment with mitochondrial toxins, suggesting a protective function at the mitochondria (Saha et al., 2009), and mitochondrial defects have been reported in fibroblasts from patients with the common G2019S mutation in *LRRK2* (Mortiboys et al., 2010). Furthermore, a recent study showed that the mitochondrial depolarisation observed in G2019S fibroblasts and neuroblastoma cells was due to a specific upregulation of the uncoupling proteins UCP2 and UCP4 (Papkovskaia et al., 2012). Meanwhile α-syn has also been found to localise to the mitochondria (Li et al., 2007), resulting in a conformational change from a 'closed' to an 'open' conformation upon membrane binding (Nakamura et al., 2008). Devi and colleagues have additionally demonstrated a cryptic mitochondrial targeting sequence in the N-terminus of α-syn, mediating import of the protein into the mitochondria where it interacts with complex I. Accumulation of α-syn (particularly mutant forms) in mitochondria was found to inhibit complex I activity and increase reactive oxygen species production, both in cultured cells and in PD brains (Devi et al., 2008). Overexpression of α-syn (mimicking gene multiplications observed in patients) results in alterations in mitochondrial function and morphology (Banerjee et al., 2010; Xie and Chung, 2012), with two studies suggesting that association of α-syn with the mitochondrial membrane results in mitochondrial fragmentation independent of the fusion/fission machinery (Kamp et al., 2010; Nakamura et al., 2011). Another recent paper suggests that α-syn is involved in tethering mitochondria to the endoplasmic reticulum (ER), thereby controlling calcium homeostasis (Cali et al., 2012).

A summary of some of the known mitochondrial functions of proteins encoded by PD genes is provided in figure 1.10 below, highlighting the importance of mitochondrial function in disease pathogenesis. This thesis aims to build on this information by investigating the mechanism of neuroprotection in HtrA2 deficiency and by identifying novel roles for the remaining PD gene products in mitochondrial function. By better understanding the mechanisms underlying mitochondrial dysfunction in the various genetic forms of PD, there is hope that common pathways will emerge which may form the basis for more effective therapeutics, enabling the development of compounds which target the pathogenesis of the disease and not only the symptoms.

Figure 1.10 Mitochondrial involvement in Parkinson's disease pathogenesis. Figure adapted from (Schapira and Tolosa, 2010).

1.4. Objectives of this thesis

As has been discussed in this chapter, mitochondrial dysfunction has been strongly implicated in PD pathogenesis and much of the evidence for this has come from studies of proteins genetically linked to the disease. This thesis aims to build on those studies by answering the following questions:

What is the mitochondrial function of HtrA2?

Mice with either a loss-of-function mutation or targeted deletion of the *HtrA2* gene exhibit a severe neurodegenerative phenotype (Jones et al., 2003; Martins et al., 2004), suggesting a crucial neuroprotective role for this protein. Using live cell imaging and respirometry to investigate mitochondrial physiology in primary neuronal cultures revealed an uncoupling event in HtrA2 deficient mitochondria. This was further investigated using biochemical analysis and physiological assays to identify the likely source of the uncoupling, identifying a hitherto unidentified role for HtrA2 in regulation of the ATP synthase.

Do other PD-associated genes encode proteins with important mitochondrial functions? And if so, what are those functions?

These questions were addressed initially by designing an shRNA screen to assess the mitochondrial effect of silencing genes associated with PD, described in chapter 4. Due to technical difficulties it was not possible to complete the screen in the time available. However, at the same time an investigation was initiated into the putative mitochondrial function of Fbxo7 (PARK15), a PD-associated protein with no published link to the mitochondria. In this case, *in silico* analysis predicted a mitochondrial localisation for this protein and further investigation by immunocytochemistry and biochemical methods revealed that Fbxo7 co-operates with two other PD proteins, PINK1 and Parkin, to mediate mitophagy.

Chapter 2

Materials and Methods

2.1. Materials

All chemicals were purchased from Sigma-Aldrich unless otherwise stated. The country of origin is only indicated for companies which do not have registered UK subsidiaries.

2.2. Bioinformatics

Protein sequences for isoforms 1 and 2 of Fbxo7 were obtained from the NIH National Center for Biotechnology Information (NCBI) server, which currently lists nine protein entries for Fbxo7 at a size of 522 amino acids (the expected size of isoform 1) and one entry for Fbxo7 at a size of 443 amino acids (the expected size of isoform 2). The sequences chosen were those first published in (Cenciarelli et al., 1999).

Isoform 1: Accession number NP_036311.3

Isoform 2: Accession number NP_ 001028196.1

2.2.1. Prediction of mitochondrial localisation

Peptide sequences were examined for putative N-terminal mitochondrial targeting sequences using four online algorithms. These were as follows:

- PSORT II (*http://psort.hgc.jp/form2.html*) is a rule-based algorithm using the MITDISC mitochondrial discriminant analysis described in (Nakai and Kanehisa, 1992)
- Mitoprot (*http://ihg.gsf.de/ihg/mitoprot.html*) uses an extension of the MITDISC approach to include further analysis of the charge, acidity and hydrophobicity of the N-terminal residues (Claros and Vincens, 1996)
- Target P (*http://www.cbs.dtu.dk/ services/TargetP/*) is a neural network-based algorithm for determination of ER, plastid and mitochondrial targeting sequences (Emanuelsson et al., 2000).
- Predotar (*http://urgi.versailles.inra.fr/predotar/predotar.html*) is a neural network-based algorithm intended for large scale proteomic screening, with further corrections applied to reduce false positives (Small et al., 2004).

2.2.2. Prediction of peptide secondary structure

To determine an appropriate site for generation of an internal FLAG tag, Fbxo7 secondary structure was predicted using the program Geneious v5.5.7 (Drummond et al., 2011), which uses the GOR (Garnier Osguthorpe Robson) method as described in (Garnier et al., 1978).

2.3. Molecular biology

2.3.1. Materials

Buffers for competent cell production:

- Buffer TF I: 100 mM KCl, 50 mM RbCl, 10 mM $CaCl_2$, 30 mM KAc, 15% (w/v) glycerin, pH adjusted to 5.8 with acetic acid.
- Buffer TF II: 10 mM MOPS, 10 mM RbCl, 75 mM $CaCl_2$, 15% (w/v) glycerin, pH adjusted to 7.0 with NaOH.

Bacterial growth medium and plates: Luria broth (LB) powder (10 g/l tryptone, 5 g/l yeast extract, 5 g/l NaCl) and LB-agar powder (as for LB broth plus 15 g/l agar powder) were purchased from Sigma-Aldrich, diluted in distilled water according to the manufacturer's protocol and sterilised by autoclaving. Ampicillin sodium salt was purchased from Sigma-Aldrich, diluted in deionised water to a stock concentration of 100

mg/ml and sterile filtered. LB-agar was allowed to cool to 50°C before addition of ampicillin to a final concentration of 100 μg/ml. The LB-ampicillin was then poured into 10 cm dishes and allowed to set at room temperature before storage at 4°C.

Constructs: A list of DNA constructs used in this thesis is shown in table 2.1 below.

Name of construct	Vector backbone	Obtained from
pcDNA3	-	Invitrogen
pEGFP	-	Clontech
Cytosolic luciferase	pcDNA3	Gyorgy Szabadkai (UCL)
FLAG-Parkin	pcDNA3	Helen Ardley (Leicester)
WT Fbxo7	pcDNA3	Heike Laman (Cambridge)
T22M Fbxo7	pcDNA3	This thesis
R378G Fbxo7	pcDNA3	Heike Laman
R498X Fbxo7	pcDNA3	Heike Laman
WT Fbxo7-HA	pcDNA3	This thesis
T22M Fbxo7-HA	pcDNA3	This thesis
R378G Fbxo7-HA	pcDNA3	This thesis
R498X Fbxo7-HA	pcDNA3	This thesis
T7-Fbxo7	pcDNA3	Heike Laman
R2D/ R6W Fbxo7	pcDNA3	This thesis
T7-R2D/ R6W Fbxo7	pcDNA3	This thesis
Fbxo7 internal FLAG	pcDNA3	This thesis
T22M Fbxo7 internal FLAG	pcDNA3	This thesis
R378G Fbxo7 internal FLAG	pcDNA3	This thesis
R498X Fbxo7 internal FLAG	pcDNA3	This thesis

Table 2.1 DNA constructs used in this thesis

Kits: QIAprep spin miniprep, QIAfilter plasmid maxiprep, QIAquick gel extraction and RNeasy mini kits were all purchased from Qiagen. QIAshredder columns were also purchased from Qiagen.

Cloning reagents: AccuPrime Pfx SuperMix (containing Pfx polymerase, dNTPs, reaction buffer) was purchased from Invitrogen. Cloning and sequencing primers were purchased from Eurofins MWG Operon (Ebersberg, Germany); for a list of primer sequences, see Appendix II. Restriction enzymes and T4 DNA ligase were purchased from New England Biolabs. RAPid alkaline phosphatase was purchased from Roche.

Electrophoresis reagents: TBE (Tris-borate-EDTA) buffer was prepared as follows: 89 mM Tris base, 89 mM boric acid, 2 mM EDTA (pH 8). Agarose powder was purchased from Sigma-Aldrich. 10x Orange G loading buffer was prepared by dissolving 2.5 g/l Orange G in 30% (v/v) glycerol. GelRed nucleic acid stain was purchased from Biotium (CA, USA).

Reverse transcription: Superscript III reverse transcriptase, dNTPs, random primers, DTT, and RNaseOUT RNase inhibitor were all purchased from Invitrogen.

Real-time PCR: Universal mastermix and Taqman probes were purchased from Applied Biosystems. FAM-labelled probes were used for HtrA2 and PINK1 (HtrA2: Hs00234883_m1; PINK1: Hs00260868_m1). A VIC-labelled probe was used for GAPDH.

2.3.2. Plasmid amplification and purification

2.3.2.1. Production of chemically competent bacteria

One vial of chemically competent Top10 *E. coli* was diluted in 5 ml LB and cultured overnight in a shaking incubator at 37°C and 220 rpm. 1 ml of this pre-culture was then transferred into 200 ml LB and incubated with shaking for ~ 4 hr until the bacteria were dividing exponentially (OD_{580} = 0.3-0.5). The bacteria were pelleted in a pre-cooled (4°C) centrifuge for 7 min at 5000 *g*, resuspended in 30 ml filter-sterilised TF buffer I and incubated on ice for 15 min. The bacteria were then pelleted for a second time at 5000 *g* for 7 min, resuspended in 7.5 ml filter-sterilised TF buffer II and incubated for 15 min on ice before aliquoting into pre-chilled autoclaved eppendorfs. Aliquots of 50 µl were snap frozen in liquid nitrogen and stored at -80°C until needed.

2.3.2.2. Transformation of bacteria by heat-shock

DNA (usually 1 µg purified DNA for re-transformation or 10 µl ligation reaction) was added to 50 µl chemically competent Top10 *E. coli* on ice, mixed gently by flicking and incubated on ice for 5 min. Bacteria were heat-shocked at 42°C for 30 s before returning to ice for a further 5 min. 200 µl pre-warmed LB medium without antibiotic was added

and the bacteria incubated for 1 hr at 37°C, shaking at 225 rpm. 30 µl bacteria (in the case of DNA re-transformation) or 200 µl bacteria (for transformation following ligation) were spread on pre-warmed LB-agar plates containing the appropriate antibiotic selection and incubated overnight at 37°C.

2.3.2.3. Plasmid purification

For preparation of small quantities of DNA, single bacterial colonies were picked using a sterile Gilson pipette tip into 2 ml LB broth containing the appropriate antibiotic selection and incubated at 37°C shaking at 220 rpm overnight. The resulting bacteria were pelleted by centrifugation at 16,000 *g* for 1 min in a 2 ml eppendorf, resuspended in 250 µl Qiagen buffer P1 and DNA extracted using a QIAprep spin miniprep kit according to the manufacturer's instructions.

For the preparation of larger quantities of DNA, bacterial colonies were picked as described above into 3 ml LB broth containing the appropriate antibiotic, and incubated at 37°C at 220 rpm for ~ 8 hr. After this time, 1 ml bacterial culture was transferred into 200 ml LB containing antibiotic and incubated overnight at 37°C, shaking at 220 rpm. The resulting bacteria were pelleted by centrifugation at 6000 *g* for 15 min, resuspended in 10 ml Qiagen buffer P1, and DNA extracted using a QiaFilter Plasmid Maxiprep kit, according to the manufacturer's protocol. Upon elution of the DNA in buffer QF, DNA was precipitated using isopropanol according to the manufacturer's instruction, but at this point the recommended purification of DNA using 70% ethanol was replaced with sodium acetate precipitation. Briefly, the precipitated DNA was resuspended in 100 µl deionised water and transferred to an eppendorf containing 1 ml 100% ethanol and 40 µl 3 M NaAc (pH 5.2). The eppendorf was kept at -80°C overnight to facilitate precipitation of DNA, then the DNA was pelleted by centrifugation at 16,000 *g* for 30 min in a cooled benchtop centrifuge. The supernatant was aspirated and the pellet allowed to air dry before resuspension in an appropriate volume of sterile deionised water. Plasmid concentration and quality was measured spectrophotometrically using a NanoDrop 2000 and the DNA diluted in water to a 1 mg/ml stock.

2.3.3. Subcloning new constructs

Plasmids containing untagged WT, R378G and R498X Fbxo7 in a pcDNA3 background were obtained in collaboration with Dr Heike Laman, University of Cambridge. The same group also provided an N-terminally FLAG-tagged T22M Fbxo7 construct. Using these

plasmids as templates, untagged T22M Fbxo7 and C-terminally HA-tagged WT and mutant Fbxo7 were cloned into pcDNA3. Mutations in the MTS of Fbxo7 were also generated by PCR to produce an untagged MTS mutant and an N-terminally T7-tagged MTS mutant (generated using a T7-Fbxo7 construct also obtained from Heike Laman). Finally, an internal FLAG tag was inserted into the WT and PD-mutant Fbxo7 sequences using a two-stage fusion PCR approach. For a description of the cloning strategy used to generate each of these constructs, see Appendix I. For a full list of the constructs used in this thesis, see table 2.1 on page 58.

2.3.3.1. Polymerase chain reaction

Polymerase chain reaction (PCR) was performed using AccuPrime Pfx SuperMix according to the manufacturer's protocol. Briefly, 100 ng template DNA and 200 nM appropriate forward and reverse primers were added to 22.5 µl AccuPrime Pfx SuperMix in a sterile PCR tube. PCR reactions were subjected to temperature cycling in an Eppendorf Mastercycler thermal cycler according to the protocol in table 2.2. The annealing temperature chosen was 5°C lower than the lowest melting temperature of the primers. For primer sequences and melting temperatures, see Appendix II.

Step	Temp	Time	Cycles
Initialisation	95°C	5 min	1
Denaturing	95°C	15 s	
Annealing	55-65°C*	30 s	35
Extension	68°C	1 min per kb	

Table 2.2 PCR thermal cycling protocol (Accuprime Pfx polymerase). * Annealing temperature was usually 5°C lower than primer melting temperature (Appendix II)

2.3.3.2. Agarose gel electrophoresis

PCR products were separated on a 1% (w/v) agarose gel made by dissolving 0.5 g agarose in 50 ml TBE buffer and heating in the microwave. GelRed was added to the gel to a dilution of 1:10,000 before setting in order to enable visualisation of DNA. Once set, the gel was submerged in TBE buffer and DNA samples diluted in Orange G loading buffer were added into the wells. DNA was electrophoresed at 80 V for 30 min or as long as required to ensure good separation of bands. DNA was visualised under UV, then correctly

sized bands were excised and DNA purified using a QIAquick Gel Extraction kit according to the manufacturer's instructions.

2.3.3.3. DNA digestion and vector dephosphorylation

Purified PCR fragments and vector DNA were digested using appropriate restriction enzymes for at least 2 hr at 37°C. 300 ng DNA was digested with 10 U enzymes in a total reaction volume of 10 µl, including the recommended buffer provided by the manufacturer and 10 µg BSA where recommended. Where 5' and 3' restriction enzymes were compatible, double digests were performed. Digested DNA was run on a 1% (w/v) agarose gel and appropriate bands excised and purified using a QIAquick Gel Extraction kit according to the manufacturer's instructions. Vector DNA was dephosphorylated using 1 U rAPid alkaline phosphatase for 10 min at 37°C in a reaction volume of 20 µl. The enzyme was then inactivated by incubation at 75°C for 2 min.

2.3.3.4. Ligation

DNA fragments and vector DNA with compatibly digested restriction sites were ligated in a 3:1 molar ratio insert:vector using T4 DNA ligase in a 10 µl reaction volume. Ligations were performed overnight at 16°C. As a negative control, an additional reaction was performed including the digested and dephosphorylated vector but not the DNA fragments to be inserted, in order to confirm that the vector was unable to re-ligate. Ligated DNA was transformed into chemically competent Top10 *E.coli* (see section 2.3.2.2).

2.3.3.5. Sequencing

For each construct generated, 6-12 colonies were picked, miniprepped and subjected to diagnostic digests to verify the presence of the insert. Those that did contain the insert were sent for Sanger sequencing at the UCL Scientific Support Service. Sequencing primers were designed across exon boundaries to exclude the possibility of genomic DNA contamination, at intervals of approximately 500 bp. The program Primer3 (*http://frodo.wi.mit.edu/*) was used to generate primer sequences, using an optimal primer length of 20 residues (acceptable range 18-27) and an optimal T_m of 60°C (acceptable range 57-63°C). For primer sequences, see Appendix II.

All sequences returned were analysed by aligning the sequenced sense and antisense fragments with the expected sequence for Fbxo7 (NCBI accession number NM_012179.3)

using Sequencher software (GeneCodes, MI, USA). This compilation was analysed by eye to check for mutations or changes to the open reading frame.

2.3.4. Quantitative PCR

2.3.4.1. RNA extraction

Cells were harvested for RNA extraction by scraping down in PBS (see section 2.4.1), transferred to an eppendorf and pelleted by centrifugation at 400 *g* for 5 min in a benchtop centrifuge. The supernatant was removed and the cell pellet either stored at -80°C, or immediately lysed for RNA extraction by resuspension in lysis buffer provided with the Qiagen RNeasy mini RNA extraction kit. Lysates were homogenised using Qiagen QIAshredder columns, then RNA was extracted using the RNA extraction kit, according to the manufacturer's protocol.

2.3.4.2. Reverse transcription

For production of cDNA, 1 µg extracted RNA was reverse transcribed using Superscript III reverse transcriptase, according to the manufacturer's protocol. Briefly, RNA was combined with random hexamer primers (final concentration 2.5 µM) and dNTP mix (final concentration 0.5 mM) in an initial volume of 13 µl and incubated at 65°C for 5 min. The mixture was then incubated on ice for 1 min before addition of the provided First-Strand 5x buffer, 5 mM DTT and 200 U reverse transcriptase enzyme, bringing the total reaction volume to 20 µl. The reaction was incubated at 25°C for 5 min, then at 50°C for 50 min and finally the enzyme was inactivated at 70°C for 15 min.

2.3.4.3. Quantitative real-time PCR

mRNA expression of HtrA2 and PINK1 was measured using Taqman quantitative PCR, performed on a Rotor-gene 6000 (Corbett). 10 ng cDNA was combined with 2X Taqman Universal Mastermix and 20X probe sets for the gene of interest and GAPDH in a total reaction volume of 6.5 µl. Assay conditions are shown in table 2.3 below.

Step	Temp	Time	Cycles
Initialisation	95°C	10 min	1
Denaturing	95°C	30 s	35
Annealing	60°C	45 s	

Table 2.3 Quantitative PCR thermal cycling protocol (Taqman).

Data were acquired on the green (FAM) and yellow (VIC) channels during the 60°C extension step (gain = 10). Data were analysed using the $2^{-\Delta\Delta CT}$ method (Livak and Schmittgen, 2001), using GAPDH as an internal standard.

2.4. Cell culture

2.4.1. Materials

Cell lines: The cell lines used, their origin and antibiotic selection are listed in table 2.4.

Media for human cell lines: For culture of SH-SY5Y, HEK293T, U2OS and patient fibroblast cell lines, Dulbecco's modified Eagle medium (DMEM) containing high glucose, sodium pyruvate and 2 mM L-glutamine was purchased from Invitrogen and supplemented with 10% (v/v) foetal bovine serum (FBS; PAA). Puromycin dihydrochloride powder was purchased from Sigma-Aldrich, dissolved in deionised water and sterile filtered before addition to the growth medium where necessary (see table 2.4). For culture of patient lymphoblasts, Roswell Park Memorial Institute medium (RPMI-1640) was purchased from Invitrogen, and supplemented with 15% (v/v) FBS (PAA). 0.25% trypsin-EDTA and sterile phosphate buffered saline (PBS) and Hanks buffered salt solution (HBSS) were purchased from Sigma-Aldrich.

Transfection reagents: Effectene was purchased from Qiagen, Lipofectamine 2000 from Invitrogen, Fugene 6 from Roche, GeneJuice from Millipore (MA, USA) and Arrest-In from Open Biosystems (LA, USA). For calcium phosphate transfection, a 2x HEPES buffered saline (HBS) was prepared containing 100mM HEPES, 281 mM NaCl and 1.5 mM Na_2HPO_4, pH adjusted to 7.12. Aliquots were stored at -20°C. DharmaFECT transfection reagent and siRNA were purchased from Dharmacon (ThermoScientific). siRNA was diluted in sterile RNase free water to a stock concentration of 100 µM.

Trypan blue: 0.4% trypan blue solution was purchased from Sigma-Aldrich;

Poly-D-lysine: Poly-D-lysine (PDL) powder was purchased from Sigma-Aldrich, diluted in deionised water and sterile-filtered.

shRNA constructs: shRNA constructs were obtained as part of the Human Lentiviral shRNAmir library from Open Biosystems. Four shRNA sequences were selected for use

Name	Cell type	Antibiotic	Origin
SH-SY5Y	Human neuroblastoma	-	ECACC
HEK293T	Human embryonic kidney cell	-	ECACC
U2OS	Human osteosarcoma	-	Heike Laman, Cambridge
WT/HtrA2 KO MEFs	Immortalised mouse embryonic fibroblasts	-	Miguel Martins, Leicester
HtrA2-TAP and TAP HEK293	Human embryonic kidney cells with stable overexpression of TAP or HtrA2-TAP	G418 (500 µg/ml)	Hélène Plun-Favreau (cell lines generated at CRUK)
Fbxo7 KD SH-SY5Y	Human neuroblastoma with stable shRNA expression	Puromycin (1 µg/ml)	Heike Laman, Cambridge
Fbxo7 KD U2OS	Human osteosarcoma with stable shRNA expression	Puromycin (2 µg/ml)	Heike Laman, Cambridge
FLAG-Parkin SH-SY5Y	Human neuroblastoma with stable FLAG-Parkin overexpression	-	Helen Ardley, Leicester
Control/ patient fibroblasts	Human primary fibroblasts	-	Extracted from skin biopsies by Selina Wray
Control/patient lymphoblasts	Immortalised patient lymphoblasts	-	Isolated from peripheral blood and immortalised with EB virus. Obtained from Henry Houlden

Table 2.4 Cell lines used. (ECACC, European collection of cell cultures; EB virus, Epstein-Barr virus; TAP, tandem-affinity purification tag)

against each target gene. The hairpin sequences for the two control genes, HtrA2 and PINK1, are shown in table 2.5 below.

shRNA	Target	Mature sense sequence	Manufacturer code
HtrA2 #1	HtrA2	ACGCTGAGGATTCAGACTA	315863
HtrA2 #2	HtrA2	CCAATGTGGAATACATTCA	315864
HtrA2 #3	HtrA2	CGAGAAACACTGACCTTAT	315866
HtrA2 #4	HtrA2	GCGAGGTCCCTATCTCGAA	315867
PINK1 #1	PINK1	GGAGCCATCGCCTATGAAA	235108
PINK1 #2	PINK1	CCGCAAATGTGCTTCATCT	238759
PINK1 #3	PINK1	GTATGTGCCTTGAACTGAA	234804
PINK1 #4	PINK1	CGCAAATGTGCTTCATCTA	319829

Table 2.5 shRNA sequences for HtrA2 and PINK1

Primary neuronal culture medium: Neurobasal medium A (Invitrogen) was supplemented with 2% (v/v) B27 (Invitrogen), 2 mM glutamine (Invitrogen), 100 I.U./ml penicillin and 100 I.U./ml streptomycin (Sigma-Aldrich).

Mouse genotyping: DNA extractions were performed using the Extract 'N' Amp tissue PCR kit, purchased from Sigma-Aldrich. Genotyping primers were purchased from Invitrogen.

2.4.2. Culture of cell lines

2.4.2.1. Conditions and culturing

Cell lines were cultured in the appropriate media (see section 2.4.1) at 37°C in 5% CO_2/95% air. Cells were passaged every 2-3 days (usually 1:3 for SH-SY5Ys, 1:6 for HEK293T cells, 1:15 for HtrA2 MEFs, 1:2 for primary human fibroblasts and 1:3 for immortalised human lymphoblasts). SH-SY5Y cells were used at passage numbers no higher than 25.

2.4.2.2. Freezing and thawing

For long-term storage of cell lines the cells were detached by incubation in 0.025% trypsin, resuspended in warm medium and pelleted by centrifugation at 400 *g* for 5 min. The cell pellet was resuspended in 90% FBS with 10% sterile DMSO and transferred to

cyovials for freezing at a rate of -1°C/min using a Nalgene Mr Frosty at -80°C. After 24 hr, the cells were transferred to liquid nitrogen for storage.

To resuscitate frozen cells, cells were thawed rapidly and resuspended in 5 ml warm growth medium. Cells were again pelleted by centrifugation at 400 *g* for 5 min, resuspended in fresh growth medium and transferred to a cell culture flask.

2.4.2.3. Cell counting

Where necessary, cells were counted using a Neubauer haemocytometer. Dead cells were detected using 0.4% trypan blue solution at a 1:1 ratio with the cell suspension. Trypan blue is excluded from intact cells, therefore any stained cells were disregarded.

2.4.2.4. Adhering cells to glass coverslips

Glass coverslips were sterilised in 100% ethanol and allowed to air dry, then, where stated in the methods, coated with 25 µg/ml PDL to improve cell adherence. Coverslips were coated with PDL for 5 min at room temperature, then washed twice with sterile water and air dried under UV light for at least 30 min.

2.4.2.5. Transient transfection of DNA and shRNA

Unless otherwise indicated, cells were transfected at approximately 90% confluency using Effectene according to the manufacturer's protocol, with the exception that for transfection of SH-SY5Y cells DNA quantity was increased. In brief, to transfect one well of a 6 well plate, 0.4 µg plasmid DNA (2 µg for transfection of SH-SY5Ys) and 3.2 µl enhancer were diluted in 100 µl buffer EC and incubated at room temperature for 2-5 min before addition of 10 µl effectene (enhancer and EC both provided by the manufacturer). The mix was incubated for a further 8 min at room temperature, during which time the medium on the cells was replaced with 1.6 ml fresh complete medium. After 8 min, 600 µl growth medium was added to the mix and the total volume added to the cells.

For optimisation of the transfection protocol in chapter 4 (section 4.2.1.1), SH-SY5Y cells seeded at a density of 8e4 cells per well were transfected with Arrest-In, Lipofectamine 2000, Fugene 6, GeneJuice, Effectene and DharmaFect in a 24 well plate according to each manufacturer's protocol. Each reagent was tested with 6 different quantities of empty vector DNA: 0.1, 0.2, 0.25, 0.3, 0.5 and 1 µg per well.

For viral packaging, cells were cotransfected with the pGIPZ shRNA construct and the two packaging vectors pMDG and p8.91 using a calcium phosphate ($CaPO_4$) protocol. Briefly, for transfection of a 20 cm dish the medium was first replaced 2 hr prior to transfection with 18 ml fresh complete growth medium. 32 µg pGIPZ, 7 µg pMDG and 16.25 µg p8.91 constructs were diluted in sterile water to a total volume of 1.125 ml before addition of 125 µl $CaCl_2$ (2.5 M). The mixture was vortexed briefly and incubated at room temperature for 5 min, then 1.25 ml 2x HBS buffer was added dropwise with continuous vortexing. The mixture was immediately added to the cells and thoroughly dispersed by back and forth and sideways movements.

2.4.2.6. siRNA-mediated gene silencing

Cells were transfected with siRNA at 80-90% confluency using DharmaFECT according to the manufacturer's protocol. Briefly, for one well of a 6 well plate 10 µl siRNA and 6 µl DharmaFECT were each diluted in a total of 200 µl serum free media. The two solutions were incubated separately for 5 min at room temperature, then combined and incubated for a further 20 min at room temperature during which time the media on the cells was replaced with 1.6 ml fresh growth media. After 20 min, the entire 400 µl siRNA/DharmFECT solution was added dropwise to the cells. For transfection in a 24 well plate, the protocol was as described above except all volumes were divided by 4.

2.4.3. Primary neuronal cultures

2.4.3.1. Genotyping

HtrA2 knockout mice were obtained in collaboration with Dr Miguel Martins (Leicester University). Heterozygous mice were bred in order to generate study populations containing homozygous wild-type (WT), homozygous knockout (KO) and heterozygous (Het) mice. For genotyping, tail samples were taken from new-born pups at the time of neuronal culture (between days 1-5), or alternatively ear snips were taken at day 14. Genomic DNA was extracted using the Extract 'N' Amp tissue PCR kit according to the manufacturer's instructions. For the PCR reaction, 4 µl extracted DNA was combined with 10 µl PCR readymix (obtained as part of the Extract 'N' Amp kit) and 200 nM each of the three primers (HtrA2genFWD, NeoR and AM52; see Appendix II for sequences) in a total volume of 20 µl. Cycling parameters for the PCR are shown in table 2.6 overleaf.

Step	Temp	Time	Cycles
Initialisation	94°C	2 min	1
Denaturing	94°C	45 s	
Annealing	60°C	45 s	35
Extension	72°C	45 s	
Extension	72°C	10 min	1

Table 2.6 PCR thermal cycling protocol for HtrA2 genotyping.

In the HtrA2 KO mice exons 2-6 and part of exons 1 and 7 of the *HtrA2* gene have been replaced by a neomycin cassette, resulting in complete loss of HtrA2 protein (Martins et al., 2004). The forward primer HtrA2genFWD anneals to a sequence in the first coding exon of *HtrA2* while the reverse primers NeoR and AM52 anneal to sequences in the neomycin cassette and the second coding exon respectively. Consequently, NeoR only primes in KO animals and AM52 only primes in WT animals, generating PCR products which can be visualised at two different molecular weights after separation by electrophoresis (see section 2.3.3.2). A higher molecular weight band indicates a WT allele and a lower molecular weight product band a KO allele. Two bands indicate a heterozygous genotype.

2.4.3.2. Preparation of neuronal cultures

Primary neurons were cultured from newborn pups aged between days 1-5. Pups were culled by cervical dislocation, then the whole brain was removed in a petri dish containing ice cold HBSS under sterile conditions. Cerebral hemispheres or midbrain were removed into sterile eppendorfs containing 1 ml chilled HBSS and kept on ice while the rest of the litter was processed. The HBSS was then removed and replaced with 1 ml pre-warmed trypsin-EDTA solution for 5 min at room temperature. The cultures were pelleted by centrifugation at 2000 rpm for 5 min, then the trypsin was gently aspirated and the cells washed first in pre-warmed HBSS, then in warm neurobasal medium. The cells were resuspended in 1 ml warm complete neurobasal medium and 3-4 drops of cells were plated per well on PDL-coated coverslips in 6 well plates (6-8 coverslips per animal). The cultures were incubated in a humidified incubator at 37°C with 5% CO_2 in air for 3-4 hr, then 2 ml pre-warmed neurobasal medium added. Half the medium was replaced after 2 days, after which half the medium was replaced weekly.

2.5. Viral work

2.5.1. Materials

Packaging vectors: Vectors p8.91 (carrying the HIV *gag* and *pol* genes) and pMDG (encoding the VSV glycoprotein) were a kind gift from Catherine King (UCL Cancer Institute).

Polybrene: Polybrene (hexadimethrine bromide) was purchased as a powder from Sigma-Aldrich, diluted in deionised water to a stock concentration of 8 mg/ml, and sterile filtered.

Fixing solution: CellFix solution for FACS analysis was purchased from BD Bioscience.

2.5.2. Virus production

shRNA was packaged into lentiviral particles using a second-generation packaging system requiring cotransfection of the shRNA, a packaging vector (p8.91) and an envelope vector (pMDG). Briefly, HEK293T cells were transfected in 20 cm dishes with the three vectors using calcium phosphate (see section 2.4.2.3). 16 hr after transfection the medium was removed and replaced with 20 ml fresh medium. 24 hr later the medium was harvested, passed through a 0.45 μm sterile filter, and stored overnight at 4°C. 20 ml fresh medium was added to the cells for a further 24 hr before this medium was also harvested in the same way. The two days' supernatants were combined and frozen at -80°C in 1 ml aliquots in order to avoid freeze-thawing the virus.

2.5.3. Virus titration

To measure viral titre, SH-SY5Y cells were plated in a 6 well plate at 4e5 cells per well in the evening. The following morning, 4-fold serial dilutions of crude virus were prepared in DMEM + 10% FBS. The media was aspirated from the plated cells and replaced with 1 ml complete medium containing 16 μg/ml polybrene, then 1 ml diluted virus was added to the cells. Four dilutions were used per virus to be titered: 1/4, 1/16, 1/64 and 1/256. After 6 hr the media was changed to fresh complete media (DMEM + 10% FBS). 3 days after viral transduction the cells were trypsinised, pelleted by centrifugation and resuspended in CellFix solution for analysis by flow cytometry using a FACSCalibur machine (BD Bioscience) to calculate the percentage of GFP-positive cells. The dilution

which gave 1-10% cells GFP-positive was used to calculate viral titre (transducing units per ml) using the following formula:

Titre = (Fraction green cells) * (number cells plated) * 1/dilution

2.5.4. Viral transduction

SH-SY5Y cells were plated in 6 well plates at a density of 5e5 cells per well in the evening. The following morning, unconcentrated virus was added to cells at an appropriate multiplicity of infection (MOI; see section 4.2.2) in the presence of 8 μg/ml polybrene. If necessary (depending on viral titre), complete growth medium containing 8 μg/ml polybrene was added in addition to the virus to bring the total volume to a minimum of 1 ml. The virus was removed after 6-10 hr and replaced with 2 ml full growth media (DMEM high-glucose with L-glutamine and 10% FBS) in order to avoid polybrene toxicity. Where stated, this process was repeated on the second day in order to improve viral incorporation into the cells.

2.6. Mitochondrial physiology

2.6.1. Materials

Fluorophores: TMRM, dihydroethidium, Mag-Fura and Fura-2 were purchased from Molecular Probes, Invitrogen and dissolved to a 100x stock solution in DMSO.

Chemicals: FCCP, rotenone, oligomycin, sodium cyanide, thapsigargin and ionomycin were purchased from Sigma-Aldrich and dissolved in DMSO; ADP and ATP were purchased from Sigma-Aldrich and dissolved in deionised water.

Buffers:

- Hanks balanced salt solution (HBSS): 156 mM NaCl, 3 mM KCl, 2 mM $MgSO_4$, 1.25 mM KH_2PO_4, 2 mM $CaCl_2$, 10 mM glucose, 10 mM HEPES, pH 7.35. A 10x stock was purchased from Invitrogen and diluted in deionised water.
- Calcium-free HBSS:
- Mitochondrial isolation buffer: 250 mM sucrose, 1 mM EDTA and 19 mM Tris-HCl, pH 7.4.
- Mitochondrial respiration buffer: 150 mM KCl and 20 mM HEPES-KOH, pH 7.0.

2.6.2. Mitochondrial membrane potential

Mitochondrial membrane potential ($\Delta\Psi_m$) was measured using tetramethylrhodamine methyl ester (TMRM), a membrane-permeable cationic dye which localises to mitochondria (see figure 2.1 below) according to the Nernst equation which governs equilibration of a charged molecule across a membrane. Mitochondrial depolarisation causes release of the dye into the cytosol and therefore a reduction in the mitochondrial signal. At low concentrations, mitochondrial TMRM fluorescence is proportional to $\Delta\Psi_m$ (Scaduto and Grotyohann, 1999).

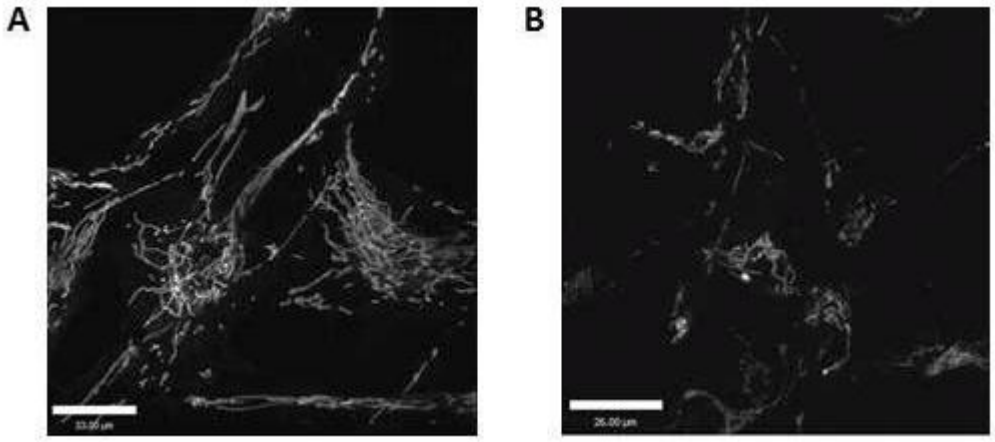

Figure 2.1 Representative images of TMRM staining. Images of TMRM staining in (**A**) fibroblasts and (**B**) neuroblastoma cells are shown. In both cases images are taken from a single focal plane. TMRM fluorescence is artificially coloured white to improve visibility. Images were obtained using a 63x oil objective as described; scale bars indicate 33 μm and 26 μm respectively.

For measurement of $\Delta\Psi_{m,}$ cells were pre-loaded with 40 nM TMRM in HBSS for 40 min at room temperature to allow equilibration of the dye into the mitochondria. The dye was present in the media at the time of recording. Z-stack confocal images were obtained using a Zeiss 710 confocal microscope with a 63x oil immersion objective. TMRM was excited using the 560 nm laser line and fluorescence measured above 580 nm. TMRM fluorescence intensity was quantified for each Z-stack in a semi-automatic manner using Volocity 3D image analysis software (PerkinElmer). In brief, the software was used to measure the average intensities of all objects above a threshold intensity, where a single threshold was manually set for each experiment and applied to each image. In order to exclude any effect of mitochondrial size on TMRM intensity, object intensities were normalised to volume by summing the total intensities in the image (calculated as mean

intensity multiplied by volume) and dividing by the total mitochondrial volume in the image to give a value that equates to the average TMRM fluorescence intensity in all the voxels containing mitochondria. Analysed in this manner, $\Delta\Psi_m$ is independent of mitochondrial mass. For each *n*, average TMRM fluorescence was normalised to control cells to enable comparison between experiments.

2.6.3. Redox index

Two redox couples are central to the action of the ETC: $NADH/NAD^+$, which provides high energy electrons for complex I; and $FADH_2/FAD^{++}$ which provides electrons for complex II. The redox state of each couple can be determined by microscopy since NADH and FAD^{++} (but not NAD^+ or $FADH_2$) are both autofluorescent in the visible spectrum (Chance et al., 1962), offering a method for investigating mitochondrial respiration on a single cell basis (see representative image of NADH autofluorescence below).

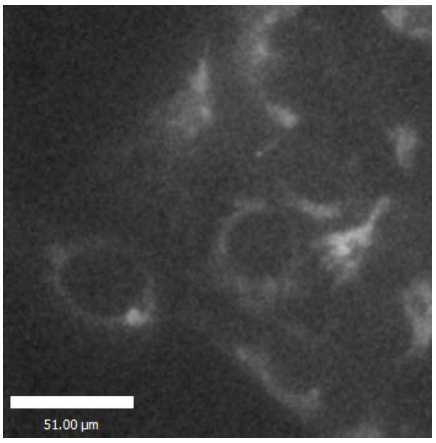

Figure 2.2 Representative image of NADH autofluorescence. NADH autofluorescence is shown for SH-SY5Y neuroblastoma cells under basal conditions. Image was obtained using a 40x oil objective; scale bar, 51 µm.

In order to distinguish the mitochondrial NADH signal from NADPH autofluorescence, which is visible at the same wavelength, an uncoupler (1 µM FCCP) is added to maximise respiration and thereby cause depletion of the mitochondrial pool of NADH, and an inhibitor of respiration (1 mM NaCN) is added to block respiration and thereby cause accumulation of NADH (Duchen and Biscoe, 1992). The NADH redox index is then calculated by expressing basal autofluorescence as a percentage of this range (see figure 2.3 overleaf). In addition, calculating the difference in autofluorescence between these

two states gives the mitochondrial NADH level, which can be indicative of substrate supply to the respiratory chain.

NADH and FAD^{++} autofluorescence was measured in cells plated on 22 mm glass coverslips using an epifluorescence inverted microscope equipped with a 20x fluorite objective. For measurement of NADH, excitation light at a wavelength of 350 nm was provided by a Xenon arc lamp, the beam passing through a monochromator (Cairn Research). Emitted fluorescence light was reflected through a 455 nm long-pass filter to a cooled CCD camera (Retiga, QImaging, Canada) and digitised to 12 bit resolution. For measurement of FAD^{++}, excitation light was provided at a wavelength of 454 nm and emitted light was measured from 505-550 nm. Imaging data were collected and analysed using software from Andor.

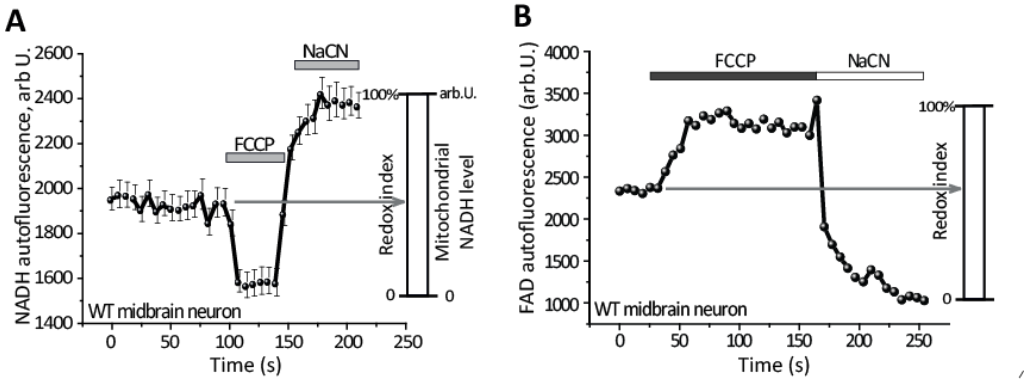

Figure 2.3 Calculation of NADH and FAD^{++} redox index. (A) Representative trace for NADH autofluorescence, showing calculation of NADH redox index (in percent) and mitochondrial NADH level (in arbitrary units). **(B)** Representative trace for FAD^{++} autofluorescence showing calculation of FAD^{++} redox index.

2.6.4. Oxygen consumption

2.6.4.1. Whole cells

Measurement of oxygen consumption is a direct indication of the rate of cellular respiration, and can therefore be used to investigate the function of the mitochondrial respiratory chain. Oxygen consumption was measured using a Clark oxygen electrode thermostatically maintained at 37°C. For measurements in whole cells, cells were cultured in flasks as previously described (section 2.4.2.1), harvested by trypsinisation, resuspended in HBSS and maintained on ice for approximately 30 min before measurement. Before recording, the instrument was calibrated by adding ~1 g sodium dithionite to determine the minimum oxygen level; air-saturated water was then assumed

to contain 406 nmol O atoms/ml at 37°C. 10^6 cells were then added to the chamber and the oxygen concentration monitored to determine the rate of consumption. Oligomycin (2 µg/ml) was then added to inhibit ATP synthesis and thereby reduce the rate of respiration, then FCCP (1 µM) was added to determine the maximal oxygen consumption. A representative trace for control cells is shown in figure 2.4 below.

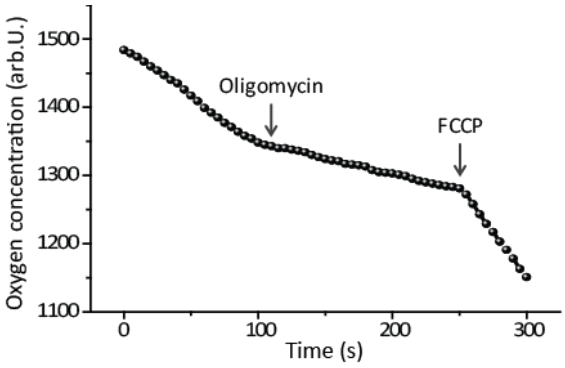

Figure 2.4 Representative trace for oxygen consumption in whole cells. Oxygen consumption was measured in control cells under basal conditions, then following addition of oligomycin (2 µg/ml), and finally following addition of FCCP (1 µM).

2.6.4.2. Isolated mitochondria

For measurements of oxygen consumption in isolated mitochondria, mitochondria were harvested from mouse brains using differential centrifugation. Brains from three WT and three HtrA2 KO animals were collected and pooled according to genotype. The brains were then homogenised using a chilled Teflon-glass homogenizer and resuspended in 50 ml mitochondrial isolation buffer (see section 2.6.1). Unbroken cells were removed by centrifugation at 600 *g* for 15 min. The supernatant was collected and spun at 8500 *g* for 15 min. The resulting pellet was resuspended in 1 ml of chilled mitochondrial respiration buffer (see section 2.6.1). In order to measure state III/IV respiration, mitochondria were added to the chamber in recording medium without ADP but supplemented with either glutamate/malate (5 mM) to investigate complex I-linked respiration, or succinate (5 mM) plus rotenone (5 µM) to investigate complex II-linked respiration. 50 nmoles ADP was then added to stimulate ATP production, resulting in an increase in respiration (state III respiration). Upon consumption of the ADP, respiration returns to an inhibited state (state IV). A representative control trace is shown in figure 2.5 overleaf.

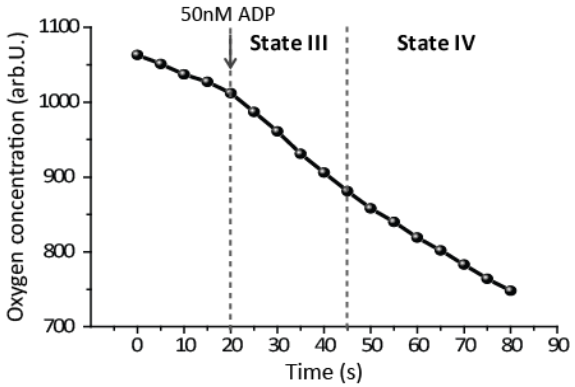

Figure 2.5 Measurement of state III and state IV respiration in isolated mitochondria.
A representative trace is shown for mitochondria isolated from control animals.

2.6.5. Reactive oxygen species production

2.6.5.1. By fluorescent/confocal microscopy

Cytosolic superoxide production was measured using dihydroethidium (DHE), a fluorescent dye which is oxidised by cytosolic reactive oxygen species to ethidium, which translocates to the nucleus, intercalates DNA and fluoresces at a different wavelength (Bindokas et al., 1996). Cells were plated on 22 mm glass coverslips and GFP-positive cells selected by excitation at 490 nm where appropriate. 80 μM DHE was then added to cells at the start of the experiment and was present throughout; no pre-loading was used in order to limit the intracellular accumulation of oxidised products. Light from a Xenon arc lamp was passed through a monochromator to provide excitation light alternately at 380 nm (for measurement of fluorescence from unoxidised DHE) and 530 nm (for measurement of fluorescence from oxidised DHE). Emitted light was passed through a 455 nm or 605 nm filter (for unoxidised or oxidised DHE respectively) to a cooled CCD camera. Images were captured and analysed using IQM software from Andor over a time period of approximately 5 minutes, during which time fluorescence at 530 nm increased and fluorescence at 380 nm decreased as the dye was oxidised. Rate of ROS production is proportional to the rate of increase in the ratio of 530 nm/380 nm fluorescence.

Mitochondrial ROS production was measured in the same way using a mitochondrially targeted derivative of DHE, mitoSOX. MitoSOX is oxidised to mito-ethidium which intercalates mtDNA and fluoresces at the same wavelength as DHE. Cells were pre-loaded with 5 μM mitoSOX for 20 min prior to start of the experiment, then fluorescence was recorded as described above.

2.6.5.2. Using the Cellomics ArrayScan

Cytosolic ROS production was optimised in 96 well plates using an ArrayScan microscope from Cellomics (Pittsburgh, PA, USA) accessed in collaboration with Eisai Pharmaceuticals, London. Cells were seeded at a density of 10^4 cells per well 10 days after transduction, on plates which had previously been coated with PDL as described in section 2.4.2.4. Immediately prior to recording, the cell culture medium was removed and replaced with HBSS containing 0.5, 1 or 3 μM DHE as indicated in the text (section 4.2.3.2). Excitation light at 543 nm and 488 nm was provided from an LED light source to measure oxidised DHE and GFP fluroscence respectively. Images were captured using a 20x LD Plan-Neofluor objective over a period of 3 hr at 37°C, 5% CO_2 and analysed in real time with the Cellomics Target Activation Bio Application, using the GFP marker to select cells of interest.

2.6.6. Measurement of ATP production

2.6.6.1. Luciferin/luciferase

Kinetic ATP measurements were performed by plating MEF cells on glass coverslips, transfecting with a cytosolic luciferase construct as described previously (section 2.4.2.3), and placing in a 37°C heated chamber in a home built luminometer in the laboratory of Dr Michelangelo Campanella, Royal Veterinary College, London. Cells were constantly perfused with HBSS at 37°C. Luciferin (5 μM) was added into this saline, followed by ATP (1 mM). Addition of ATP stimulates calcium uptake into the cells and thereby stimulates mitochondrial ATP production (Jouaville et al., 1999). Under these conditions, the light output of a coverslip of transfected cells was in the range of up to 8000 counts/s for each measurement compared to a background lower than 150 counts/s. Luminescence was entirely dependent on the presence of luciferin.

2.6.6.2. Mag-Fura

ATP may be measured indirectly in single cells using Mag-Fura, an indicator of cytosolic magnesium, since ATP binds magnesium at an affinity ten times that of ADP and therefore cellular ATP levels correlate inversely with free magnesium (Leyssens et al., 1996). To measure cytosolic free magnesium levels, cells were pre-loaded with 5 μM Mag-Fura AM ester and 0.005% pluronic in HBSS for 30 min at room temperature. Cells were then washed three times prior to recording. Measurements were taken using an Olympus microscope, using light from a Xenon arc lamp passed through a monochromator to

provide excitation light alternately at 340 nm and 380 nm. Emitted light was passed through a 515 nm long-pass filter to a cooled CCD camera. Images were captured and analysed using software from Andor. Free magnesium concentration is proportional to the ratio of fluorescence at 340 nm (magnesium-bound) divided by 380 nm fluorescence (unbound).

2.6.7. Mitochondrial calcium

Mitochondrial calcium can be quantified indirectly using Fura-2, a ratiometric indicator of cytosolic calcium (Abramov and Duchen, 2003). Cells were pre-loaded with 5 μM Fura-2 AM and 0.005% pluronic in HBSS containing calcium for 30 min at room temperature, then washed three times with calcium-free HBSS prior to recording. Basal cytosolic calcium levels were recorded in calcium-free HBSS, then 1 μM thapsigargin was added to empty the endoplasmic reticulum (ER), resulting in a peak in cytosolic calcium which corresponds to the ER calcium level. After cytosolic calcium levels had returned to baseline, 5 μM ionomycin (an ionophore) was added to permeabilise all membranes, allowing calcium release from the mitochondria (the only significant calcium gradient remaining). This peak in cytosolic calcium therefore corresponds to mitochondrial calcium levels. Fura-2 fluorescence measurements were taken exactly as described for Mag-Fura (section 2.6.6.2). A representative trace for one WT cell is shown in figure 2.6 overleaf.

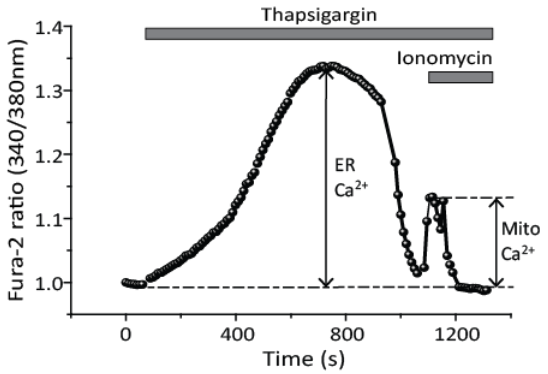

Figure 2.6 Representative trace showing measurement of mitochondrial calcium. Trace shows response of cytosolic calcium to thapsigargin and ionomycin in one WT U2OS cell. Response to thapsigargin may be considered an indication of ER calcium, while response to ionomycin is an indication of mitochondrial calcium.

2.7. Protein biochemistry

2.7.1. Materials

Buffers:

- 2% CHAPS buffer: 10 mM Tris (pH8), 150 mM NaCl, 2% (w/v) CHAPS. EDTA-free protease inhibitor cocktail tablets (Roche) were added immediately before cell lysis.
- Mitochondrial isolation buffer: 70 mM Tris base, 0.25 M sucrose, 1 mM EDTA, pH 7.4
- MES buffer: 19.8 mM EDTA, 0.25 M D-mannitol, 19.8 mM MES, pH 7.4
- Sample loading buffer: NuPAGE 4x LDS Sample buffer (Invitrogen) plus DTT to a final concentration of 1 mM.
- Gel running buffer: NuPAGE MES SDS (Invitrogen)
- Transfer buffer: Tris-glycine (National Diagnostics, Georgia, USA) plus 20% (v/v) methanol
- PBST: 1x phosphate buffered solution (PBS) was made from tablets (Invitrogen) diluted in deionised ultrapure water with 0.1% (v/v) Tween-20 (Sigma-Aldrich)
- Milk: Marvel skimmed milk powder was dissolved in PBST to the appropriate percentage.
- TEV cleavage buffer: 10 mM Tris-HCl (pH 8), 150 mM NaCl, 2% (w/v) CHAPS, 0.5mM EDTA, 1 mM DTT (DTT added immediately before use)
- Calmodulin binding buffer: 10 mM Tris-HCl (pH 8), 150 mM NaCl, 2% (w/v) CHAPS, 10 mM β-mercaptoethanol, 1 mM Mg-acetate, 1 mM imidazole, 2 mM $CaCl_2$
- Calmodulin elution buffer: 10 mM Tris-HCl (pH 8), 150 mM NaCl, 2% (w/v) CHAPS, 10 mM β-mercaptoethanol, 1 mM Mg-acetate, 1 mM imidazole, 2 mM EGTA
- PK buffer: 20 mM HEPES (pH 7.4), 250 mM sucrose, 80 mM KOAc, 5 mM MgOAc

Antibodies: A list of antibodies used for western blotting is shown in table 2.7 overleaf. Antibodies were prepared at the specified dilution in 5% (w/v) milk/PBST. Rabbit and mouse secondary antibodies were purchased from Santa Cruz Biotechnology (CA, USA) and diluted 1:2000 in 5% (w/v) milk/PBST.

Antibody-bound agarose beads: ATP synthase immunocapture beads were purchased from MitoSciences (Eugene, OR, USA); rabbit IgG beads were purchased from Sigma-Aldrich; calmodulin affinity resin was purchased from Stratagene.

Protein	Species	Dilution	Obtained from
HtrA2	Rabbit	1:4000	R&D Systems
α-tubulin	Mouse	1:2000	Sigma
β-actin	Mouse	1:1000	Sigma
ATP synthase α subunit	Mouse	1:1000	MitoSciences
ATP synthase α subunit	Rabbit	1:1000	Proteintech Group
ATP synthase b subunit	Rabbit	1:10,000	Prof John Walker (University of Cambridge)
GAPDH	Mouse	1:2000	Abcam
Fbxo7	Rabbit	1:1000	Dr Heike Laman (University of Cambridge)
TOM20	Rabbit	1:1000	Santa Cruz
TIM23	Mouse	1:1000	BD Bioscience
Hsp60	Rabbit	1:1000	Cell Signalling
Apotrack cocktail*	Mouse	1:1000	MitoSciences

Table 2.7 List of antibodies for western blotting. * Apotrack cocktail is composed of antibodies against ATP synthase α subunit, pyruvate dehydrogenase E1α and GAPDH.

Consumables: Bio-Rad DC (detergent compatible) protein assay kit was purchased from Bio-Rad (CA, USA). NuPAGE 4-12% Bis-Tris protein gels, NuPAGE LDS sample buffer and Novex Sharp Standard protein ladder were purchased from Invitrogen. Immobilon-P transfer membrane was purchased from Millipore. Amersham chemiluminescent substrate (ECL) was purchased from GE Healthcare. CL-Xposure X-ray film was purchased from Thermo Scientific. RG Universal X-ray fixer and developer were purchased from Champion Photochemistry.

Enzymes: TEV protease was purchased from Invitrogen. Protease K was purchased from Sigma-Aldrich.

Silver staining solutions: (sensitiser, stainer A and B, developer and stopper all purchased as part of the SilverXpress kit from Invitrogen)

- Fixing solution: 50% (v/v) methanol, 10% (v/v) acetic acid in ultrapure water
- Sensitising solution: 50% (v/v) methanol, 2.5% (v/v) sensitiser in ultrapure water
- Staining solution: 5% (v/v) stainer A, 5% (v/v) stainer B in ultrapure water
- Developing solution: 5% (v/v) developer in ultrapure water

2.7.2. Harvesting and lysing of cells

Cells were first washed with PBS, then harvested by adding 2% CHAPS buffer with protease inhibitors on ice and scraping into an eppendorf. Lysates were snap frozen in liquid nitrogen, then thawed and incubated at 4°C on a turning wheel for 1 hr to ensure complete lysis. Insoluble cellular components were removed by centrifugation at 16,000 *g* for 10 min at 4°C, then the supernatant was transferred to a fresh eppendorf and stored at -80°C. Protein levels were estimated using the Bio-Rad DC protein assay kit, using protein standards prepared by diluting BSA to concentrations of 0.2, 0.4, 0.6, 0.8 and 1.0 mg/ml in lysis buffer.

2.7.3. Mitochondrial isolation for biochemistry

2.7.3.1. From brain tissue

For isolation of mitochondria from brain tissue, mice were culled by cervical dislocation and the brains immediately removed into cold PBS or snap frozen and stored at -80°C for use at a later date. The tissue was roughly chopped, rinsed in PBS to remove blood, then transferred into ~7 ml cold mitochondrial isolation buffer for homogenisation.

Homogenisation was carried out using an electrical Teflon-glass homogeniser (20 passes at 290 rpm), taking care to avoid introducing bubbles. The homogenate was centrifuged at 900 *g* for 2 min to remove intact cells and debris, then the supernatant was centrifuged at 16,000 *g* for 10 min to pellet mitochondria. The mitochondrial pellet was rinsed once in PBS, then resuspended in PBS with protease inhibitors.

2.7.3.2. From cells (Samali protocol)

To isolate mitochondria from cultured cells, unless otherwise stated a protocol was followed from (Samali et al., 1999). Briefly, the media was aspirated from the cells and the monolayer rinsed once with PBS. An appropriate volume of mitochondrial isolation buffer (100 µl for one well of a 6 well plate) was added directly to the cells, then an equal volume of MES buffer with 0.2 mg/ml digitonin added and incubated at room temperature for 10 min. The cells were scraped into an eppendorf and pelleted at 900 *g* for 2 min to remove intact cells and debris. The supernatant was then centrifuged at 16,000 *g* for 10 min to separate the mitochondrial pellet from the cytosolic fraction (the supernatant). The cytosolic fraction was removed and diluted directly in sample buffer for western blot analysis, while the mitochondrial pellet was rinsed once with PBS, resuspended in diluted sample buffer and sonicated before loading.

2.7.3.3. From cells (Gegg protocol)

Permeabilisation of the cells by digitonin in the previous method may strip loosely associated proteins from the outer mitochondrial membrane. For this reason, where stated it was necessary to use an alternative protocol for isolation of mitochondria from cells (Gegg et al., 2010). Briefly, a large volume of cells (10 x 10cm plates) were harvested by trypsination, pelleted and frozen at -80°C for at least 3 hr to aid permeabilisation. The cell pellet was thawed on ice and resuspended in 2 ml ice cold homogenisation buffer, then homogenised using an ice-cold Teflon-glass homogeniser at 1000 rpm. The homogenate was centrifuged at 1500 *g* for 10 min to remove nuclei, cell debris and unbroken cells. The supernatant was transferred to a fresh tube, then the pellet was again homogenised in 2 ml homogenisation buffer and pelleted at 1500 *g* for 10 min. The supernatants were combined and centrifuged at 1500 *g* for a further 10 min, and the pellet discarded. Mitochondria were pelleted by centrifugation at 11,500 *g* for 12 min, resuspended in 1 ml fresh homogenisation buffer, transferred to an eppendorf and pelleted a second time at 11,500 *g* for 12 min. Mitochondria were resuspended directly in sample buffer and sonicated for western blot analysis.

2.7.4. Immunoprecipitation

2.7.4.1. ATP synthase immunocapture from mitochondria

For immunocapture of intact F_1F_0 ATP synthase complexes, mitochondria were first isolated as previously described (section 2.7.3) from the whole brains of mice aged P20 killed by cervical dislocation. Isolated mitochondria were resuspended in PBS and diluted to a concentration of 5.5 mg/ml, then incubated with 0.1 volume 10% (w/v) n-dodecyl β-D-maltopyranoside (DDM) on ice for 30 min to disrupt the membranes. The sample was then centrifuged at 72,000 *g* for 30 min at 4°C and the supernatant transferred to a new tube containing 30 µl pre-washed ATP synthase immunocapture beads. The sample was incubated with the beads for at least 3 hr at room temperature or overnight at 4°C, then the beads were collected by centrifugation at 2000 *g* for 1 min and washed three times in 100 volumes of PBS + 1 mM DDM. Finally the proteins were eluted by incubating the beads with a solution of 1% (w/v) sodium dodecyl sulphate (SDS) in ultrapure water for 10 min with frequent agitation.

2.7.4.2. Tandem-affinity purification

Ten to 15 10 cm dishes of stable overexpressing TAP or HtrA2-TAP HEK293T cells were harvested by trypsinisation, pooled and frozen as a dry pellet overnight at -80°C. Pellets were then lysed in 7.5 ml ice cold 2% CHAPS buffer, homogenised in a chilled Teflon-glass douncer (20 passes at 1000 rpm) and centrifuged at 3000 *g* for 20 min to remove insolubles. 500 µl cleared lysate was saved to run as input, while the remaining lysate was added to 150 µl rabbit IgG beads which had been pre-washed 3 times in 10 ml lysis buffer. The lysate was rotated with the beads for at least 2 hr at 4°C to allow binding of the Protein A tag to the IgG, then the beads were collected by centrifugation at 400 *g* for 4 min. The beads were washed 3 times in the falcon tube with 10 ml 2% CHAPS buffer before transferring into a column and washing a further time with 10 ml 2% CHAPS. Beads were then washed once in 10 ml TEV cleavage buffer before the column was closed and the beads incubated with 950 µl TEV cleavage buffer plus 10 µl TEV protease for 1.5 hr at room temperature. The eluate was then transferred to a second column containing 150 µl calmodulin affinity resin which had been pre-washed 3 times in 10 ml calmodulin binding buffer. A further 3 ml calmodulin binding buffer was run through the IgG column to bring through any remaining TEV eluate, then 3.2 µl 1M $CaCl_2$ was added directly to the calmodulin beads and the column capped and rotated for 2 hr at 4°C to allow the calmodulin binding peptide tag to bind the beads. The beads were washed three times in

the column with 10 ml calmodulin binding buffer before finally eluting in 500 µl calmodulin elution buffer.

2.7.5. Protease K digestion

To determine the submitochondrial localisation of Fbxo7, a protease K (PK) digest was performed on isolated mitochondria. Mitochondria were first isolated from untransfected HEK293T cells using the protocol from (Gegg et al., 2010) (see section 2.7.3.3), resuspended in PK buffer and split into eight equal samples. PK enzyme was added on ice for 30 min, then stopped with protease inhibitor cocktail. Samples were immediately diluted in sample loading buffer and boiled prior to loading on a gel (see section 2.7.6). PK concentrations used were as follows: 0, 0.25, 0.5, 1, 5, 10, 25, 50 µg/ml.

2.7.6. Protein electrophoresis and western blotting

Samples were diluted in 4x sample buffer containing DTT, boiled at 100°C for 5 min and loaded on a precast 4-12% NuPAGE polyacrylamide gel. Bands were separated by electrophoresis at 120 V, then transferred to a PVDF microporous membrane for 80 min at 80 V or overnight at 15 V at 4°C. The membrane was blocked by incubation in PBST/5% milk for 30 min, then incubated in primary antibody either overnight at 4°C or for 2 hr at room temperature. The membrane was washed 3-5 times in PBST, incubated with the appropriate HRP-conjugated secondary antibody for 1 hr at room temperature, and washed again in PBST. Finally the membrane was developed by incubation with 1 ml ECL for 1 min, then exposure to X-ray film for an appropriate period of time to record the resultant chemiluminescence. Bands were quantified by scanning the developed film and analysing using Image J software.

2.7.7. Silver staining

Samples were electrophoresed using a 1 mm 10% NuPAGE BisTris gel as previously described (section 2.7.5), then instead of transferring proteins onto a PVDF membrane the gel was incubated in fixing solution for 10 min and stained using the SilverXpress kit according to the manufacturers' instructions. Briefly, the fixed gel was incubated on an orbital shaker in two changes of sensitising solution for a total of one hour, rinsed twice in ultrapure water, then incubated for 15 min in staining solution. The gel was then washed twice more in ultrapure water before developing solution was added and incubated at

room temperature until the desired intensity was reached. At this point stopping solution (0.05 volumes) was added for 10 min and the gel washed three times in ultrapure water.

2.8. Immunocytochemistry

2.8.1. Materials

Antibodies: Primary antibodies used for immunofluorescence are listed in table 2.8 below. Alexa Fluor fluorescently labelled secondary antibodies were purchased from Invitrogen and used at a dilution of 1:2000.

Protein	Species	Dilution	Obtained from
FLAG	Mouse	1:2000	Sigma
FLAG	Rabbit	1:5000	Sigma
HA	Rat	1:500	Roche
HtrA2	Rabbit	1:1000	R&D Systems
CxVβ	Mouse	1:1000	MitoSciences
Fbxo7	Rabbit	Various	Dr Heike Laman
Fbxo7	Mouse	Various	Abnova
Fbxo7	Rabbit	Various	Novus

Table 2.8 Primary antibodies used for immunofluorescence

Consumables: FBS and PBS were as described previously (section 2.4.1). Normal goat serum (NGS) was purchased from Invitrogen. Triton X-100 was purchased from Sigma-Aldrich. DAPI was purchased from Sigma-Aldrich and dissolved in water. Fluorescent mounting medium was purchased from Dako.

2.8.2. Cell staining

Cells for immunofluorescent analysis were cultured on 13 mm glass slides previously coated with 25 μg/ml PDL as previously described (section 2.4.2.4). Unless otherwise stated, cells were fixed for 10 min in 4% (w/v) PFA/PBS, then rinsed twice with PBS to remove any residual PFA. Cells were permeabilised in 0.5% (v/v) triton X-100/PBS solution for 5 min, rinsed twice in PBS and blocked with 10% (v/v) FBS/PBS for 30 min to

prevent non-specific antibody binding. Primary antibodies were diluted in blocking solution, then coverslips were inverted onto a 50 µl drop of antibody solution on parafilm and incubated either for 2 hr at room temperature or overnight at 4°C. Cells were rinsed three times in PBS, then incubated for 30 min at room temperature with fluorescently labelled secondary antibodies in blocking solution. Excess antibody was removed by washing five times with PBS for five min each; one of these washes included 1 µM DAPI in PBS to stain cell nuclei. Finally, coverslips were mounted onto glass slides using fluorescence mounting medium and allowed to dry at room temperature. Cells were protected from light at all times following the addition of the fluorescent secondary antibody to prevent fading of the signal.

2.8.3. Antibody optimisation

2.8.3.1. FLAG and HA antibodies

To optimise FLAG and HA antibodies, untransfected SH-SY5Y cells and cells transfected with either FLAG-Parkin or PINK1-HA were stained using primary antibody dilutions of 1:500, 1:1000, 1:2000 and 1:5000. The concentration was chosen which resulted in a clear signal in transfected cells with minimal background in untransfected cells. To ensure background staining was kept to a minimum, four different blocking solutions were also tested. These were: 10% (v/v) FBS/PBS; 15% (v/v) FBS/PBS; 10% (v/v) normal goat serum (NGS)/PBS; 15% NGS/PBS. For all three antibodies, FBS proved a more effective block than NGS and no difference could be observed between 10% and 15% FBS. The optimal blocking solution was therefore 10% (v/v) FBS/PBS.

2.8.3.2. HtrA2 and ATP synthase β antibodies

To optimise HtrA2 and ATP synthase β (CxVβ) antibodies, untransfected SH-SY5Y cells were stained using primary antibody dilutions of 1:200, 1:500, 1:1000 and 1:2000. The concentration was chosen which resulted in a clear mitochondrial distribution of the staining with minimal cytosolic (non-specific) staining.

2.8.3.3. Fbxo7 antibodies

As described in section 5.2.1, three different Fbxo7 antibodies were tested in an attempt to detect endogenous Fbxo7. Each antibody was tested in untransfected cells and in cells transfected with Fbxo7 siRNA at four different dilutions: 1:50, 1:150, 1:500 and 1:2000. Alternative fixation and permeabilisation methods were tested, including fixation with ice-

cold 90% (v/v) methanol/PBS for 20 min at -20°C or fixation with 4% (w/v) PFA/PBS followed by permeabilisation for 15 min in 100% at room temperature. Blocking solutions tested were: 1% (w/v) BSA/PBS; 5% (w/v) BSA/PBS, 10% (v/v) FBS/PBS; 15% (v/v) FBS/PBS; 10% (v/v) NGS/PBS; 15% (v/v) NGS/PBS. None of the conditions tested resulted in detection of a signal in untransfected cells which was absent or visibly reduced in cells transfected with Fbxo7 siRNA.

2.8.4. Visualisation of protein relocation

As previously (section 2.6.2), representative images were captured using a Zeiss LSM 710 confocal microscope with a 63x oil immersion objective. Excitation/emission wavelengths are shown in table 2.9 below.

Dye	Excitation (nm)	Emission (nm)
DAPI	405	410-585
Alexa Fluor 488 (anti-rabbit/anti-rat)	488	496-573
Alexa Fluor 568 (anti-mouse)	561	573-630
Alexa Fluor 633 (anti-rabbit)	633	638-747

Table 2.9 Excitation and emission wavelengths for immunocytochemistry

2.9. Statistical analysis

Unless otherwise stated, experiments were performed at least three times and data is presented as mean ± standard error of the mean (S.E.M.). In the majority of cases, differences between groups were analysed using an unpaired *t*-test assuming an equal normal distribution. Where it was necessary to normalise each experiment to control data in order to exclude differences in experimental setup between *n* (e.g. analysis of $\Delta\Psi_m$ by TMRM), a two-sample *t*-test was no longer appropriate as the control data were not normally distributed (standard deviation = 0). Under these circumstances a single-sample *t*-test was used to determine whether the sample population differed significantly from the control value (usually 1). Scientific significance was assumed at $p < 0.05$.

Chapter 3

Mitochondrial dysfunction in HtrA2 deficient mice

3.1. Introduction

As described in section 1.3.3.2, HtrA2, or Omi, is a mitochondrial serine protease with a dual function. Upon its release from the mitochondria HtrA2 induces apoptosis, both by degrading IAPs and thereby releasing their inhibitory effect on caspases, and additionally via a caspase-independent mechanism (Hegde et al., 2002; Martins et al., 2002; Suzuki et al., 2001; Verhagen et al., 2002). In the mitochondria, however, HtrA2 appears to have an important neuroprotective function revealed by a loss-of-function mutation or targeted deletion of the gene in mice (Jones et al., 2003; Martins et al., 2004).

HtrA2 is expressed as a 49 kDa peptide with an N-terminal presequence responsible for targeting the protein to the mitochondria, where it spans the IMM facing the IMS (Martins et al., 2002). Autocatalytic cleavage at the Ala133 site removes the transmembrane domain (Seong et al., 2004), releasing the mature protein into the IMS and revealing an IAP binding motif (IBM) (Martins et al., 2002). The catalytic protease activity of HtrA2 is regulated by homotrimerisation, which depends on three conserved residues and is essential for proteolysis (Li et al., 2002a). The trimeric complex is pyramid-shaped, with the N-terminal IBM domains at the top and the C-terminal PDZ protein-protein interaction domains at the bottom (Li et al., 2002a). In the inactive protein the PDZ physically blocks the protease domain, but substrate binding induces a conformational change which

exposes the protease domain and activates the protein (Li et al., 2002a). Figure 3.1 shows the domain structure of HtrA2.

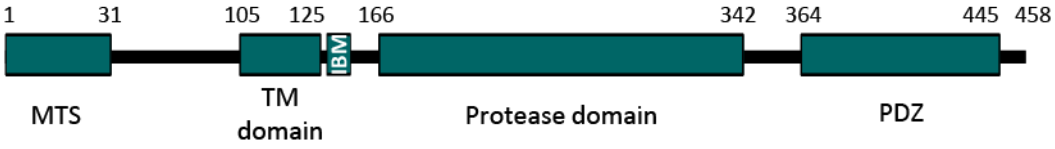

Figure 3.1 Domain structure of HtrA2. Adapted from (Strauss et al., 2005). Abbreviations: MTS, mitochondrial targeting sequence; TM, transmembrane; IBM, IAP binding motif.

Since HtrA2 was initially identified as an interactor of XIAP (X-linked inhibitor of apoptosis protein) (Hegde et al., 2002; Martins et al., 2002; Suzuki et al., 2001; Verhagen et al., 2002), it was expected that transgenic mice lacking HtrA2 would have a cancer phenotype. Surprisingly, however, the *mnd2* mouse model which carries a protease dead mutation in the *HtrA2* gene was found to exhibit a severe neurodegenerative disorder (Jones et al., 2003) which was recapitulated in homozygous HtrA2 KO mice (Martins et al., 2004). Both mouse models demonstrate striatal neurodegeneration leading to a progressive akinetic syndrome including rigidity and tremor, similar to the clinical features of PD. The mice fail to gain weight after weaning, develop symptoms around day 20 and die around day 40 after birth. Furthermore, mouse embryonic fibroblasts (MEFs) derived from the mice exhibit signs of mitochondrial dysfunction (Kieper et al., 2010; Martins et al., 2004) and HtrA2 deficient flies have increased numbers of defective mitochondria (Tain et al., 2009), indicating that HtrA2 has a function in the mitochondria which is essential for its neuroprotective action.

The parkinsonian phenotype of the HtrA2 KO and *mnd2* mice raised the question of whether HtrA2 could play a role in PD pathogenesis in humans. In 2005, Strauss and colleagues identified a novel mutation (G399S) in HtrA2 in German PD patients which was absent in controls, and a novel polymorphism (A141S) which was significantly associated with PD (Strauss et al., 2005). Interestingly both sites are located next to a putative phosphorylation site for a proline-directed serine/threonine kinase, and p38-dependent phosphorylation on both the S142 and S400 sites has been found to increase HtrA2 protease activity (Plun-Favreau et al., 2007). Furthermore, phosphorylation of the S142 site was shown to require the PD-associated kinase PINK1 (Plun-Favreau et al., 2007), while phosphorylation of the S400 is mediated by Cdk5, a kinase implicated in several neurodegenerative disorders (Fitzgerald et al., 2012). However, a subsequent larger study

identified the same mutations in *HtrA2* in neurologically normal controls (Simon-Sanchez and Singleton, 2008), casting doubt on the link between HtrA2 and PD. Since then a number of smaller studies have identified HtrA2 mutations in Belgian, Chinese and Taiwanese PD patients (Bogaerts et al., 2008; Lin et al., 2011; Wang et al., 2011a), but another large genetic association study identified no strong association with PD in populations worldwide (Kruger et al., 2011).

Although the human genetic link between HtrA2 and PD remains controversial, the severe phenotype of the KO and *mnd2* mice clearly indicates an important and as yet undetermined role for HtrA2 in mitochondrial function. HtrA2 has substantial homology to both the bacterial chaperone protein DegP and the unfolded protein response protease DegS, leading some groups to suggest that HtrA2 could participate in a mitochondrial unfolded protein response (mtUPR). In support of this, HtrA2 protein levels are upregulated in response to heat shock or tunicamycin (Gray et al., 2000) and phosphorylation of HtrA2 downstream of the stress-activated kinase p38 increases its protease activity (Plun-Favreau et al., 2007). Radke and colleagues propose that HtrA2 acts as a 'second check-point' in the IMS, degrading misfolded proteins which have evaded degradation by the proteasome system (Radke et al., 2008), while another study shows that loss of HtrA2 results in activation of a transcriptional integrated stress response including upregulation of CHOP, a key transcription factor of the mtUPR (Moisoi et al., 2009). HtrA2 itself is also transcriptionally regulated: accumulating proteins in the IMS have been shown to result in ROS-dependent activation of the oestrogen receptor (ER) and upregulation of HtrA2 (Papa and Germain, 2011). It may also act via several pathways, as another study has found that HtrA2 is involved in the degradation of pathogenic proteins such as A53T α-synuclein through autophagy (Li et al., 2010). In addition to this general role in mitochondrial maintenance, HtrA2 has also been shown to interact with and modulate the mitochondrial fusion protein OPA1, suggesting a possible role in mitochondrial dynamics (Kieper et al., 2010) .

This study aims to identify the primary mitochondrial function of HtrA2 in neurons, using live cell imaging approaches to dissect the mitochondrial physiology of HtrA2 deficient cells and biochemical techniques to probe the molecular mechanism. Wherever possible, primary neuronal cultures will be used to most closely model the cells of interest. These cultures are prepared from neonatal pups and aged no more than 20 days in culture, and consequently represent neurons from pre-symptomatic mice, suggesting that any

mitochondrial defect uncovered would likely be due directly to the loss of HtrA2 function, rather than the accumulation of unfolded mitochondrial proteins which has been reported in these animals in later life (Moisoi et al., 2009).

3.2. Results

3.2.1. A knockout mouse model to investigate HtrA2 function

Loss of HtrA2 protease function in mice has been shown to result in a severe neurodegenerative phenotype (Jones et al., 2003; Martins et al., 2004), and studies in both HtrA2 KO mice and flies have shown signs of mitochondrial dysfunction (Kieper et al., 2010; Martins et al., 2004; Moisoi et al., 2009; Tain et al., 2009). In order to further investigate the function of HtrA2 in the mitochondria, an HtrA2 KO mouse model was obtained through collaboration with Miguel Martins (Leicester University, UK). Primary neuronal/glial co-cultures were prepared from the midbrain and cortex of WT and HtrA2 KO mouse pups, enabling comparison of the effects of HtrA2 deficiency on two different cell types from two different brain regions. Immortalised mouse embryonic fibroblasts (MEFs) from WT and HtrA2 KO mice were also kindly provided by Miguel Martins, providing a more readily manipulatable cell model. Probing lysates from WT and HtrA2 KO mouse brains or MEFs confirms the complete disappearance of a band at 36 kDa, corresponding to the processed HtrA2 peptide (figure 3.2). It was not possible to detect the full length protein due to the presence of a non-specific band at the expected molecular weight (50 kDa).

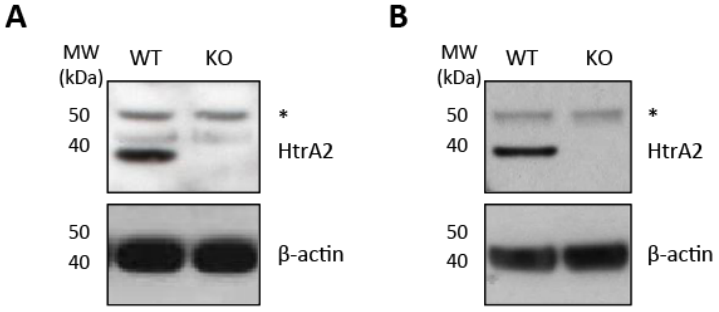

Figure 3.2 HtrA2 levels in WT and KO models. (A-B) Lysates from WT and HtrA2 KO midbrain (A) and MEFs (B) were probed for HtrA2 and β-actin (as a loading control). * indicates non-specific band.

3.2.2. Loss of HtrA2 causes mitochondrial depolarisation across cell types

A primary function of the mitochondria is oxidative phosphorylation, which requires the pumping of protons out of the mitochondrial matrix by the ETC to generate a potential across the IMM ($\Delta\Psi_m$). This potential is harnessed for the production of ATP and is thus an important indicator of mitochondrial function or dysfunction.

Consistent with previous reports (Kieper et al., 2010; Martins et al., 2004; Moisoi et al., 2009; Plun-Favreau et al., 2007) loading WT and HtrA2 KO MEFs with the $\Delta\Psi_m$-sensitive dye TMRM revealed a significant reduction in $\Delta\Psi_m$ in HtrA2 KO cells compared to WT (figure 3.3a). The same pattern was additionally observed in neuron and astrocyte co-cultures from the midbrains and cortices of WT and HtrA2 KO mice (figure 3.3b). Furthermore, the mitochondrial depolarisation observed in HtrA2 KO midbrain neurons was significantly greater than that observed in KO cortical neurons, suggesting a functional link between the mitochondrial dysfunction observed and the parkinsonian behavioural phenotype.

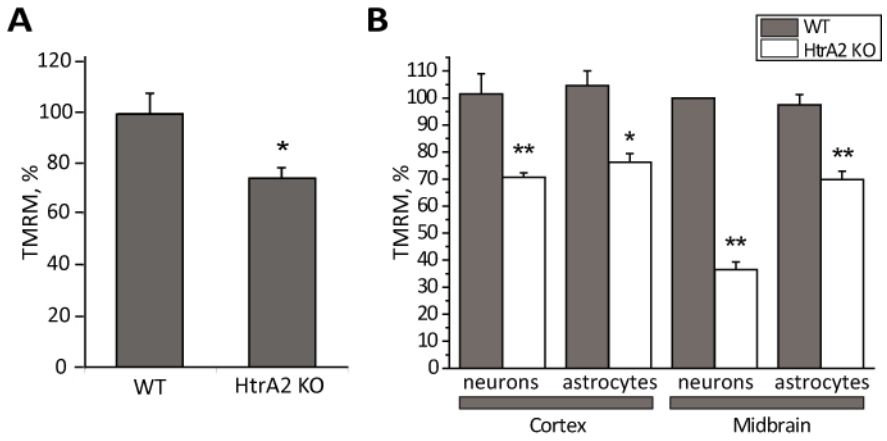

Figure 3.3 Mitochondrial membrane potential in WT and HtrA2 KO cells. (A-B) $\Delta\Psi_m$ was assessed using TMRM in WT and HtrA2 KO MEFs (A) and primary neuronal cultures (B). Histograms show average TMRM intensity over 3 independent experiments, normalised to WT cells in panel A and to WT midbrain in panel B. Data are represented as mean ± S.E.M. * p <0.05, ** p <0.005.

3.2.3. NADH and FAD^{++} redox states are more oxidised in HtrA2 KO cells

Since $\Delta\Psi_m$ is generated by the mitochondrial respiratory complexes, a decrease in $\Delta\Psi_m$ could indicate a defect in respiration. In order to investigate mitochondrial respiration specifically in neurons and not glia, NADH redox index was calculated based on the autofluorescence of NADH. NADH is generated by the reduction of NAD^+ during β-oxidation, glycolysis and the TCA cycle, and is oxidised back to NAD^+ by complex I (see section 1.2.1); consequently, relative levels of NADH and NAD^+ are a function of both respiratory chain activity and the rate of substrate supply. NADH, but not NAD^+, fluoresces in the UV range and can therefore be measured by confocal microscopy on a single cell basis. Increased respiration results in depletion of the NADH pool and a reduction in autofluorescence; conversely, impaired respiration increases NADH autofluorescence. Resting redox state can therefore be measured as a function of its most oxidised state (following addition of the uncoupler FCCP, 1 μM) and most reduced state (after addition of 1 mM sodium cyanide to block respiration) (figure 3.4a). This value is independent of NADPH autofluorescence, which occurs at the same wavelength, since NADPH is not a substrate for the mitochondrial respiratory chain.

NADH redox index was measured in cortical and midbrain neuron/glia co-cultures from WT and HtrA2 KO mice. In HtrA2 KO cells, the reduction in NADH levels in response to FCCP was notably smaller than in WT cells while the response to sodium cyanide (NaCN) was much larger (figure 3.4b), resulting in a significant reduction in redox index in all the cell types tested (figure 3.4c). This finding indicates that mitochondrial respiration is in fact closer to maximal in HtrA2 deficient cells, in contrast to the respiratory impairment expected. The reduction in redox index was greater in neurons than in their neighbouring astrocytes and was most dramatic in the midbrain neurons, indicating that the defect observed is most severe in these cells.

The difference in absolute values between the minimum and maximum NADH signal is termed the mitochondrial NADH pool (figure 3.4a) and is an indication of the total pool of NADH available to the respiratory chain. In all cell types measured, HtrA2 KO cells had a significant increase in mitochondrial NADH level compared to WT cells (figure 3.4d), possibly indicating an increase in glycolysis or upregulation of the TCA cycle to compensate for the low $\Delta\Psi_m$.

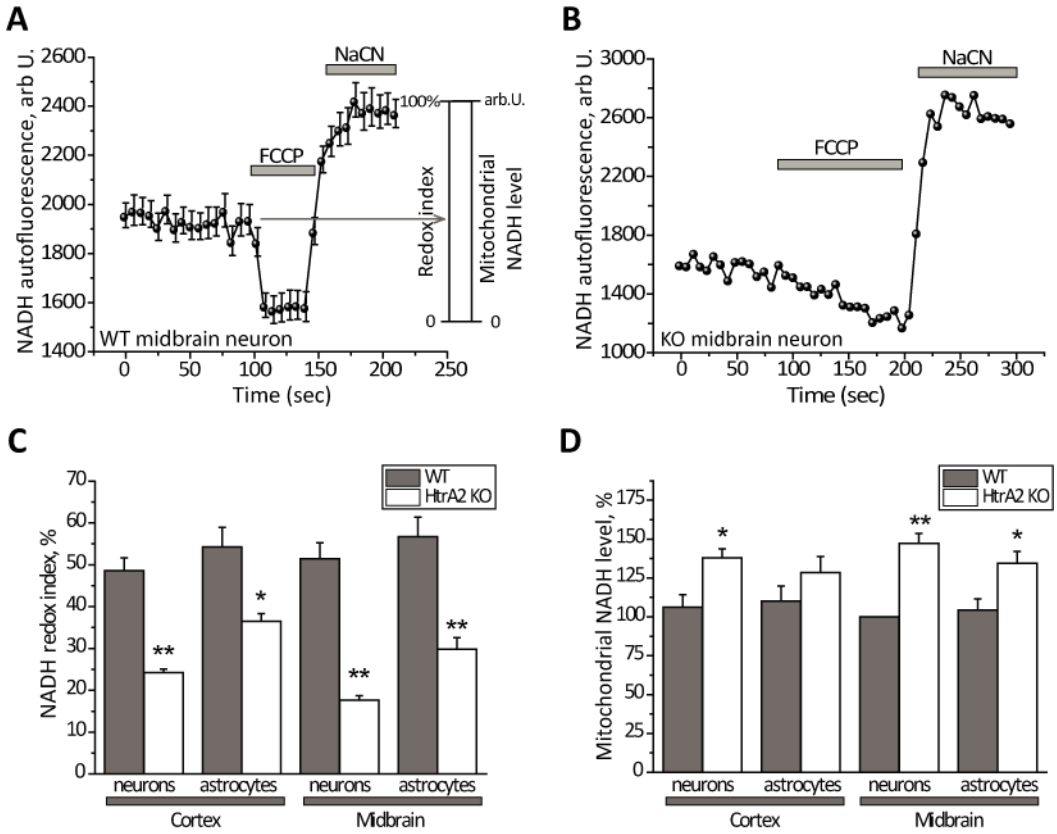

Figure 3.4 NADH redox index in WT and HtrA2 KO cells. **(A, B)** Representative traces are shown for one WT (A) and one HtrA2 KO (B) midbrain neuron following addition of FCCP (1 µM) and NaCN (1 mM). **(C)** Redox index was calculated as shown in panel A for WT and HtrA2 KO neurons and astrocytes. **(D)** Mitochondrial NADH pool was calculated for WT and HtrA2 KO neurons and normalised to WT midbrain neurons. Data are represented as mean ± S.E.M. *$p < 0.05$, **$p < 0.005$

Just as NADH autofluorescence may be used to monitor mitochondrial respiration through complex I, the electron donor for complex II, $FADH_2$, can be monitored in the same way. FAD^{++} is a cofactor of the flavoprotein succinate dehydrogenase (complex II), which functions both as part of the TCA cycle, oxidising succinate to fumarate, and as a complex of the respiratory chain (see section 1.2.1). During the TCA cycle FAD^{++} is reduced to $FADH_2$ by the addition of two electrons, which are then passed through an iron-sulphur relay to ubiquinone, feeding the electron transport chain and, in so doing, oxidising $FADH_2$ back to FAD^{++}. FAD^{++} is autofluorescent when excited at 458 nm, therefore an increase in respiratory chain activity at complex II is observed as an increase in autofluorescence, while a reduction in respiration is observed as a reduction in autofluorescence. Maximally oxidised and maximally reduced signals are measured by addition of FCCP and NaCN and the basal autofluorescence converted to a redox index as described for NADH, thus

distinguishing FAD^{++} used by complex II in mitochondrial respiration from FAD^{++} reduced during β-oxidation. FADH redox index was found to be significantly increased (i.e. oxidised) compared to WT in all HtrA2 KO cell types and particularly in midbrain neurons (figure 3.5). Therefore mitochondrial respiration through both complex I and complex II is closer to maximal levels in HtrA2 KO neurons and glia, indicating an increase in mitochondrial respiration in HtrA2 deficient cells.

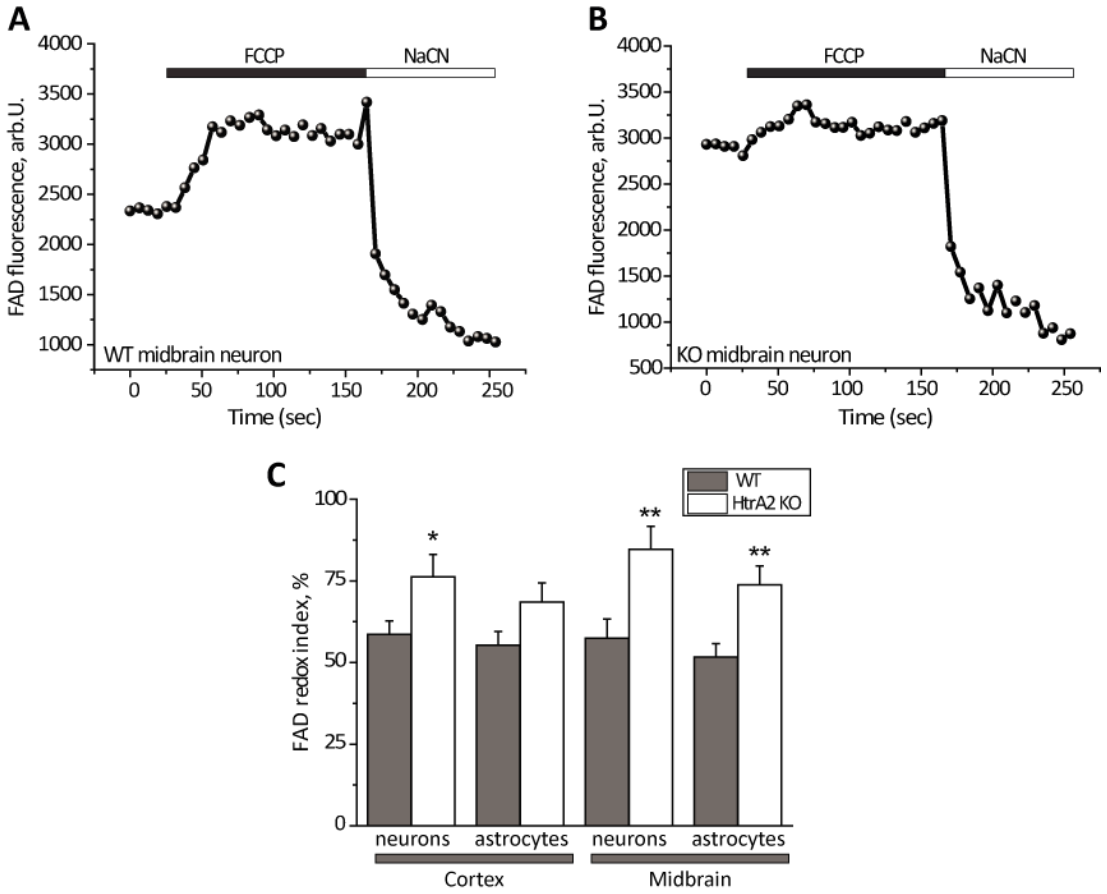

Figure 3.5 FAD redox index in WT and HtrA2 KO cells. **(A, B)** Representative traces are shown for one WT (A) and one HtrA2 KO (B) midbrain neuron following addition of FCCP (1 μM) and NaCN (1 mM). **(C)** FAD redox index was calculated as previously described (figure 3.4a) for WT and HtrA2 KO neurons and astrocytes. Data are represented as mean ± S.E.M. $*p < 0.05$, $**p < 0.005$

3.2.4. Oxygen consumption is increased in HtrA2 KO mitochondria

The NADH/FAD redox index data suggest that mitochondrial respiration is closer to maximal in HtrA2 deficient cells. In order to confirm this increase in respiration by a different method, oxygen consumption was measured in whole MEFs using a Clark oxygen electrode. Consistent with the previous data, the basal rate of oxygen consumption was higher in HtrA2 KO MEFs than WT, indicating an increase in respiration (figure 3.6). Addition of oligomycin to block the ATP synthase inhibited respiration in both WT and KO cells, and addition of the uncoupler FCCP increased respiration to the same maximal rate, suggesting that expression and maximal activity of the mitochondrial complexes are not affected.

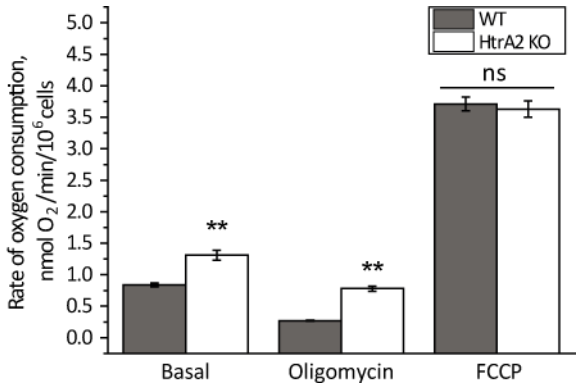

Figure 3.6 Oxygen consumption in whole WT and HtrA2 KO MEFs. Rate of oxygen consumption was measured in WT and KO MEFs under basal conditions and following addition of oligomycin (2 μg/ml) and FCCP (1 μM). Data are represented as mean ± S.E.M. ns, not significant; ** $p < 0.005$

One explanation for both an increase in oxygen consumption and a reduction in $\Delta\Psi_m$ could be a leak of protons across the IMM, effectively uncoupling mitochondrial respiration from oxidative phosphorylation. To test this hypothesis, respiratory control ratio was measured in intact mitochondria isolated from the brains of WT and HtrA2 KO mice. Mitochondrial oxgyen consumption was initially measured in an intracellular-like solution (see Methods) containing mitochondrial substrates but no ADP. A fixed quantity of ADP was then added to enable ATP production and therefore stimulate oxygen consumption: this ADP-stimulated state is termed state III. After a few minutes the added ADP is consumed and the rate of oxygen consumption returns to its original level, termed state IV. The ratio of state III to state IV respiration is the respiratory control ratio and is an

indication of how efficiently mitochondrial respiration is coupled to oxidative phosphorylation. A representative trace for control mitochondria indicating state III and IV respiration can be seen in Methods (figure 2.5)

Respirometry in isolated brain mitochondria revealed a small increase in state III respiration in HtrA2 KO mitochondria (figure 3.7a) but a large increase in state IV respiration (figure 3.7b), resulting in a dramatic reduction in respiratory control ratio compared to WT mitochondria (figure 3.7c). This reduction in control ratio occurred irrespective of whether the substrates provided fed into complex I (glutamate plus malate) or complex II (succinate). This indicates that HtrA2 KO mitochondria are severely uncoupled and this uncoupling does not occur at either complex I or complex II.

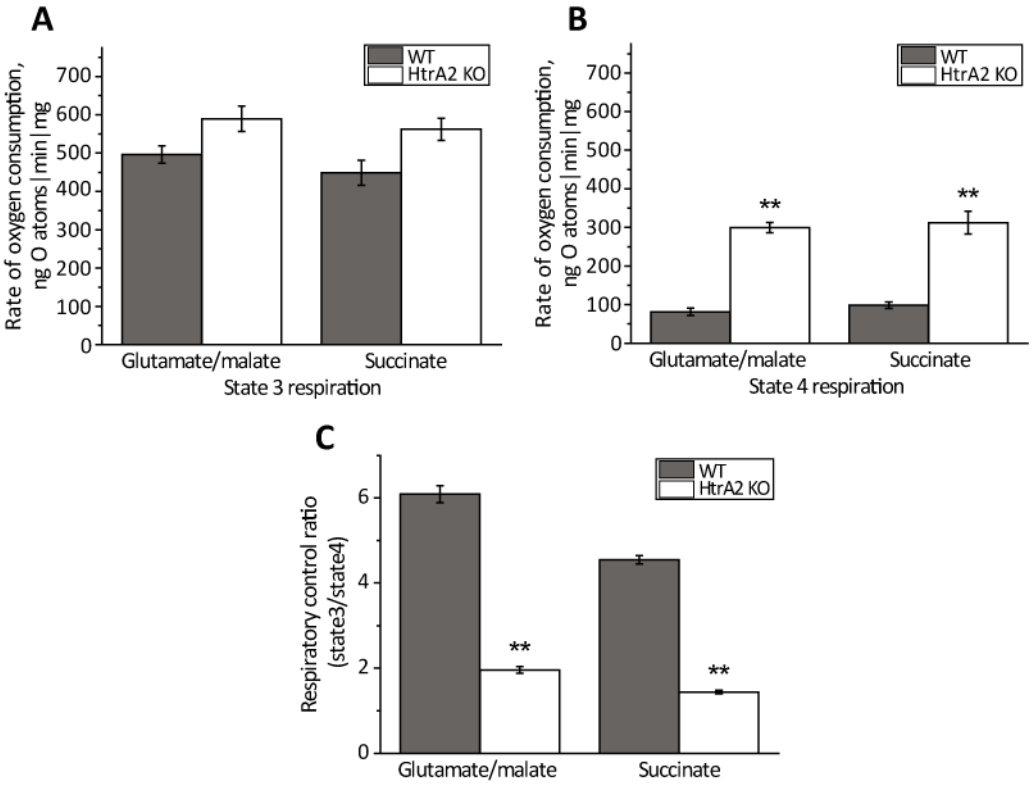

Figure 3.7 Respiratory control ratio in brain mitochondria. (A, B) Mitochondria were isolated from the brains of WT and HtrA2 KO animals and oxygen consumption measured in state III (ADP stimulated; A) and state IV (no ADP present; B). **(C)** Respiratory control ratio (the ratio of state III to state IV) was calculated for WT and HtrA2 KO mitochondria. Data are represented as mean ± S.E.M.

3.2.5. ROS production in HtrA2 KO neurons

Mitochondrial reactive oxygen species (ROS) production has previously been shown to be reduced under conditions of mitochondrial uncoupling (reviewed by Brand et al., 2004; Casteilla et al., 2001). Consistent with the previous data, measurement of mitochondrial ROS using mitoSOX (a mitochondrially-targeted derivative of the redox probe dihydroethidium) revealed a significant reduction in basal mitochondrial ROS in HtrA2 KO neurons compared to WT (figure 3.8a; data generated by Andrey Abramov). No difference was observed in maximal ROS production, which was induced by inhibiting complex I with rotenone (5 μM), resulting in reverse electron flux from complex II (Votyakova and Reynolds, 2001). Interestingly, cytosolic ROS production measured using dihydroethidium was significantly increased in HtrA2 KO neurons (figure 3.8b), indicating an increase in ROS from a non-mitochondrial source.

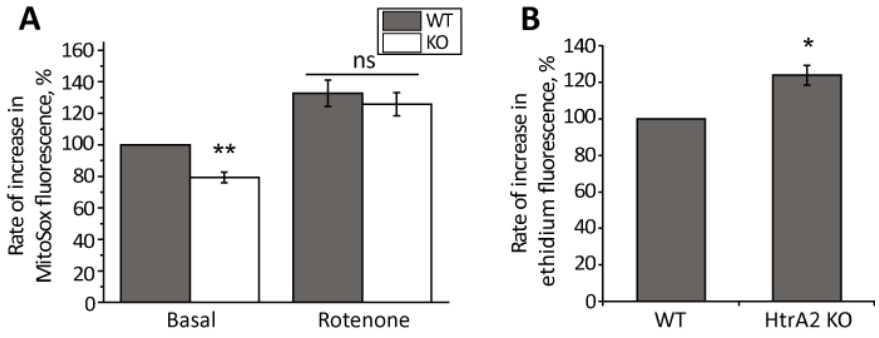

Figure 3.8 ROS production in WT and HtrA2 KO midbrain neurons. (A) Rate of increase in oxidised MitoSOX fluorescence before and after addition of rotenone (5 μM). **(B)** Rate of increase in 530/380nm (oxidised/reduced dihydroethidium) fluorescence. Results are normalised to WT in each case and represented as mean ± S.E.M. * $p < 0.05$, ** $p < 0.005$.

3.2.6. Proton entry through the ATP synthase is increased in HtrA2 KO neurons

Under normal conditions, the F_1F_0-ATP synthase generates ATP by allowing protons to enter the mitochondria down the electrochemical gradient generated by the ETC. However, under conditions of very low $\Delta\Psi_m$, such as those observed in HtrA2 KO midbrain neurons, the ATP synthase may reverse its activity such that ATP is hydrolysed and protons are pumped out of the mitochondrial matrix, thereby maintaining the $\Delta\Psi_m$. This may be investigated by using the potential-sensitive dye TMRM to monitor the effect of mitochondrial toxins on $\Delta\Psi_m$ (Rego et al., 2001; Ward et al., 2000). In WT cells (figure

3.9a), the addition of oligomycin to block the pore of the ATP synthase has no effect on $\Delta\Psi_m$, or causes a slight hyperpolarisation as proton entry into the matrix is inhibited. Rotenone, an inhibitor of complex I, then depolarises the mitochondria and the uncoupler FCCP results in complete depolarisation. If the ATP synthase acts in reverse, as has been shown previously in PINK1 KO neurons, the addition of oligomycin causes a loss of $\Delta\Psi_m$ as proton pumping through the synthase is prevented (Gandhi et al., 2009). In HtrA2 KO midbrain neurons, however, the addition of oligomycin produced a hyperpolarisation (figure 3.9b), indicating that $\Delta\Psi_m$ is still maintained solely through the electron transport chain despite the low resting $\Delta\Psi_m$. Furthermore, this hyperpolarisation was found to be significantly larger in HtrA2 KO cells than in WT (figure 3.9c), indicating that proton entry into the mitochondria through the pore of the ATP synthase is increased.

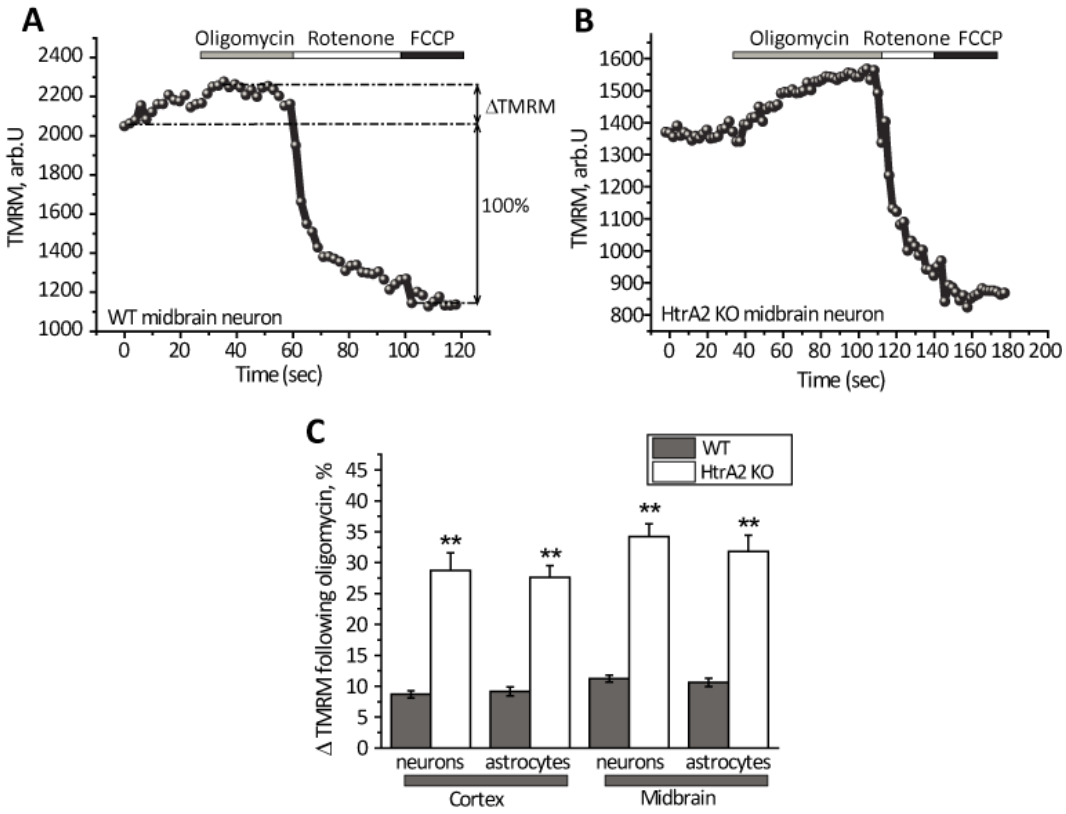

Figure 3.9 Mechanism of maintenance of $\Delta\Psi_m$ in WT and HtrA2 KO midbrain neurons. (A, B) Representative traces are shown for one WT (A) and one HtrA2 KO (B) midbrain neuron in response to oligomycin (2 µg/ml), rotenone (5 µM) and FCCP (1 µM). **(C)** Hyperpolarisation in response to oligomycin (ΔTMRM) was quantified as a percentage of the difference between the initial TMRM intensity and the minimum TMRM fluorescence achieved after addition of FCCP (see panel A). Data are represented as mean ± S.E.M. ** $p < 0.005$

3.2.7. Oxidative phosphorylation is impaired in HtrA2 deficient cells

An increase in proton translocation through the ATP synthase might indicate a leak of protons through the pore, explaining the mitochondrial uncoupling observed. To investigate whether the increased proton translocation represents a leak of protons or an increase in oxidative phosphorylation, ATP production by the ATP synthase was measured using a kinetic luciferin/luciferase assay. The firefly enzyme luciferase catalyses the conversion of luciferin to oxyluciferin, a bioluminescent compound, in an ATP-dependent manner (Neufeld et al., 1975). ATP levels therefore correlate with luminescence and can be measured using a luminometer. In order to apply this principle to specifically investigate ATP production by the F_1F_0-ATP synthase, MEF cells were transfected with a cytosolic luciferase construct and perfused with 5 µM luciferin. Perfusion with 1 mM ATP stimulated purinergic receptors on the cell surface, leading to uptake of calcium into the mitochondria and therefore an increase in ATP production by the ATP synthase (Jouaville et al., 1999). In WT MEFs this was observed as a sudden increase in luminescence following addition of ATP; in HtrA2 KO MEFs, however, the relative increase was significantly smaller (figure 3.10a, b). Thus ATP production by the ATP synthase is reduced in HtrA2 KO cells even though proton translocation through the pore of the synthase is increased, suggesting a leak of protons through the ATP synthase.

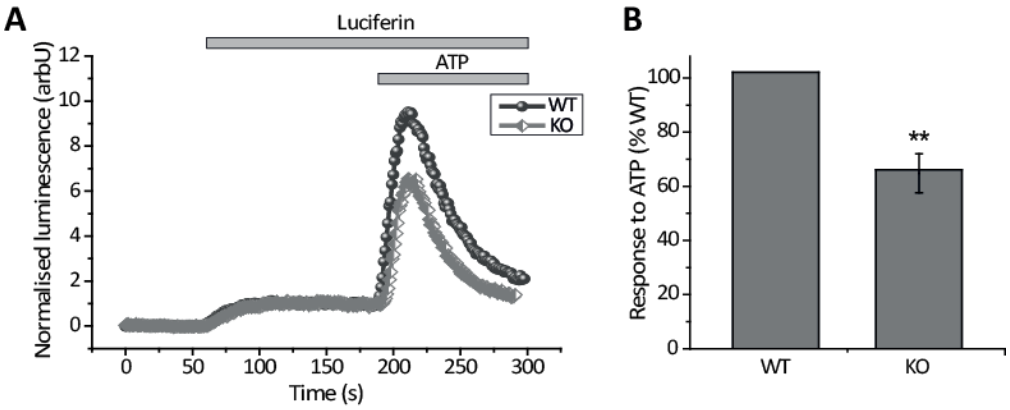

Figure 3.10 Oxidative phosphorylation in HtrA2 deficient cells. (A) Representative traces are shown for one WT and one HtrA2 KO coverslip. Initial luminescence was normalised to 0 and response to luciferin normalised to 1. **(B)** ATP response curves were normalised to luciferin response, then for each pair of coverslips the KO response was expressed as a percentage of the WT. Data are represented as mean ± SEM. ** indicates $p < 0.005$ compared to WT.

3.2.8. HtrA2 interacts with the ATP synthase

To investigate the uncoupling further on a biochemical level, an affinity purification approach was employed to determine whether HtrA2 interacts with the ATP synthase. A prior tandem-affinity purification (TAP) screen for interactors of HtrA2 had identified a peptide fragment of the α subunit of the ATP synthase by mass spectrometry (Hélène Plun-Favreau, unpublished data). To confirm this interaction, lysates from HEK293T cells overexpressing TAP-tagged HtrA2 (figure 3.11a) were first immunoprecipitated using IgG beads to bind the protein A sequence, then cleaved with TEV protease to separate the complexes from the beads before a second immunoprecipitation (IP) using calmodulin beads to bind the calmodulin binding peptide sequence. HtrA2 complexes were finally eluted with calcium and subjected to western blot analysis (figure 3.11b).

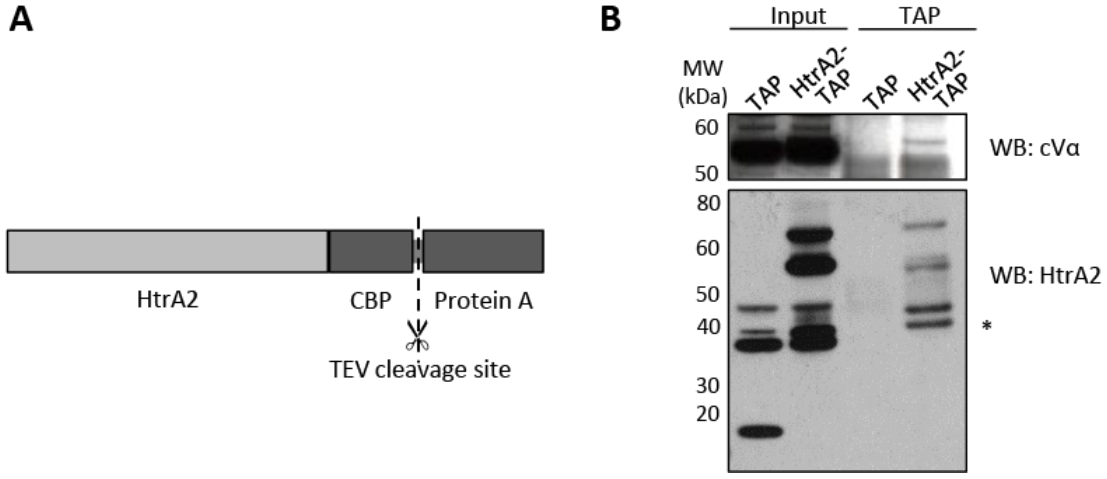

Figure 3.11 ATP synthase F_1 α subunit interacts with HtrA2 by tandem affinity purification. (A) HtrA2 was tagged at the C terminus with a tandem affinity purification (TAP) tag consisting of a protein A sequence (for IP with IgG beads) and a calmodulin binding peptide (CBP) sequence (for IP with calmodulin resin) separated by a TEV cleavage site. **(B)** The F_1 α subunit (cVα) was identified in TAP eluates from HtrA2-TAP cells but not from TAP control cells. WB for HtrA2 shows endogenous processed HtrA2 (37 kDa) in TAP and HtrA2-TAP inputs, full length and processed TAP-tagged HtrA2 (58 and 69 kDa) in the HtrA2-TAP inputs, and CBP-tagged processed HtrA2 (42 kDa) in the final eluate. * indicates non-specific band.

The mammalian F_1F_0-ATP synthase complex is composed of ~16 different subunits, many of which have no commercially available antibodies. In order to investigate whether HtrA2's interaction with the ATP synthase has any effect on its composition, an

immunocapture approach was therefore applied as described by Giorgio and colleagues (Giorgio et al., 2009). Mitochondria were isolated from the brains of littermate WT and HtrA2 KO mice aged P20, solubilised, and intact ATP synthase complexes immunoprecipitated using a commercially available immunocapture kit. Complexes were subjected to denaturing gel electrophoresis, then silver stained (figure 3.12a, overleaf). Subunits were identified on the basis of their size and band pattern.

Although there are no immediately obvious differences between the WT and KO samples, densitometry using Image J revealed a significant reduction in the intensity of the doublet corresponding to the α and β subunits of the F_1 part of the synthase, when normalised either to the total intensity per lane (figure 3.12b) or to a non-specific band (figure 3.12c). In order to confirm this, expression of the α subunit in the immunoprecipitated ATP synthase complexes was analysed by western blot, using the b subunit of the F_0 part of the complex as a loading control (figure 3.12d). Although there did appear to be a reduction in α subunit protein levels in the KO samples by western blot, the same pattern was also observed in b subunit protein levels, suggesting that this difference was either due to loading or that both subunits are equally affected by loss of HtrA2. No alteration in processing of either subunit was detected in KO mitochondria compared to WT.

3.2.9. HtrA2 deficiency reduces ATP levels and increases vulnerability to chemical ischaemia

In order to investigate the effect of the observed uncoupling on cellular ATP levels and cell viability, primary neuronal cultures were loaded with the dye Mag-Fura-2, a fluorescent chelator of free magnesium. Since ATP is always bound to magnesium in the cell, free magnesium levels have been shown to inversely correlate with ATP levels (Leyssens et al., 1996) and Mag-Fura can thus be used as an indirect indicator of ATP levels. This approach has the advantage that it can be analysed on a single cell basis and can therefore be used to investigate neurons independently from astrocytes in co-culture. In addition to binding magnesium ions with a high affinity, Mag-Fura is also a low-affinity chelator of calcium ions, a property which can be utilised to investigate cell viability in response to chemical ischaemia by monitoring the fluorescence following addition of sodium cyanide (figure 3.13a). Cyanide blocks respiration at complex IV, causing depletion of ATP levels and a steady increase in Mag-Fura ratio until ATP levels fall below a critical threshold. At this point there is no longer sufficient ATP to maintain ionic homeostasis and the cell floods

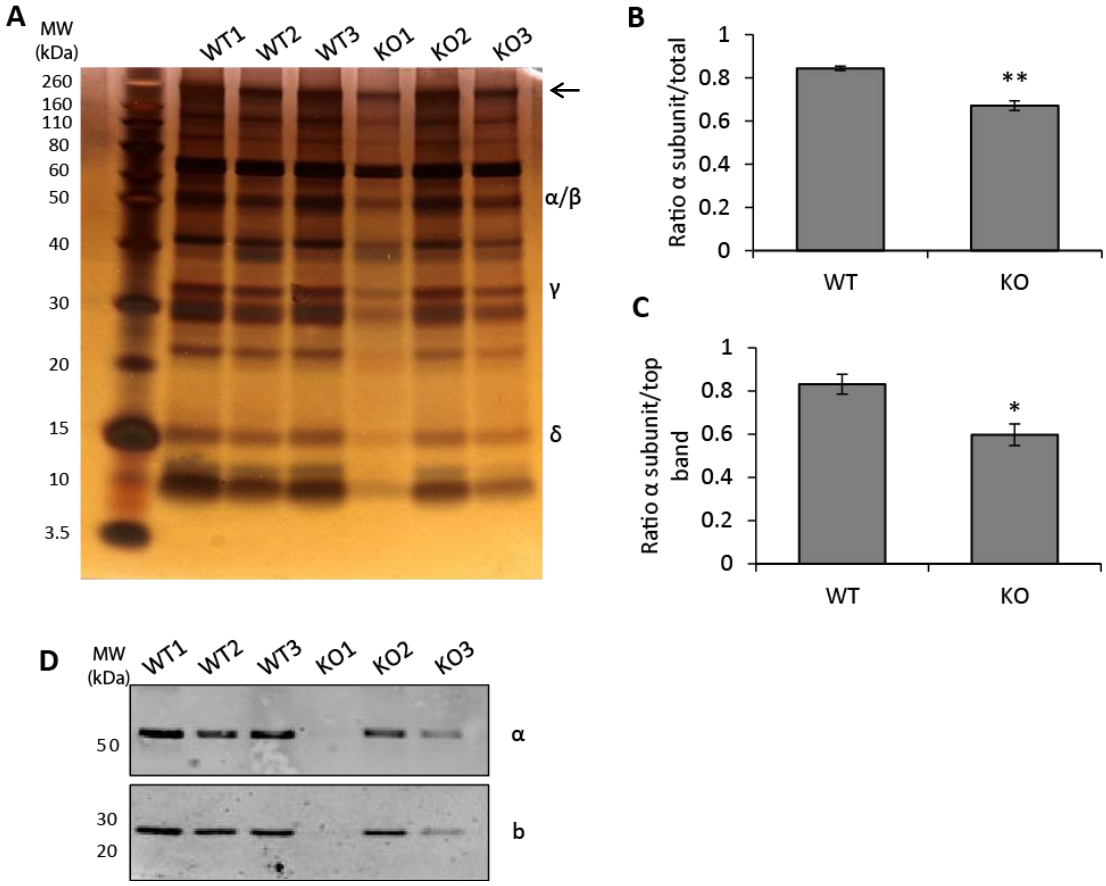

Figure 3.12 Investigation of alteration in ATP synthase complex formation. (A) The ATP synthase complex was immunoprecipitated from mitochondria isolated from the brains of three WT and three HtrA2 KO mice. Bands were separated on a 10% SDS-PAGE gel and visualised by silver staining. **(B, C)** Relative expression of the α/β subunits normalised either to total protein (B) or a non-specific band indicated with an arrow (C) was decreased in the KO samples compared to WT. **(D)** ATP synthase immunoprecipitated from WT or HtrA2 KO mouse brain mitochondria was probed using antibodies against the α and b subunits. No difference in expression of α relative to b was observed. Error bars indicate mean ± S.E.M. * $p < 0.05$, ** $p < 0.005$

with calcium, causing a sudden increase in Mag-Fura ratio. This sudden increase indicates the complete bioenergetic collapse of the cell and consequent cell lysis.

In primary midbrain neurons, HtrA2 KO cells were found to exhibit significantly higher basal Mag-Fura ratio than WT cells (figure 3.13b), indicating a reduction in cellular ATP level consistent with the reduction in oxidative phosphorylation observed in MEFs and KD SH-SY5Y cells. Furthermore, the time taken for HtrA2 KO cells to undergo bioenergetic collapse (ΔT) following addition of cyanide was significantly shorter than their WT counterparts (figure 3.13c), indicating that the lack of ATP renders these cells more vulnerable to cytotoxicity in response to chemical ischaemia. This vulnerability might help to explain the death of striatal neurons *in vivo* in the HtrA2 KO mice.

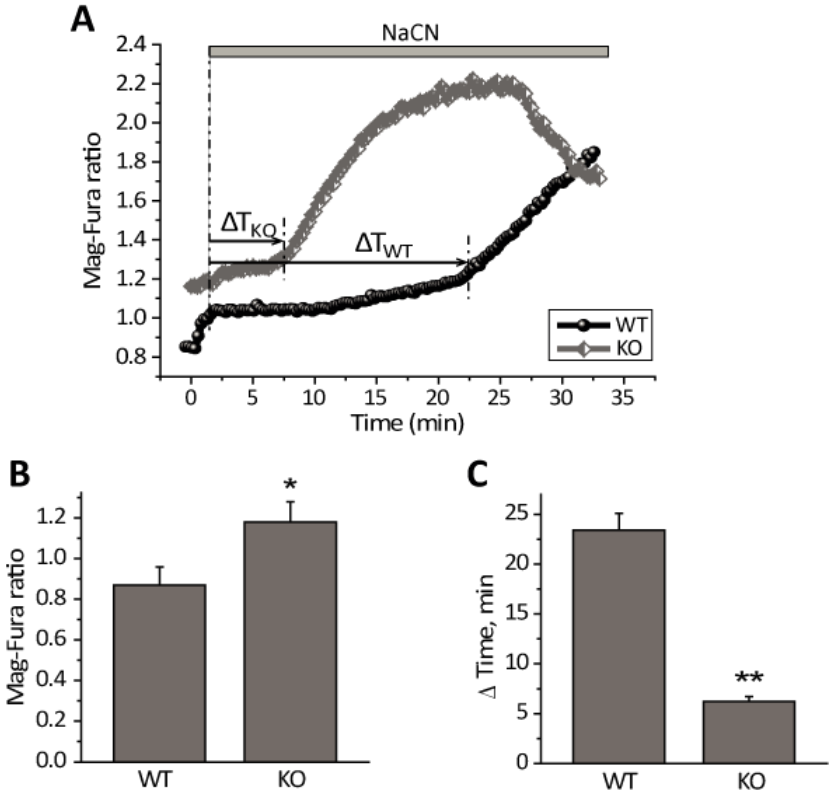

Figure 3.13 Effect of HtrA2 deficiency on ATP levels and vulnerability to chemical ischaemia. (A-C) ATP levels were assessed indirectly using an indicator of free magnesium, Mag-Fura (5 μM). Panel A shows representative traces for one WT and one HtrA2 KO midbrain neuron. Initial Mag-Fura ratio is quantified in panel B, data represented as mean ± SEM. Inhibition of mitochondrial respiration by NaCN (1 mM) causes a slow increase in Mag-Fura ratio as ATP levels are depleted, followed by a sudden increase in Mag-Fura ratio as the cell floods with calcium. The time to onset of this bioenergetic collapse (ΔT) is quantified in panel C, data represented as mean ± SEM. * $p < 0.05$, ** $p < 0.005$ compared to WT.

3.3. Discussion

HtrA2 is a mitochondrial serine protease with both a pro-apoptotic and a neuroprotective function. Previous studies in MEFs from HtrA2 KO or mutant mice have observed low $\Delta\Psi_m$ and altered mitochondrial ultrastructure, indicating mitochondrial dysfunction in these cells (Jones et al., 2003; Kieper et al., 2010; Martins et al., 2004; Moisoi et al., 2009). In this study mitochondrial physiology was examined in primary neuronal cultures from pre-symptomatic mice, enabling investigation of the mitochondrial function of HtrA2 prior to induction of the unfolded protein response which has previously been reported in HtrA2 KO mice over 15 days of age (Moisoi et al., 2009).

3.3.1. Mitochondrial uncoupling: protective or pathogenic?

As previously discussed in chapter 1 (section 1.2.2), mitochondria are a major source of free radical production in the cell, with the primary culprits being respiratory complexes I and III. Superoxide ($O_2^{\cdot}$) is generated at these sites because the free energy released by the transfer of an electron to molecular oxygen is greater than that released by its transfer to either ubiquinone or cytochrome c, and consequently the reaction is more thermodynamically favourable (Balaban et al., 2005). The greater the existing proton gradient across the mitochondrial inner membrane, the greater the energy required to pump further protons out of the matrix and therefore the more energetically favourable $O_2^{\cdot}$ production becomes. Mitochondrial ROS production has been consistently shown to increase with $\Delta\Psi_m$, with H_2O_2 production rising steeply above a threshold $\Delta\Psi_m$ which slightly exceeds normal state III levels (Korshunov et al., 1997). Consequently, it has long been suggested that mitochondria have an endogenous mechanism for mildly uncoupling respiration from oxidative phosphorylation, reducing $\Delta\Psi_m$ and therefore avoiding potentially damaging ROS production (Brand, 2000; Skulachev, 1996). More recently, the identification of mitochondrial uncoupling proteins (UCPs) 2 and 3 (Boss et al., 1997; Fleury et al., 1997) has provided a mechanism by which this uncoupling could occur. Both proteins are mitochondrial proton channels which are activated by $O_2^{\cdot}$ and derivatives of ROS (Echtay et al., 2003; Echtay et al., 2002), and inhibition or genetic deletion of either protein results in an increase in ROS production (Arsenijevic et al., 2000; Negre-Salvayre et al., 1997; Vidal-Puig et al., 2000).

The work described in this chapter reveals for the first time that mitochondria lacking HtrA2 are severely uncoupled, resulting in low $\Delta\Psi_m$ but increased respiration. Consistent

with the evidence discussed above, mitochondrial ROS production was significantly reduced in HtrA2 KO primary neurons, although this data is in contrast to previously reported results in HtrA2 KO MEFs (Kieper et al., 2010; Moisoi et al., 2009). This difference in findings may arise from a difference in cell type (MEFs versus primary neurons) or experimental approach (flow cytometry versus confocal microscopy). It should also be noted that the increase in mitochondrial ROS in KO MEFs has been shown to be rescued by protease-dead as well as WT HtrA2 (Kieper et al., 2010), indicating that this effect is not due to its catalytic function. Interestingly an increase in cytosolic ROS was observed in HtrA2 KO cells, consistent with the results reported in MEFs. This ROS appears not to originate from the mitochondria in KO neurons, but may be due to activation of plasmalemmal NADPH oxidase, perhaps due to an alteration in calcium handling: *mnd2* mutant MEFs have previously been shown to exhibit impaired mitochondrial calcium handling and increased vulnerability to calcium induced mitochondrial permeability transition (Jones et al., 2003).

In contrast to the mild uncoupling described above, the severe uncoupling observed in HtrA2 KO neurons is extremely pathogenic, leading to a lack of ATP which increases the cell's vulnerability to bioenergetic collapse during chemical ischaemia and may account for the neurodegeneration observed *in vivo*. Interestingly, another study has recently reported mitochondrial uncoupling in fibroblasts from patients with a pathogenic G2019S mutation in LRRK2, although in this case the uncoupling was found to result from transcriptional upregulation of UCP4 in fibroblasts and UCP2 in a neuroblastoma model (Papkovskaia et al., 2012). Together with the data in this chapter, this provides further support to the notion that pathological uncoupling might result in a parkinsonian phenotype.

3.3.2. Region-specific effect of HtrA2 deficiency

Given the specificity of the neuronal cell death observed in the HtrA2 KO mice, it is interesting to note that the mitochondrial defect observed affected HtrA2-deficient primary neurons more than astrocytes, MEFs or neuroblastoma cells, and furthermore that midbrain neurons were more severely affected than cortical neurons. The neuronal selectivity of the phenotype may plausibly be explained by the difference in bioenergetic profile between neurons, astrocytes and fibroblasts. Neurons are unusual in having very low levels of glycolysis due to the continuous proteasomal degradation of a key glycolytic enzyme (Herrero-Mendez et al., 2009), and consequently they are heavily dependent on

mitochondria for ATP production. Interestingly, the behavioural phenotype of the HtrA2 KO mice only appears after weaning, perhaps because lactate in the mother's milk can be oxidised to pyruvate which is a direct substrate of the TCA cycle. HtrA2 has previously been suggested to degrade two enzymes of the TCA cycle (Johnson and Kaplitt, 2009) and figure 3.4 showed an increase in the mitochondrial pool of NADH in KO cells consistent with upregulation of this pathway. Potentially, this upregulation might be sufficient to compensate for the mitochondrial uncoupling in mouse pups, but once weaned the mice would need to obtain TCA cycle substrates from glucose, and consequently the brain, which is least able to upregulate glycolysis, would be most severely affected.

While differences between neurons and astrocytes can be easily explained by the difference in bioenergetic profile, the difference between midbrain and cortical neurons is more difficult to explain. The experiments were carried out in primary cultures rather than whole brains, so there should be no difference in the extracellular environment between the genotypes. A possible explanation is that differences in the transcriptional profile of the different brain regions may account for the different mitochondrial phenotype, perhaps by impacting on the energy demands or oxidative state of the cell. For example, it has been suggested that the expression of pacemaking L-type calcium channels in the dopaminergic neurons of the substantia nigra may account for their vulnerability in Parkinson's disease due to the increased energy required for calcium homeostasis (Chan et al., 2009). Similarly, dopamine itself may result in oxidative stress through auto-oxidation (Berg et al., 2004). It should be noted that although a difference in mitochondrial physiology was observed between midbrain and cortical cultures from HtrA2 KO mice, it is likely that the underlying difference is a broad regional phenomenon rather than a specifically dopaminergic effect because the dissection of neonatal brains for culture is relatively crude, resulting in a mixed population of cells which include neighbouring regions such as the striatum. Interestingly, maternally inherited mutations in the mitochondrial *ATP6* gene underlie a subgroup of disorders characterised by striatal lesions (Schon et al., 1997). *ATP6* encodes subunit a of the ATP synthase (see figure 3.14 on page 109), suggesting that this region may be especially vulnerable to failure of the ATP synthase. Understanding the basis of this regional selectivity may therefore be relevant both in understanding HtrA2-linked striatal degeneration and parkinsonian dopaminergic neurodegeneration.

3.3.3. ATP synthase structure and function

The mammalian ATP synthase is composed of ~16 different subunits and accessory proteins, arranged in two associated complexes: the membrane bound F_0 complex, and the F_1 complex in the mitochondrial matrix (figure 3.14a). The F_1 complex comprises a hexameric ring of alternating α and β subunits surrounding the γ subunit, which forms a central rotor shaft. The δ and ε subunits couple the F_1 ATPase to the F_0 complex, composed of the membrane bound a and c subunits and the 'stator stalk' made up of the b, d, F_6 and OSCP subunits. A second domain of the F_0 complex contains the e, f, g and A6L subunits whose structure and function are less well understood, although all four contain a single transmembrane domain (Belogrudov et al., 1996) and the e and g subunits appear to be important for the formation of ATP synthase dimers (Arnold et al., 1998). Proton translocation through the F_0 a subunit results in a rotation of the c ring which in turn rotates the central γ subunit. The α/β ring is held stationary by the stator stalk, thus each 120° rotation of the γ subunit brings it into contact with a different α/β subunit pair (Diez et al., 2004). At any given moment, each of the three catalytic sites (located at the subunit interface on the clockwise side of the β subunit) is in a different conformation such that one is empty, one binds ADP and inorganic phosphate, and the third binds ATP (Abrahams et al., 1994). Rotation of the γ subunit induces a conformational change (Masaike et al., 2008) such that the ADP site changes to an ATP site, catalysing the addition of P_i to ADP, while the ATP site changes to empty releasing the ATP molecule and the empty site becomes an ADP binding site (figure 3.14b). In this manner each 120° rotation results in one molecule of ADP binding, one molecule of ATP being produced, and one molecule of ATP being released.

The data presented in this chapter provides the first evidence that HtrA2 is required for proper function of the ATP synthase. In the absence of HtrA2, proton entry into the mitochondria was increased (demonstrated by increased mitochondrial hyperpolarisation in response to oligomycin) yet mitochondrial ATP production was reduced (since ATP production in response to extracellular ATP was reduced), suggesting a leak of protons through the ATP synthase. Furthermore, HtrA2 was shown to interact with the ATP synthase, suggesting that it may have a direct modulatory effect. This is not the first evidence of mitochondrial uncoupling through the ATP synthase: mutations in several of the subunits of both the F_1 and F_0 complexes have been shown to have a similar effect. Point mutations in the γ and c subunits of the ATP synthase of *Escherichia coli* have been found to cause intrinsic mitochondrial uncoupling by affecting subunit interactions in the

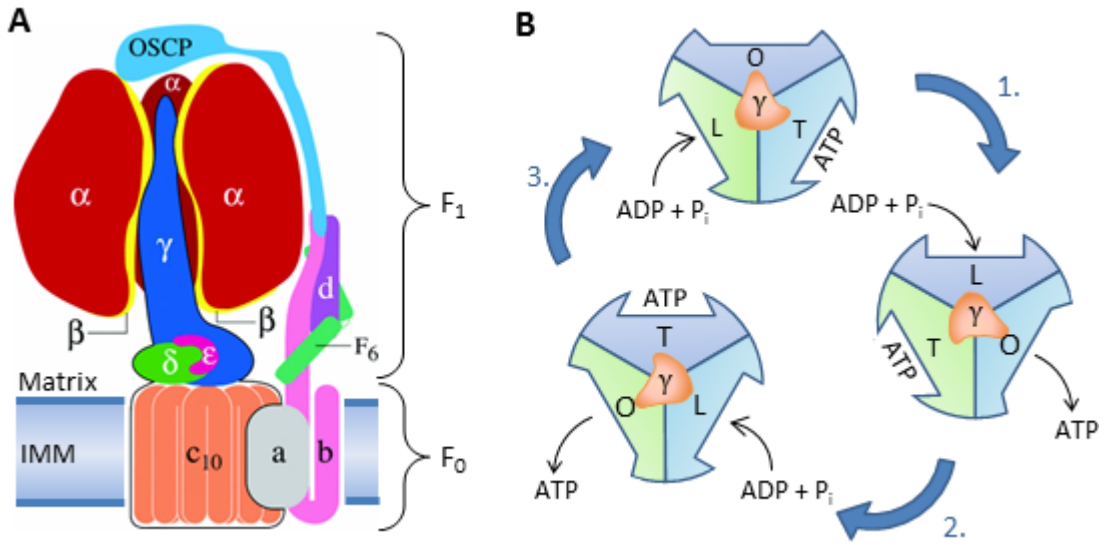

Figure 3.14 ATP synthase structure and function. (A) Holoenzyme of the mammalian F_1F_O ATP synthase, lacking the peripheral F_0 subunits. Modified from (Gledhill and Walker, 2006). **(B)** The 'binding change hypothesis' for ATP production. ADP and P_i enter the catalytic site of the subunit in the 'loose' conformation (L), then rotation of the γ subunit by 120° changes the conformation to 'tight' (T), generating a molecule of ATP (1). A further rotation changes the subunit to the 'open' conformation (O), releasing the ATP (2). The final rotation returns the subunit to its loose conformation to bind another molecule of ADP + P_i (3).

F_1 domain (Shin et al., 1992; Zhang et al., 1994), while in mammalian cells a disease-causing mutation in subunit a of the ATP synthase (encoded by *ATP6*) was shown to result in a proton leak through the ATP synthase (Majander et al., 1997). A recent study found that loss of the anti-apoptotic Bcl2 family protein Bcl-xL also causes uncoupling through the ATP synthase, and in this case an interaction was demonstrated with the F_1 β subunit (Alavian et al., 2011). Finally, the transmembrane regions of subunits e, f, g, A6L and the adenine nucleotide transporter (ANT) have been suggested to form a proton pore across the membrane which is occluded by coupling factor B (Lee et al., 2008), offering an alternative mechanism of uncoupling.

3.3.4. Neuroprotective function of HtrA2

This study aimed to dissect the mitochondrial phenotype of HtrA2 deficiency in order to understand the fundamental neuroprotective function of HtrA2. Loss of HtrA2 was found to lead to mitochondrial uncoupling through the ATP synthase; the question, therefore, is how HtrA2 prevents this uncoupling under normal conditions.

As discussed in section 3.1, a number of studies suggest that HtrA2 functions to degrade unfolded mitochondrial proteins in the intermembrane space as part of a stress response (Moisoi et al., 2009; Papa and Germain, 2011; Radke et al., 2008). One possibility is therefore that the loss of this protein quality control mechanism could result in aberrant forms of the ATP synthase subunits becoming incorporated into the complex and preventing its proper function. On the other hand, there are a number of discrepancies between the data in this chapter and that published in the study by Moisoi and colleagues: most notably, where we observe an increase in oxygen consumption in isolated mitochondria, they show a reduction concomitant with an accumulation of unfolded mitochondrial proteins. The major experimental difference is the age of the animals used: where this study used mitochondria isolated from the brains of mice aged P18 (presymptomatic), theirs used mice aged P30 (after development of the phenotype). This implies that the defect observed in this study precedes the role of HtrA2 in the mitochondrial unfolded protein response, with the increase in cytosolic ROS potentially contributing to the subsequent accumulation of damaged and misfolded mitochondrial proteins and consequent impairment in respiration. Consistent with this hypothesis, upregulation of CHOP (a transcription factor upregulated as part of the integrated stress response) in HtrA2 KO mice was shown to begin only at P15 in the basal ganglia and did not reach the cerebellum until P28 (Moisoi et al., 2009). Furthermore, the identification of

the F_1 α subunit in HtrA2-TAP complexes suggests that HtrA2 may have a more direct and specific effect on the ATP synthase complex, in addition to this more general role in response to mitochondrial stress.

There are a number of possible mechanisms by which HtrA2 could directly affect ATP synthase function. As a protease, one possibility is that HtrA2 could be responsible for the processing of one or more subunits of the ATP synthase as they pass through the IMS (figure 3.15a). Interestingly, two studies in yeast have independently identified a metalloprotease of the IMS as being responsible for cleavage of the N-terminal 10 kDa leader sequence of Atp6 (F_0 subunit a). The same protein, named Atp23 in yeast, also acts as a chaperone to mediate the assembly of mitochondrially translated Atp6 into the F_0 complex (Osman et al., 2007; Zeng et al., 2007). HtrA2 could feasibly perform a similar subunit processing role in mammalian cells, and it has additionally been shown to have a protease-independent chaperone activity in preventing amyloid β oligomerisation (Kooistra et al., 2009), raising the possibility that it could directly participate in complex assembly.

An alternative possibility is that HtrA2 could act in a protease-independent manner to prevent mitochondrial uncoupling, by physically blocking the proton leak. Factor B is a matrix metalloprotein which is almost entirely absent from chromatography purified F_1F_0 ATP synthase but increases the efficiency of ATP production 2.5-fold when reconstituted with the ATP synthase *in vitro*, leading some to consider it a subunit of the ATP synthase (reviewed by Belogrudov, 2009). Crystallography studies suggest that factor B increases coupling at the ATP synthase by occluding a second proton-translocating pathway composed of the transmembrane domains of subunits e, f, g, A6L and the ANT (Lee et al., 2008). Potentially HtrA2 could act in a similar way but block the pathway from the IMS side (figure 3.15b).

Figure 3.15 Mechanisms by which HtrA2 could protect against uncoupling through the ATP synthase. (A) HtrA2 may be required to process and/or chaperone one or more subunits of the ATP synthase, in this case the F_0 a subunit (green). The subunit peptide sequence is translated by mitoribosomes in the matrix and simultaneously inserted into the inner mitochondrial membrane. HtrA2 on the IMS side of the membrane could cleave the leader sequence from the peptide (1) and may act as a chaperone to ensure correct folding of the peptide (2) and assembly into the complex (3). Figure adapted from (Osman et al., 2007). **(B)** HtrA2 may physically block a second proton-translocating pathway formed by subunits A6L, e, f, g and the adenine nucleotide transporter (ANT). Figure based on (Wang and Oster, 1998) and (Gledhill and Walker, 2006). Topology of putative proton pore based on crosslinking experiments described in (Belogrudov et al., 1996).

3.3.5. Conclusions

In summary, this study has shown that the mitochondrial depolarisation previously described in HtrA2 KO MEFs occurs to a greater extent in primary neurons, particularly midbrain neurons, and that it is observed in combination with an increase in mitochondrial respiration. This indicates a severe mitochondrial uncoupling which was confirmed by a dramatic reduction in respiratory control ratio in isolated brain mitochondria. The proton leak described occurs through the ATP synthase, since proton entry through the synthase is increased but ATP production by the synthase is decreased, and HtrA2 interacts with the complex suggesting that it may have a direct modulatory effect. Finally, uncoupling in HtrA2 deficient mitochondria results in a severe depletion of ATP which is not sufficiently compensated for by upregulation of alternative pathways, rendering HtrA2 KO neurons vulnerable to conditions in which respiration is inhibited. This vulnerability may explain the neurodegeneration observed in HtrA2 KO mice *in vivo*. A schematic highlighting the major points outlined above is shown in figure 3.16.

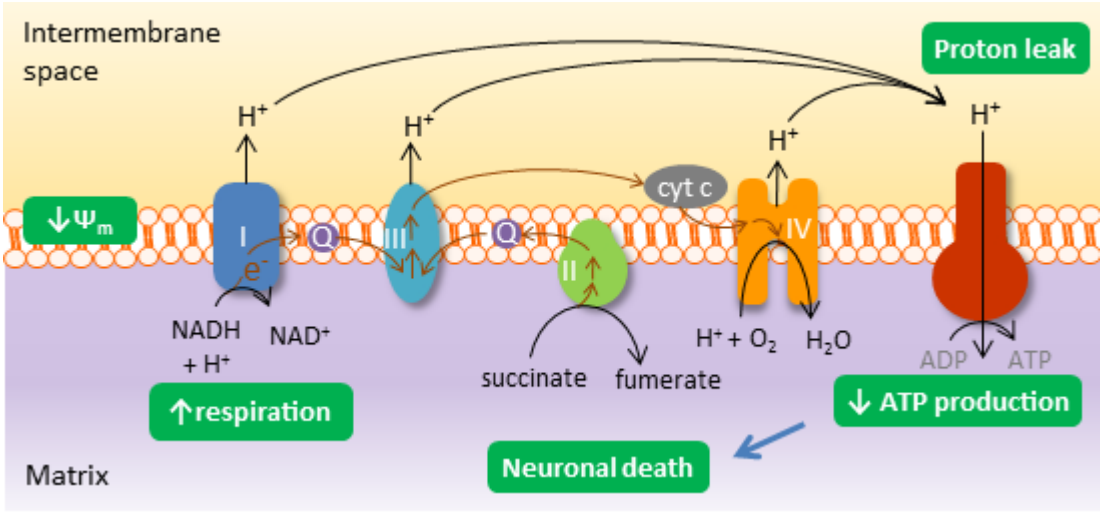

Figure 3.16 Summary of the mitochondrial effect of HtrA2 deficiency.

3.3.6. Future perspectives

The work presented in this chapter represents the first link between HtrA2 and the F_1F_0 ATP synthase. While this is interesting in understanding the function of HtrA2 and therefore the mechanism underlying HtrA2-linked neurodegeneration, it may have additional importance in improving our understanding of the ATP synthase. The ATP synthase is the most highly expressed protein complex of the mitochondrial inner

membrane and accounts for the majority of the ATP produced in a healthy neuron (Vander Heiden et al., 2009), yet despite this only a handful of modulators of its function have been identified (Johnson and Ogbi, 2011). Further work is needed to identify how HtrA2 mediates its effect on the ATP synthase. In the first instance, it is important to determine whether the effect is protease-dependent, indicating that HtrA2 is required either for the specific processing of a subunit or associated protein of the ATP synthase or for a non-specific unfolded protein quality control mechanism, or whether it is independent of protease function, suggesting that HtrA2 might physically block the proton leak or that it might act as a chaperone similar to its bacterial homologue, DegP. This could be determined by generating HtrA2 KO MEFs stably overexpressing either WT or protease dead HtrA2; however, our data shows that the mitochondrial defect is far more severe in HtrA2 KO primary neurons than in MEFs. Lentiviral transduction could instead be used to introduce WT or protease dead HtrA2 into primary neurons, or an elegant solution would be to repeat the experiments in primary cultures from *mnd2* mice, which carry a spontaneous mutation in HtrA2 which ablates protease function (Jones et al., 2003).

If the coupling effect of HtrA2 is protease-independent, it would also be interesting to know whether it is reversible. In the case of factor B, a pair of cysteine residues located close to the N-terminal helix has the potential to form a disulphide bridge under oxidising conditions (Lee et al., 2008). In this oxidised state factor B has a 3-fold lower affinity for the ATP synthase (Belogrudov, 2009), suggesting that under conditions of oxidative stress factor B may dissociate from the synthase to provide a rapid mechanism of uncoupling to reduce mitochondrial ROS production. HtrA2 is phosphorylated on two serine residues in response to the MEKK3/p38 stress pathway, resulting in activation of its protease function (Fitzgerald et al., 2012; Plun-Favreau et al., 2007). Potentially this activation could involve a conformational change along the lines of that described for factor B, resulting in its dissociation from the ATP synthase.

Assuming the effect of HtrA2 on the ATP synthase is specific and not simply the effect of a failure of mitochondrial protein quality control, a key question is which subunit(s) of the ATP synthase HtrA2 interacts with. Although the data in figure 3.11 shows that HtrA2 interacts with the F_1 α subunit, this should only be taken as evidence of interaction with the complex as a whole since the synthase would be expected to immunoprecipitate as a complex. Using *in vitro* immunoprecipitation to detect a direct interaction would also be difficult as expressing one subunit independently of the rest of the complex may allow

interactions to occur which *in vivo* would be physically prevented by other subunits. In one study an interaction between Bcl-xL and the β subunit was demonstrated by overexpressing FLAG-tagged ATP synthase subunits and immunoprecipitating using FLAG beads (Alavian et al., 2011), although this again has the danger that overexpressing a single subunit of the ATP synthase might interfere with complex formation and therefore affect physiological interactions. Alternatively, a photocross-linking approach has previously been successfully used to identify the subunits of the ATP synthase in proximity to the N-terminal α-helix of factor B (Belogrudov, 2008). The approach requires replacing a tryptophan residue with the unnatural photoreactive amino acid *p*benzoyl-L-phenylalanine (*p*Bpa), which forms cross-links with neighbouring proteins when exposed to UV light. In the study described, bacterially generated photoreactive factor B was UV-irradiated in the presence or absence of F_1F_O ATP synthase purified from bovine mitochondria, then cross-linked products were separated by electrophoresis and probed by western blot or identified by mass spectrometry. A similar approach could potentially be applied to investigate HtrA2 binding to the ATP synthase, although without knowing which domain of HtrA2 mediates the interaction it would be necessary to generate several mutants with photoreactive *p*Bpa sites at various sites on the protein surface.

Whether as a necessary participant in the correct assembly of the ATP synthase or a modulator of mitochondrial coupling under stress conditions, it is clear that HtrA2 has an important and previously undiscovered role in ATP synthase function. Further work in this area thus has the potential not only to improve our understanding of HtrA2 and the mechanisms underlying the neurodegeneration in mice, but also to improve our understanding of the ATP synthase. As the primary source of ATP, particularly in the brain, the ATP synthase is of increasing therapeutic interest (Johnson and Ogbi, 2011). If HtrA2 acts as a modulator, rather than an assembly factor, elucidating the mechanism by which it modulates ATP synthase function could therefore have enormous therapeutic value.

Chapter 4

An shRNA screen to investigate the roles of PD-associated genes in mitochondrial function

4.1. Introduction

In the last chapter, live cell imaging approaches were used to investigate the mitochondrial phenotype of HtrA2 deficient cells, revealing a novel role for this protein in ATP synthase function. This chapter will follow on from that work by investigating the mitochondrial functions of other genes associated with PD, using RNA interference (RNAi) to silence each gene in cultured cells and then using similar techniques to assess the effect on mitochondrial function. Issues of study design, optimisation and development will be discussed throughout.

As discussed in section 1.1.5, scientific understanding of the mechanisms underlying idiophathic PD has been significantly furthered in the last two decades by the discovery of genetic mutations which cause familial forms of the disease. The proteins encoded by these genes have been implicated in a wide variety of cellular processes associated with PD pathogenesis (Farrer, 2006) such as proteasomal dysfunction, protein aggregation or oxidative stress. In particular, an increasing body of evidence has linked mitochondrial dysfunction to the disease (see section 1.3).

Of the 11 PARK genes, only two are known to encode proteins with a mitochondrial targeting sequence: *PINK1* (Valente et al., 2004) and *HtrA2* (Strauss et al., 2005). Despite this, a number of other proteins encoded by these genes have been linked to mitochondrial function: most notably Parkin, which has been found to function in a common pathway with PINK1 (Clark et al., 2006; Park et al., 2006). Furthermore, it increasingly appears that pathways can impact on each other: for example, mitochondrial dysfunction increases ROS production, which damages proteins and causes them to aggregate, overloading the proteasomal degradation system (Abou-Sleiman et al., 2006). It therefore seems likely that other PD-associated proteins may be directly or indirectly required for mitochondrial function.

RNAi was chosen as a method for investigating this hypothesis as it has been routinely used in screens of up to tens of thousands of genes to systematically reduce the expression of each gene and investigate the physiological consequences (reviewed by (Campeau and Gobeil, 2011). This non-hypothesis-driven approach enables the identification of unexpected hits, opening up new paths of research (Hirsch, 2010; Wolters and MacKeigan, 2008). By applying a similar approach to a smaller, more focused screen, it was thus hoped that novel roles in mitochondrial function would be identified for one or more proteins genetically associated with PD. Due to experimental issues it was not possible to complete the optimisation stages of this study in the time available; possible reasons for these difficulties, potential solutions and alternative approaches will be discussed in section 4.3.

4.1.1. Study design

4.1.1.1. Selection of RNAi approach

RNAi may be divided into three categories: micro RNAs (miRNAs), which are the cell's endogenous mechanism for regulating gene expression (Lagos-Quintana et al., 2001), small interfering RNA (siRNA), and short hairpin RNA (shRNA), both of which are exogenous nucleotides which use the cell's endogenous system to mediate silencing of a target gene. Both siRNA and shRNA act through the same mechanism, but siRNA is a double-stranded RNA sequence which mimics the processed miRNA (Carthew and Sontheimer, 2009), while shRNA is introduced to the cell in a DNA vector whereupon it is transcribed by the Pol III RNA polymerase and processed to siRNA through the same mechanism as endogenous miRNAs (Brummelkamp et al., 2002b; Paddison et al., 2002a).

Both siRNA and shRNA have advantages and disadvantages. siRNA is a popular choice for individually arrayed screens (one gene silenced per well, e.g. (Brass et al., 2008)) as transfection is quick, effective and can easily be automated for use in high throughput screens. On the other hand, because shRNA is encoded on a DNA plasmid it has greater flexibility: where siRNA-mediated gene silencing only lasts a few days before the siRNA is degraded, shRNA can integrate into the genome of the target cell to mediate stable knockdown (Brummelkamp et al., 2002a; Paddison et al., 2002b), which can be important for proteins with long half-lives (Kok et al., 2009). shRNA can be packaged into virus for transduction of hard to transfect cells such as primary neurons (e.g. (Hayashi-Takagi et al., 2010); discussed further in section 4.2.1), and it has been suggested that shRNA sequences are less prone to off-target effects than siRNA sequences (Rao et al., 2009). Finally, an shRNA construct can include additional genes such as fluorescent markers or antibiotic resistance elements which are co-expressed with the hairpin, enabling identification of transfected or transduced cells. For these reasons, shRNA was selected as the method of RNAi in this study.

Numerous shRNA libraries are commercially available, offering different combinations of selection markers and fluorescent labels in either stable or inducible systems. The Open Biosystems pGIPZ human lentiviral library was chosen because the pGIPZ vector included both a GFP marker, enabling cells expressing the hairpin to be identified in live cell imaging assays, and a puromycin resistance gene, offering the flexibility of producing stable knockdown cell lines at later stages in the project.

4.1.1.2. Selection of genes for inclusion

All genes with a documented association with PD, whether through linkage analysis or association studies, were included in the screen. These included all 11 identified PARK genes, even those whose link to PD has been disputed: *UCHL-1* (Healy et al., 2006), *HtrA2* (Simon-Sanchez and Singleton, 2008) and *GIGYF2* (Bras et al., 2009). *GBA* was also included as heterozygous mutations have been shown to be a significant risk factor for PD and dementia with Lewy bodies (Lwin et al., 2004). Although *NPC1* and *PANK2* have not been associated with PD, mutations in both underlie diseases for which Lewy body pathology has been reported (Arawaka et al., 1998; Saito et al., 2004) and some scientists have suggested that in order to identify common pathogenic mechanisms in PD the pathology of the disease, rather than the clinical symptoms, should be considered paramount (Bras et al., 2008; Hardy et al., 2009). Finally, at the time of study design

genome-wide association studies (GWAS) had identified common variants in two genes as increasing risk for PD: *SCNA* (*PARK1/4*) and *MAPT* (Edwards et al., 2010; Satake et al., 2009; Simon-Sanchez et al., 2009). *MAPT*, encoding the protein tau, was therefore additionally included. Table 4.1 summarises the genes included, the proteins they encode and the reason for their selection. *HtrA2* and *PINK1* were chosen as positive controls because previous work has shown that cells lacking either protein have a clear mitochondrial phenotype (Gandhi et al., 2009; Martins et al., 2004; Wood-Kaczmar et al., 2008; chapter 3).

Gene	Reason for selection
α-syn (PARK1/4)	PARK genes
Parkin (PARK2)	
UCLH1 (PARK5)	
PINK1 (PARK6) *	
DJ-1 (PARK7)	
LRRK2 (PARK8)	
ATP13A2 (PARK9)	
GIGYF2 (PARK11)	
HtrA2 (PARK 13) *	
PLA2G6 (PARK14)	
FBXO7 (PARK 15)	
GBA	Genes associated with Lewy body disorders
NPC1	
PANK2	
MAPT (Tau)	Genome-wide association studies

Table 4.1 Genes included in the screen. * indicates positive control.

4.1.1.3. Selection of cell model

The cell line selected for this study was the human dopaminergic neuroblastoma cell SH-SY5Y. This is by far the most common cell model for PD research because it more closely models a dopaminergic neuron than other immortal cell lines such as HEK293T cells, but is relatively cheap and easy to manipulate compared to primary neuronal lines such as the ReNcell human neuronal progenitor cell from Millipore.

4.1.1.4. Selection of readouts

Five readouts were selected for this screen with the intention that, in combination, they would give an insight into the mechanism underlying the mitochondrial phenotype. These were as follows: mitochondrial membrane potential ($\Delta\Psi_m$); cytosolic and mitochondrial ROS production; oxygen consumption in whole cells; and basal mitochondrial calcium levels ($[Ca^{2+}]_m$).

- **$\Delta\Psi_m$** is an important indicator of mitochondrial bioenergetic function, since generation of ATP by the ATP synthase depends on this potential across the IMM (Alberts et al., 2002). Lower $\Delta\Psi_m$ also predisposes mitochondria to opening of the PTP (Rasola and Bernardi, 2007; see section 1.2.5), an important route of cell death due to mitochondrial dysfunction. $\Delta\Psi_m$ is measured using the membrane-permeable cationic dye TMRM, which is taken into mitochondria in a $\Delta\Psi_m$-dependent manner (Scaduto and Grotyohann, 1999). TMRM fluorescence can then be measured by confocal microscopy (see methods).

- **Mitochondrial and cytosolic ROS production** are both indirect indicators of mitochondrial function, but are informative in combination with other assays. A major source of ROS in both the mitochondria and the cytosol is the mitochondrial ETC, which releases superoxide into the matrix at complex I (Kushnareva et al., 2002) and into the cytosol at complex III (Chen et al., 2003) (see section 1.2.2). Damage to the respiratory chain can significantly increase ROS production at either complex by impairing electron transfer between the complexes, resulting in a leakage of electrons (Balaban et al., 2005). Other factors to affect ROS production include $\Delta\Psi_m$: mitochondrial depolarisation reduces ROS production (Korshunov et al., 1997), so the reduction in mitochondrial ROS combined with reduced $\Delta\Psi_m$ observed in HtrA2 KO mice is consistent with a mitochondrial uncoupling defect (chapter 3). Either a significant increase or decrease in mitochondrial ROS production should therefore be considered a hit in the screen. Mitochondrial dysfunction can also increase cytosolic ROS, either directly by increasing superoxide production at the ETC, or indirectly due to altered mitochondrial calcium handling leading to calcium-induced activation of NADPH oxidase (Gandhi et al., 2009). Although both assays should be interpreted with caution, they were included in the screen because they are robust, simple assays which could be optimised for use with a high throughput system (section 4.2.3). Cytosolic or mitochondrial ROS production can be measured by loading the cells with either dihydroethidium (DHE) or its mitochondrially targeted derivative, mitoSOX. DHE and mitoSOX are oxidised by ROS to ethidium or mito-ethidium which are

fluorescent in the red spectrum, enabling oxidation of the probe to be monitored over time by fluorescent microscopy. The rate of increase in fluorescence is indicative of ROS levels.

- The **rate of oxygen consumption** is a direct indicator of the rate of mitochondrial respiration. A decrease in basal oxygen consumption thus suggests impaired respiration as in the case of PINK1 deficiency (Gandhi et al., 2009), while an increase can indicate mitochondrial uncoupling as in the case of HtrA2 deficiency (chapter 3). Furthermore, addition of the mitochondrial toxins oligomycin (an inhibitor of the ATP synthase) and FCCP (a mitochondrial uncoupler) can provide further information as described in the last chapter. Oxygen consumption can be measured in trypsinised cells using a Clark oxygen electrode, or in cultured cells in a 24 well plate using a Seahorse Extracellular Flux Analyser. The latter enables oxygen consumption to be measured in a higher throughput manner, but this would still be a highly labour-intensive readout. Consequently oxygen consumption was selected for the screen but it was decided that it would only be used to investigate genes that had already been shown to affect $\Delta\Psi_m$, thus reducing the number of constructs to be tested.

- Finally, $\mathbf{[Ca^{2+}]_m}$ was selected as a readout for the screen because calcium toxicity is a major route of neuronal death and mitochondrial calcium mishandling is frequently implicated in that process (see section 1.2.3). It can measured indirectly using the cytosolic calcium indicator Fura-2, by first adding the SERCA (sarcoplasmic/endoplasmic reticulum calcium ATPase) inhibitor thapsigargin in calcium-free medium to empty the ER, and then adding the ionophore ionomycin to release calcium from the sole remaining intracellular store: the mitochondria (Abramov and Duchen, 2003). Because this requires the addition of compounds at variable intervals, it would be very difficult to optimise for high throughput. Like oxygen consumption, it was therefore decided that mitochondrial calcium would be assessed only for those genes that had already shown an effect on $\Delta\Psi_m$.

The selected readouts are summarised in table 4.2 overleaf.

	Method	Physiological relevance	Hit definition	Positive controls
$\Delta\Psi_m$	Microscopy – TMRM	Indicates bioenergetic function	Decrease	Decreased
cROS	Microscopy – DHE	Can indicate broad mitochondrial dysfunction	Increase	Increased
mROS	Microscopy – mitoSOX	Indication of respiratory chain function/ dysfunction	Increase or decrease	HtrA2 decreased; PINK1 increased
O_2 consumption	Respirometry – Clark electrode /Seahorse	Indicates basal, min and max respiration	Increase or decrease	HtrA2 increased; PINK1 decreased
Basal $[Ca^{2+}]_m$	Microscopy – Fura-2	Common factor in neuronal pathology	Increase or decrease	HtrA2 unknown; PINK1 increased

Table 4.2 List of mitochondrial readouts. Abbreviations: $\Delta\Psi_m$, mitochondrial membrane potential; cROS, cytosolic reactive oxygen species; mROS, mitochondrial reactive oxygen species; $[Ca^{2+}]_m$, mitochondrial calcium; TMRM, tetramethylrhodamine methylester; DHE, dihydroethidium.

4.1.1.5. Hit validation

Any hits from the screen would need to be validated to ensure that the phenotype is due to silencing of the target gene and not an off-target effect. In large scale RNAi screens this is most commonly achieved through redundancy: by testing multiple si/shRNA sequences against a target gene and verifying that the phenotype correlates with the degree of gene silencing (Kassner, 2008). In the original plan for this study, it was intended that each gene would be silenced using a pool of four shRNA constructs; however, as will be discussed in this chapter there was too much variability in knockdown using pools of shRNA for this approach to be used, requiring individual constructs to be used throughout. An advantage to this system is that redundancy is already built in, as any phenotype only caused by one of the four constructs targeting a single gene can immediately be disregarded as an off-target effect. Any genes identified as 'hits' in the screen would then be validated initially by assessing the level of silencing produced by each of the four shRNA sequences. Finally, the 'gold standard' of hit validation is rescue (Kassner, 2008), whereby cells expressing shRNA are transfected with cDNA of the gene of interest containing silent mutations in the shRNA target sequence to prevent its degradation. If the observed phenotype is real, it should be possible to reverse it by expressing the WT protein.

4.1.1.6. Intended workflow

Figure 4.1 (overleaf) shows the planned workflow for the screen, from optimisation to validation. In order to maximise the sensitivity of the screen it was necessary to optimise both the shRNA delivery system, to achieve the best possible knockdown, and the readouts, to ensure they were robust. The first round of hit identification would then be performed in 96 well plates using a high content imaging system in collaboration with Eisai Pharmaceuticals. In this round, all the shRNAs would be tested for effects on $\Delta\Psi_m$, cytosolic and mitochondrial ROS. Any hits, defined as shRNAs which produced a significant effect in these readouts, would then be carried forward to the second round of testing where they would be assayed for oxygen consumption using the 24 well Seahorse respirometer and $[Ca^{2+}]_m$ using a standard fluorescent microscope. Hits would be validated by verification of knockdown as described in section 4.1.1.5. One or more hits could then be followed up by using more focused experiments to investigate the mechanisms underlying the phenotype, as shown for HtrA2 in the previous chapter.

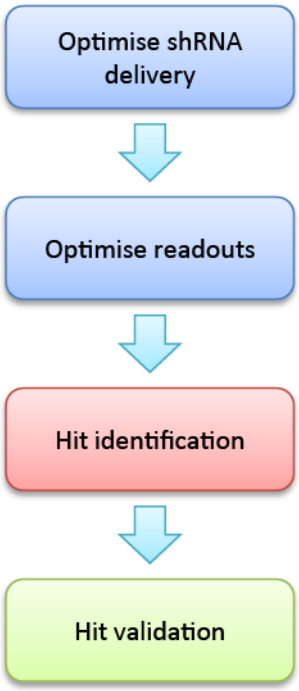

Figure 4.1 Schematic of the intended workflow.

4.2. Results

4.2.1. Transfection of cells with shRNA

The shRNA vector chosen for this screen was designed to be introduced into the cell either by transient or stable transfection, or by lentiviral transduction. Transient or stable transfection involves the use of a cationic lipid which aggregates with the DNA to facilitate its transfer across the plasma membrane (Felgner et al., 1987). In the majority of cells, this DNA does not integrate into the genome and so expression of the shRNA only lasts three to five days (transient transfection), after which time the DNA is either diluted out by mitosis or degraded. In some cells, however, the introduced DNA is integrated into the host genome by random recombination, and by treating the transfected cells with the appropriate antibiotic over at least 10-14 days, it is possible to select only those cells which stably express the construct (stable transfection). These cells may be maintained as a pool, or clonal cell lines may be generated by separating them into single cells and expanding them. Finally, viral transduction requires packaging the construct into a lentiviral particle which infects the target cell and integrates the DNA into the genome, producing stable cell lines without the need for antibiotic selection.

Each of these methods has both advantages and disadvantages. The primary advantage of transfection, particularly transient transfection, is that it is very quick: cells transfected on day 0 can be assayed on day 3. A disadvantage, however, is that not all cell types are equally transfectable and SH-SY5Y cells are relatively resistant to transfection, with typical transfection efficiencies around 40%. Viral transduction, on the other hand, is efficient even in very difficult to transfect cells such as primary neurons (Naldini et al., 1996), but is time-consuming to optimise and carry out and is subject to greater regulation by the Health and Safety Executive (HSE).

Given the technical challenges inherent in lentiviral transduction, the decision was taken to start by using transient transfection. It was therefore necessary to optimise seeding density, transfection reagent and DNA concentration to maximise transfection efficiency.

4.2.1.1. Optimisation of transfection conditions

The majority of the mitochondrial assays chosen for this study used live cell imaging approaches, enabling transfected cells to be selected visually using GFP expression as a marker. However, this meant that it was essential that cells were well separated to allow the signal from a transfected cell to be distinguished from its untransfected neighbour. Cell seeding density was therefore optimised to result in a final confluency of approximately 80%, which meant transfecting the cells when they were approximately 50% confluent. This is substantially lower than the recommended confluency for any of the available transfection reagents, so it was necessary to test a range of transfection reagents with varying quantities of shRNA construct to maximise the number of transfected cells. Transfection efficiency was estimated using a fluorescent microscope to check cells for GFP expression.

Six transfection reagents were tested with quantities of empty vector DNA ranging from 0.1 µg to 1 µg per well of a 24 well plate. These were: Arrest-In; Lipofectamine 2000; GeneJuice; DharmaFect; Effectene and Fugene 6. The results are summarised in figure 4.2a overleaf. Transfection with Arrest-In, Lipofectamine 2000 or GeneJuice resulted in no GFP-positive cells two days after transfection. Some cells transfected with DharmaFect were GFP-positive but almost all of those were dead, indicating high toxicity. Transfection with Fugene 6 was successful in a small percentage of cells (5%) with the lowest amount of DNA, but was unsuccessful at higher DNA concentrations. By far the most effective transfection reagent was Effectene, which gave transfection efficiencies up to 25% at the highest DNA concentration. These conditions were scaled up to a 6 well plate (a two-fold increase in quantity of transfection reagent and buffers) by testing DNA concentrations from 1 to 5 µg per well. Optimal conditions were achieved using 3 µg DNA per well, which produced the maximum number of GFP-positive cells without affecting cell morphology or resulting in high levels of cell death (figure 4.2b).

A

	0.1 ug	0.2 ug	0.25 ug	0.35 ug	0.5 ug	1 ug
Arrest-In	0%					
Lipofectamine 2000	0%					
GeneJuice	0%					
DharmaFect	Some green cells, almost all dead					
Effectene	0%	2%	2%	5%	10%	25%
Fugene6	5%	0%				

B

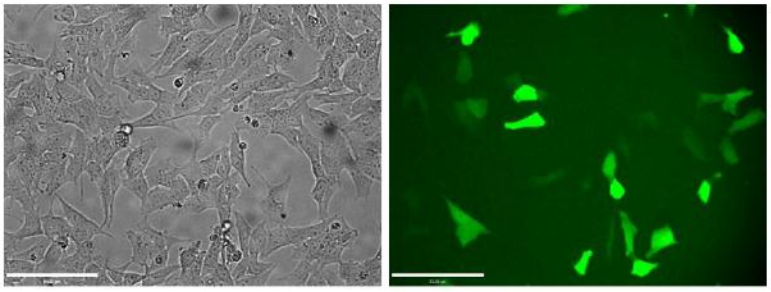

Figure 4.2 Optimisation of transfection conditions. (A) Results of transfection optimisation for transfection reagent and quantity of DNA. Percentages indicate the estimated percentage of cells that were positive for GFP when viewed using a fluorescent microscope. **(B)** A bright-field and a fluorescent image showing cells transfected using optimised conditions in a 6 well plate. Scale bar 85 µm. Image obtained using a 20x objective and a 490 nm filter.

4.2.1.2. Measurement of $\Delta\Psi_m$ and cytosolic ROS production

The data shown in chapter 3, in agreement with previous studies (Kieper et al., 2010; Martins et al., 2004; Moisoi et al., 2009; Plun-Favreau et al., 2007), demonstrated that cells derived from *HtrA2* KO mice have significantly lower $\Delta\Psi_m$ than cells derived from their WT littermates. Similarly, PINK1 deficient cells have been repeatedly shown to have depolarised mitochondria compared to controls (Exner et al., 2007; Gandhi et al., 2009; Gautier et al., 2008; Gegg et al., 2009; Wood-Kaczmar et al., 2008). It was therefore expected that SH-SY5Y cells transfected with pools of shRNA constructs targeting either *HtrA2* or *PINK1* would have significantly lower $\Delta\Psi_m$ than cells transfected with either the empty vector or a non-targeting shRNA sequence (scrambled). Cells were transfected according to the optimised conditions and TMRM used to measure $\Delta\Psi_m$ as previously described. Although mitochondrial depolarisation was observed on some occasions, the data were very inconsistent and over three independent experiments no significant reduction in $\Delta\Psi_m$ could be detected in cells transfected with shRNA against either gene (figure 4.3)

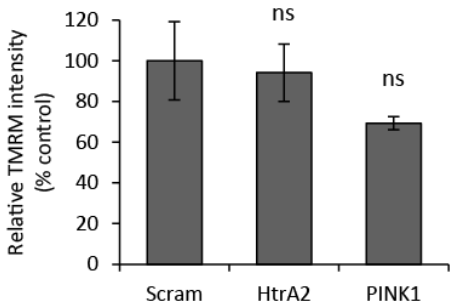

Figure 4.3 Mitochondrial membrane potential in transfected SH-SY5Ys. Relative TMRM intensity is shown for SH-SY5Y cells transfected with scrambled control shRNA (Scram) or pools of shRNA constructs targeting either HtrA2 or PINK1. Histograms indicate mean ± S.E.M. ns, not significant vs. control.

Since shRNAs targeting *HtrA2* and *PINK1* did not have the expected effect on $\Delta\Psi_m$, a second readout was tested. Several studies have also previously reported an increase in cytosolic ROS production in cells lacking either HtrA2 (Kieper et al., 2010; Moisoi et al., 2009) or PINK1 (Gandhi et al., 2009; Wood-Kaczmar et al., 2008) compared to controls. Consistent with these reports, work in the last chapter showed a significant increase in basal cytosolic ROS production in *HtrA2* KO mouse neurons. However, this data could not be recapitulated by transfecting SH-SY5Y cells with shRNA against either gene, as measurement of ROS production using DHE revealed no significant difference between HtrA2 or PINK1 knockdown cells and controls (figure 4.4).

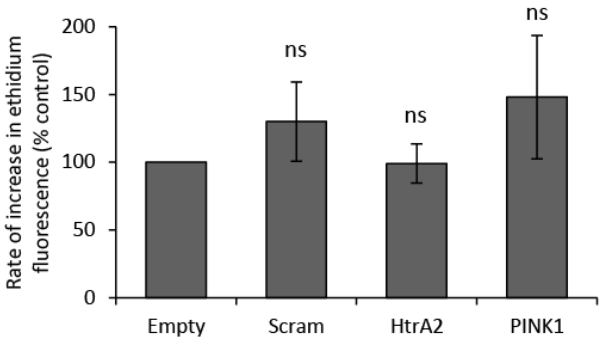

Figure 4.4 Cytosolic ROS production in transfected SH-SY5Ys. Rate of increase in ethidium fluorescence in cells transfected with empty, scrambled (scram), HtrA2 or PINK1 shRNA is shown as a percentage of the rate of increase in empty vector control cells. Histograms indicate mean ± S.E.M. ns, not significant compared to empty control.

4.2.1.3. Knockdown of HtrA2 in transfected SH-SY5Y cells

The absence of a consistent mitochondrial phenotype in cells transfected with shRNA could perhaps be explained by poor knockdown at the protein level. To investigate this, SH-SY5Y cells were transfected with the empty vector, scrambled control shRNA or a pool of shRNA constructs targeting *HtrA2* and selected with puromycin for 48 hr to kill the majority of untransfected cells. The cells were then lysed, electrophoresed and subjected to immunoblotting (figure 4.5) using an anti-HtrA2 antibody which had previously been validated using HtrA2 KO mouse tissue (chapter 3). As previously described, two bands were observed at 37 and 48 kDa, the expected sizes for full length and processed HtrA2, but the upper band was non-specific (appears equally in WT and HtrA2 KO mouse samples, fig 3.2). No striking difference in the bottom band could be observed between the three samples, indicating that the shRNA mediates little or no knockdown of HtrA2 at protein level.

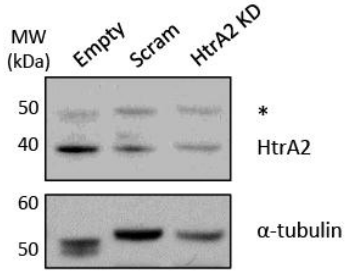

Figure 4.5 HtrA2 protein levels in transfected SH-SY5Y cells. Lysates from cells transfected with an empty vector, scrambled control (scram) or shRNA targeting *HtrA2* (HtrA2 KD) were probed with antibodies against HtrA2 and α-tubulin for loading. * indicates non-specific band.

4.2.1.4. Knockdown of HtrA2 and PINK1 in transfected HEK293T cells

A number of factors can influence the level of protein knockdown by shRNA. One is the sequence of the shRNA: empirical studies have revealed a number of 'rules' of shRNA design which improve gene silencing (Hannon and Rossi, 2004) but there remains a good deal of variation in efficiency between different hairpins. Another important factor is the amount of shRNA taken into the cell. SH-SY5Y are relatively resistant to transfection (Jiang et al., 2006; Jiang et al., 2004a) and so to investigate whether poor transfections account for the poor knockdown, the same experiment was repeated in HEK293T cells, which are more readily transfectable. In all the experiments described thus far, cells were transfected with a pool of four shRNA constructs targeted against *HtrA2* or four against *PINK1*. To determine whether some constructs are more capable of gene silencing than others, HEK293T cells were thus transfected with the empty vector, the scrambled control, the pool of four HtrA2 shRNAs, and with each individual shRNA against *HtrA2*. Probing the HEK293T lysates for HtrA2 revealed significant silencing of HtrA2 protein expression by each of the individual HtrA2 shRNAs (average of 70-80% by densitometry, figure 4.6), suggesting that poor transfection efficiency, and not the hairpin sequence, was the cause of the poor knockdown in SH-SY5Ys. The effect of transfecting the pool of shRNA constructs was highly variable, suggesting that this may also have contributed to the poor knockdown previously observed.

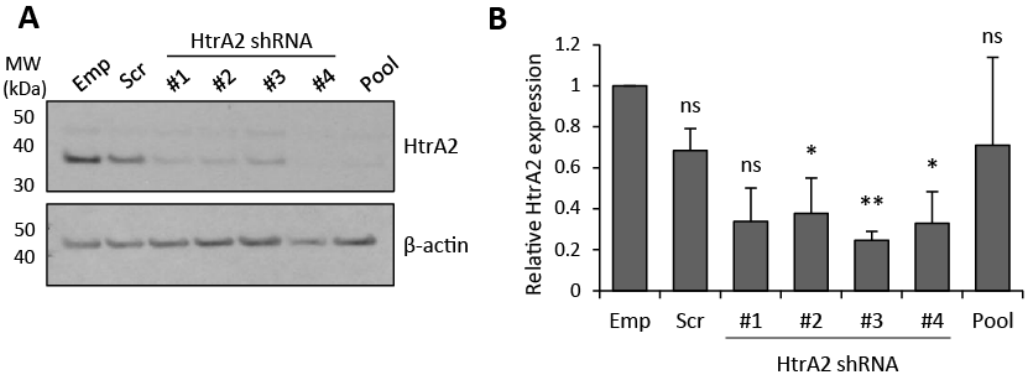

Figure 4.6 HtrA2 protein levels in transfected HEK293T cells. (A) Representative western blot for HtrA2 in cells transfected with empty vector (emp), scrambled control (scr), individual HtrA2 shRNA sequences or a pool of all four shRNAs. β-actin is used as a loading control. **(B)** HtrA2 expression was quantified by densitometry and expressed relative to empty vector control. Histograms indicated mean of three independent experiments ± S.E.M. ns, not significant; * $p < 0.05$, ** $p < 0.005$ compared to empty control.

To confirm the efficiency of shRNA against a different gene, HEK293T cells were also transfected with individual constructs or a pool targeting *PINK1*. Extensive antibody testing by Dr Emma Deas (UCL Institute of Neurology) has shown that none of the currently available antibodies are capable of detecting endogenous PINK1 under basal conditions (Deas et al., 2011). It was therefore necessary to employ a different technique to assess PINK1 knockdown, using quantitative PCR (qPCR) to investigate expression at the mRNA level (figure 4.7). Of the four PINK1 constructs tested, two (#3 and #4) resulted in almost total silencing, while constructs 1 and 2 had much more moderate effects. Once again, transfecting HEK293T cells with a pool of shRNA produced inconsistent results and no significant reduction in *PINK1* mRNA expression overall.

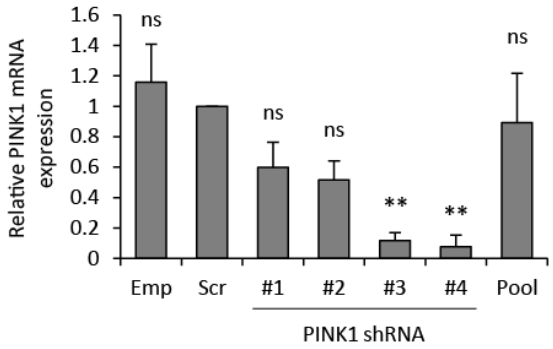

Figure 4.7 *PINK1* mRNA levels in transfected HEK293T cells. *PINK1* mRNA levels were measured by quantitative PCR and expressed relative to scrambled control. Data presented as mean ± S.E.M. ns, not significant; ** $p < 0.005$ vs scrambled control.

4.2.2. Transduction of SH-SY5Y cells with shRNA

Since more efficient knockdown was achieved in a more transfectable cell line, it was hypothesised that increasing shRNA expression in the SH-SY5Y cells by using an alternative approach for shRNA delivery might improve the knockdown efficiency. As discussed in section 4.2.1, one such method for introducing shRNA into the cell is to use lentiviral transduction. This is a more efficient method, enabling more copies of the shRNA sequence to enter the cell (Hwang and Gilboa, 1984) and thus potentially improving knockdown. The decision was therefore taken to move from transfection to viral transduction.

The shRNA constructs are provided in a pGIPZ vector which includes most of the essential lentiviral genes to allow generation of the virus. As a safety precaution, three essential genes, *gag* (encoding structural elements of the virus), *pol* (encoding the reverse polymerase and integrase) and *env* (encoding a surface envelope protein) are not included

in the vector. Cotransfection of a packaging cell line with the shRNA construct and vectors containing these genes (see Methods section 2.5.2) thus enables the production and release of recombinant viral particles which contain the shRNA hairpin, GFP marker and puromycin resistance element incorporated in their genome (Wu et al., 2000). Media containing infectious virus can then be removed from the packaging cells and added to the cells of interest.

4.2.2.1. Optimisation of transduction conditions

An important variable in viral transduction is multiplicity of infection (MOI), which is defined as the number of infectious viral particles added per cell plated. Adding more virus particles would be expected to increase the expression of the shRNA hairpin and therefore increase the level of gene silencing; on the other hand, incorporating several copies into the genome of the target cell increases the likelihood of off target effects and may increase toxicity (An et al., 2006).

To determine the optimal MOI for the screen, an shRNA construct targeting GAPDH was packaged into lentivirus and the harvested media was titered to determine the concentration of infectious viruses (see Methods). This construct was selected because it had been used by the manufacturers of the shRNA library as a positive control for library validation, and was therefore guaranteed to produce effective knockdown (Open Biosystems product literature). SH-SY5Y cells were then transduced at a range of MOIs, cultured without antibiotic selection, and harvested for analysis by flow cytometry and western blot. Flow cytometry was used to accurately determine the percentage of cells expressing GFP (transduction efficiency), while western blot was used to estimate the percentage knockdown at protein level (knockdown efficiency).

Figure 4.8 shows the results of the optimisation for both transduction and knockdown efficiency. The range of MOIs that could be tested was limited by the titre of the virus produced, which could not be concentrated without increasing the risk category according to the HSE. In order to increase the quantities of virus that could be added to the cells, both single and double transductions were tested: in a single transduction the virus was added to the cells for 8-10 hr and then removed, while in a double transduction this process was repeated a second time 24 hr later. For the purposes of the graph in figure 4.8a, two transductions using 2 viruses/cell on consecutive days was considered equivalent to an MOI of 4. Both transduction efficiency (figure 4.8a) and knockdown (figure 4.8b) were improved at higher MOIs, but there was no substantial difference

between the two highest MOIs. The optimal transduction conditions were therefore considered to be a double transduction with 2 viruses/cell (a total MOI of 4).

An unexpected result was that although a double transduction with 1 virus/cell resulted in almost exactly the same percentage tranduced cells as a single transduction with 2 viruses/cell (figure 4.8a), their effects on GAPDH protein levels were not equivalent. A double transduction was substantially more effective at silencing protein expression than a single transduction using twice the virus concentration (figure 4.8b), indicating that the length of time for which the cells are exposed to the virus is an important factor. To determine whether knockdown efficiency could be further improved by even longer exposure to the virus, virus was added to the cells and left on for 24 hr instead of the usual 8-10 hr. This resulted in high levels of cell death (approx. 50% after 24 hr), indicating that prolonged exposure to the virus is toxic. By contrast, very little cell death was observed following two consecutive transductions for 8 hr and the cells appeared morphologically normal (figure 4.8c).

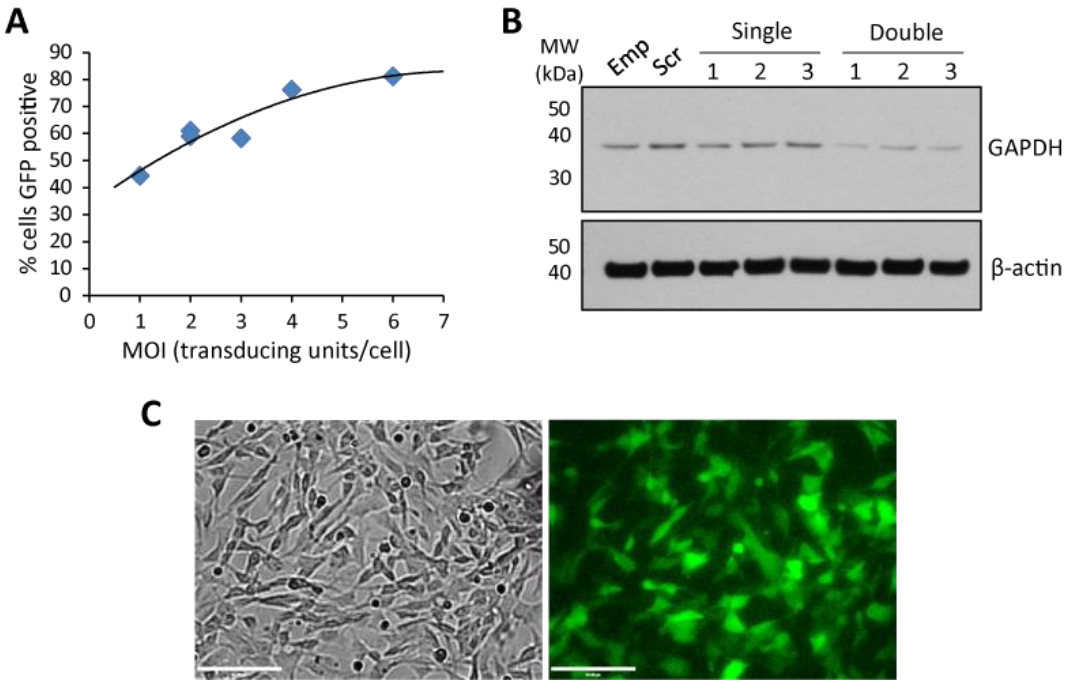

Figure 4.8 Optimisation of multiplicity of infection (MOI). (A) The percentage of cells transduced at varying MOIs was assessed by flow cytometry. A double transduction using an MOI of 2 was considered equal to an MOI of 4. **(B)** WB showing GAPDH expression following either a single or double transduction with an MOI of 1, 2 or 3 viruses/cell. **(C)** A bright-field and a fluorescent image showing cells transduced using the optimised conditions. Scale bar 84 μm.

4.2.2.2. Knockdown of HtrA2 and PINK1 in transduced SH-SY5Ys

To determine whether the issue of poor silencing of *HtrA2* and *PINK1* could be resolved by using viral transduction instead of transfection, SH-SY5Y cells were infected with lentivirus carrying either the empty vector, scrambled control or the individual HtrA2 shRNA constructs. Consistent with the hypothesis, figure 4.9 below shows that HtrA2 protein levels were reduced in cells transduced with each of the four shRNA constructs, with the most efficient silencing achieved using constructs 3 and 4 (approx. 80% knockdown).

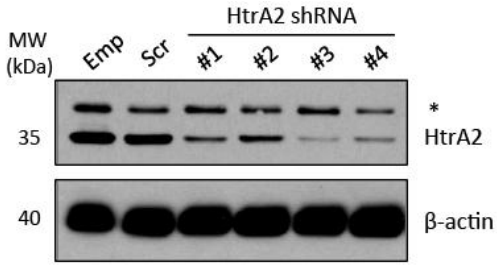

Figure 4.9 HtrA2 protein levels in transduced SH-SY5Y cells. Lysates from cells transduced with empty vector (emp), scrambled control (scr) or HtrA2 shRNA constructs were probed for HtrA2 and β-actin. * indicates non-specific band.

To confirm the findings using a second gene of interest, *PINK1* silencing was again assessed by qPCR. SH-SY5Y cells transduced with shRNA constructs targeting *PINK1* showed consistent and significant silencing of *PINK1* at mRNA level, with knockdown of at least 80% observed for three of the four constructs (#1, 3 and 4; figure 4.10).

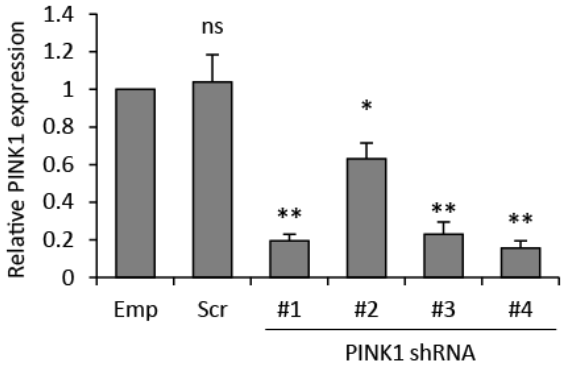

Figure 4.10 *PINK1* mRNA levels in transduced SH-SY5Y cells. *PINK1* mRNA levels were assessed by quantitative PCR relative to empty vector. Histograms indicate mean ± S.E.M. ns, not significant; * $p < 0.05$; ** $p < 0.005$

4.2.3. Optimisation of ROS production for high throughput screening

Having confirmed that shRNA-mediated gene silencing could be achieved in SH-SY5Y cells using viral transduction, the next challenge was to optimise the readouts for higher throughput screening. The use of imaging readouts in large scale screens, termed high content screening, has become possible with the advent of 96- and 384-well microscopes such as the ArrayScan automated microscope from Cellomics. The first readout chosen for optimisation was cytosolic ROS production, as once successfully optimised, it was assumed that similar principles would then be applied to the assay for mitochondrial ROS since both require recording of fluorescence on the red channel over a timecourse. The assay for $\Delta\Psi_m$ was expected to present less of a challenge as it only requires images to be taken at a single timepoint (see section 4.1.1.4 for a description of the assays).

4.2.3.1. Optimisation of seeding conditions

The Cellomics system automatically analyses the images as they are taken, a capability which is invaluable in large screens. In order for the software to differentiate the cells, however, it is essential that they are clearly separated in the wells. Seeding density was therefore optimised by testing a range of cell densities with and without poly-D-lysine (PDL) coating. Optimal cell separation was achieved by seeding at a density of 10,000 cells per well after coating with 25 μg/ml PDL.

4.2.3.2. Optimisation of dye concentration

As described in section 4.1.1.4, measurement of ROS levels by either DHE or mitoSOX involves monitoring the fluorescence of the oxidised products (ethidium or mito-ethidium) over a timecourse. The rate of increase in fluorescence is a function of both the levels of oxidants in the cell and the concentration of dye added. When cytosolic ROS was measured on coverslips in chapter 3 and section 4.2.1.2, DHE was used at a high concentration over a short period (5 min), with measurements taken every 10 s. This is not possible in a 96 well plate as the microscope head must scan each well individually before returning to the first. It was therefore necessary to record over a longer timecourse, using a lower dye concentration in order to avoid saturation of the signal.

To determine the optimal dye concentration, SH-SY5Y cells transduced with either the empty vector, scrambled shRNA, or an shRNA targeting *HtrA2* (construct #2) were loaded with DHE at concentrations of 0.5, 1 and 3 μM and the fluorescence monitored for 3 hr. At

least six replicates of each condition were included in order to estimate intra-plate variation, and the outermost wells were not used and were filled with water to exclude edge effects (Delmas et al., 1993). Representative traces for each concentration of DHE are shown in figure 4.11 below.

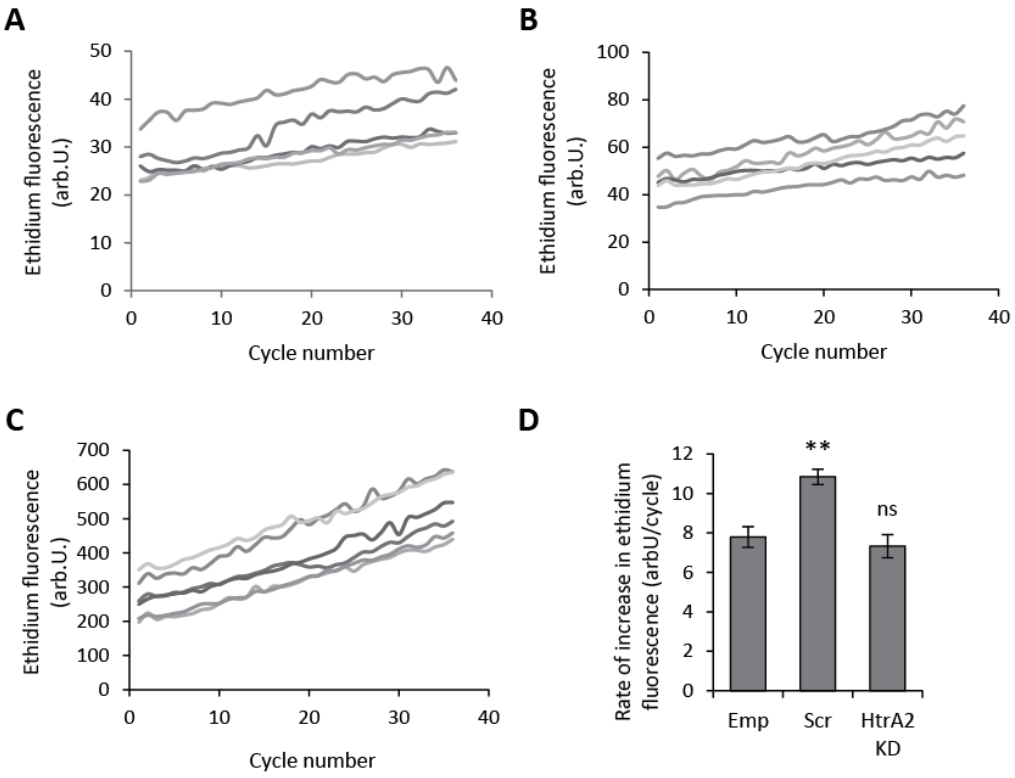

Figure 4.11 Optimisation of DHE concentration for high content analysis. (A-C) Representative ethidium traces are shown for SH-SY5Y cells transduced with empty vector and loaded with DHE at a concentration of 0.5 μM (A), 1 μM (B) or 3 μM (C). **(D)** Mean rate of increase of ethidium fluorescence in cells transduced with empty (emp), scrambled (scr) or HtrA2 shRNA (HtrA2 KD) and loaded with 3 μM DHE. Histograms indicate mean ± S.E.M. ns, not significant; ** $p < 0.005$ compared to empty vector.

In all three cases, DHE fluorescence was found to increase steadily over time, with little fluctuation and no saturation at later timepoints. Each of the graphs above shows five replicates of the same condition and in all cases the lines are parallel, indicating low variability in the rate of increase across the plate. Of the three concentrations, the highest (3 μM) appeared the most suitable as it showed the largest percentage increase in signal over time, with typical values doubling from approx. 200 to 400 units; by contrast, at the lowest concentration of DHE fluorescence only increased from approx. 20 to 25 units. However, analysis of the average rate of increase in ethidium fluorescence did not indicate any increase in cytosolic ROS production in the HtrA2 knockdown cells compared to those

transduced with the empty vector (figure 4.11d). This suggested that either: (i) the cytosolic ROS assay was not sufficiently sensitive using this method and required further optimisation; or (ii) the expected mitochondrial phenotype was not recapitulated in SH-SY5Y cells transduced with HtrA2 shRNA.

4.2.3.3. Verification of ROS production and $\Delta\Psi_m$ in transduced cells

To determine whether the failure to detect a difference in ROS production in the previous experiment was due to a lack of sensitivity in the method, ROS production was again measured on coverslips using a method that previously had been successfully used to demonstrate increased cytosolic ROS in HtrA2 KO mouse neurons compared to WT (fig 3.8). SH-SY5Y cells were transduced with each of the HtrA2 and PINK1 shRNA constructs and the empty and scrambled controls and ROS production measured in three independent experiments. Despite relatively consistent results for all the constructs except HtrA2 shRNA #3, no significant increase in ROS could be detected in cells transduced with any of the constructs compared to controls (figure 4.12).

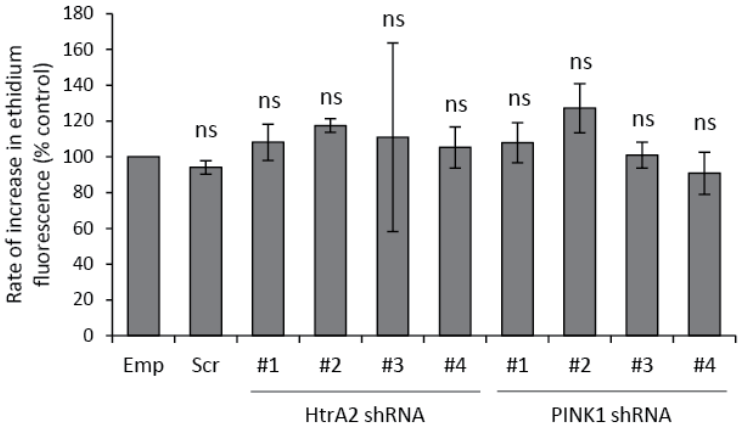

Figure 4.12 Cytosolic ROS production in transduced SH-SY5Y cells. Rate of increase in ethidium fluorescence in cells transduced with empty vector (emp), scrambled (scr) or shRNA against either *HtrA2* or *PINK1*. Values normalised to empty vector control. Histograms indicate mean ± S.E.M. ns, not significant compared to empty vector control.

Despite having demonstrated shRNA-mediated knockdown of both *HtrA2* and *PINK1* in transduced SH-SY5Y cells, the last experiment showed that this level of silencing had no effect on cytosolic ROS production. To investigate the effect of gene silencing on a different assay, $\Delta\Psi_m$ was also measured in two independent experiments (figure 4.13). The results were extremely variable, with little consensus between the two repeats and no correlation between the phenotype and the degree of knockdown: the most convincing

mitochondrial depolarisation was observed in cells transduced with HtrA2 shRNA #2, which was the least effective by western blot (figure 4.9).

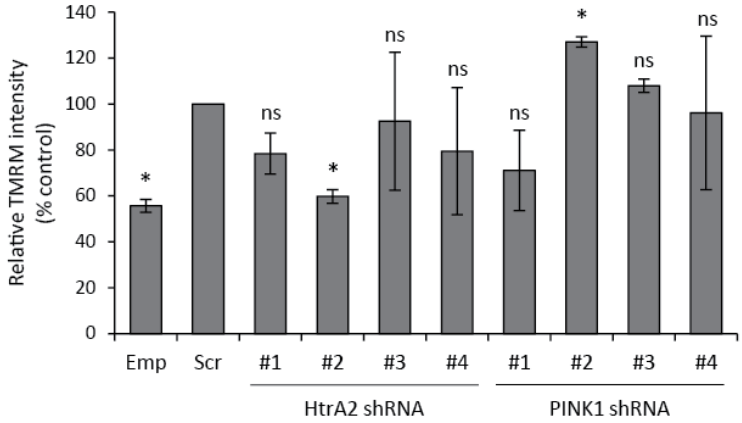

Figure 4.13 $\Delta\Psi_m$ in transduced SH-SY5Y cells. TMRM fluorescence in cells transduced with empty vector (emp), scrambled (scr) or shRNA against either *HtrA2* or *PINK1*. Values normalised to scrambled control. Histograms indicate mean ± S.E.M. ns, not significant; * $p < 0.05$ compared to empty vector control.

In summary, although the work presented in this chapter successfully demonstrated shRNA-mediated silencing of both *HtrA2* and *PINK1* in SH-SY5Y cells, it was unable to recapitulate the expected phenotype in these cells and so further optimisation would still be needed before the screen could be taken to the next stage. These experiments will be discussed in the next section of this chapter.

4.3. Discussion

The aim of this chapter was to design and implement a screen for mitochondrial functions of PD genes by systematically silencing each gene with shRNA and investigating the effect on mitochondrial parameters such as $\Delta\Psi_m$. Due to difficulties in experimental optimisation it was not possible to complete the study in the time available; this section will thus focus on the issues faced and possible solutions, the feasibility of the approach, and the possible outcomes of the screen had it been successful.

4.3.1. shRNA delivery by transfection

In the initial planning stages of this study, transfection was chosen as the method of shRNA delivery because it has previously been shown to mediate effective gene silencing

(Draviam et al., 2007), and avoids the need for viral packaging and titration. In section 4.2.1.1, six different liposomal and non-liposomal transfection reagents were tested with varying amounts of DNA but only one, Effectene, transfected more than a few cells. Why should this be? It is difficult to analyse the difference between the reagents because all were commercially obtained and are therefore patented technologies. However, both Effectene, which transfected up to 25% of cells, and Fugene 6, which transfected some cells (5%) at the lowest DNA quantities, are non-liposomal formulations whereas Lipofectamine 2000 and Arrest-in are both liposome-based technologies and were unsuccessful. This may suggest that SH-SY5Y cells are refractory to liposome-based transfection. It is also important to note that the empty pGIPZ vector is relatively large (11.6 kb) and this may affect lipoplex size and charge ratio, explaining the unusually poor performance of common transfection reagents such as Lipofectamine 2000. The lack of transfection using Arrest-in is surprising, however, because it is sold by Open Biosystems as a reagent specifically intended for use with shRNA and one study has been published in which SH-SY5Y cells were transfected with pGIPZ constructs using this reagent (Ansaloni et al., 2010). One possibility is that the low cell confluency at the time of transfection reduced transfection efficiency in this study.

Although optimising the transfection conditions increased the number of transfected cells, the level of knockdown achieved in SH-SY5Y cells was not sufficient and so the decision was taken to switch to viral transduction. Before taking this decision, however, a number of alternatives were considered and discounted. Electroporation has been shown to be effective in hard-to-transfect cell lines (Jordan et al., 2008), but is prohibitively expensive for even a small screen. Alternatively, cells could have been selected with a high concentration of puromycin or sorted on GFP intensity by fluorescence-activated cell sorting (FACS) with the aim of enriching the population of highly expressing cells, but access to a FACS sorter would again have been too expensive, and selecting cells with high concentrations of puromycin was discounted because puromycin has been shown to increase ROS production (Zent et al., 1995). In retrospect, however, before starting to use viral transduction it would have been worth revisiting the transfection optimisation using individual HtrA2 constructs to confirm that the effect of using a pool of constructs had not confounded the knockdown result (discussed further in the next section). Had knockdown been possible by transfection, it would have saved a considerable amount of time in packaging and titering virus. On other hand, transfection using commercial transfection reagents would have become very expensive if the constructs were used individually, so it

would have been necessary to investigate cheaper transfection methods such as calcium phosphate or polyethylenimine (PEI). These were not considered originally because of concerns over their efficiency and toxicity (Dennig and Duncan, 2002; Regnstrom et al., 2003) – PEI in particular would not be appropriate since PEI-DNA polyplexes have been found to associate with mitochondria and cause mitochondrial depolarisation (Grandinetti et al., 2011).

4.3.2. Pools of shRNA vs individual constructs

An unexpected result of transfecting HtrA2 and PINK1 shRNA constructs into HEK293T cells was the finding that transfecting a pool of four constructs against the same gene resulted in a far more variable knockdown than transfection with individual shRNA constructs (figure 4.6; figure 4.7). The original decision to use pools of constructs had been based on the fact that a number of large scale RNAi screens have used this approach (Berns et al., 2004; Brass et al., 2008), and of course it reduces the number of samples to be assayed by a factor of four. One report even directly compared the effects of individual shRNA constructs with pools and found that using pools increased the likelihood of a loss-of function phenotype (Parsons et al., 2009). However, it is possible that using a pool of constructs resulted in a mixed population of cells where those cells with the poorest knockdown had a selective advantage, enabling them to proliferate more rapidly and thus resulting in a poorer overall knockdown. This level of variability would severely compromise the screen and with this in mind the decision was taken to move from pools to individual constructs.

4.3.3. shRNA delivery by transduction

Due to the poor knockdown of *HtrA2* in shRNA-transfected SH-SY5Y cells, it was necessary to increase expression of the hairpin in the cells. Viral transduction was not originally favoured as a method for shRNA delivery because of the time required to produce and titre virus for each construct; however, it is a more efficient method of gene delivery and therefore results in higher gene expression (Hwang and Gilboa, 1984). It was therefore hypothesised that improved knockdown could be mediated by using viral transduction.

Before silencing the genes of interest, transduction conditions were optimised using the validated positive control provided with the shRNA library, GAPDH (section 4.2.2.1). Surprisingly, although the percentage of cells transduced with the construct depended on

the number of virus particles added to cell, the efficiency of GAPDH silencing appeared to be determined to a greater extent by the amount of time for which the virus was added. Thus transducing cells once with an MOI of 2 viruses/cell was substantially less effective at silencing GAPDH than transducing them with an MOI of 1 virus/cell on two consecutive days, presumably because the probability of a virus particle reaching a cell by random diffusion increases with time. On the other hand, transducing cells twice with an MOI of 1 produced almost exactly the same number of GFP-positive cells as transducing cells once with an MOI of 2, suggesting that under the former conditions the same cells are transfected with more copies of the plasmid than under the latter. This might indicate that some cells in the dish are inherently more readily transduced than others, although the reason for this remains unclear.

4.3.4. High content screening for mitochondrial physiology

The advent of high content screening has enabled a revolution in the types of assays that can be used in large scale screens, enabling dynamic measurements of a range of readouts such as protein localisation or phosphorylation in fixed cells (Moffat et al., 2006; Orvedahl et al., 2011) or mitochondrial morphology and $\Delta\Psi_m$ in live cells (Reis et al., 2012). In this study a high content approach was attempted for the measurement of cytosolic ROS, but it failed to detect an increase in ROS production in cells transduced with an shRNA construct targeting *HtrA2*. Using a previously validated method to measure ROS production also failed to detect any increase in HtrA2 or PINK1 knockdown cells, however (figure 4.12), suggesting that this lack of sensitivity was not due to the high content approach. In fact, one of the major advantages of high content analysis is that a large number of cells can be assayed simultaneously, reducing the impact of outliers and thus potentially improving the detection of subtle phenotypes (Dragunow, 2008). Since the entire system is automated, the images are both acquired and analysed in a standardised, objective manner which can also improve assay robustness (Dragunow, 2008). Perhaps for these reasons, the variation between wells (intra-plate variation) was very small using the high content system, resulting in small standard errors. It was not possible to assess the inter-plate variation (variation between plates) as no effect was detected for the positive controls, which would have been used to normalise the data from each plate for comparison (Malo et al., 2006). Nonetheless, the consistency in the rate of increase in ethidium fluorescence between wells should be considered a positive indication of the robustness and suitability of this assay for high content screening.

4.3.5. Experimental difficulties

Two major difficulties were encountered in this project: first, achieving a reasonable level of gene silencing in the chosen cell line; and second, detecting any reproducible effect of HtrA2 or PINK1 shRNA on either $\Delta\Psi_m$ or ROS production. The former was solved by using viral transduction to deliver shRNA into the cell, but the latter persisted despite efficient silencing eventually being achieved for both genes.

Several factors may contribute to this difficulty in detecting a phenotype. The level of gene silencing achieved could be insufficient to cause the reported mitochondrial phenotype (discussed below), or the assays may not be sufficiently sensitive at present to detect the phenotype. Perhaps it takes time for the mitochondrial phenotype to develop, and so culturing the cells for longer after transduction would improve the result. Another possibility is that mitochondrial function could be affected by viral toxicity even in cells transduced with either empty or scrambled controls, masking the phenotype in the HtrA2 or PINK1 knockdown cells. All these options require further investigation and will be discussed in detail in section 4.3.8.

Although in this study it was not possible to observe any effect of HtrA2 or PINK1 knockdown on mitochondrial physiology, it is important to note that several different groups have previously reported mitochondrial depolarisation and increased ROS production in HtrA2 and PINK1 deficient cell models. In the case of HtrA2, the majority of published mitochondrial physiology has been performed using cells derived from HtrA2 KO mice (Fitzgerald et al., 2012; Kieper et al., 2010; Martins et al., 2004; Moisoi et al., 2009; Plun-Favreau et al., 2007), raising the possibility either that HtrA2 is more important for mitochondrial function in mice than in humans, or that absolute knockout of the gene is required in order to recapitulate the phenotype. For PINK1, however, several different groups have reported mitochondrial depolarisation in human cells, both following transient transfection with siRNA (Exner et al., 2007; Gegg et al., 2009) and in stable knockdown cells (Gandhi et al., 2009; Wood-Kaczmar et al., 2008), strongly suggesting that the failure to detect such an effect in the present study was due to experimental issues.

4.3.6. Critical evaluation of study design

This study took the unusual approach of applying some of the principles of high-throughput screening to a much smaller and more focused screen. At the time, decisions

regarding study design were taken based on the best information available, but in retrospect it is useful to consider the effects of these decisions on the experimental outcome.

In this chapter it has proven difficult to achieve high levels of gene silencing, and impossible to recapitulate the expected phenotype in knockdown SH-SY5Y cells. One possibility which was not considered at the time is that SH-SY5Y cells are simply not a good model for this study, and that attempting the screen in HEK293T cells might have been more effective. This is far from ideal because HEK293T cells are a kidney cell line and are therefore a poor model for the dopaminergic neurons which are selectively affected by mutations in the genes of interest. However, in most cases the proteins encoded by these genes are ubiquitously expressed and are likely to have the same function in all cells. It may therefore have been worth investigating whether a more consistent effect of HtrA2 and PINK1 knockdown could be achieved in an alternative cell line.

Another factor in achieving adequate levels of knockdown is the shRNA itself. All four HtrA2 constructs and two out of four PINK1 constructs resulted in at least 60% knockdown in transfected HEK293T cells (figure 4.6 and figure 4.7), indicating that the hairpin sequences were able to mediate effective gene silencing. However, it proved difficult to achieve sufficiently high expression of the plasmid in SH-SY5Y cells to produce good levels of knockdown, and this may be due in part to the vector design. The pGIPZ library was chosen because, unlike most shRNA vectors, the pGIPZ vector contained both a puromycin resistance gene and a GFP marker to enable selection of shRNA-expressing cells by either method. However, a consequence of this flexibility is that the vector is very large at 11.6 kb. By contrast, shRNA hairpins from SAB Biosciences (Qiagen) are available in either a puromycin vector (4.6 kb) or a GFP-containing vector (5.3 kb), which may have improved delivery to the cell and therefore knockdown. It would be interesting to compare knockdown of *HtrA2* in SH-SY5Y cells using the same hairpin in different vectors to determine their effect.

One of the most important decisions in the design of a screen is readout selection. To make a good readout, an assay should have several attributes. First, it should be conclusive: for this study, any mitochondrial dysfunction should be detected by the assay, and any effect on the assay should be indicative of mitochondrial dysfunction. Assays should be cheap, quick, and ideally have the potential to be scaled up to high throughput

systems. Above all, they must be reliable, and large effects should be detected for at least one of the positive controls. Of the readouts selected for this screen, $\Delta\Psi_m$ and cytosolic and mitochondrial ROS were expected to fulfil all the criteria listed, while oxygen consumption and $[Ca^{2+}]_m$ were expected to be more difficult assays but were chosen because of the information they could provide. However, within the timeframe available it was not possible to detect a consistent effect of either HtrA2 or PINK1 shRNA on either $\Delta\Psi_m$ or ROS production, suggesting that these assays are less reliable than initially thought. While reliability may be improved by further optimisation (discussed in section 4.3.8), alternative approaches for assessing mitochondrial function should also be considered. For example, both $\Delta\Psi_m$ and ROS production have previously been measured by flow cytometry (Mukhopadhyay et al., 2007; Rottenberg and Wu, 1998), which is an alternative method to quantify fluorescence in a large number of cells. Although not a high throughput method as only one sample can be tested at a time, the time taken to measure each sample is substantially less than is possible using microscopy. A disadvantage of this technique, however, is that it is not possible to visually confirm that the dye has localised to the mitochondria, potentially making the technique more vulnerable to artefacts (Solaini et al., 2007). Alternatively, different mitochondrial parameters could have been used as readouts. One such possibility could be an assay to detect sensitivity to mitochondrial toxins, since loss of both HtrA2 and PINK1 have been shown to increase sensitivity to toxins including 6-hydroxydopamine (6-OHDA) (Plun-Favreau et al., 2007), rotenone (Deng et al., 2005; Martins et al., 2004) and MPTP (Deng et al., 2005; Haque et al., 2008). Cell death readouts are often included in high content screens (Abraham et al., 2004; Zanella et al., 2010) because the cells can be fixed, reducing some of the variability inherent in live cell assays. Numerous spectrophotometric or luminescent cell death assays are also available for use in a 96 well plate reader.

A final consideration is whether it was the right decision to run the study as a screen at all. An alternative design could have been to generate stable knockdown cell lines for each of the genes of interest and verify the knockdown by western blot or qPCR for each gene before investigating the mitochondrial physiology. One advantage of this approach is that once the stable cell lines were made the experiment could be repeated three times in the same cell line rather than using three independent transductions, saving time and potentially improving reliability. There would also have only been one cell line to test for each gene rather than four constructs, enabling more repeats to be run per plate. Finally, by confirming the knockdown of all the target genes in the study, this approach would also

enable the gathering of negative data, producing the first direct comparison of the mitochondrial functions of all the mendelian PD genes in the same cell line. On the other hand, the major disadvantage of this approach would be that the generation and testing of cell lines for 15 different genes would be extremely time consuming and labour-intensive.

4.3.7. Conclusions

In this chapter, two methods of shRNA delivery were optimised to achieve silencing of *HtrA2* and *PINK1* in SH-SY5Y cells. Transfection of shRNA was not found to mediate effective gene silencing using the conditions tested, so lentiviral transduction was used instead. Optimisation of transduction conditions revealed that repeating the transduction on two consecutive days substantially improved knockdown compared to a single transduction, and that knockdown only improved with increasing MOI up to an MOI of 4 (two transductions with 2 viruses/cell), after which it appeared to plateau.

By using viral transduction to deliver the shRNA it was possible to demonstrate successful shRNA-mediated silencing of both *HtrA2* and *PINK1* in SH-SY5Y cells. However, this knockdown was not found to result in a reproducible mitochondrial phenotype under the conditions tested. Further optimisation would therefore be required before these techniques could be applied to screen for mitochondrial functions of PD genes.

4.3.8. Future perspectives

Before this screen could be taken to the hit identification stage, the readouts would need to be capable of consistently detecting a significant effect in cells expressing shRNA against either positive control, *HtrA2* or *PINK1*. Future work would therefore focus on optimisation of the assays in order to improve sensitivity, and optimisation of the transduction in order to improve knockdown.

Optimisation of a high content assay for ROS production was started in section 4.2.3, but was taken no further because no effect of gene silencing could be detected using a previously validated method. However, further work should revisit the high content approach as it may have the potential to improve assay sensitivity and robustness for the reasons previously discussed (section 4.3.4). To better optimise DHE concentration for ROS production using the Cellomics system, untransfected SH-SY5Y cells could be treated with a dose response to rotenone, which stimulates ROS production through complex I, then loaded with varying concentrations of DHE to determine which dye concentration

allows the best detection of low doses of rotenone. This approach would exclude questions over the degree of gene silencing achieved and solely address the issue of assay sensitivity. The $\Delta\Psi_m$ assay could also be optimised for the Cellomics, since this approach may improve reliability for the reasons discussed above. However, these strengths do come with weaknesses. Measuring $\Delta\Psi_m$ on individual coverslips using a confocal microscope allows optical slicing of the cell layer and the generation of a 3D image, thus excluding any effects arising from differences in focal plane. The high content system would use a lower magnification and would not enable optical slicing, which could reduce the accuracy of the measurement and therefore the sensitivity of the assay. Careful validation of the method would therefore be necessary to avoid false positives. Previous high content screens have included assays for $\Delta\Psi_m$ using this approach, however, demonstrating its feasibility (Rausch, 2006; Reis et al., 2012).

In addition to improving the sensitivity of the readouts, future work must address the question of why, despite achieving knockdown of both *HtrA2* and *PINK1* using viral transduction, it was not possible to detect any effect on ROS production or $\Delta\Psi_m$ using methods which had been previously validated in both HtrA2 KO mouse neurons (chapter 3) and PINK1 stable knockdown SH-SY5Ys (Gandhi et al., 2009; Wood-Kaczmar et al., 2008). A number of possible reasons for this have already been suggested in section 4.3.5; further work should therefore aim to identify and solve the underlying problem.

One likely explanation is that although the transduction conditions used in this study produced some degree of gene silencing, the remaining gene expression was sufficient to maintain normal physiological function: it should be noted here that *HtrA2*$^{+/-}$ mice have no phenotype and neither do patients with heterozygous *PINK1* mutations, indicating that a 50% reduction in the levels of the functional proteins has little or no effect on mitochondrial function. Further optimisation of the transduction conditions would therefore be necessary in order to improve knockdown at the protein level. MOI is limited by the titre of the virus produced, since concentrating the virus is not possible under the existing HSE approval, but by optimising the protocol for virus packaging it may be possible to improve titre and thereby enable higher MOIs to be tested. The concentration of polybrene, a cationic polymer used to increase adsorption of the virus through the cell membrane (Davis et al., 2002), should also be optimised. One possible reason for poor knockdown could stem from the period between transduction of the cells and measurement of the phenotype: too short, and proteins with long half-lives may not be

degraded; too long, and cells poorly expressing the plasmid may grow faster than those with better knockdown, reducing the overall knockdown and increasing the variability. In this chapter, all the experiments using viral transduction used an incubation of ten days to ensure sufficient time for even proteins with the longest half-lives to be turned over, but future work should optimise this by testing both knockdown and mitochondrial physiology over a timecourse. Alternatively, selecting the cells with puromycin for a short period soon after transduction may select for only the high-expressing cells and thus reduce the variation by another means.

If improving knockdown by optimising these parameters does not improve the mitochondrial phenotype, other potential causes should be considered. For example, one such possibility is that viral transduction in itself produces a mitochondrial phenotype that masks the effects due to gene silencing. To investigate this, ROS production and $\Delta\Psi_m$ should be measured in untransduced SH-SY5Y cells and cells transduced with the empty vector. If a difference were detected, it would then be necessary to revisit transfection conditions with individual constructs, using cheaper transfection reagents such as calcium phosphate. A number of publications have reported improvements in the transfection of hard to transfect cell lines by modifying existing protocols: for example, one study reports increased transfection of primary neurons by calcium phosphate by altering the vortexing of solutions during complex formation, and by removing the precipitate using a slightly acidic solution after 1-3 hr (Jiang et al., 2004b). It would therefore be necessary to test such modified protocols to find conditions that allow sufficient transfection of SH-SY5Y cells without stressing the cells and affecting mitochondrial physiology.

Finally, it is interesting to consider what hits might have been identified if it had been possible to take the screen forward. Of the genes included, some are already known to have roles in mitochondrial function, such as *Parkin* or *DJ-1* (Canet-Aviles et al., 2004; Greene et al., 2003; see section 1.3.3), so these would be expected to produce a mitochondrial phenotype. The proteins PINK1 and Parkin have recently been found to mediate the clearance of damaged mitochondria through the lysosome (Geisler et al., 2010a; Narendra et al., 2008; Narendra et al., 2010; Vives-Bauza et al., 2010), suggesting that silencing expression of the lysosomal proteins ATP13A2 or GBA might impact on mitochondrial function by interfering with this process. Consistent with this hypothesis, a recent paper has reported mitochondrial abnormalities in ATP13A2 knockdown SH-SY5Y cells, including increased reactive oxygen species and increased mitochondrial mass

(Gusdon et al., 2012). Interestingly, data in the next chapter will show that Fbxo7 also plays a role in PINK1/Parkin-mediated mitophagy, so the screen would also be expected to identify mitochondrial defects in Fbxo7 knockdown cells and it would be interesting to determine how closely these cells phenocopy cells transduced with PINK1 or Parkin shRNA.

Chapter 5

Role of Fbxo7 in PINK1/Parkin mediated mitophagy

5.1. Introduction

In last chapter of this thesis, an shRNA screen was attempted with the aim of identifying a novel mitochondrial function for one or more proteins genetically linked to PD. One such protein is F-box only protein 7 (Fbxo7), which was first found to be mutated in an Iranian family with early-onset L-DOPA responsive parkinsonian-pyramidal syndrome in 2008 (Shojaee et al., 2008). Since then two further PD mutations in the Fbxo7 gene have been identified in an Italian and a Dutch family (Di Fonzo et al., 2009a) and in Pakistani and Turkish families (Paisan-Ruiz et al., 2010). This chapter continues the work of the last by identifying a novel role for Fbxo7 in mitochondrial function, and in particular in the removal of damaged mitochondria from the cell.

Up until the identification of a link to PD, Fbxo7 was a relatively understudied protein and consequently much remains unknown about its function. It is a member of the F-box family of proteins, which are known to function as variable adaptors for E3 ubiquitin ligase complexes termed SCF (Skp1-Cul1-F-box) complexes (Skowyra et al., 1997). E3 ubiquitin ligases may catalyse the addition of a single ubiquitin molecule to a substrate (monoubiquitination), which can serve signalling roles (Woelk et al., 2007), or the addition of a chain of ubiquitin molecules (polyubiquitination) which may target the substrate for proteasomal degradation or signal for other cellular events (Trempe, 2011).

Within the SCF complex, the F-box protein (FBP) is responsible for binding both to the substrate for ubiquitination, through its C-terminal protein-protein interaction domain, and to Skp1, though the F-box domain (Bai et al., 1996). Skp1 in turn binds Cullin, which interacts with both an E2-ubiquitin conjugating enzyme and a RING-domain containing protein which together catalyse the ubiquitination event (Patton et al., 1998). An SCF complex may interact with several different FBPs in order to mediate the ubiquitination of different targets in response to different events, placing FBPs at the heart of a highly dynamic and versatile system.

In addition to its F-box domain, Fbxo7 has a number of additional functional domains as can be seen in figure 5.1. At the C-terminus, a proline-rich region (PRR) is responsible for binding the substrate for ubiquitination (Hsu et al., 2004), while a region immediately upstream of the F-box domain is necessary for its homodimerisation or heterodimerisation with the proteasome inhibitor PI31 (Kirk et al., 2008) and upstream of that is a Cdk6 interacting domain (Laman et al., 2005). Fbxo7 is also unique among the identified FBPs in having a ubiquitin-like domain (UBL) at its N-terminus, but the function of this domain remains unclear. In addition to the major isoform of Fbxo7 (isoform 1), three further isoforms have been described as a result of splice variation in the N-terminus (Di Fonzo et al., 2009a). Of these additional isoforms, only isoform 2, which lacks the UBL domain, is detectable at the protein level (Zhao et al., 2011).

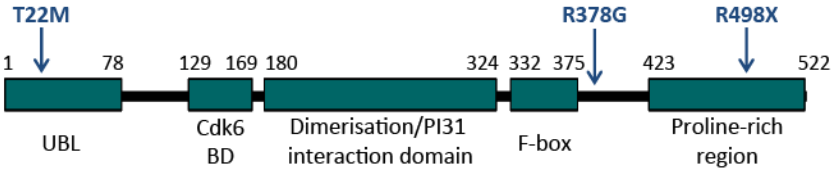

Figure 5.1 Domain structure of Fbxo7 (isoform 1). The three PD mutations are shown in blue above the domains. Abbreviations: UBL, ubiquitin-like domain; Cdk6 BD, Cdk6 binding domain.

Much of the research into the function of Fbxo7 to date has focused on its role in cell cycle and cell growth, and closely linked to this, its potentially tumorigenic effect. Fbxo7-SCF complexes have been shown to mediate the ubiquitination and degradation of HURP (hepatoma upregulated protein; Hsu et al., 2004), a protein involved in cell growth in G_2/M phase (Tsou et al., 2003), and cIAP-1, an inhibitor of apoptosis (Chang et al., 2006). It additionally interacts with Cdk6 but does not mediate its degradation, instead enhancing its interaction with Cyclin D and therefore increasing the catalytic activity of the

CyclinD/Cdk6 complex which translates growth signals into cell cycle progression (Laman et al., 2005). Upregulation of *Fbxo7* was capable of transforming mouse fibroblasts into tumour-forming cells in a Cdk6-dependent manner and Fbxo7 was found to be highly expressed in epithelial tumours (Laman et al., 2005), suggesting that it may have proto-oncogenic role in human cancers. Its cellular localisation is controversial, with one group suggesting a predominantly nuclear localisation due to an N-terminal nuclear targeting sequence (Zhao et al., 2011) but another demonstrating that Fbxo7 is targeted to the nucleus but exported back out to the cytosol, only residing in the nucleus of cells entering S/G_2 phase of the cell cycle (Laman et al., 2005; Nelson and Laman, 2011).

In parallel with the work described in chapter 4, this study specifically investigated a potential role for Fbxo7 at the mitochondria. This work was performed in collaboration with Dr Hélène Plun-Favreau (UCL Institute of Neurology) and Dr Heike Laman (University of Cambridge), who performed experiments where indicated in the text. All necessary molecular biology, immunocytochemistry and mitochondrial physiology was performed by the candidate.

5.2. Results

5.2.1. Mitochondrial localisation of Fbxo7

Fbxo7 localisation has previously been described as both cytosolic and nuclear (Laman et al., 2005; Nelson and Laman, 2011; Zhao et al., 2011). However, analysis of the protein sequence of Fbxo7 using four different mitochondrial prediction algorithms (Mitoprot, PSORT, Target P and Predotar; for further details see Methods section 2.2.1) consistently suggested a mitochondrial localisation for isoform 1 of the protein (figure 5.2a). Interestingly isoform 2 of Fbxo7, which lacks the N-terminal UBL domain, was not predicted to localise to the mitochondria, indicating that the mitochondrial targeting sequence (MTS) is in the first 79 amino acids of isoform 1. MTS prediction using Mitoprot suggested a cleavage site at amino acid 12, suggesting that the first 11 residues comprise the MTS (figure 5.2b).

In order to confirm the predicted mitochondrial localisation, mitochondria were separated from the cytosol of untransfected SH-SY5Y cells by differential centrifugation and both fractions were probed for endogenous Fbxo7 by western blot. As predicted, a fraction of Fbxo7 was detected in the mitochondrial fraction. Moreover, two bands were observed in

the cytosolic fraction corresponding to isoforms 1 and 2, but only the higher molecular weight band corresponding to isoform 1 was present in the mitochondrial fraction (figure 5.2c). The specificity of the antibody was verified using siRNA against Fbxo7 (figure 5.3).

A

	Mitoprot	PSORT	Target P	Predotar
Fbxo7 isoform 1	0.8505	Matrix: 0.485	0.597	0.36
Fbxo7 isoform 2	0.0528	Matrix: 0.100	0.087	0.01

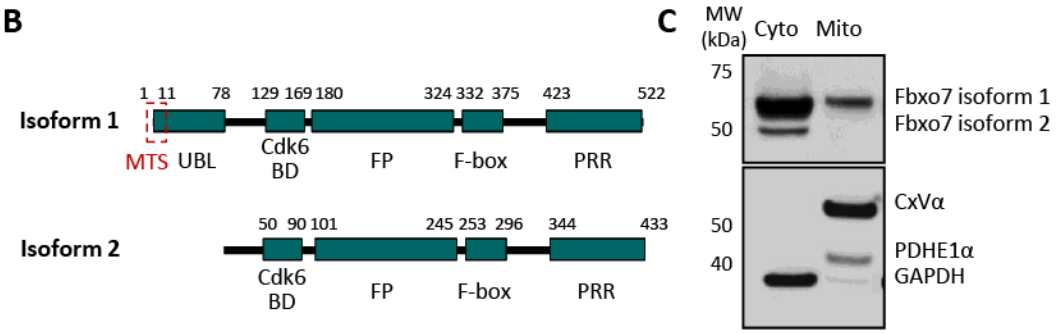

Figure 5.2 Mitochondrial localisation of Fbxo7. (A) Table showing mitochondrial prediction scores for Fbxo7 isoforms 1 and 2. **(B)** Structure of Fbxo7 isoforms 1 and 2 indicating the predicted mitochondrial targeting sequence (MTS). Abbreviations: UBL, ubiquitin-like domain; Cdk6 BD, Cdk6 binding domain; FP, Fbxo7-PI31 domain; PRR, proline-rich region. **(C)** Cytosolic and mitochondrial fractions of SH-SY5Y cells were probed for Fbxo7 and with an antibody cocktail composed of complex V α subunit (CxVα) and pyruvate dehydrogenase E1α (PDHE1α) as mitochondrial markers and GAPDH as a cytosolic marker.

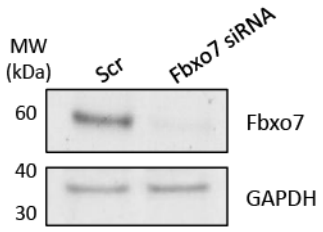

Figure 5.3 Verification of Fbxo7 antibody using siRNA. Lysates from cells transfected with scrambled siRNA (Scr) or Fbxo7 siRNA were probed for Fbxo7 and for GAPDH (as a loading control).

In order to confirm the predicted MTS, two point mutations were generated (see Appendix I) which in combination substantially reduced the mitochondrial prediction score (figure 5.4a). These residues were chosen as they were predicted to have the maximal effect on the mitochondrial localisation, whilst keeping the number of changes to the amino acid sequence to a minimum in order to avoid interfering with any interactions occurring at the N-terminus of the protein. HEK293T cells were transfected with either WT or mutant Fbxo7, both tagged with T7 at the N-terminus, then separated into mitochondrial and cytosolic fractions by differential centrifugation. Probing the fractions for T7 showed that WT Fbxo7 localises to the mitochondria as previously shown, but mutant Fbxo7 does not (figure 5.4b).

A

	Mitoprot	PSORT	Target P	Predotar
Fbxo7 isoform 1	0.8505	0.391	0.597	0.36
Fbxo7 mutant MTS (R2D, R6W)	0.1536	0.174	0.103	0.03

B

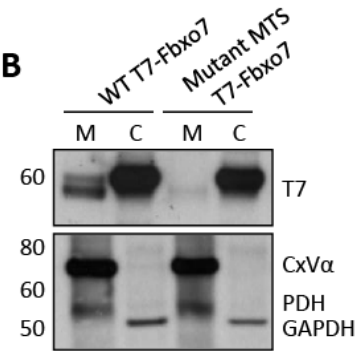

Figure 5.4 Mutations in the MTS abolish the mitochondrial localisation of Fbxo7. **(A)** Mutating two residues in the predicted MTS of Fbxo7 reduces the mitochondrial prediction scores generated by all four algorithms. **(B)** T7 tagged mutant, but not WT, Fbxo7 is absent in the mitochondrial fraction of transfected HEK cells.

To further identify the submitochondrial localisation of Fbxo7, mitochondria were isolated from untransfected HEK293T cells and subjected to digestion with protease K (PK) for 30 minutes over a range of concentrations. PK is a serine protease with broad substrate specificity, and therefore digests proteins primarily according to their availability to the enzyme; internal mitochondrial proteins are protected from the protease by the OMM and are therefore degraded only at higher concentrations. Digested mitochondria were lysed and analysed by western blot to determine the degradation of Fbxo7 and markers of the OMM, IMS, IMM and matrix (figure 5.5 overleaf). Fbxo7 degradation began to occur at PK concentrations of 1 µg/ml and above, similar to the pattern observed for the OMM protein TOM20. By contrast, the translocase of the inner membrane, TIM23, was degraded at

higher concentrations and the matrix protein Hsp60 was only partially degraded at the highest concentration, 50 μg/ml. This data thus suggests that Fbxo7 localises to the OMM.

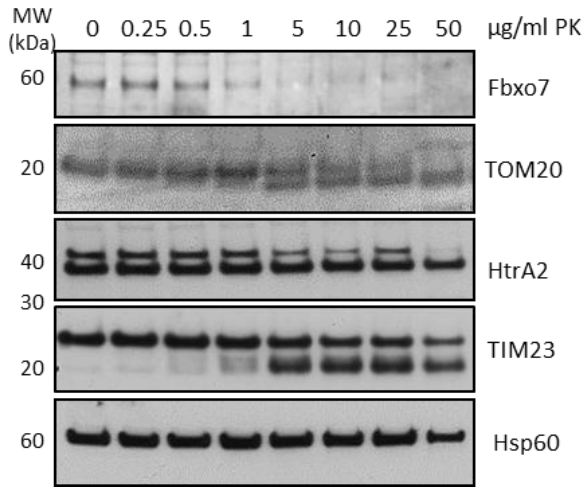

Figure 5.5 Protease K digestion of isolated mitochondria. Mitochondria were isolated from untransfected HEK293T cells and digested with increasing concentrations of protease K (PK). Lysates were then probed for Fbxo7 and markers of the OMM (TOM20), IMS (HtrA2), IMM (TIM23) and matrix (Hsp60). Experiment performed in collaboration with Hélène Plun-Favreau.

To investigate the mitochondrial localisation of Fbxo7 by an alternative technique, immunofluorescence was employed using Fbxo7 antibodies to probe the subcellular localisation of endogenous protein. Three different antibodies were optimised over a range of dilutions between 1:50 and 1:2000 using various fixation/permeabilisation methods and blocking solutions (see Methods), but no difference could be detected between untransfected cells and cells transfected with Fbxo7 siRNA (figure 5.6).

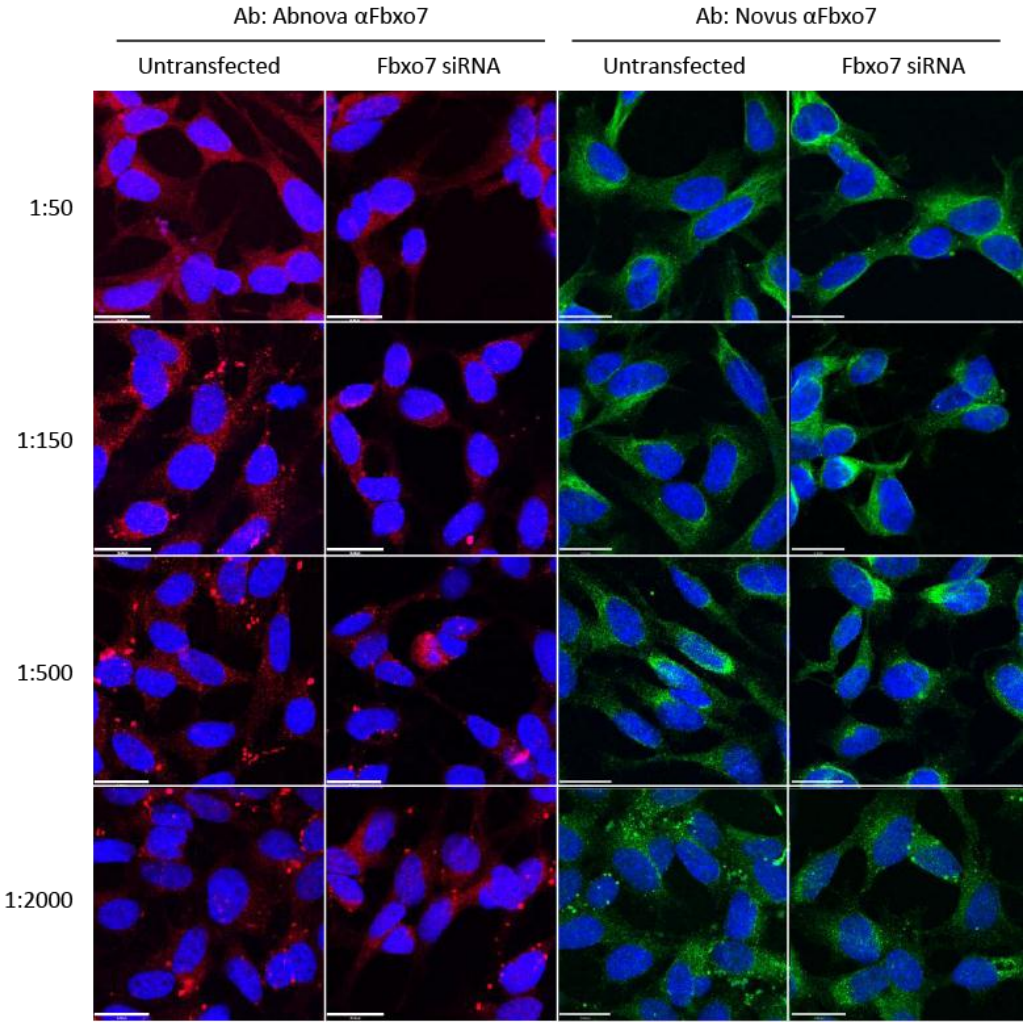

Figure 5.6 Fbxo7 antibody optimisation. Representative images are shown for staining using anti-Fbxo7 antibodies from Abnova (red) and Novus (green) over a range of dilutions. For each pair of images, gain and laser power settings were set to give the clearest image for the untransfected coverslip, then kept the same for the siRNA-treated cells. Nuclei were stained with DAPI (blue). Scale bar 20 μm.

Since it was not possible to detect endogenous Fbxo7 by immunocytochemistry, a construct for expression of a FLAG-Fbxo7 fusion was obtained from Heike Laman (University of Cambridge). To exclude the possibility that an N-terminal tag might interfere with the localisation of the protein, an Fbxo7-HA construct was also generated (see Appendix I for cloning strategy). SH-SY5Y cells were transfected with either N- or C-terminally tagged Fbxo7, fixed and stained using antibodies against FLAG or HA (to detect Fbxo7), HtrA2 or ATP synthase β subunit (to identify mitochondria), and DAPI (to label nuclei) (figure 5.7). Consistent with previous reports (Nelson and Laman, 2011), Fbxo7 localisation appeared predominantly cytosolic, with nuclear staining in a population of cells. Any mitochondrial staining was masked by cytosolic Fbxo7, in keeping with the western blot data which indicated that only a small pool of the total Fbxo7 is found in the mitochondrial fraction (figure 5.2).

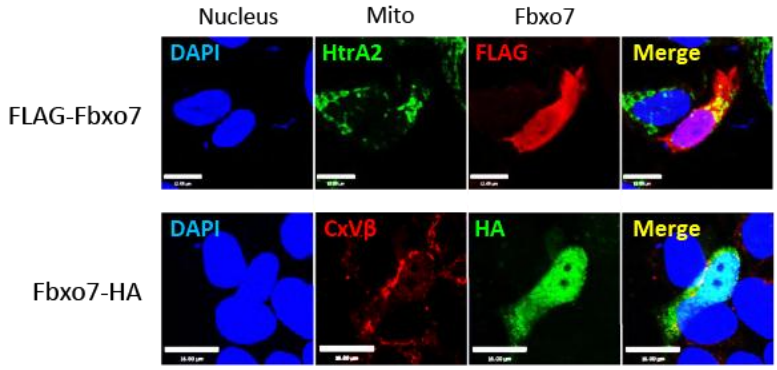

Figure 5.7 Localisation of tagged Fbxo7. SH-SY5Y cells transfected with N- or C-terminally tagged Fbxo7 were stained with the appropriate antibody. Antibodies against HtrA2 or complex V β subunit were used as mitochondrial markers (CxVβ). Scale bar 14 μm.

5.2.2. Fbxo7 relocates to depolarised mitochondria

The data thus far indicates that Fbxo7 has an MTS and yet localises predominantly to cytosol. As discussed in chapter 1, similar findings have been described for the mitochondrial kinase PINK1, which is targeted to the IMM but is immediately cleaved by the protease PARL and released into the cytosol (Jin et al., 2010). Upon mitochondrial depolarisation, however, PINK1 accumulates on the OMM of depolarised mitochondria (Geisler et al., 2010a; Narendra et al., 2010; Vives-Bauza et al., 2010). To investigate whether the same might be true for Fbxo7, SH-SY5Y cells transfected with either FLAG-Fbxo7 or Fbxo7-HA were treated with the mitochondrial uncoupler CCCP (10 μM), fixed

and stained with antibodies against FLAG or HA. No difference in Fbxo7 localisation could be detected following CCCP treatment (figure 5.8), suggesting that either Fbxo7 does not relocate to depolarised mitochondria, or that any relocation is masked by the cytosolic pool.

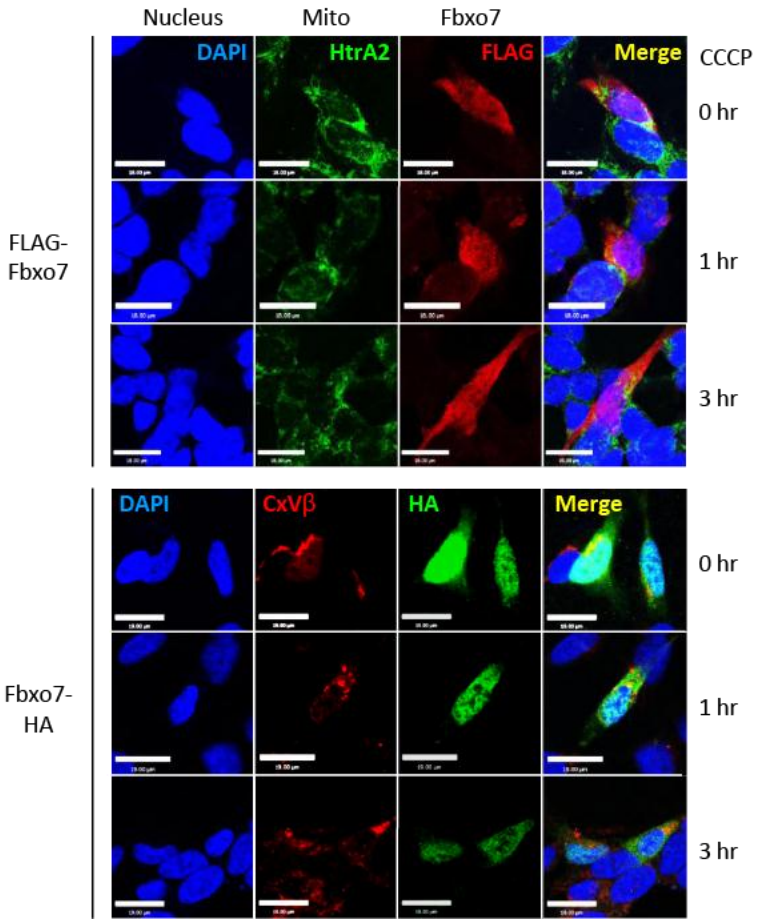

Figure 5.8 Relocation of tagged Fbxo7 following CCCP treatment. HA or FLAG staining in SH-SY5Y cells transfected with N- or C-terminally tagged Fbxo7 and treated with CCCP (10 μM) for the indicated time. HtrA2 or ATP synthase β subunit (CxVβ) antibodies were used as a mitochondrial marker. Scale bar: 18 μm.

Although relocation of Fbxo7 to the mitochondria was not observed using immunofluorescence of tagged constructs, an alternative explanation for this could be that the tags interfere with the translocation. To exclude this possibility an internally FLAG-tagged Fbxo7 construct was generated with the tag inserted into the region between the UBL domain and the Cdk6 binding domain (see Appendix I for details), but this construct was not expressed, presumably because the tag interfered with the protein's folding. Instead, relocation of endogenous Fbxo7 was therefore investigated by western blot, by

treating untransfected SH-SY5Y cells with CCCP for 0, 1 and 5 hr and then isolating mitochondria by differential centrifugation. Western blot of the mitochondrial and cytosolic fractions reveals a clear relocation of Fbxo7 from the cytosol to the mitochondria, in a pattern mimicking that of the E3 ubiquitin ligase Parkin (figure 5.9).

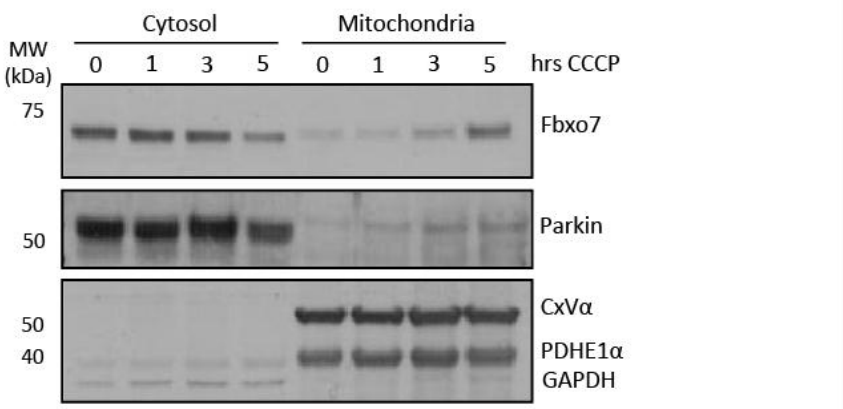

Figure 5.9 Fbxo7 relocates to mitochondria following CCCP treatment. Cytosolic and mitochondrial fractions of SH-SY5Y cells were probed for endogenous Fbxo7 and Parkin. Antibodies against complex V α subunit (CxVα), pyruvate dehydrogenase E1α (PDHE1α) and GADPH were used as controls for fractionation. Experiment performed by Hélène Plun-Favreau.

5.2.3. Fbxo7 interacts with Parkin

As discussed in section 1.2.4.2, PINK1 and Parkin have been shown to act in a common pathway to mediate the autophagic clearance of damaged mitochondria from the cell, a process termed mitophagy. Briefly, depolarisation of the mitochondria causes PINK1 to accumulate on the OMM (Geisler et al., 2010a; Narendra et al., 2010; Vives-Bauza et al., 2010), which in turn recruits Parkin (Narendra et al., 2008). Parkin ubiquitinates mitofusins 1 and 2 (Mfn1 and Mfn2) to signal their degradation by the proteasome (Gegg et al., 2010; Poole et al., 2010; Tanaka et al., 2010; Ziviani et al., 2010), resulting in fragmentation of the damaged mitochondria and enabling their engulfment by the autophagosome (Tanaka et al., 2010). Parkin may additionally ubiquitinate other targets in the mitochondria to mediate their autophagic removal (see section 1.2.4.2).

Since Fbxo7 also appears to relocate to depolarised mitochondria, we hypothesised that it may act in the same pathway as PINK1 and Parkin to mediate mitophagy. In order to determine whether Fbxo7 physically interacts with Parkin, FLAG immunoprecipitation

was performed on cell lysates from HEK293T cells transfected with Fbxo7 and FLAG-Parkin. Fbxo7 could be detected in FLAG-Parkin complexes at both the overexpressed (figure 5.10a) and endogenous (figure 5.10b) level.

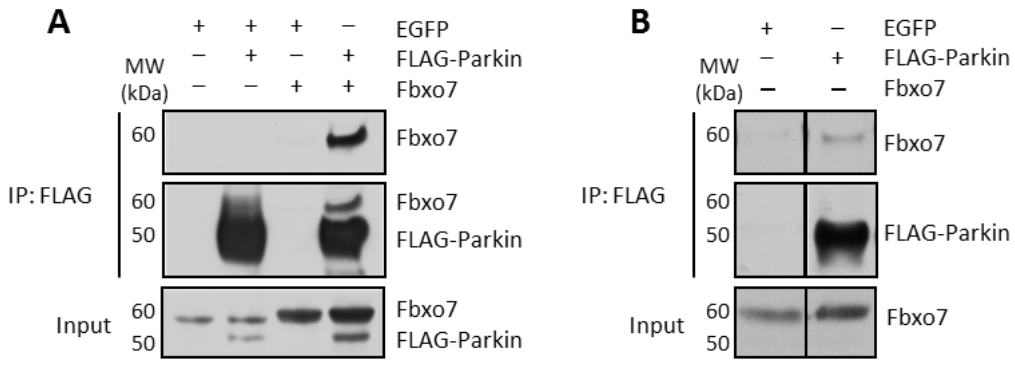

Figure 5.10 Co-immunopreciptation of FLAG-Parkin and Fbxo7. (A-B) FLAG-Parkin was immunoprecipitated from HEK293T cells transfected with combinations of enhanced green fluorescent protein (EGFP), FLAG-Parkin and Fbxo7. Immunoprecipitated complexes were probed for Fbxo7 and FLAG (as a control). Experiment performed by Hélène Plun-Favreau.

To determine where in the cell the interaction occurred, the same experiment was repeated using mitochondrial and cytosolic fractions from transfected HEK293T cells (figure 5.11). Probing the FLAG complexes for Fbxo7 revealed that the interaction occurs in both the cytosol and the mitochondria, with a slightly stronger band detected in the cytosolic fraction. However, given the overwhelming majority of Parkin in the cytosol compared to the mitochondria, it appears that only a small fraction of cytosolic Parkin is in complex with Fbxo7 compared to the majority of mitochondrial Parkin. This suggests that the interaction may have functional significance in the mitochondria. Interestingly, FLAG-Parkin was only detected at very low levels in the mitochondrial fraction of cells transfected with FLAG-Parkin with a GFP control (lane 2), but in cells overexpressing both FLAG-Parkin and Fbxo7 (lane 4), FLAG immunoreactivity is substantially increased in the mitochondrial fraction, suggesting that overexpression of Fbxo7 is in itself sufficient to cause a slight redistribution of Parkin to the mitochondria.

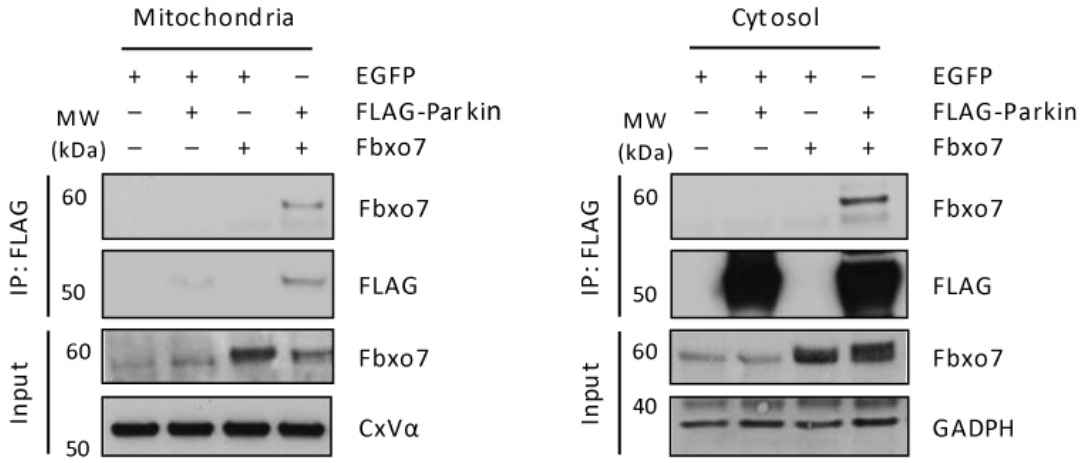

Figure 5.11 Co-immunoprecipitation of FLAG-Parkin and Fbxo7 in mitochondria and cytosol. HEK293T cells were transfected with combinations of EGFP, FLAG-Parkin and Fbxo7 and subjected to fractionation by differential centrifugation. FLAG immunoprepitation was then performed on both the mitochondrial and cytosolic fractions. Immunoprecipitated complexes were probed for FLAG and Fbxo7. Experiment performed by Hélène Plun-Favreau.

5.2.4. Fbxo7 is involved in the recruitment of Parkin to mitochondria

To investigate whether Fbxo7 participates in Parkin's translocation to the mitochondria, Fbxo7 was silenced in SH-SY5Y cells using siRNA. Cells were then transfected with FLAG-Parkin, treated with CCCP (10 μM) and stained with anti-FLAG antibody to observe mitochondrial relocation. As previously reported (Narendra et al., 2008), in control cells transfected with scrambled siRNA Parkin staining changed from a diffuse cytosolic staining before treatment to a punctate mitochondrial staining following treatment. In cells in which Fbxo7 expression had been silenced, on the other hand, the number of cells in which Parkin staining co-localised with a mitochondrial marker was significantly reduced at both 1 hr and 3 hr post treatment (figure 5.12), indicating that the recruitment of Parkin to the mitochondria is at least partially dependent on Fbxo7. The mitochondrial localisation of Fbxo7 appears to be important for this function, since Parkin relocation could be rescued in Fbxo7 knockdown cells by transfection with WT Fbxo7 but not with the MTS mutant described previously (figure 5.13).

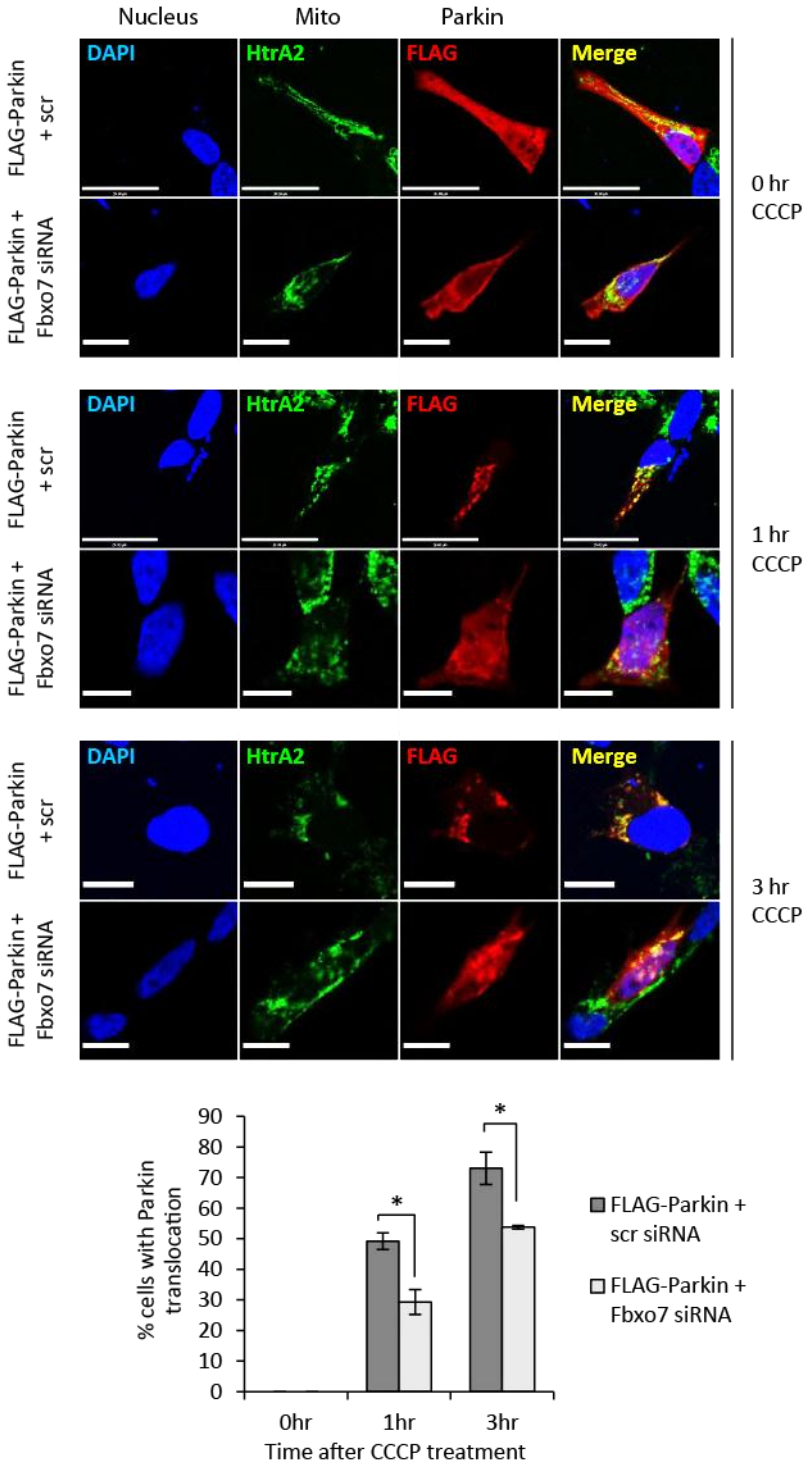

Figure 5.12 Effect of Fbxo7 on CCCP-induced Parkin translocation. Parkin localisation at the mitochondria was analysed by immunocytochemistry in SH-SY5Y cells transfected with FLAG-Parkin plus scrambled (scr) or Fbxo7 siRNA following 1 or 3 hr treatment with CCCP (10 μM). Cells in which FLAG-Parkin co-localised with mitochondrial staining were counted by eye (min 150 cells per coverslip). Data are presented as mean ± S.E.M., * $p < 0.05$. Scale bar, 20 μm.

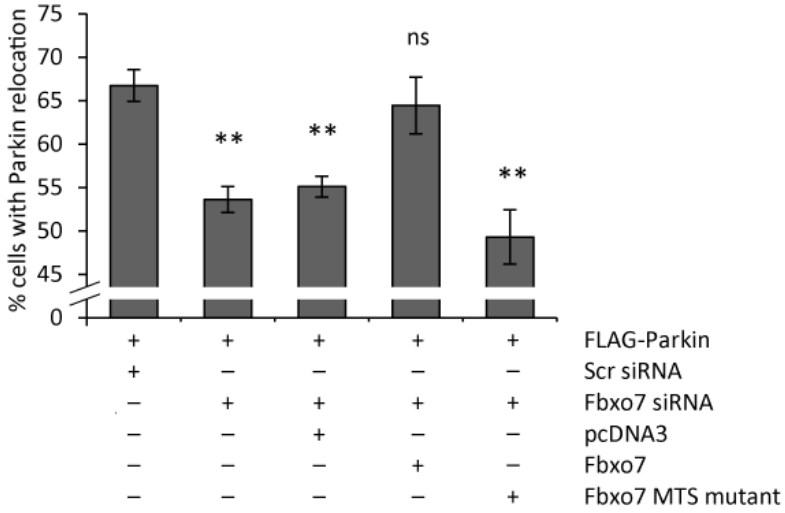

Figure 5.13 Rescue of Parkin relocation by Fbxo7 overexpression. SH-SY5Y cells were transfected with either scrambled (Scr) or Fbxo7 siRNA, then 24 hr later transfected with FLAG-Parkin cDNA plus either WT Fbxo7, R2D/R6W mutant Fbxo7 (MTS) or a vector control (pcDNA3). Cells were treated with CCCP (10 μM) for 3 hr, then stained with anti-FLAG and anti-HtrA2 antibodies. Cells in which Parkin co-localised with mitochondrial staining were counted by eye (at least 150 cells per coverslip). Histograms represent mean of at least 3 coverslips ± S.E.M. ns, not significant; ** $p < 0.005$.

5.2.5. Fbxo7 and PINK1

Parkin recruitment is dependent on the accumulation of PINK1 at the mitochondria (Geisler et al., 2010a; Narendra et al., 2010; Vives-Bauza et al., 2010). To investigate whether Fbxo7 also interacts with PINK1, FLAG immunoprecipitation was performed by Heike Laman at the University of Cambridge on cells transfected with FLAG-Fbxo7 and PINK1-myc. Fbxo7 was found to interact with both full length and processed PINK1 (unpublished data). To determine whether Fbxo7 is therefore implicated in the accumulation of PINK1 depolarised mitochondria, SH-SY5Y cells were transfected with PINK1-HA and either scrambled or Fbxo7 siRNA, treated with CCCP (10 μM) and stained with anti-HA antibody. PINK1 staining relocated from a diffuse cytosolic localisation before treatment to a distinct mitochondrial localisation after treatment, irrespective of whether cells were transfected with scrambled or Fbxo7 siRNA (figure 5.14), indicating that Fbxo7 is not required for PINK1 accumulation at the mitochondria.

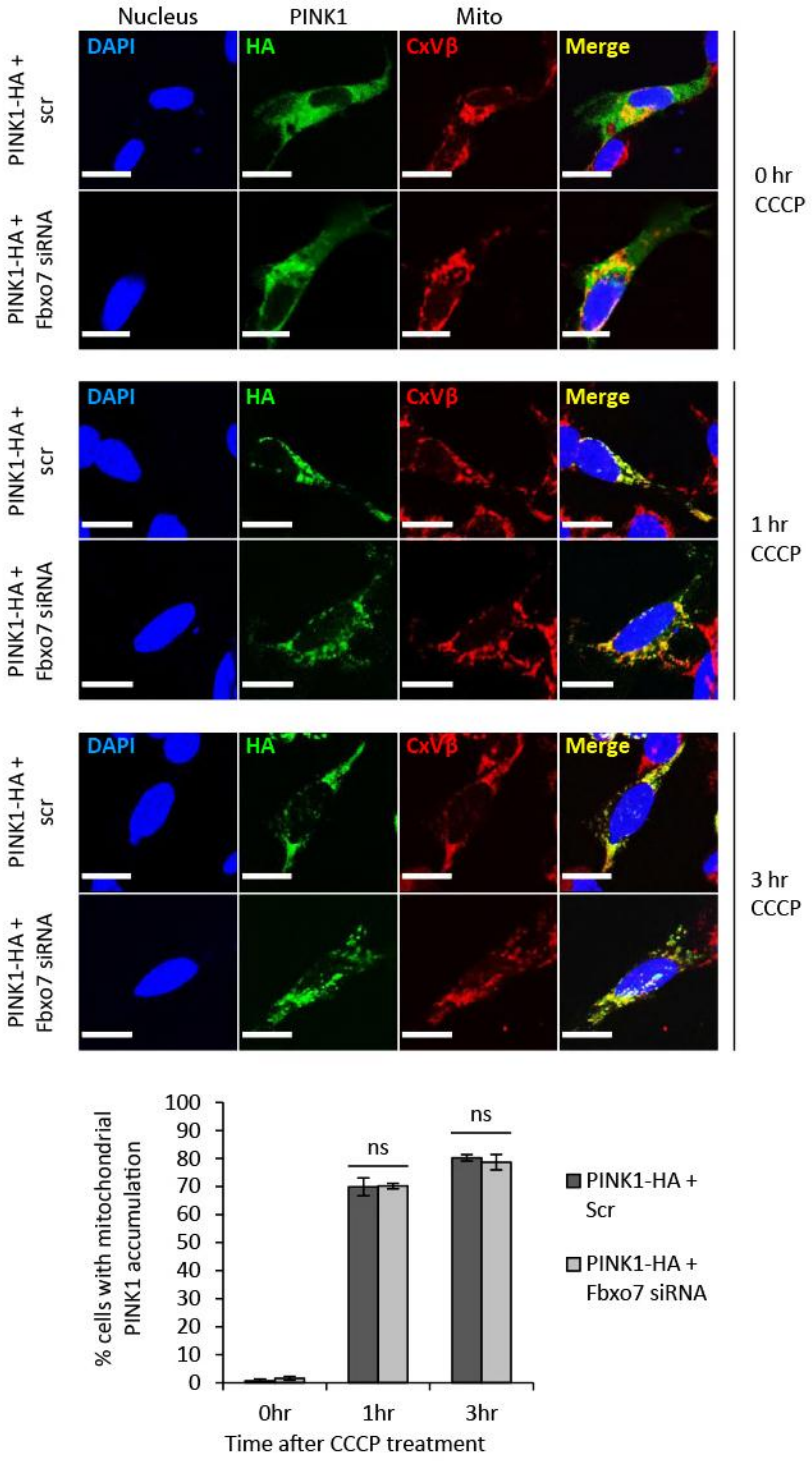

Figure 5.14 Effect of Fbxo7 on mitochondrial PINK1 accumulation. PINK1 localisation at the mitochondria was analysed by immunocytochemistry in SH-SY5Y cells transfected with PINK1-HA plus scrambled (scr) or Fbxo7 siRNA following treatment with CCCP (10 μM). Histograms show the percentage of cells with mitochondrial localisation of PINK1-HA. Data are presented as mean ± S.E.M., ns, not significant. Scale bar, 20 μm.

5.2.6. Fbxo7 is required for Mfn1 ubiquitination and mitophagy

To investigate the influence of Fbxo7 on downstream effectors of the PINK1/Parkin pathway, SH-SY5Y cells transfected with either control or Fbxo7 shRNA were treated with CCCP for 0, 3 and 5 hr and the mitochondria isolated by differential centrifugation. Previous studies have reported the appearance of higher molecular weight forms of Mfn1 and Mfn2 following CCCP treatment: these bands were shown to be ubiquitinated forms of the proteins and their appearance is dependent on expression of both PINK1 and Parkin (Gegg et al., 2010). Probing isolated mitochondria for Mfn1 revealed that ubiquitinated forms occur to a much greater extent in CCCP-treated control cells than in Fbxo7 KD cells (figure 5.15), indicating that Parkin-mediated ubiquitination of Mfn1 occurs in an Fbxo7-dependent manner.

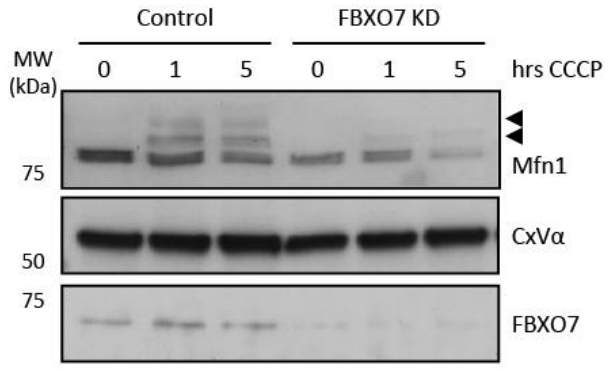

Figure 5.15 Mfn1 ubiquitination in Fbxo7 KD cells. Control and Fbxo7 knockdown SH-SY5Y cells were treated with CCCP (10 μM) for the indicated time, then mitochondria were isolated and probed for Mfn1. Complex V α subunit (CxVα) was used as a loading control. Arrows indicate ubiquitinated species.

The PINK1/Parkin/mitofusin pathway has been repeatedly shown to mediate mitophagy of depolarised mitochondria (Gegg et al., 2010; Tanaka, 2010; Ziviani and Whitworth, 2010). In SH-SY5Y cells overexpressing Parkin, mitophagy may be visualised by immunocytochemistry as the complete disappearance of mitochondrial staining in a cell following 24 hr CCCP treatment (Geisler et al., 2010a). This mitochondrial disappearance was inhibited by 3-methyl adenine (3-MA; 10 mM), an inhibitor of autophagosome formation (Seglen and Gordon, 1982), confirming that it was due to mitophagy and not an alternative mechanism of mitochondrial clearance (figure 5.16). To determine the effect of Fbxo7 on mitophagy, SH-SY5Y cells stably overexpressing FLAG-Parkin (kindly provided by Helen Ardley, University of Leicester) were transfected with scrambled or

Fbxo7 siRNA, treated with CCCP for 24 hr and stained for the presence of mitochondria (figure 5.17). The percentage of cells with no mitochondria remaining after CCCP treatment was significantly reduced in cells transfected with Fbxo7 siRNA compared to control, confirming that Fbxo7 participates in CCCP-driven mitophagy.

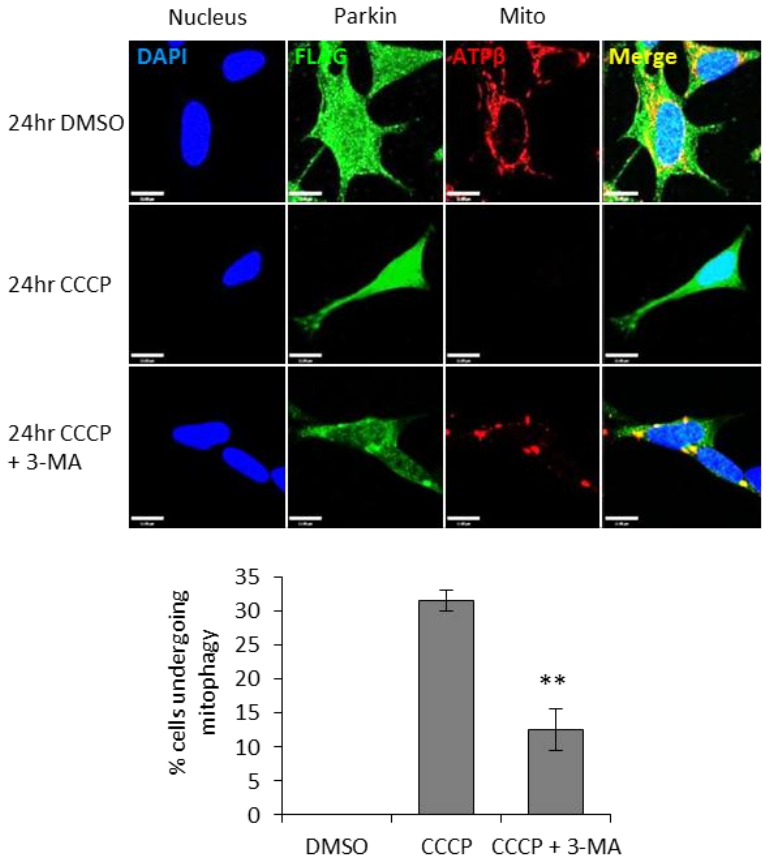

Figure 5.16 Mitochondrial clearance following CCCP is dependent on autophagosome formation. FLAG-Parkin overexpressing SH-SY5Ys were treated with DMSO, CCCP (10 μM) or CCCP + 3-MA (10 mM) for 24 hr as indicated. Histograms indicate the percentage of cells with no remaining mitochondria. Data are presented as mean ± S.E.M., ** $p < 0.005$. Scale bar, 20 μm.

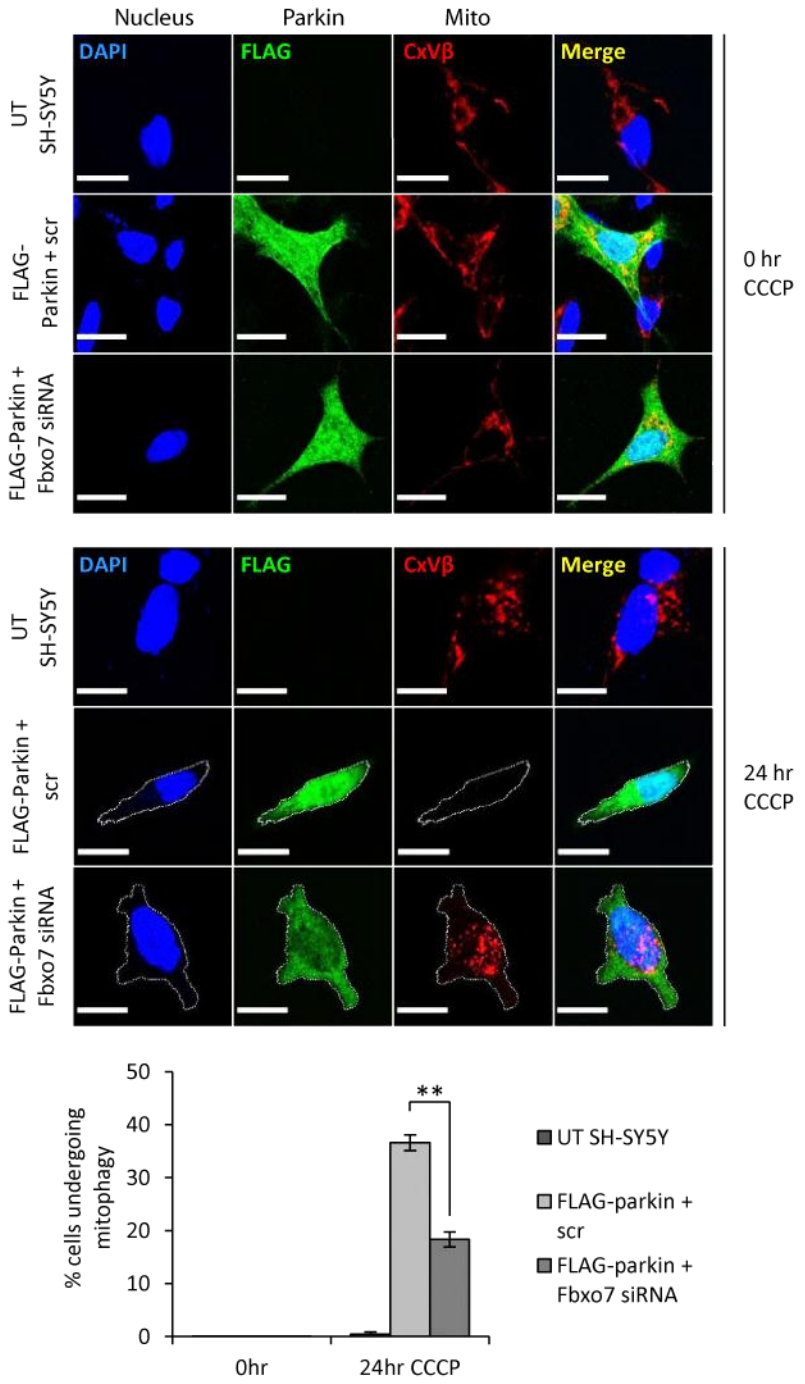

Figure 5.17 Effect of Fbxo7 on mitophagy. Untransfected SH-SY5Ys and FLAG-Parkin overexpressing SH-SY5Ys transfected with either scrambled (Scr) or Fbxo7 siRNA were treated with CCCP (10 µM) for 24 hr and mitophagy analysed by immunocytochemistry. Histograms indicate the percentage of cells with no mitochondrial staining. Data are presented as mean ± S.E.M., ** $p < 0.005$. Scale bar, 20 µm. Experiment was performed in collaboration with Marta Delagado-Camprubi.

5.2.7. Effect of PD mutations on Fbxo7 function

Three missense mutations in Fbxo7 have been shown to give rise to a parkinsonian-pyramidal syndrome: R378G (Shojaee et al., 2008); R498X (Di Fonzo et al., 2009a); and T22M, which was identified in a compound heterozygous state with a IVS7 + 1G/T mutation (Di Fonzo et al., 2009a). To investigate the effect of these mutations on the role of Fbxo7 in PINK1/Parkin-mediated mitophagy, experiments were performed at the University of Cambridge to investigate the mitochondrial localisation of the mutants under basal conditions and to determine whether any of the mutations interfered with the interaction with either Parkin or PINK1. Despite the close proximity of the T22M mutation to the predicted MTS, no alteration in mitochondrial localisation was observed for any of the mutants. However, the T22M was found to prevent the interaction between Fbxo7 and Parkin, although the R378G and R498X mutations had no effect (Heike Laman, unpublished data).

To investigate whether the mutations had any further effect on the relocation of Parkin to mitochondria following CCCP, a Parkin relocation rescue experiment was performed as described in figure 5.13. Parkin relocation in cells transfected with Fbxo7 siRNA was rescued by expression of WT or R378G mutant Fbxo7, but not by either the T22M or the R498X mutants (figure 5.18).

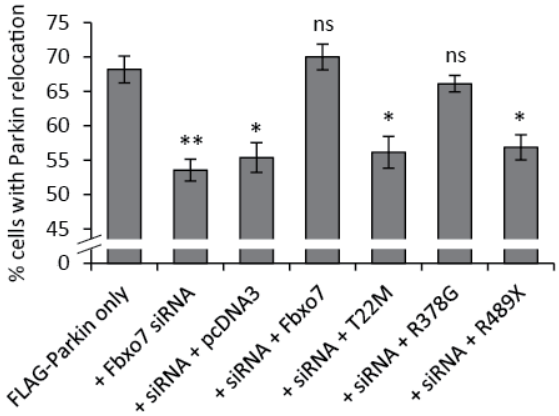

Figure 5.18 Rescue of Parkin translocation with WT Fbxo7 and PD mutants. SH-SY5Y cells were transfected with Fbxo7 siRNA, then 24 hr later transfected with FLAG-Parkin cDNA plus either WT or mutant Fbxo7 or a control vector (pcDNA3). Cells were treated with CCCP (10 μM) for 3 hr, then stained with anti-FLAG and anti-HtrA2 antibodies. Cells in which Parkin co-localised with mitochondrial staining were counted by eye. Histograms represent mean of a least 3 coverlips ± S.E.M. * $p < 0.05$; ** $p < 0.005$; ns, not significant compared to FLAG-Parkin only control.

The data above showed that the R378G mutation was able to rescue Parkin relocation to the mitochondria, suggesting that this mutation may have no effect on the role of Fbxo7 in this pathway. However, to investigate the effect of this mutation on downstream targets of Parkin, Mfn1 ubiquitination was investigated in fibroblasts from a patient with a homozygous R378G mutation. Similar to the previous results in SH-SY5Y cells, treatment of fibroblasts from an unaffected individual with CCCP resulted in the appearance of higher molecular weight ubiquitinated Mfn1 species, but this ubiquitination was virtually abolished in the R378G patient fibroblasts (figure 5.19). This data indicates that all three of the PD mutations interfere with this pathway at different stages, and furthermore, suggests that Fbxo7 plays a key role not only in bringing Parkin to the mitochondria but also in facilitating Parkin-mediated ubiquitination of at least one substrate.

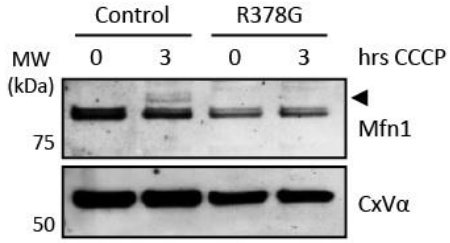

Figure 5.19 Ubiquitination of Mfn1 in control and R378G fibroblasts. Control and patient fibroblasts were treated with 10 μM CCCP for the time indicated, then mitochondria isolated and probed with antibodies against Mfn1 and ATP synthase α subunit (CxVα) as a loading control. The arrow indicates ubiquitinated forms.

5.2.8. Mitochondrial physiology in Fbxo7 deficient cells

The data already shown in this chapter indicates that Fbxo7 localises partially to mitochondria under basal conditions, and furthermore that it functions in a common pathway with PINK1 and Parkin, both of which are important for basal mitochondrial function since cells lacking either protein have been shown to exhibit severe mitochondrial dysfunction (Exner et al., 2007; Greene et al., 2003; Palacino et al., 2004; Valente et al., 2004). To determine whether Fbxo7 is similarly essential for mitochondrial function, clonal cell lines were generated stably expressing Fbxo7 shRNA in either U2OS or SH-SY5Y cells (Heike Laman, University of Cambridge). Knockdown levels of approx. 90% and 80% respectively were observed for the two cell lines (figure 5.20).

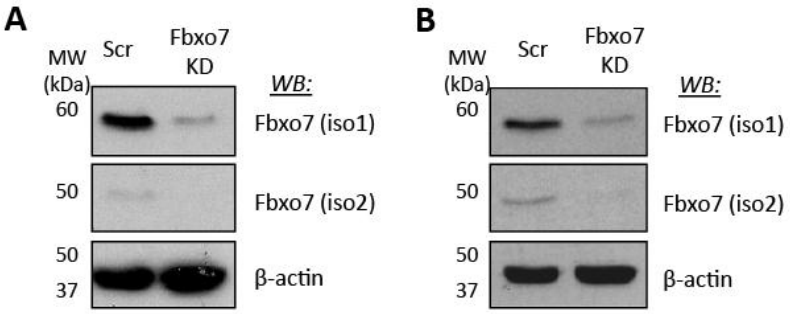

Figure 5.20 Fbxo7 protein levels in stable KD U2OS and SH-SY5Y cells. (A-B) Lysates from U2OS (A) and SH-SY5Y (B) cells stably expressing either scrambled (Scr) or Fbxo7 shRNA were probed for Fbxo7 and β-actin for loading.

As previously described (chapters 3 and 4), $\Delta\Psi_m$ is an important indicator of mitochondrial function. Using TMRM to measure $\Delta\Psi_m$ by confocal microscopy revealed a significant mitochondrial depolarisation in Fbxo7 KD U2OS and SH-SY5Y cell lines (figure 5.21), suggesting an effect of Fbxo7 on basal mitochondrial function.

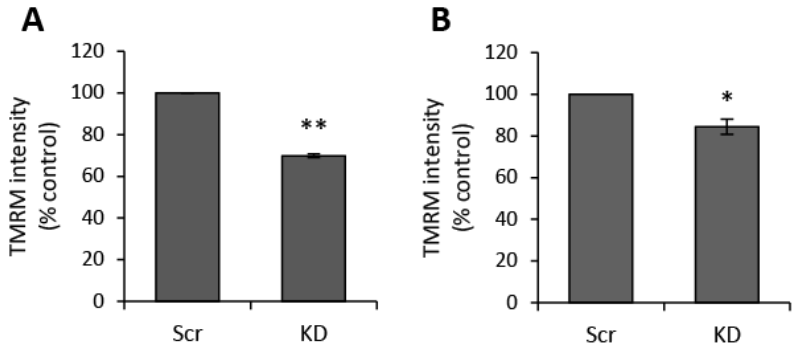

Figure 5.21 Mitochondrial membrane potential in Fbxo7 knockdown cells. (A-B) $\Delta\Psi_m$ was measured in U2OS cells (A) and SH-SY5Y cells (B) stably expressing either a scrambled shRNA (Scr) or shRNA targeting Fbxo7 (knockdown, KD). Histograms represent mean of three independent experiments ± S.E.M. * $p < 0.05$, ** $p < 0.005$. Data in panel B were generated in collaboration with Marta Delgado-Camprubi.

Neither patient fibroblasts carrying the R378G mutation nor immortalised lymphoblasts carrying the R498X mutation were found to exhibit significant mitochondrial depolarisation on average, but both had clear mitochondrial abnormalities. Whereas fibroblasts from a healthy control individual and from a heterozygote carrier for the R378G mutation had uniformly high $\Delta\Psi_m$ in all cells, the homozygous R378G fibroblasts were extremely variable, with a minority of cells exhibiting profound mitochondrial depolarisation, often accompanied by fragmentation of the mitochondrial network (figure

5.22a). Immortalised lymphoblasts from a patient homozygous for the R498X mutation had normal $\Delta\Psi_m$ but TMRM staining in some cells showed a fused mitochondrial morphology in the patient compared to controls (figure 5.22b). It should be noted that mitochondrial morphology cannot be accurately assessed using TMRM as the staining is $\Delta\Psi_m$-dependent. It may therefore be interesting to repeat the staining using a potential-independent dye or by using an antibody in fixed cells and to quantify the morphology to determine whether this is a significant effect. If so, it may be suggestive of a role for Fbxo7 in control of mitochondrial morphology.

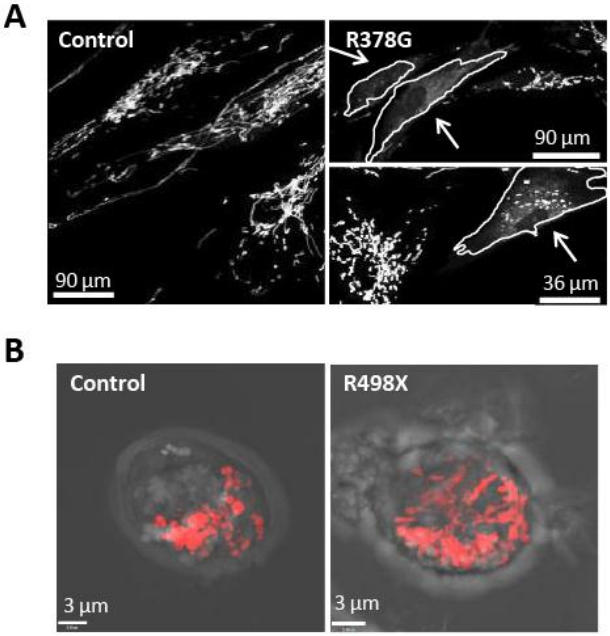

Figure 5.22 Representative images of TMRM staining in control and patient fibroblasts and lymphoblasts. **(A)** TMRM staining of fibroblasts from a control individual (left) and a patient with a homozygous R378G mutation in Fbxo7 (right). TMRM staining is falsely coloured in white to improve contrast. Arrows indicate depolarised cells. **(B)** TMRM staining of a control (left) and homozygous R498X (right) lymphoblast. TMRM staining in red is superimposed on a bright-field image.

In order to determine whether the mitochondrial depolarisation observed in Fbxo7 deficient cells is the result of a defect in respiration, NADH redox index was measured in Fbxo7 KD U2OS cells as previously described (see chapter 3), by calculating the basal NADH autofluorescence as a percentage of the range between the minimum (FCCP-stimulated) and maximum (NaCN-stimulated) values. A significant increase in NADH redox index was observed in KD cells compared to WT (figure 5.23a), indicating a reduction in basal mitochondrial respiration. Meanwhile the total NADH pool (absolute

difference between maximum and minimum NADH autofluorescence) was reduced in KD cells (figure 5.23b) suggesting a potential defect upstream of the ETC (e.g. in the TCA cycle).

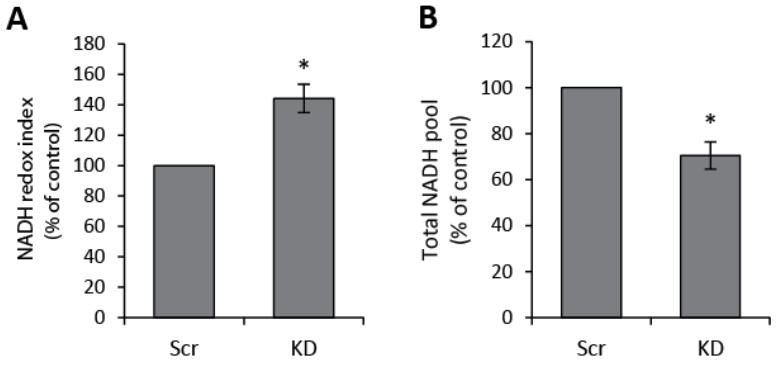

Figure 5.23 NADH redox index in control and Fbxo7 KD U2OS cells. (A-B) NADH redox index (A) and total pool (B) in U2OS cells stably expressing scrambled (Scr) or Fbxo7 shRNA. Histograms indicate a mean of 3 independent experiments (each normalised to control) ± S.E.M. * $p < 0.05$ compared to control.

Preliminary data also suggested an increase in cytosolic and mitochondrial ROS production in Fbxo7 KD U2OS cells (figure 5.24, n=1 experiment), consistent with a possible defect in the ETC. Finally, measurement of mitochondrial calcium using Fura-2 as described in the last chapter (section 4.1.1.4) suggested a possible reduction in basal mitochondrial calcium levels and increase in ER calcium in KD U2OS cells compared to control (figure 5.25), although these results are extremely preliminary (n=1 pair of coverslips) and would need to be confirmed.

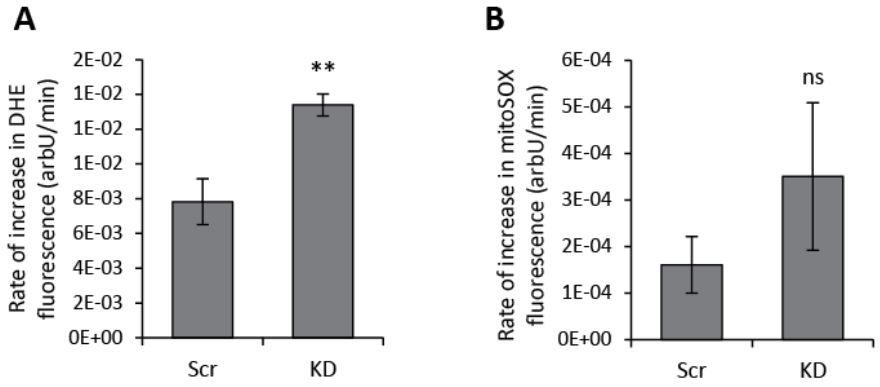

Figure 5.24 ROS production in Fbxo7 KD U2OS cells. (A-B) Cytosolic (A) and mitochondrial (B) ROS were assessed by measuring the rate of increase in fluorescence at 530 nm in cells loaded with dihydroethidium (DHE) or mitoSOX respectively. Histograms represent mean of 3 pairs of coverslips in 1 experiment, ± S.E.M. ** $p < 0.005$ compared to control; ns, not significant.

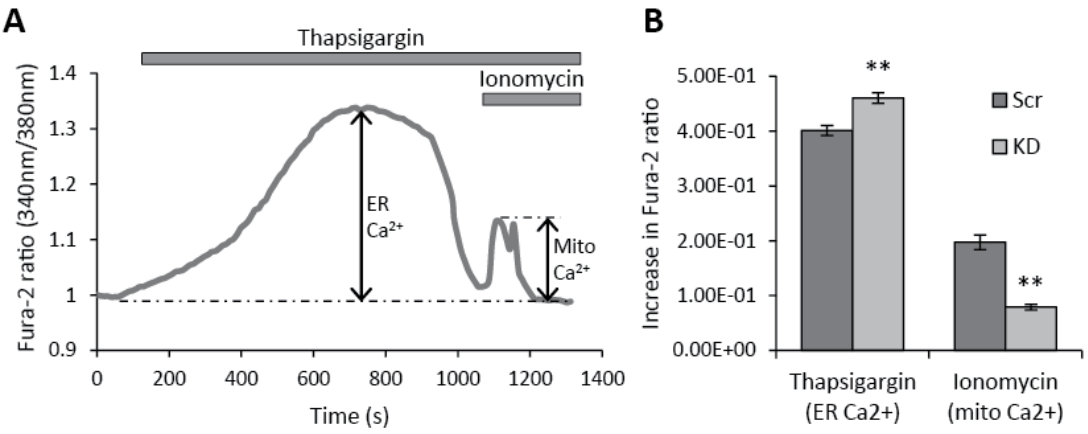

Figure 5.25 Basal mitochondrial calcium levels in Fbxo7 KD U2OS cells. (A) Representative Fura-2 trace for a control cell to illustrate response to toxins. Addition of thapsigargin, a SERCA inhibitor, causes gradual emptying of the ER. Addition of ionomycin, a calcium ionophore, then releases the remaining store of calcium, the mitochondrial calcium pool. **(B)** Response to thapsigargin (ER calcium pool) and to ionomycin (mitochondrial calcium pool) in control and Fbxo7 KD cells. Histograms indicate mean of at least 20 cells in one coverslip ± S.E.M. ** $p < 0.005$ compared to control.

While preliminary, together these results are suggestive of a defect in mitochondrial respiration and calcium handling in Fbxo7 deficient cells. Further experiments will be required in order confirm these data and determine the underlying cause of the defect.

5.3. Discussion

The PINK1/Parkin mitophagy pathway has been the subject of intense study over the past few years, yet despite this, large gaps in our knowledge remain. The work described in this chapter introduces a new PD protein into the pathway upstream of Parkin, and provides insight into the mechanism of both Parkin recruitment and mitofusin ubiquitination.

5.3.1. Mitophagy in PD

Where mutations in several different members of a pathway cause the same disease, it strongly suggests that that cellular process plays a critical role in protecting against that disease. In this case, mutations in Fbxo7, PINK1 or Parkin all interfere with mitophagy and all cause autosomal-recessive PD. Understanding the mechanism by which these

mutations prevent mitophagy, and more importantly how impaired mitophagy leads to nigral degeneration, may thus have enormous therapeutic value.

The idea that mitochondria may be destroyed by autophagy is not a new one: autophagosomes containing mitochondria were observed by electron microscopy as far back as 1962 (Ashford and Porter, 1962). Studies by Lemasters and colleagues have shown that starvation-induced mitophagy in hepatocytes is preceded by mitochondrial depolarisation (Elmore et al., 2001) and used confocal microscopy to visualise recruitment of GFP-LC3 in real time following laser-induced mitochondrial depolarisation (Kim et al., 2007; Rodriguez-Enriquez et al., 2006), indicating that mitophagy can be a selective process. In recent years, rapid advances have been made in understanding the mechanism by which damaged mitochondria are targeted for mitophagy following the finding by Narendra *et al.* that Parkin translocates to depolarised mitochondria and is necessary for their removal (Narendra et al., 2008). Further work has shown that this recruitment is dependent on the kinase activity of PINK1 (Geisler et al., 2010a; Narendra et al., 2010; Vives-Bauza et al., 2010), which is usually cleaved out of the mitochondria by the IMM protease PARL (Deas et al., 2011; Jin et al., 2010) but accumulates on the OMM of depolarised mitochondria (Jin et al., 2010; Narendra et al., 2010). Parkin has been shown to ubiquitinate multiple mitochondrial substrates (see section 1.2.4.2) including mitofusins 1 and 2, which targets them for excision from the membrane by the AAA^+ protease p97 and degradation by the proteasome (Gegg et al., 2010; Tanaka et al., 2010). The removal of mitofusins prevents the damaged mitochondrion from fusing back to the healthy mitochondrial network and allows Drp1-mediated fragmentation of the mitochondria, which is essential to allow the depolarised mitochondria to be engulfed by the autophagosome for degradation (Tanaka et al., 2010). For a more comprehensive review of the literature surrounding PINK1/Parkin-mediated mitophagy, see section 1.2.4.2 of the Introduction. A schematic indicating the previously described pathway for ubiquitination of mitofusins and subsequent mitophagy is shown in figure 5.26 overleaf.

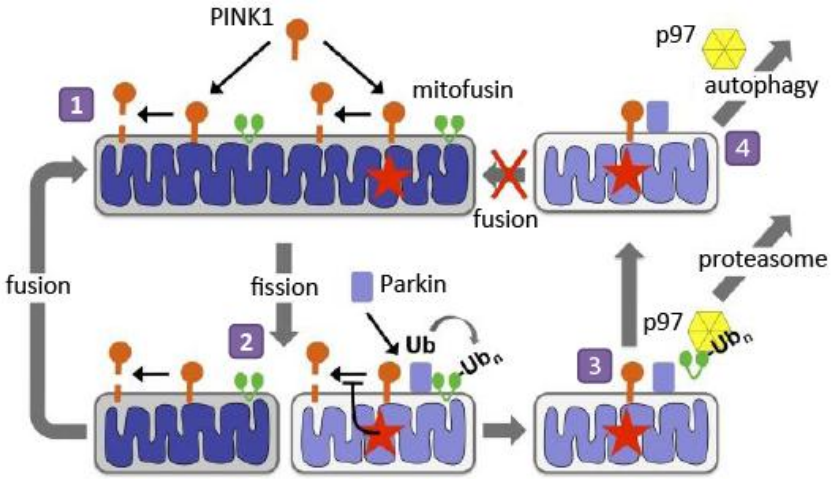

Figure 5.26 Schematic of PINK1/Parkin/mitofusin-mediated mitophagy. When a healthy mitochondrion (1) becomes damaged (red star), it divides unequally (2). The daughter mitochondrion with the higher $\Delta\Psi_m$ fuses back the mitochondrial network, but in the depolarised daughter mitochondrion PINK1 accumulates, Parkin is recruited, and mitofusin is ubiquitinated and degraded (3), preventing it from fusing back to the mitochondrial network and targeting it for mitophagy (4). Figure adapted from (Pallanck, 2010).

Interest in mitophagy has surged in the last few years, but investigation of this pathway has been hampered by the lack of availability of good antibodies against either PINK1 or Parkin, coupled with the low endogenous expression of these proteins in most cell lines. This has led the majority of studies (including this one) to rely on overexpression of tagged proteins to investigate their function, raising concerns over potential artefacts. Similarly, the use of high concentrations of CCCP is not physiological. However, there have been encouraging signs that this is a physiologically relevant pathway. Mitofusin ubiquitination is observed following treatment with either CCCP or valinomycin in fibroblasts from control individuals, but not in patient fibroblasts carrying PD-causing mutations in either PINK1 or Parkin (Rakovic et al., 2011) and in figure 5.19 the same effect was observed in fibroblasts from a patient with a homozygous Fbxo7 mutation, demonstrating that the mutant proteins can affect the pathway at endogenous levels. Furthermore, endogenous Parkin has recently been shown to relocate to mitochondria following CCCP treatment in cultured mouse neurons, albeit over a longer timescale than reported in HeLa and SH-SY5Y cells, and silencing Parkin expression prevented removal of damaged mitochondria in these cells (Cai et al., 2012). The question of whether CCCP treatment models a physiological process has also been elegantly addressed using

mitofusin double knockout MEFs. Cells lacking both Mfn1 and Mfn2 have previously been shown to exhibit fragmented and heterogeneous mitochondria, some of which are relatively depolarised (Chen et al., 2005). Transfecting these cells with YFP-Parkin and staining with $\Delta\Psi_m$-sensitive mitotracker red revealed that Parkin selectively localised to those mitochondria with lower $\Delta\Psi_m$ (Narendra et al., 2008), demonstrating that Parkin can selectively recognise depolarised mitochondria in a physiological setting.

5.3.2. Role of Fbxo7 in Parkin recruitment to mitochondria

The data presented here show that in Fbxo7 knockdown cells treated with CCCP, the mitochondrial relocation of Parkin, but not PINK1, is substantially reduced. This strongly suggests that Fbxo7 is involved in the recruitment of Parkin to the mitochondria, potentially by physically binding Parkin in the cytosol and translocating with it to the mitochondria. Several lines of evidence support this hypothesis. Fbxo7 interacts with Parkin in both the cytosol and the mitochondria, and cotransfection of Fbxo7 with FLAG-Parkin resulted in higher expression of FLAG-Parkin in the mitochondrial fraction than in cells only transfected with FLAG-Parkin. Fbxo7 has a mitochondrial targeting sequence, and this is essential for its effect on Parkin relocation to the mitochondria. Finally, Fbxo7 itself relocates from the cytosol to the mitochondria following CCCP treatment, in a similar time-frame to that reported for Parkin, consistent with the idea that it might physically recruit the E3 ligase to the mitochondria.

Mechanistically, however, questions still remain. How does Fbxo7 accumulate specifically on depolarised mitochondria? And what factors control its translocation? Interestingly, the fact that both N- and C-terminal tags interfere with relocation of Fbxo7 to the mitochondria suggests that both termini may be important for this relocation. The C-terminal PRR domain of Fbxo7 has previously been shown to be responsible for substrate binding (Hsu et al., 2004), raising the possibility that Fbxo7 is stabilised at the mitochondria by binding to a substrate (discussed further in section 5.3.4). On the other hand, the requirement for the N-terminus is more difficult to explain and further work will be required in order to fully investigate the mechanistic detail and to better understand this observation.

5.3.3. Role of Fbxo7 in Parkin-mediated ubiquitination

The R378G mutation was found not to affect Parkin recruitment to the mitochondria (figure 5.18) and yet surprisingly the same mutation prevented Mfn1 ubiquitination

following CCCP treatment in patient fibroblasts (figure 5.19), suggesting that the role of Fbxo7 in this pathway extends beyond the recruitment of Parkin to the mitochondria. This mutation has previously been shown to disrupt the interaction of Fbxo7 with Skp1 (Nelson and Laman, 2011), raising the possibility that ubiquitination of Mfn1 by Parkin might require additional members of the SCF protein complex.

In support of this idea, a previous study has also suggested that Parkin may function as part of an atypical 'SCF-like' complex. Starapoli and colleagues showed that Parkin interacts with another FBP, hSel-10 (also called Fbw7), and this interaction was important for Parkin's catalytic activity (Staropoli et al., 2003). In a canonical SCF complex, the protein components are arranged in a crescent shape such that the FBP, Skp1 and Cullin act as a bridge between the substrate and the E3 ubiquitin ligase and E2 ubiquitin conjugating enzyme (Skowyra et al., 1997) (figure 5.27a, overleaf). In the Parkin/hSel-10 complex, however, the interaction between Parkin and hSel-10 was direct and the complex included Cullin but not Skp1, indicating an alternative protein configuration (Staropoli et al., 2003). Although in the case of hSel-10 the FBP was found to directly interact with both the E3 ubiquitin ligase and the substrate, the fact that Cullin was found in the complex suggests that it has an important function, perhaps in recruiting the E2 ubiquitin conjugating enzyme to the complex (figure 5.27b). Since the T22M mutation in the UBL domain of Fbxo7 interferes with its binding to Parkin, one possibility is that, like hSel-10, Fbxo7 binds Parkin directly but in this case via its N-terminus. An interaction with Skp1 may then be necessary in order to facilitate the ubiquitination, explaining the effect of the R378G mutation (figure 5.27c). In the future it would be interesting to investigate this further by silencing Skp1 and Cullin expression using siRNA and assessing the effect on Mfn1 ubiquitination following CCCP treatment.

A major strength of SCF-dependent ubiquitination is its versatility, enabling different E3 ubiquitin ligases to interact with different substrates under different conditions. By binding different FBPs such as Fbxo7 and hSel-10, Parkin may thus be capable of ubiquitinating different substrates in response to different cellular signals. It is also worth noting that while silencing Fbxo7 expression substantially reduces Parkin relocation and Parkin-mediated ubiquitination, it does not abolish it. While this may simply indicate that not all cells were transfected with the siRNA, another possibility is that a different FBP might mediate this residual effect.

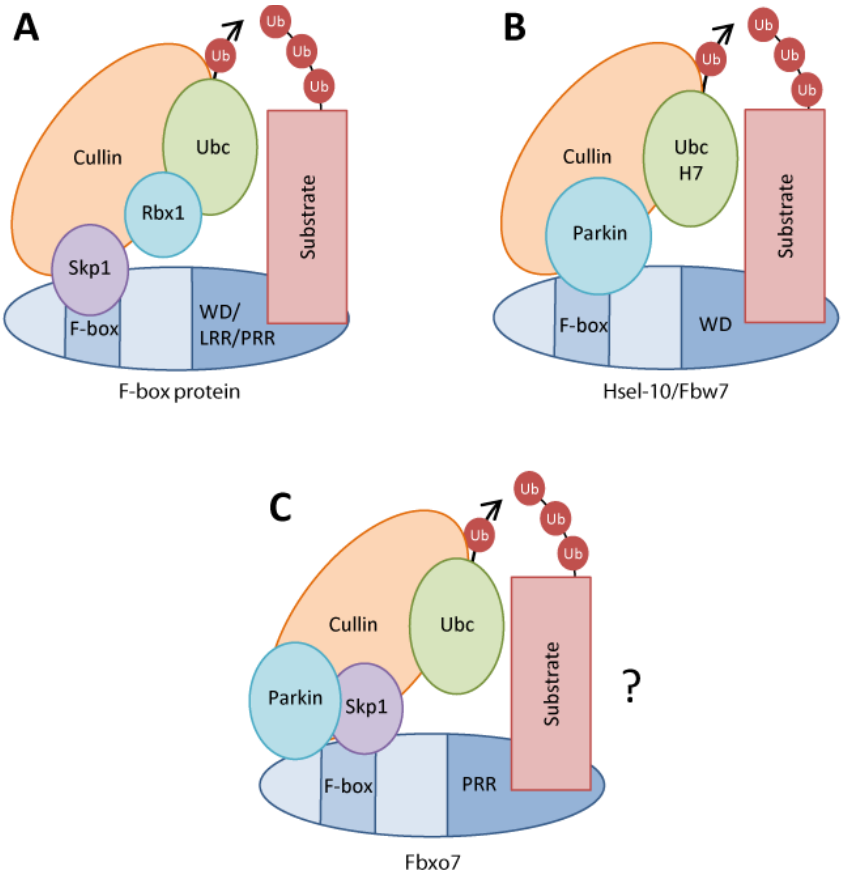

Figure 5.27 Typical and atypical SCF complexes. **(A)** A typical SCF complex, in which the FBP interacts with Skp1 through its F-box domain and the substrate through its C-terminal protein-protein interaction domain. Skp1 in turn binds Cullin, which binds the E3 ubiquitin ligase Rbx1 and a ubiquitin conjugating enzyme (Ubc). Figure based on (Kipreos and Pagano, 2000). **(B)** The FBP hSel-10 was found to interact directly with Parkin through its F-box domain. The complex included Cullin, but not Skp1 (Staropoli et al., 2003). **(C)** Hypothetical model by which Fbxo7 might mediate ubiquitination of Mfn1 by Parkin.

5.3.4. Role of PINK1

Silencing Fbxo7 had no effect on PINK1 accumulation at the mitochondria, indicating either that it functions in a second pathway parallel to PINK1, or that it functions downstream of PINK1 in the PINK1/Parkin pathway. Although the first possibility cannot be absolutely excluded on the basis of the results presented here, the fact that Fbxo7 interacts with PINK1, and that Parkin relocation to the mitochondria has been previously shown to be dependent on PINK1 (Geisler et al., 2010a; Narendra et al., 2010; Vives-Bauza et al., 2010), makes the second possibility far more likely. It is interesting to note that FBPs generally target phosphorylated substrates (Skowyra et al., 1997), and Fbxo7 in particular has been shown to mediate ubiquitination of the substrate HURP only after its phosphorylation by Cdk1-cyclin B (Hsu et al., 2004). It has previously been shown that PINK1 kinase activity is essential for Parkin recruitment to depolarised mitochondria (Geisler et al., 2010a), so a possible explanation could be that PINK1 phosphorylates a mitochondrial substrate which Fbxo7 can then interact with, stabilising its mitochondrial localisation selectively on depolarised mitochondria. Consistent with this idea, PK digestion suggested that Fbxo7 localises primarily to the OMM where it would be well positioned to interact with PINK1, Parkin and any substrates of PINK1 after CCCP treatment.

5.3.5. Fbxo7: one protein, many functions?

In addition to providing new mechanistic insight into PINK1/Parkin-mediated mitophagy, the results described in this chapter indicate a previously unrecognised role for Fbxo7 in mitochondrial function. Like many FBPs, Fbxo7 appears to participate in a diverse range of cellular processes, with previous studies suggesting possible roles in control of the cell cycle (Hsu et al., 2004) or apoptosis (Chang et al., 2006) (see section 5.1 and figure 5.28 overleaf). Two groups have reported that Fbxo7 can localise to the nucleus (Nelson and Laman, 2011; Zhao et al., 2011), with the former finding that this occurs specifically in cells entering the G_1-S transition in the cell cycle. Given that several FBPs have been shown to modulate transcription, for example Mdm30p in yeast (Muratani et al., 2005; Shukla et al., 2009) or Skp2 or Fbw7 in mammalian systems (Reavie et al., 2010; von der Lehr et al., 2003), it thus seems plausible that Fbxo7 may mediate transcription of genes involved in the G_1-S transition. While it is by no means impossible that the function of Fbxo7 at the mitochondria is completely independent of its function at the nucleus, it is interesting to consider that the two could be linked. Recent studies have investigated the

effect of mitochondrial function on the cell cycle, with one study showing that at the G_1-S transition mitochondria rearrange themselves into a highly fused network which enables more efficient ATP production, a step which was essential to enable the cell to enter S phase (Mitra et al., 2009). The data in this chapter indicate that Fbxo7 is capable of mediating the degradation of Mfn1 via Parkin-mediated ubiquitination; it is tempting to speculate, therefore, that it might also play a role in controlling basal mitofusin levels, perhaps by interacting with a different E3 ubiquitin ligase. If so, it is its translocation to the nucleus would occur at exactly the point in the cell cycle when mitofusins would be needed to mediate an increase in mitochondrial fusion.

If Fbxo7 is involved in controlling basal mitofusin levels, another function might also be possible. In yeast, an FBP called Mdm30p is known to interact with and mediate the degradation of the yeast homologue of mitofusins, fuzzy onion (Fzo1) (Cohen et al., 2008; Escobar-Henriques et al., 2006). Recent work has shown that this degradation occurs after Fzo-mediated tethering of the two mitochondria, and is essential to allow mitochondrial fusion to complete (Cohen et al., 2011). The present study has not investigated the possibility of a role for Fbxo7 in mitochondrial dynamics, but in the future it would be interesting to perform electron microscopy on Fbxo7 deficient cells to properly investigate mitochondrial morphology. Interestingly, some lymphoblasts homozygous for the R498X mutation did appear to exhibit a hyper-fused mitochondrial morphology, while fibroblasts carrying the R378G mutation seemed to have more fragmented mitochondria, potentially indicating an involvement of Fbxo7 in controlling both mitochondrial fusion and fission.

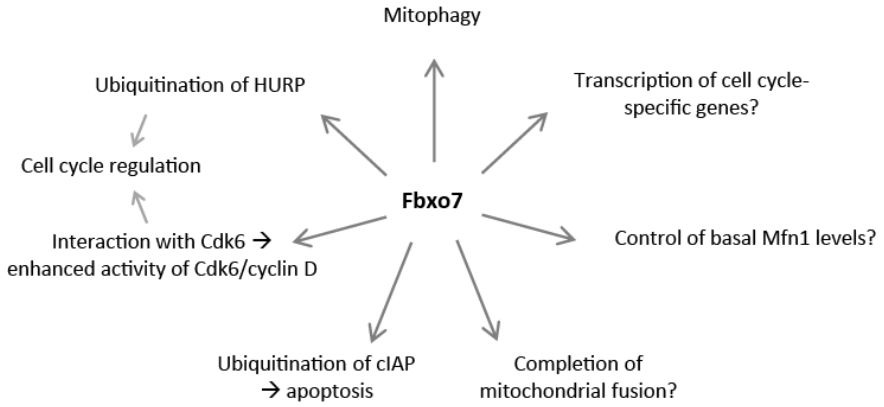

Figure 5.28 Known and putative functions of Fbxo7. On the left of the figure are previously published functions of Fbxo7 (see section 5.1), whilst on the right are possible novel functions discussed in this section.

5.3.6. Conclusions

In summary, this study shows that Fbxo7 has an N-terminal MTS but under basal conditions localises primarily to the cytosol. Upon treatment of the cell with CCCP, PINK1 and Fbxo7 both accumulate at the mitochondria, recruiting Parkin. Parkin translocation requires both PINK1 kinase activity and Fbxo7, giving rise to a possible model in which PINK1 phosphorylation of an OMM protein (probably Mfn1) allows Fbxo7 to bind it and therefore stabilise its localisation on the outer membrane. Fbxo7 binds Parkin in both the cytosol and the mitochondria, suggesting that Parkin might 'hitchhike' to the mitochondria by binding Fbxo7 and using its MTS. Once at the mitochondria, Parkin ubiquitinates Mfn1 in an Fbxo7-dependent manner, resulting in degradation of Mfn1 through the ubiquitin-proteasome system which in turn allows fragmentation of the damaged mitochondria and their degradation by mitophagy. The three PD-causing mutations all interfere with this pathway, but at different stages. The main findings of the study are summarised in figure 5.29 below.

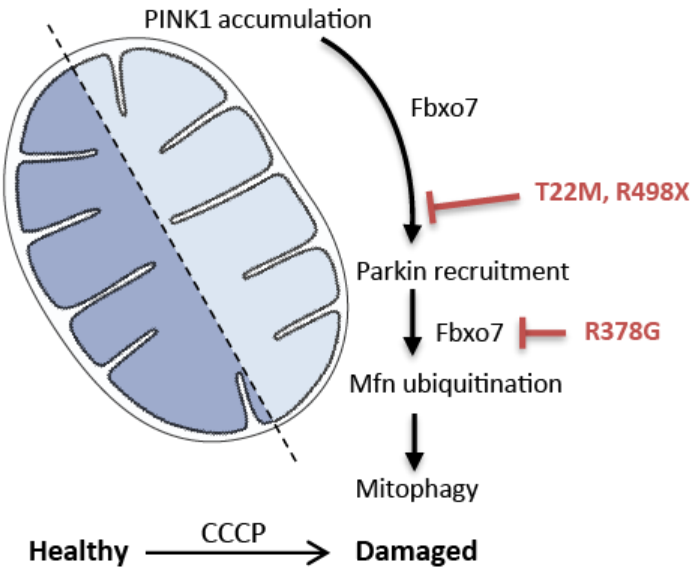

Figure 5.29 The role of Fbxo7 in PINK1/Parkin-mediated mitophagy.

5.3.7. Future perspectives

This work represents the first evidence linking Fbxo7 to mitochondria in general, and to PINK1/Parkin-mediated mitophagy in particular. However, many questions remain unanswered. Does Fbxo7 physically bring Parkin to the mitochondria, or merely stabilise it on the OMM once it reaches it? Why are both termini of Fbxo7 required for its

relocation to the mitochondria? Is PINK1 required for Fbxo7 relocation, and if so, does it phosphorylate Mfn1 to allow Fbxo7 to bind? Are Skp1 and Cullin involved in Parkin-mediated ubiquitination of Mfn1? Are other OMM proteins ubiquitinated in an Fbxo7/Parkin-dependent manner, and what function does that ubiquitination serve?

All of these questions are important, but some can be addressed more easily than others. To determine whether Mfn1 ubiquitination is SCF-dependent, for example, it would be interesting to assess the appearance of ubiquitinated forms in cells transfected with Skp1 or Cullin siRNA as previously mentioned. Similarly, relocation of Fbxo7 could be monitored by western blot in PINK1 knockdown cells to determine whether it is PINK1-dependent. Unfortunately, other questions are severely impacted by the inability to visualise Fbxo7 relocation by immunocytochemistry, either using antibodies to detect endogenous protein or by using tags at either terminus. To confirm the order of events, ideally all three proteins (PINK1, Fbxo7 and Parkin) would be tagged with fluorescent tags and their translocation to the mitochondria monitored in real time following CCCP treatment. This should make it possible to see in a single cell whether Fbxo7 relocation to the mitochondria precedes Parkin's relocation, or whether they translocate together. Still more elegant would be to monitor the interaction of Fbxo7 with Parkin following CCCP treatment using fluorescence resonance energy transfer (FRET), where both proteins are tagged with a fluorophore such that when the two interact the emission from the first fluorophore excites the second. Unfortunately, tagging the protein at either terminus appears to prevent its relocation, making these experiments impossible.

As well as further investigating the role of Fbxo7 in mitophagy, it would be interesting to identify other substrates for Fbxo7-mediated ubiquitination, perhaps by identifying interactors using tandem-affinity purification and mass spectrometry. Parkin has previously been described to ubiquitinate a number of substrates at the OMM, most notably VDAC1, which was modified by K27-linked ubiquitination to recruit p62 to the mitochondria (Geisler et al., 2010a). In addition to VDAC1, two recent studies have shown that Miro, an OMM component of the mitochondrial trafficking machinery, is phosphorylated by PINK1 which triggers its ubiquitination and degradation in a Parkin-dependent manner (Liu et al., 2012; Wang et al., 2011b). Since FBPs are known to primarily interact with phosphorylated substrates (Skowyra et al., 1997), an attractive possibility is that Parkin may mediate this ubiquitination as part of an SCF-like complex, either with Fbxo7 or a different FBP. Finally, it may also be interesting to determine

whether Fbxo7 has substrates on other organelle membranes. A recent study from the group of Richard Youle has shown that ectopically targeting PINK1 to the OMM is sufficient to recruit Parkin and mediate mitochondrial clearance in the absence of a depolarising stimulus, and furthermore, that targeting PINK1 to the peroxisome is sufficient to recruit Parkin and mediate pexophagy (Lazarou et al., 2012). The authors conclude that no mitochondria-specific proteins are thus required for mitophagy, but an alternative interpretation is that the PINK1/Fbxo7/Parkin machinery is adaptable to substrates on different subcellular membranes.

The finding that Fbxo7 is present at low levels in the mitochondrial fraction of harvested cells under basal conditions raises further questions. Is it expressed at low levels in all mitochondria, or in the mitochondria of some cells, or in a subpopulation of mitochondria in all cells? Given that it appears to have an MTS, why does Fbxo7 not localise to a greater extent to the mitochondria? In the case of PINK1, the full length protein is targeted to the mitochondria by the MTS, but in healthy mitochondria it is cleaved out, explaining its largely cytosolic localisation (Jin et al., 2010). This seems unlikely in the case of Fbxo7, since there is no difference in molecular weight between the cytosolic and mitochondrial protein; however, another possibility is that Fbxo7 could be degraded by proteases in the mitochondria. Fbxo7 also has a functional nuclear targeting sequence (Zhao et al., 2011), so its localisation may also be regulated by interactions that mask one or both sequences.

A final question is whether Fbxo7 has a function in healthy mitochondria, or only in removing those that have been damaged. In this study the investigation of mitochondrial physiology in Fbxo7 deficient cells was extremely preliminary, but suggested a mitochondrial defect along similar lines to that previously reported for PINK1 deficient cells (Exner et al., 2007; Gautier et al., 2008; Wood-Kaczmar et al., 2008), although basal mitochondrial calcium levels appeared reduced in the Fbxo7 knockdown cells whereas they were found to be elevated in PINK1 deficient cells (Gandhi et al., 2009). Whether this dysfunction is the result of an accumulation of damaged mitochondria, or a role for mitochondrial Fbxo7 in basal mitochondrial function, will be the subject of further discussion in the next chapter.

Chapter 6

Discussion

This thesis has focused on the role of mitochondrial dysfunction in PD, and particularly in familial forms of the disease. The direct conclusions and implications of the results presented have already been discussed; this chapter will therefore seek to address the broader questions raised by the work and the implications for the field at large.

6.1. Mitochondrial dysfunction in neurodegeneration and PD

A wealth of evidence has implicated mitochondrial dysfunction in both sporadic and familial forms of PD (see section 1.3), but in many cases it remains unclear exactly what causes that mitochondrial dysfunction, and what part it plays in the eventual cell death. In mice, the loss of HtrA2 function results in striatal neurodegeneration and a severe parkinsonian behavioural phenotype (Jones et al., 2003; Martins et al., 2004). To investigate the cause of this phenotype, in chapter 3 the mitochondrial physiology of WT and KO mouse neurons was assessed by live cell imaging approaches, revealing a pathological mitochondrial uncoupling through the ATP synthase which resulted in ATP depletion and vulnerability to ischaemic cell death.

Chapter 4 of this thesis next aimed to provide further evidence of a role for mitochondrial dysfunction in PD pathogenesis by identifying a novel mitochondrial function for one or more of the proteins encoded by PD genes. Using an shRNA screen approach to investigate all the PD genes proved impossible in the time available, but in chapter 5, *in silico* analysis of the peptide sequence of Fbxo7 (encoded by the PD gene *Fbxo7*/*PARK15*)

suggested a previously unrecognised mitochondrial localisation for the protein. Further work indicated that Fbxo7 participates in the previously described PINK1/Parkin pathway to mediate the selective clearance of damaged mitochondria by mitophagy, providing yet more evidence of a mitochondrial link to PD. Overall, therefore, the work described in this thesis complements existing knowledge of mitochondrial involvement in disease pathogenesis by uncovering a novel mechanism of mitochondrial dysfunction in HtrA2 KO mice and by identifying a previously unrecognised mitochondrial function for Fbxo7.

6.2. Mitochondrial maintenance in neurodegeneration

As described in chapter 1, the integrity of the mitochondrial network is maintained through two pathways: at the protein level, by system of chaperones and proteases, and at an organellar level by the removal of damaged mitochondria through mitophagy. Both pathways have been implicated in neurodegeneration by the identification of disease-causing mutations in genes such as *PINK1*, *Parkin* and *Fbxo7* in the mitophagy pathway or *mortalin* and *paraplegin* in the mitochondrial protein quality control pathway (see section 1.2.4). Mutations in many of these genes result in early onset neurodegeneration, consistent with the idea that accumulation of mitochondrial damage underlies the ageing process (Green et al., 2011). Any defect in the processes that repair or remove damaged mitochondria would thus be expected to cause an acceleration of age-related diseases such as PD.

6.2.1. PINK1: a 'master regulator' of mitochondrial quality control?

This thesis has focused on two proteins in detail: HtrA2 and Fbxo7. As discussed previously (chapter 3), a number of groups have suggested that HtrA2 may function in mitochondrial protein quality control, since loss of HtrA2 results in an accumulation of unfolded mitochondrial proteins (Moisoi et al., 2009) and damaged proteins found in the IMS following proteasomal inhibition were shown to be substrates for HtrA2 (Radke et al., 2008). The data in chapter 5 shows that Fbxo7 also has a role in mitochondrial maintenance, since loss of Fbxo7 impaired Parkin recruitment to depolarised mitochondria and subsequent mitophagy. Interestingly, these two proteins also have another factor in common as both appear to function either downstream of, or in concert with, PINK1 (see below). The observation that PINK regulates proteins involved in both

processes has led some to suggest that it could act as a 'master regulator' of mitochondrial quality control, co-ordinating the actions of the two pathways described (Dagda and Chu, 2009; Desideri and Martins, 2012).

A number of factors make PINK1 an attractive candidate to perform this function. As a mitochondrial kinase, PINK1 would be well placed to control signalling pathways in response to mitochondrial stress. It has been described variously to localise to the cytosol (Haque et al., 2008; Takatori et al., 2008), IMM (Muqit et al., 2006; Pridgeon et al., 2007; Silvestri et al., 2005), OMM (Muqit et al., 2006; Zhou et al., 2008), and IMS (Pridgeon et al., 2007), with recent evidence suggesting that it is continually synthesised and targeted to the IMM where it is cleaved, released to the cytosol and rapidly degraded by the proteasome (Jin et al., 2010; Narendra et al., 2010). This perpetual cycling of PINK1 could allow its regulation by either mitochondrial or cytosolic factors that might impact on the protein's import, cleavage, release or degradation. Mitochondrial depolarisation has long been known to impair import of mitochondrial proteins (Schleyer et al., 1982), causing mitochondrially targeted PINK1 to instead accumulate on the OMM (Narendra et al., 2010). This allows PINK1 to interact with the predominantly cytosolic proteins Parkin and Fbxo7 on the OMM, which is essential in order to target the mitochondria for its subsequent removal through the lysosome (Geisler et al., 2010a; Narendra et al., 2010; Vives-Bauza et al., 2010). On the other hand, PINK1-dependent phosphorylation of HtrA2 in the IMS requires activation of the mitogen-activated protein kinase (MAPK) p38 (Plun-Favreau et al., 2007), which may be triggered by various cellular stressors (Cuadrado and Nebreda, 2010). PINK1 has additionally been shown to phosphorylate the mitochondrial chaperone protein tumour necrosis factor receptor-activated protein 1 (TRAP1), and this phosphorylation enabled TRAP1 to protect cells against oxidative damage and apoptosis in response to oxidative stress (Pridgeon et al., 2007). A pathway thus emerges whereby milder stresses such as oxidative damage may activate PINK1 in the IMM, where it activates HtrA2 to degrade the resultant damaged proteins and TRAP1 to prevent apoptosis, while severe mitochondrial damage would cause mitochondrial depolarisation and thus PINK1 accumulation on the OMM to mediate mitophagy (figure 6.1).

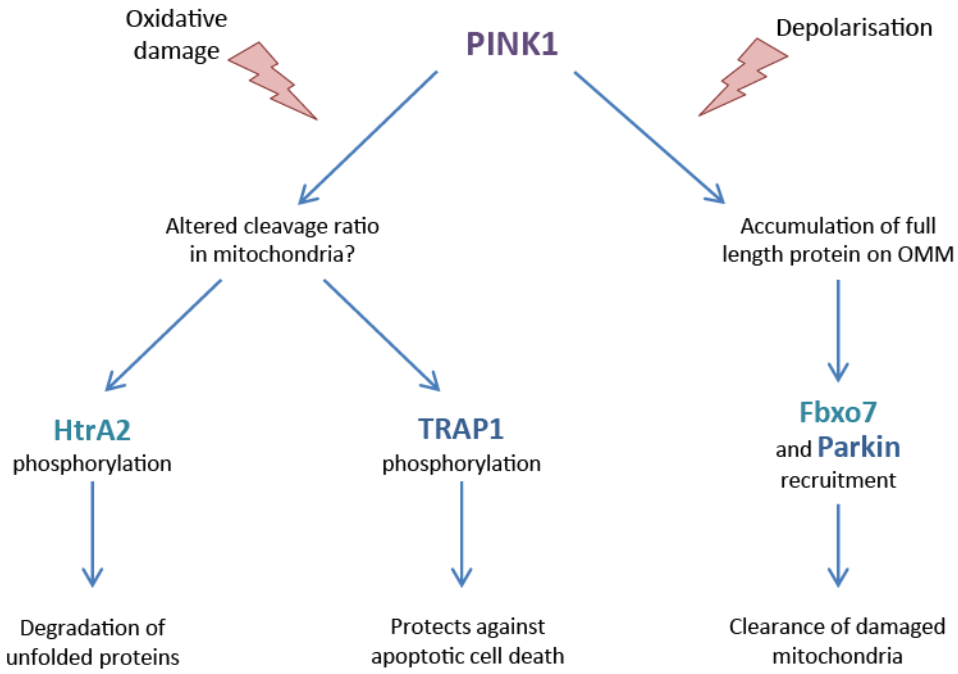

Figure 6.1 PINK1 as a regulator of mitochondrial maintenance. A hypothetical system by which PINK1 could activate distinct pathways for mitochondrial maintenance in response to either oxidative stress (resulting in phosphorylation of HtrA2 and TRAP1) or mitochondrial depolarisation (resulting in Fbxo7 and Parkin recruitment and mitophagy).

Another factor which could also be considered in this hypothetical system is the effect of PINK1 cleavage on its protective function. Although it has been reported that the processed form of PINK1 is released to the cytosol and rapidly degraded (Lin and Kang, 2008; Narendra et al., 2010), a study by Deas *et al.* introduced mutations close to the cleavage site of PINK1 to either enhance or impair its cleavage and thereby investigate the effects of both full length and cleaved PINK1 on mitochondrial function (Deas et al., 2011). This study revealed that mutations that increase the ratio of full length to processed PINK1 cause mitochondrial depolarisation and increased ROS, while mutations that decreased the ratio were found to increase $\Delta\Psi_m$ (Deas et al., 2011), suggesting that the processed form has a protective function in the mitochondria. Factors that either interfere with cleavage of PINK1 or stabilise either full length or processed PINK1 may thus have important effects on PINK1 function and may participate in the activation of PINK1 in response to mitochondrial stress. Interestingly the chaperone protein Hsp90 and its co-chaperone Cdc37 have been previously shown to protect PINK1 from proteasomal degradation (Lin and Kang, 2008; Moriwaki et al., 2008) and to control the ratio of full length to processed PINK1 in the mitochondria (Weihofen et al., 2008). Hsp90 in complex with Cdc37 was found to stabilise the full length PINK1 peptide, increasing the ratio of full length to processed PINK1, but Cdc37 acting independently of Hsp90 was able to reduce the ratio by increasing levels of processed PINK1 in the mitochondrial fraction and reducing levels in the cytosol (Weihofen et al., 2008). It is thus tempting to speculate that oxidative stress might affect mitochondrial PINK1 levels and ratio via an effect on Hsp90 levels, perhaps providing a mechanism by which PINK1 could mediate an oxidative stress response. In support of this hypothesis, one study has shown that Hsp90 is cleaved in response to oxidative stress (Beck et al., 2009).

6.2.2. Additional functions of Fbxo7 and HtrA2

As attractive as the scheme proposed in figure 6.1 is, it is important to note that each of these proteins have also been described to have additional functions, any of which may contribute to the pathological effects of disease-causing mutations. As discussed in chapter 3, the mitochondrial uncoupling caused by HtrA2 deficiency appeared to precede the accumulation of unfolded proteins which has been described in older HtrA2 KO mice (Moisoi et al., 2009) and HtrA2 was found to interact with the ATP synthase, suggesting that it may have a direct effect on ATP synthase function in additional to its role in mitochondrial protein quality control (see section 3.3.4). Similarly, Fbxo7 has a number of

previously reported functions in control of cell cycle and apoptosis, and the finding that it has a mitochondrial localisation under basal conditions may indicate an additional role in basal mitochondrial function (section 5.3.7). These additional functions do not negate the importance of mitochondrial maintenance in PD pathogenesis, but in the future it will be interesting to see to what extent failure of mitochondrial quality control can be observed in patients with sporadic disease.

The additional protein functions mentioned above may also help to explain the variation in the mitochondrial phenotypes of cells lacking Fbxo7, Parkin, PINK1, or HtrA2. The data shown in chapter 3 of this thesis showed that HtrA2 deficiency results in mitochondrial depolarisation similar to that observed in PINK1 deficient cells (Exner et al., 2007; Valente et al., 2004; Wood-Kaczmar et al., 2008), but whereas in PINK1 deficient cells this was shown to arise from a reduction in respiration (Liu et al., 2009; Piccoli et al., 2008), in HtrA2 KO mouse neurons it is instead due to mitochondrial uncoupling which is observed as an increase in respiration (figure 3.4 and figure 3.6). The KO mice also have very different behavioural phenotypes *in vivo*, with PINK1 KO mice displaying only a mild movement phenotype in old age (Gispert et al., 2009) while the HtrA2 KO mice exhibit striatal neurodegeneration and severe parkinsonsim (Martins et al., 2004), consistent with HtrA2 having both PINK1-dependent and -independent functions. Similarly, although only a preliminary examination of mitochondrial physiology in Fbxo7 deficient cells was carried out it suggested that while $\Delta\Psi_m$ and mitochondrial respiration were reduced compared to control cells as has been described for PINK1, basal mitochondrial calcium levels were significantly reduced in the knockdown cells whereas the reverse has been reported in PINK1 deficient cells (Gandhi et al., 2009). In the case of Fbxo7 it is also interesting to consider the difference in mitochondrial phenotype between cells in which the *Fbxo7* gene was silenced with shRNA, and cells from patients with PD-causing mutations (figure 5.21 and figure 5.22). The experiments cannot be properly compared because of the difference in cell types between the patient cells and the knockdown cell lines, but a possibility is that the R378G or R498X mutations may interfere with some, but not all functions of Fbxo7. Further investigation of the patient fibroblasts and lymphoblasts may thus have potential in teasing out the most relevant functions of Fbxo7 to disease pathogenesis.

Overall, therefore, it seems likely that the mitochondrial dysfunction observed in cells lacking either of these genes is not simply due to a failure of mitochondrial maintenance

but also reflects a basal mitochondrial function of both proteins. Nonetheless, the fact that four PARK genes can be linked in a putative pathway to control mitochondrial quality control certainly serves to underline the importance of this process in neuronal function, and may highlight a pathway prone to deregulation in sporadic forms of the disease. Further work will be required to fully investigate this contribution to the disease in the future.

6.3. Future directions and therapeutic targets

Nearly 200 years after James Parkinson first described the disease that was to bear his name, our understanding of the pathogenic mechanisms that underlie the disease has substantially improved but this has failed to translate into effective therapeutic strategies. As discussed in chapter 1, PD appears to result from a combination of defective pathways arising from both genetic and environmental factors. While mitochondrial dysfunction is by no means the only pathway to disease pathogenesis (see section 1.1.5), it has been strongly implicated in both familial and sporadic PD and as such has been previously suggested as a potential therapeutic target (Burchell et al., 2010a, b). Looking to the future, it is useful to consider which questions still need to be answered, and how existing knowledge may be applied to treating the disease.

6.3.1. Future directions in PD research

Following directly from this thesis, an important direction for future research will be the further investigation of the mitophagy pathway. The discovery that Fbxo7 participates in this pathway requires further study along the lines already discussed (section 5.3) in order to fully elucidate each protein's part in the mechanism; however, future research should also focus on the identification of other novel members of the pathway as this may contribute further pieces of the puzzle. One approach to identify these proteins could be whole genome RNAi screening using high content analysis, following a similar approach to that described in chapter 4. Although the shRNA screen attempted in this thesis was not successful, RNAi screening remains an extremely powerful tool which, performed on a whole-genome scale, enables investigation of a problem in a non-hypothesis-driven manner (Hirsch, 2010; Wolters and MacKeigan, 2008). In the case of mitophagy, using immunocytochemical assays for Parkin relocation or mitochondrial disappearance as readouts for a whole genome RNAi screen may allow the identification of novel

participants in the pathway which could not have been predicted on the basis of existing knowledge. Interestingly, one recent genome-wide siRNA screen along these lines used GFP-LC3 colocalisation with a viral capsid protein to identify mediators of virophagy in live cells (Orvedahl et al., 2011). Of 141 hits that could be confirmed using individual siRNAs, 96 were also found to affect mitophagy, which was assessed using cells overexpressing mCherry-Parkin (Orvedahl et al., 2011), highlighting the large number of proteins involved in this process. Using pathway analysis to identify common pathways in the hits identified by this and future screens may offer new directions for future research in this area.

On a broader level, a whole genome approach is also being applied in a different form to identify new genes associated with PD. This thesis has focused primarily on the investigation of genes that have been linked to PD either by linkage analysis in affected families or by relatively small hypothesis-driven association studies. This approach has proven extremely fruitful in the past decade (Lesage and Brice, 2012), with the identification of heritable mutations accounting for the majority of familial PD cases. While there remains some way to go in understanding the physiological functions of all these proteins, genetic studies are now increasingly looking to identify common SNPs which affect disease risk by using large scale genome-wide association studies. A number of polymorphisms have already been identified (Martin et al., 2011), but determining the causative mutations (as opposed to harmless polymorphisms in linkage disequilibrium with the lead SNP) and their functional effects will be a major challenge for the field in the future.

6.3.2. Lessons from other diseases: neurodegeneration and cancer

As a scientist working on one specific disease, it is easy to be blinded to the lessons that can be learnt from research into similar or even apparently disparate diseases. PD bears numerous similarities to the other common neurodegenerative disorders, AD, HD and ALS. For example, all four diseases commonly occur in later life, indicating a slow disease progression prior to onset of symptoms; all have strong genetic elements, at least in some forms of the disease (Lill and Bertram, 2011); all are characterised pathologically by protein aggregation (Weydt and La Spada, 2006); and all have been associated with mitochondrial dysfunction (Filosto et al., 2011). Perhaps more surprisingly, each of these

statements could equally be applied to cancer, even though at first glance it seems the opposite of neurodegeneration: a disease caused by inappropriate cell survival as opposed to inappropriate cell death. Like PD, however, cancer occurs most commonly in later life and, although usually sporadic in aetiology, may in rare cases be caused by germline mutations (Plun-Favreau et al., 2010). Protein aggregation has been implicated in the disease since aggregation and consequent inactivation of tumour suppressor proteins has been suggested to play a key role in tumorigenesis (Scott and Frydman, 2003), and mitochondria have also been linked to cancer by the observation that tumour cells exhibit an increased reliance on glycolysis rather than oxidative phosphorylation for ATP production (Warburg, 1956). Most strikingly of all, mutations in many of the genes found to associate with PD had already been identified in various cancers (Devine et al., 2011). As mentioned previously (section 5.1), Fbxo7 has previously been described as a proto-oncogene and was found to be highly expressed in epithelial cancers (Laman et al., 2005), suggesting that a gain of function may cause cancer while a loss of function causes PD. By contrast, loss of function of Parkin has been described in both PD (Kitada et al., 1998) and cancer (Cesari et al., 2003), suggesting that the same protein can have both a neuroprotective and a tumour-suppressor function.

The similarities between these diseases may have enormous value in therapeutic strategy, as compounds that target a disease process in one disease may be used in another: for example, a compound that targets amyloid β aggregation in AD may prove equally effective against α-synuclein aggregation in PD. However, they also raise countless questions. If the underlying pathology in different neurodegenerative diseases is similar, what causes the dopaminergic neurons to die in PD while the cortex is predominantly affected in AD and the striatum in HD? Why does a germline mutation result in neuronal death, while a somatic mutation in the same gene in a non-neuronal cell lead to tumour formation? Determining the answers to any of these questions would be a major advance in our understanding of each of these diseases.

6.3.3. Mitochondria as a therapeutic target

The identification of a role for mitochondrial dysfunction in PD pathogenesis has led several groups to devise therapeutic strategies that directly target the mitochondria. In particular, therapies targeting ROS have long held potential for the treatment of neurodegenerative disease, with the first antioxidant therapies going into clinical trials over ten years ago (Fahn, 1991; LeWitt, 1991; Shoulson, 1989). So far, however, results

have been disappointing. In PD, administering the mitochondrial antioxidant coQ_{10} has produced varying results in clinical trials depending on dosage (Shults et al., 2002; Storch et al., 2007), while mitoQ, a mitochondrially targeted derivative of coQ_{10} (Kelso et al., 2001), had no significant effect on disease progression in a double-blind placebo controlled study of 128 PD patients (Snow et al., 2010). In the future alternative approaches to target oxidative stress may be more successful, such as activation of the Nrf2 signalling pathway to upregulate endogenous antioxidants (Cuadrado et al., 2009). Other mitochondrial targets are also being considered, including the ETC itself: for example, one recent study tested the therapeutic effects of a non-coding RNA derived from the human cytomegaloviral β2.7 transcript which has been found to directly interact with mitochondrial complex I in infected cells, preventing cell death and maintaining energy production (Kuan et al., 2012). Linking the RNA to a peptide derived from a rabies virus glycoprotein enabled its effective delivery to the brain, where it had a significant protective effect on rat toxin models of PD without showing any immunogenic effect (Kuan et al., 2012).

Since mitochondrial damage appears to play a key role in the pathogenesis of both familial and sporadic PD (see section 1.3), and mitophagy is an important mechanism for the removal of damaged mitochondria (see section 1.2.4), it is also interesting to consider the therapeutic potential of upregulating this process to treat PD. Mitophagy is already of therapeutic interest in the cancer field, since a dramatic increase in mitophagy can deplete ATP levels to the point at which the cell can no longer maintain its ionic homeostasis (Narendra et al., 2008), offering a mechanism of cell death in cells which are intrinsically resistant to apoptosis (Gargini et al., 2011; Hughson et al., 2012). Some existing anti-cancer drugs have been suggested to induce mitophagy by causing opening of the PTP, leading to mitochondrial depolarisation which triggers mitophagy (Hughson et al., 2012). This approach would be of little therapeutic value, however, in cases where the pathology is the result of an impairment of the mitophagy pathway. An alternative approach could be instead to target more generalised mechanisms of autophagy (Harris and Rubinsztein, 2012). As was discussed in the introduction (section 1.2.4.2), a number of common mechanisms underlie both general macroautophagy, which is triggered by nutrient deprivation under the control of the mammalian target of rapamycin, mTOR (Ravikumar et al., 2010), and selective forms of autophagy such as mitophagy. A number of FDA-approved drugs have been found to upregulate autophagy through mTOR-independent pathways (Harris and Rubinsztein, 2012). These include the mood stabilisers lithium,

sodium valproate and carbamazepine, all of which act on inositol signalling pathways (Sarkar et al., 2005), and the anti-hypertensive agents clonidine and rilmenidine, both of which induce inhibitory G-protein signalling pathways leading to a reduction in levels of cAMP (Williams et al., 2008). Several of these compounds have been shown to improve clearance of aggregated proteins in *in vivo* models of either Huntington's disease or PD (Harris and Rubinsztein, 2012), although none of these studies investigated their effect on mitochondrial function in these models.

In addition to these general upregulators of autophagy, in the future new therapeutic targets may arise from an increased understanding of the pathways underlying selective mitophagy. High content screening of existing compounds to identify those that increase LC3 colocalisation with mitochondrial markers or reduce mitochondrial mass following mitochondrial depolarisation may reveal new compounds, which could in turn provide new tools to investigate the mechanisms involved. Since the discovery that Parkin participates in targeting mitochondria for mitophagy there has been a surge in research in this area, raising hopes that this improvement in mechanistic understanding may in the future be translated into therapeutic targets.

Finally, despite the promise of mitochondrial therapeutics it is important to recognise their limitations. Most PD patients do not present clinically until a large percentage of the nigral neurons are already lost, and mitochondrial therapies will not be able to bring those neurons back. For this reason it is essential that biomarkers are identified to allow earlier diagnosis and treatment of the disease (Henchcliffe et al., 2011). As more effective mitochondrial therapeutics are developed and diagnosis is improved, these approaches may yet have the potential to significantly slow the progress of the disease, enabling it to be controlled with dopamine agonists and precursors for longer and thereby improving quality of life for a large number of people.

Appendices

Appendix I

Fbxo7 cloning strategy

1. Untagged T22M Fbxo7

Unlike the WT, R378G and R498X mutant Fbxo7 sequences, the T22M mutation could only be obtained with an N-terminal FLAG tag, which could potentially obscure the mitochondrial targeting sequence. In order to produce an untagged version of the construct, cloning primers were designed against the 5' and 3' termini of the Fbxo7 sequence as follows:

Fbxo7Hind3F 5'- CCGAAGCTTGCCACCATGAGGCTGCGGGTGCGG -3'

HindIII Kozak Fbxo7 coding sequence

Fbxo7XhoIR 3'- GCCTCGAGTCACATGAATGACAGCCGG -5'

XhoI Fbxo7 coding sequence (RC)

(RC = reverse complement)

The PCR product was inserted between the HindIII and XhoI sites of pcDNA3 (Invitrogen; figure I.1).

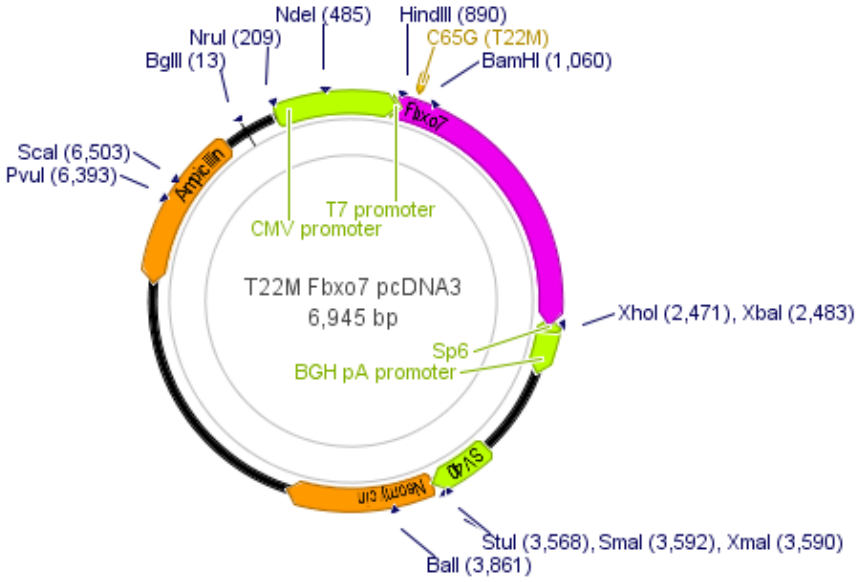

Figure I.1 Vector map of T22M-Fbxo7 in pcDNA3. Inserted Fbxo7 is shown in magenta; sites for common restriction enzymes are indicated in navy.

2. WT and PD mutant Fbxo7-HA constructs

C-terminal HA fusions were produced by incorporating the HA tag into the reverse primer between the end of the coding sequence and the stop codon, resulting in a direct fusion with no additional amino acids between the Fbxo7 sequence and the tag. Primers used were **Fbxo7Hind3F** and **Fbxo7Xho1HAR** for the WT, T22M and R378G mutant forms of Fbxo7; **Fbxo7Hind3F** and **Fbxo7R498XXho1HAR** for the R498X truncated form. Primer sequences and annealing temperatures may be found in Appendix II. The Fbxo7-HA PCR products were inserted into pcDNA3 between the HindIII and XhoI restriction sites (figure I.2).

Fbxo7Xho1HAR

3′–GCCTCGAGTCAAGCGTAATCTGGTACGTCGTATGGGTATCACATGAATGACAGCCGGCC–5′

XhoI | **Stop codon** | **HA sequence (RC)** | **Fbxo7 CDS (RC)**

Fbxo7R498XXho1HAR

3'-GCCTCGAGTCAAGCGTAATCTGGTACGTCGTATGGGTACCCTGGCAAGATGGGGTTAGG-5'

XhoI | **Stop codon** | **HA sequence (RC)** | **Fbxo7 CDS 1471-91 (RC)**

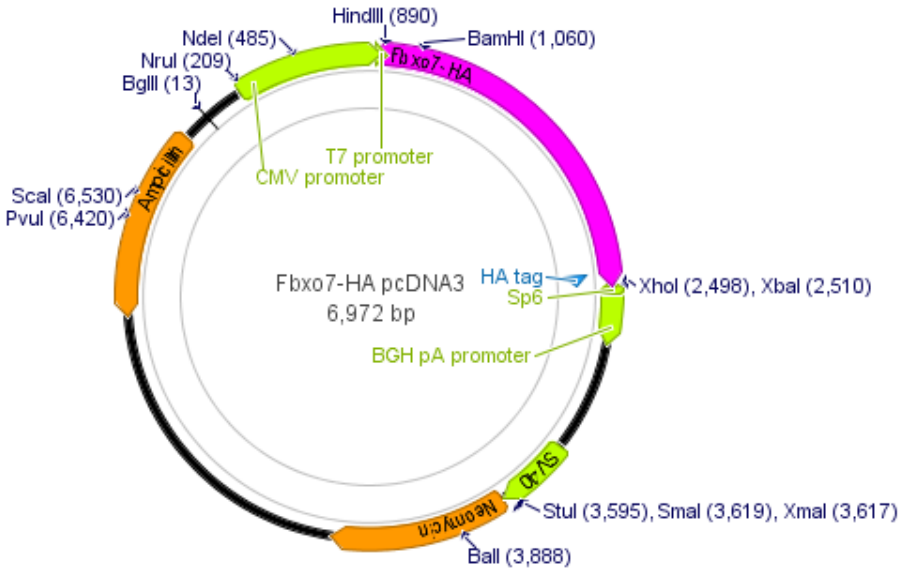

Figure I.2 Vector map of Fbxo7-HA in pcDNA3. Fbxo7 is indicated in magenta, with the C-terminal HA tag highlighted in blue. Common restriction sites are marked.

3. Mutant mitochondrial targeting sequence

In order to examine the function of the mitochondrial targeting sequence of Fbxo7, it was necessary to generate a construct with mutations in the putative MTS. These mutations should destroy the predicted mitochondrial localisation but have the minimum possible effect on protein structure in order to avoid affecting any interactions. By systematically mutating each residue of the MTS *in silico*, two amino acid mutations were chosen (R2D and R6W) which in combination substantially reduced the mitochondrial prediction scores generated by the four algorithms shown in table I.1 below.

	Mitoprot	PSORT	Target P	Predotar
Fbxo7 isoform 1	0.8505	0.391	0.597	0.36
Fbxo7 mutant MTS (R2D, R6W)	0.1536	0.174	0.103	0.03

Table I.1 Mitochondrial prediction of WT and mutant Fbxo7

Since these mutations are very close to the N-terminus of the protein, it was possible to incorporate the mutations in a cloning primer in a similar manner to the HA tag described above, rather than performing site directed mutagenesis. Two constructs were generated: one containing the untagged double-mutant Fbxo7, and another containing a version with an N-terminal T7 tag.

For the untagged construct, a forward primer was designed including an EcoRI site (**FBXO7_MTS_EcoRI**). PCR was performed using the reverse primer **Fbxo7XhoIR** and the PCR product inserted into pcDNA3 (figure I.3 overleaf).

FBXO7_MTS_EcoRI

5'-CGGAATTCGCCACCATGGACCTGCGGGTGTGGCTTCTGAA-3'

EcoRI Kozak Fbxo7 coding sequence (mutations underlined)

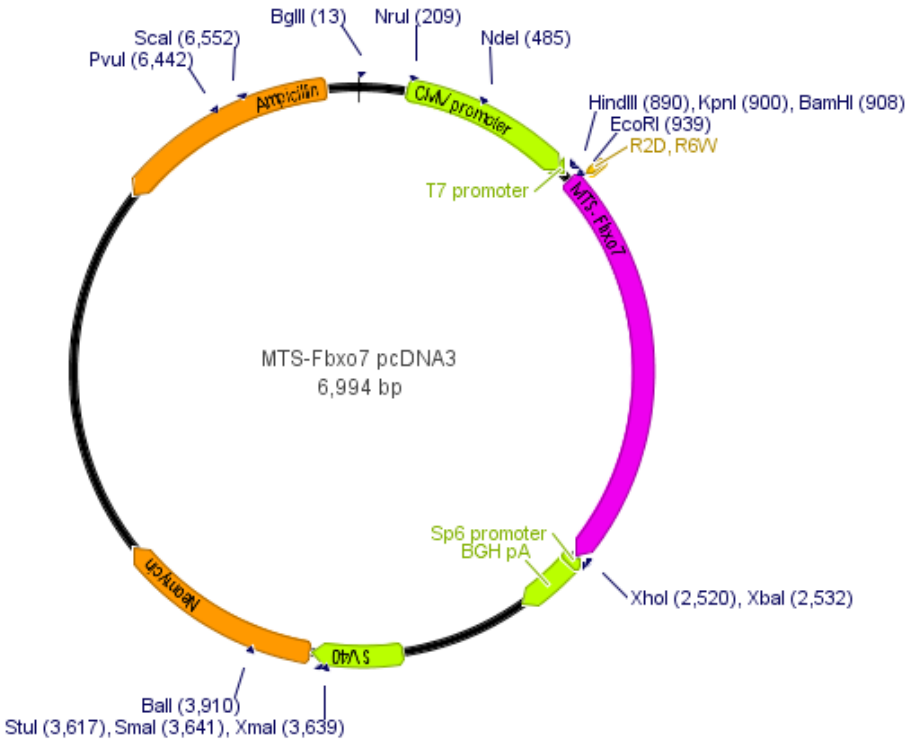

Figure I.3 Fbxo7 with mutant MTS inserted into pcDNA3. Fbxo7 is indicated in magenta; inserted mutations (R2D and R6W) are indicated in brown. Common restriction sites are marked.

For the T7-tagged construct, a T7-Fbxo7 construct obtained from Heike Laman (Cambridge University) was used as a template. This construct had been generated by cloning a Kozak and T7 sequence into pcDNA3 between the HindIII and BamHI sites, then cloning Fbxo7 into the same vector between the BamHI and XhoI sites. To generate the new T7-mutant construct, an EcoRI forward primer (**FBXO7_MTS_EcoRI_T7)** was used with the same reverse primer (**Fbxo7XhoIR**), then the T7-Fbxo7 construct was digested with EcoRI and XhoI to remove the original sequence and the digested PCR product ligated in in its place (figure I.4). The forward primer does not contain a Kozak sequence but does contain two additional bases in order to keep the Fbxo7 sequence in frame with the T7 tag.

FBXO7_MTS_EcoRI_T7

5'-CGGAATTCTTATGGACCTGCGGGTGTGGCTTCTGAA-3'

EcoRI | **2bp to keep phase** | **Fbxo7 coding sequence (mutations underlined)**

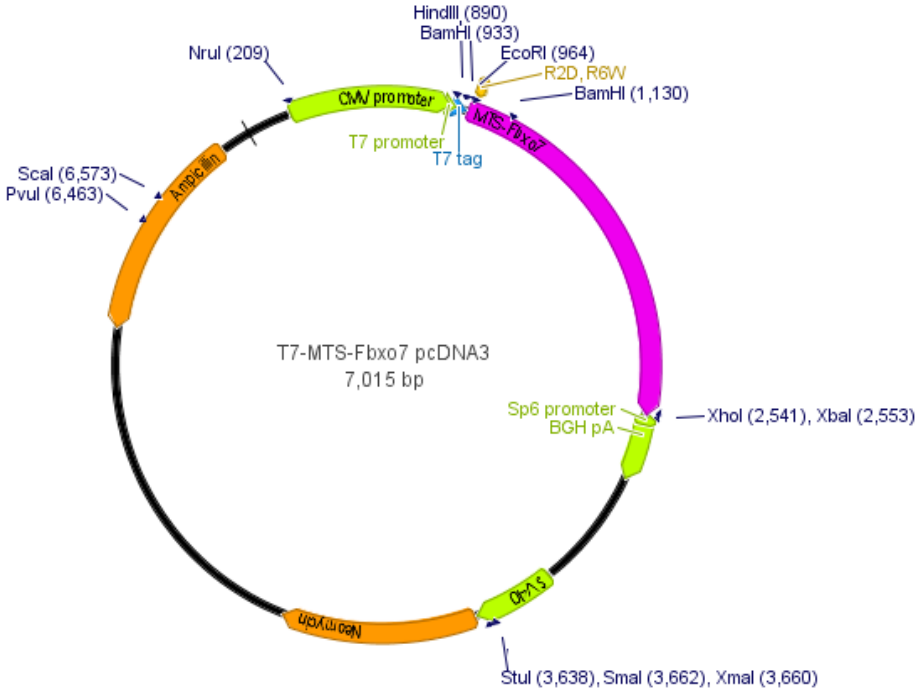

Figure I.4 T7-tagged Fbxo7 with mutated MTS. T7 tag is shown in blue between the HindIII and BamHI sites; Fbxo7 is in magenta between the EcoRI and XhoI sites. The two MTS mutations (R2D and R6W) are indicated in brown.

4. Internal FLAG-tagged constructs

Since tags at either the N- or C-termini appeared to interfere with Fbxo7 relocation to the mitochondria (section 5.2.2), constructs were generated with an internal FLAG tag. This tag was inserted between the UBL domain and the Cdk6 binding domain, as this region has no known function and analysis of the amino acid sequence using the program Geneious version 5.5.7 (Drummond et al., 2011) suggested the region to be disordered in structure (figure I.5)

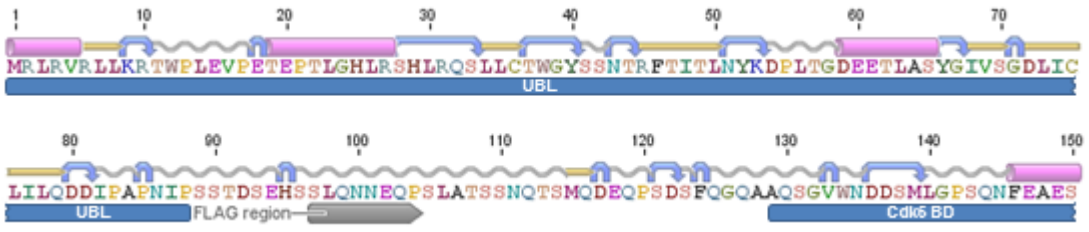

Figure I.5 Predicted secondary structure for N-terminal Fbxo7 peptide (aa 1-150). The UBL and Cdk6 binding domains of Fbxo7 are indicated in blue; the region selected for insertion of the FLAG sequence is indicated in grey.

In order to generate these constructs, a fusion PCR approach was used (see figure I.6). Two pairs of primers were designed, the first to amplify the N-terminus of Fbxo7 up to the FLAG tag, and the second to amplify the C-terminus from the FLAG tag to the end. The reverse primer for the first pair included the reverse complement of the FLAG sequence, while the forward primer for the second pair included the forward sequence of FLAG (see below). The first pair used the **Fbxo7Hind3F** primer described previously with the **Fbxo7_FLAG-IT_R** primer below, while the second pair used the **Fbxo7_FLAG-IT_F** primer below with the **Fbxo7XhoIR** primer described previously.

Fbxo7_FLAG-IT_R

3'- GACTACAAGGACGACGACGACAAGCCTCAGGTGCGAGCGC –5'

FLAG sequence (RC) Fbxo7 coding sequence (RC)

Fbxo7_FLAG-IT_F

5'- CTTGTCGTCGTCGTCCTTGTAGTCTACAGTTCTAATACCCGATTTAC -3'

FLAG sequence Fbxo7 coding sequence

The first PCR therefore resulted in two products: the N-terminal portion of Fbxo7 with a C-terminal FLAG tag, and the C-terminal portion of Fbxo7 with an N-terminal FLAG tag. These products were purified, combined in an equimolar ratio and used as the template for a second PCR, this time only using the 5' and 3' forward and reverse primers. Since the two PCR products had complementary FLAG sequences, a single PCR product was generated. Figure I.6 shows a schematic of the fusion PCR protocol. The final PCR product was then inserted into pcDNA3 using the HindIII and XhoI restriction sites in the 5' and 3' primers (figure I.7).

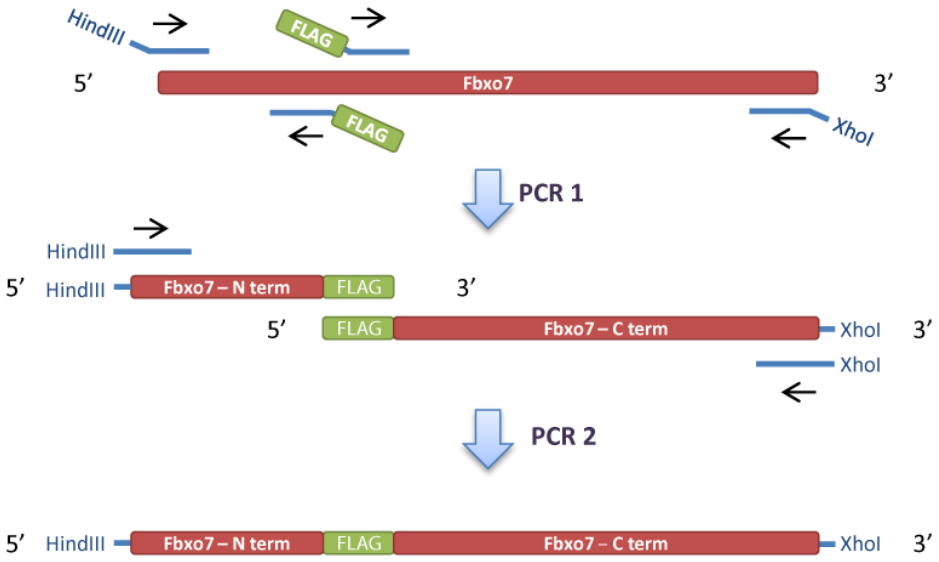

Figure I.6 Schematic showing fusion PCR protocol. In PCR 1, two primer pairs are used resulting in two PCR products: one is the N-terminus of Fbxo7 with a HindIII site inserted at the 5' end and the FLAG sequence at the 3', while the other is the C-terminus of Fbxo7 with the FLAG at the 5' and an XhoI site at the 3' end. In PCR 1, both products are used as the template but only HindIII and XhoI primers are included in the mix, resulting in a single PCR product.

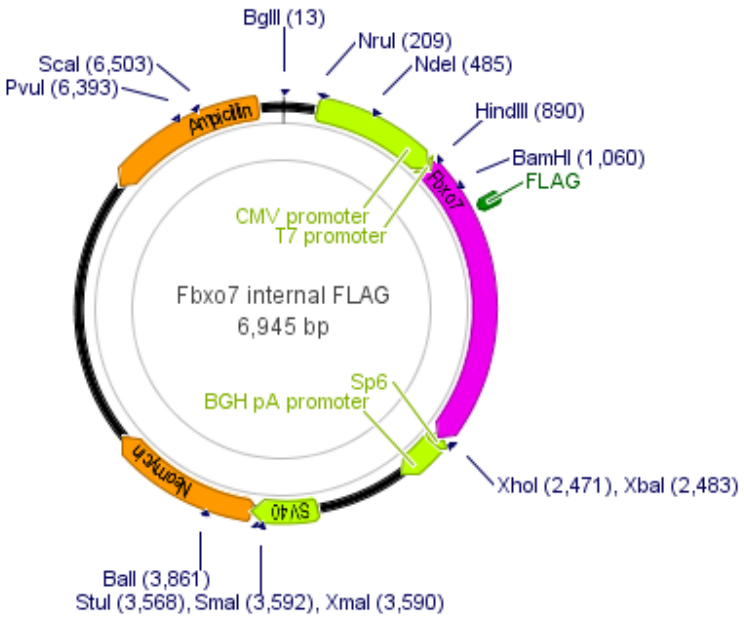

Figure I.7 Vector map showing Fbxo7 with internal FLAG inserted into pcDNA3. Fbxo7 is indicated in magenta; FLAG sequence is indicated in green. Common restriction sites are shown in navy.

Appendix II

Primer sequences

1. HtrA2 genotyping primers

Name	Sequence
HtrA2genFWD	ATGGCTGCGCTGAAAGCGGGGCGGG
NeoR	TCGGCAGGAGCAAGGTGAGATGACA
AM52	ATCCCCGCTAGGCAGCCTCACTCGTA

Table II.1 List of HtrA2 genotyping primers

2. Fbxo7 cloning primers

Name	Sequence	T_m (°C)
Fbxo7Hind3F	CCGAAGCTTGCCACCATGAGGCTGCGGGTGCGG	57
Fbxo7XhoIR	GCCTCGAGCACATGAATGACAGCCGG	48
Fbxo7Xho1HAR	GCCTCGAGTCAAGCGTAATCTGGTACGTCGTATGGGTACATGAATGAC	55
Fbxo7R498XXho1HAR	GCCTCGAGTCAAGCGTAATCTGGTACGTCGTATGGGTACCCTGGCAAG	58
FBXO7_MTS_EcoRI	CGGAATTCGCCACCATGGACCTGCGGGTGTGGCTTCTGAA	57
FBXO7_MTS_EcoRI_T7	CGGAATTCTTATGGACCTGCGGGTGTGGCTTCTGAA	52
Fbxo7_FLAG-IT_F	CTTGTCGTCGTCGTCCTTGTAGTCTACAGTTCTAATACCCGATTTAC	53
Fbxo7_FLAG-IT_R	GACTACAAGGACGACGACGACAAGCCTCAGGTGCGAGCGC	58

Table II.2 List of Fbxo7 cloning primers. Melting temperature (T_m) was determined using the BioMath calculator at *http://www.promega.com/techserv/tools/biomath/calc11.htm#melt_results*.

3. Sequencing primers

Sequencing primers for Fbxo7 were designed using Primer3 (see methods). The 5' terminus of Fbxo7 was sequenced using a standard primer against the T7 promoter provided by the UCL Sequencing Service (sequence TAATACGACTsCACTATAGGG).

Name	Sequence	Annealing site (bp)	T_m (°C)
Fbxo7Seq1	GGAATGACGACAGTATGTTAGGG	400	54
Fbxo7Seq2	GACAAGCACTGAACCTACCAG	961	54

Table II.3 List of sequencing primers for Fbxo7

References

References

Aasly, J.O., Toft, M., Fernandez-Mata, I., Kachergus, J., Hulihan, M., White, L.R., and Farrer, M. (2005). Clinical features of LRRK2-associated Parkinson's disease in central Norway. Ann Neurol *57*, 762-765.

Abou-Sleiman, P.M., Muqit, M.M., and Wood, N.W. (2006). Expanding insights of mitochondrial dysfunction in Parkinson's disease. Nat Rev Neurosci *7*, 207-219.

Abraham, V.C., Taylor, D.L., and Haskins, J.R. (2004). High content screening applied to large-scale cell biology. Trends Biotechnol *22*, 15-22.

Abrahams, J.P., Leslie, A.G., Lutter, R., and Walker, J.E. (1994). Structure at 2.8 A resolution of F1-ATPase from bovine heart mitochondria. Nature *370*, 621-628.

Abramov, A.Y., and Duchen, M.R. (2003). Actions of ionomycin, 4-BrA23187 and a novel electrogenic Ca2+ ionophore on mitochondria in intact cells. Cell Calcium *33*, 101-112.

Adams, J.M., and Cory, S. (2001). Life-or-death decisions by the Bcl-2 protein family. Trends Biochem Sci *26*, 61-66.

Agarwal, A., Banerjee, A., and Banerjee, U.C. (2011). Xanthine oxidoreductase: a journey from purine metabolism to cardiovascular excitation-contraction coupling. Crit Rev Biotechnol *31*, 264-280.

Akundi, R.S., Huang, Z., Eason, J., Pandya, J.D., Zhi, L., Cass, W.A., Sullivan, P.G., and Bueler, H. (2011). Increased mitochondrial calcium sensitivity and abnormal expression of innate immunity genes precede dopaminergic defects in Pink1-deficient mice. PLoS One *6*, e16038.

Alavian, K.N., Li, H., Collis, L., Bonanni, L., Zeng, L., Sacchetti, S., Lazrove, E., Nabili, P., Flaherty, B., Graham, M.*, et al.* (2011). Bcl-xL regulates metabolic efficiency of neurons through interaction with the mitochondrial F1FO ATP synthase. Nat Cell Biol *13*, 1224-1233.

Alberts, B., Johnson, A., Lewis, J., Raff, M., Roberts, K., and Walter, P. (2002). Molecular Biology of the Cell, 4th edn (New York, Garland Science).

Alexander, C., Votruba, M., Pesch, U.E., Thiselton, D.L., Mayer, S., Moore, A., Rodriguez, M., Kellner, U., Leo-Kottler, B., Auburger, G.*, et al.* (2000). OPA1, encoding a dynamin-related GTPase, is mutated in autosomal dominant optic atrophy linked to chromosome 3q28. Nat Genet *26*, 211-215.

An, D.S., Qin, F.X., Auyeung, V.C., Mao, S.H., Kung, S.K., Baltimore, D., and Chen, I.S. (2006). Optimization and functional effects of stable short hairpin RNA expression in primary human lymphocytes via lentiviral vectors. Mol Ther *14*, 494-504.

Ansaloni, S., Lelkes, N., Snyder, J., Epstein, C., Dubey, A., and Saunders, A.J. (2010). A streamlined sub-cloning procedure to transfer shRNA from a pSM2 vector to a pGIPZ lentiviral vector. J RNAi Gene Silencing *6*, 411-415.

Arawaka, S., Saito, Y., Murayama, S., and Mori, H. (1998). Lewy body in neurodegeneration with brain iron accumulation type 1 is immunoreactive for alpha-synuclein. Neurology *51*, 887-889.

Arnold, I., Pfeiffer, K., Neupert, W., Stuart, R.A., and Schagger, H. (1998). Yeast mitochondrial F1F0-ATP synthase exists as a dimer: identification of three dimer-specific subunits. EMBO J *17*, 7170-7178.

Arsenijevic, D., Onuma, H., Pecqueur, C., Raimbault, S., Manning, B.S., Miroux, B., Couplan, E., Alves-Guerra, M.C., Goubern, M., Surwit, R.*, et al.* (2000). Disruption of the uncoupling protein-2 gene in mice reveals a role in immunity and reactive oxygen species production. Nat Genet *26*, 435-439.

Ashford, T.P., and Porter, K.R. (1962). Cytoplasmic components in hepatic cell lysosomes. J Cell Biol *12*, 198-202.

Azad, N., Iyer, A., Vallyathan, V., Wang, L., Castranova, V., Stehlik, C., and Rojanasakul, Y. (2010). Role of oxidative/nitrosative stress-mediated Bcl-2 regulation in apoptosis and malignant transformation. Ann N Y Acad Sci *1203*, 1-6.

Bai, C., Sen, P., Hofmann, K., Ma, L., Goebl, M., Harper, J.W., and Elledge, S.J. (1996). SKP1 connects cell cycle regulators to the ubiquitin proteolysis machinery through a novel motif, the F-box. Cell *86*, 263-274.

Baines, C.P., Kaiser, R.A., Purcell, N.H., Blair, N.S., Osinska, H., Hambleton, M.A., Brunskill, E.W., Sayen, M.R., Gottlieb, R.A., Dorn, G.W.*, et al.* (2005). Loss of cyclophilin D reveals a critical role for mitochondrial permeability transition in cell death. Nature *434*, 658-662.

Baines, C.P., Kaiser, R.A., Sheiko, T., Craigen, W.J., and Molkentin, J.D. (2007). Voltage-dependent anion channels are dispensable for mitochondrial-dependent cell death. Nat Cell Biol *9*, 550-555.

Balaban, R.S., Nemoto, S., and Finkel, T. (2005). Mitochondria, oxidants, and aging. Cell *120*, 483-495.

Banerjee, K., Sinha, M., Pham Cle, L., Jana, S., Chanda, D., Cappai, R., and Chakrabarti, S. (2010). Alpha-synuclein induced membrane depolarization and loss of phosphorylation capacity of isolated rat brain mitochondria: implications in Parkinson's disease. FEBS Lett *584*, 1571-1576.

Basso, E., Fante, L., Fowlkes, J., Petronilli, V., Forte, M.A., and Bernardi, P. (2005). Properties of the permeability transition pore in mitochondria devoid of Cyclophilin D. J Biol Chem *280*, 18558-18561.

Basso, E., Petronilli, V., Forte, M.A., and Bernardi, P. (2008). Phosphate is essential for inhibition of the mitochondrial permeability transition pore by cyclosporin A and by cyclophilin D ablation. J Biol Chem *283*, 26307-26311.

Beck, R., Verrax, J., Gonze, T., Zappone, M., Pedrosa, R.C., Taper, H., Feron, O., and Calderon, P.B. (2009). Hsp90 cleavage by an oxidative stress leads to its client proteins degradation and cancer cell death. Biochem Pharmacol *77*, 375-383.

Belogrudov, G.I. (2008). The proximal N-terminal amino acid residues are required for the coupling activity of the bovine heart mitochondrial factor B. Arch Biochem Biophys *473*, 76-87.

Belogrudov, G.I. (2009). Recent advances in structure-functional studies of mitochondrial factor B. J Bioenerg Biomembr *41*, 137-143.

Belogrudov, G.I., Tomich, J.M., and Hatefi, Y. (1996). Membrane topography and near-neighbor relationships of the mitochondrial ATP synthase subunits e, f, and g. J Biol Chem *271*, 20340-20345.

Benabid, A.L., Chabardes, S., Mitrofanis, J., and Pollak, P. (2009). Deep brain stimulation of the subthalamic nucleus for the treatment of Parkinson's disease. Lancet Neurol *8*, 67-81.

Benazzouz, A., Gross, C., Feger, J., Boraud, T., and Bioulac, B. (1993). Reversal of rigidity and improvement in motor performance by subthalamic high-frequency stimulation in MPTP-treated monkeys. Eur J Neurosci *5*, 382-389.

Berg, D., Youdim, M.B., and Riederer, P. (2004). Redox imbalance. Cell Tissue Res *318*, 201-213.

Bernardi, P., and Rasola, A. (2007). Calcium and cell death: the mitochondrial connection. Subcell Biochem *45*, 481-506.

Berns, K., Hijmans, E.M., Mullenders, J., Brummelkamp, T.R., Velds, A., Heimerikx, M., Kerkhoven, R.M., Madiredjo, M., Nijkamp, W., Weigelt, B.*, et al.* (2004). A large-scale RNAi screen in human cells identifies new components of the p53 pathway. Nature *428*, 431-437.

Berridge, M.J., Lipp, P., and Bootman, M.D. (2000). The versatility and universality of calcium signalling. Nat Rev Mol Cell Biol *1*, 11-21.

Betarbet, R., Sherer, T.B., MacKenzie, G., Garcia-Osuna, M., Panov, A.V., and Greenamyre, J.T. (2000). Chronic systemic pesticide exposure reproduces features of Parkinson's disease. Nat Neurosci *3*, 1301-1306.

Bindokas, V.P., Jordan, J., Lee, C.C., and Miller, R.J. (1996). Superoxide production in rat hippocampal neurons: selective imaging with hydroethidine. J Neurosci *16*, 1324-1336.

Birkmayer, W., and Hornykiewicz, O. (1962). [The L-dihydroxyphenylalanine (L-DOPA) effect in Parkinson's syndrome in man: On the pathogenesis and treatment of Parkinson akinesis]. Arch Psychiatr Nervenkr Z Gesamte Neurol Psychiatr *203*, 560-574.

Biskup, S., Moore, D.J., Celsi, F., Higashi, S., West, A.B., Andrabi, S.A., Kurkinen, K., Yu, S.W., Savitt, J.M., Waldvogel, H.J., *et al.* (2006). Localization of LRRK2 to membranous and vesicular structures in mammalian brain. Ann Neurol *60*, 557-569.

Bogaerts, V., Nuytemans, K., Reumers, J., Pals, P., Engelborghs, S., Pickut, B., Corsmit, E., Peeters, K., Schymkowitz, J., De Deyn, P.P., *et al.* (2008). Genetic variability in the mitochondrial serine protease HTRA2 contributes to risk for Parkinson disease. Hum Mutat *29*, 832-840.

Bonifati, V., Rizzu, P., van Baren, M.J., Schaap, O., Breedveld, G.J., Krieger, E., Dekker, M.C., Squitieri, F., Ibanez, P., Joosse, M., *et al.* (2003). Mutations in the DJ-1 gene associated with autosomal recessive early-onset parkinsonism. Science *299*, 256-259.

Borghi, R., Marchese, R., Negro, A., Marinelli, L., Forloni, G., Zaccheo, D., Abbruzzese, G., and Tabaton, M. (2000). Full length alpha-synuclein is present in cerebrospinal fluid from Parkinson's disease and normal subjects. Neurosci Lett *287*, 65-67.

Boss, O., Samec, S., Paoloni-Giacobino, A., Rossier, C., Dulloo, A., Seydoux, J., Muzzin, P., and Giacobino, J.P. (1997). Uncoupling protein-3: a new member of the mitochondrial carrier family with tissue-specific expression. FEBS Lett *408*, 39-42.

Braak, H., Del Tredici, K., Bratzke, H., Hamm-Clement, J., Sandmann-Keil, D., and Rub, U. (2002). Staging of the intracerebral inclusion body pathology associated with idiopathic Parkinson's disease (preclinical and clinical stages). J Neurol *249 Suppl 3*, III/1-5.

Brand, M.D. (2000). Uncoupling to survive? The role of mitochondrial inefficiency in ageing. Exp Gerontol *35*, 811-820.

Brand, M.D., Buckingham, J.A., Esteves, T.C., Green, K., Lambert, A.J., Miwa, S., Murphy, M.P., Pakay, J.L., Talbot, D.A., and Echtay, K.S. (2004). Mitochondrial superoxide and aging: uncoupling-protein activity and superoxide production. Biochem Soc Symp, 203-213.

Bras, J., Simon-Sanchez, J., Federoff, M., Morgadinho, A., Januario, C., Ribeiro, M., Cunha, L., Oliveira, C., and Singleton, A.B. (2009). Lack of replication of association between GIGYF2 variants and Parkinson disease. Hum Mol Genet *18*, 341-346.

Bras, J., Singleton, A., Cookson, M.R., and Hardy, J. (2008). Emerging pathways in genetic Parkinson's disease: Potential role of ceramide metabolism in Lewy body disease. FEBS J *275*, 5767-5773.

Brass, A.L., Dykxhoorn, D.M., Benita, Y., Yan, N., Engelman, A., Xavier, R.J., Lieberman, J., and Elledge, S.J. (2008). Identification of host proteins required for HIV infection through a functional genomic screen. Science *319*, 921-926.

Browne, S.E., Bowling, A.C., MacGarvey, U., Baik, M.J., Berger, S.C., Muqit, M.M., Bird, E.D., and Beal, M.F. (1997). Oxidative damage and metabolic dysfunction in Huntington's disease: selective vulnerability of the basal ganglia. Ann Neurol *41*, 646-653.

Brummelkamp, T.R., Bernards, R., and Agami, R. (2002a). Stable suppression of tumorigenicity by virus-mediated RNA interference. Cancer Cell *2*, 243-247.

Brummelkamp, T.R., Bernards, R., and Agami, R. (2002b). A system for stable expression of short interfering RNAs in mammalian cells. Science *296*, 550-553.

Brundin, P., Li, J.Y., Holton, J.L., Lindvall, O., and Revesz, T. (2008). Research in motion: the enigma of Parkinson's disease pathology spread. Nat Rev Neurosci *9*, 741-745.

Burbulla, L.F., Schelling, C., Kato, H., Rapaport, D., Woitalla, D., Schiesling, C., Schulte, C., Sharma, M., Illig, T., Bauer, P.*, et al.* (2010). Dissecting the role of the mitochondrial chaperone mortalin in Parkinson's disease: functional impact of disease-related variants on mitochondrial homeostasis. Hum Mol Genet *19*, 4437-4452.

Burchell, V.S., Gandhi, S., Deas, E., Wood, N.W., Abramov, A.Y., and Plun-Favreau, H. (2010a). Targeting mitochondrial dysfunction in neurodegenerative disease: Part I. Expert Opin Ther Targets *14*, 369-385.

Burchell, V.S., Gandhi, S., Deas, E., Wood, N.W., Abramov, A.Y., and Plun-Favreau, H. (2010b). Targeting mitochondrial dysfunction in neurodegenerative disease: Part II. Expert Opin Ther Targets *14*, 497-511.

Butterfield, D.A., Perluigi, M., and Sultana, R. (2006). Oxidative stress in Alzheimer's disease brain: new insights from redox proteomics. Eur J Pharmacol *545*, 39-50.

Cai, Q., Zakaria, H.M., Simone, A., and Sheng, Z.H. (2012). Spatial parkin translocation and degradation of damaged mitochondria via mitophagy in live cortical neurons. Curr Biol *22*, 545-552.

Cain, K., Bratton, S.B., Langlais, C., Walker, G., Brown, D.G., Sun, X.M., and Cohen, G.M. (2000). Apaf-1 oligomerizes into biologically active approximately 700-kDa and inactive approximately 1.4-MDa apoptosome complexes. J Biol Chem *275*, 6067-6070.

Cali, T., Ottolini, D., Negro, A., and Brini, M. (2012). Alpha-synuclein controls mitochondrial calcium homeostasis by enhancing endoplasmic reticulum-mitochondria interactions. J Biol Chem.

Campbell, C.L., and Thorsness, P.E. (1998). Escape of mitochondrial DNA to the nucleus in yme1 yeast is mediated by vacuolar-dependent turnover of abnormal mitochondrial compartments. J Cell Sci *111 (Pt 16)*, 2455-2464.

Campeau, E., and Gobeil, S. (2011). RNA interference in mammals: behind the screen. Brief Funct Genomics *10*, 215-226.

Canet-Aviles, R.M., Wilson, M.A., Miller, D.W., Ahmad, R., McLendon, C., Bandyopadhyay, S., Baptista, M.J., Ringe, D., Petsko, G.A., and Cookson, M.R. (2004). The Parkinson's disease protein DJ-1 is neuroprotective due to cysteine-sulfinic acid-driven mitochondrial localization. Proc Natl Acad Sci U S A *101*, 9103-9108.

Carstam, R., Brinck, C., Hindemith-Augustsson, A., Rorsman, H., and Rosengren, E. (1991). The neuromelanin of the human substantia nigra. Biochim Biophys Acta *1097*, 152-160.

Carthew, R.W., and Sontheimer, E.J. (2009). Origins and Mechanisms of miRNAs and siRNAs. Cell *136*, 642-655.

Casari, G., De Fusco, M., Ciarmatori, S., Zeviani, M., Mora, M., Fernandez, P., De Michele, G., Filla, A., Cocozza, S., Marconi, R.*, et al.* (1998). Spastic paraplegia and OXPHOS impairment caused by mutations in paraplegin, a nuclear-encoded mitochondrial metalloprotease. Cell *93*, 973-983.

Casteilla, L., Rigoulet, M., and Penicaud, L. (2001). Mitochondrial ROS metabolism: modulation by uncoupling proteins. IUBMB Life *52*, 181-188.

Cenciarelli, C., Chiaur, D.S., Guardavaccaro, D., Parks, W., Vidal, M., and Pagano, M. (1999). Identification of a family of human F-box proteins. Curr Biol *9*, 1177-1179.

Cesari, R., Martin, E.S., Calin, G.A., Pentimalli, F., Bichi, R., McAdams, H., Trapasso, F., Drusco, A., Shimizu, M., Masciullo, V.*, et al.* (2003). Parkin, a gene implicated in autosomal recessive juvenile parkinsonism, is a candidate tumor suppressor gene on chromosome 6q25-q27. Proc Natl Acad Sci U S A *100*, 5956-5961.

Chan, C.S., Gertler, T.S., and Surmeier, D.J. (2009). Calcium homeostasis, selective vulnerability and Parkinson's disease. Trends Neurosci *32*, 249-256.

Chan, N.C., Salazar, A.M., Pham, A.H., Sweredoski, M.J., Kolawa, N.J., Graham, R.L., Hess, S., and Chan, D.C. (2011). Broad activation of the ubiquitin-proteasome system by Parkin is critical for mitophagy. Hum Mol Genet *20*, 1726-1737.

Chance, B., Cohen, P., Jobsis, F., and Schoener, B. (1962). Intracellular oxidation-reduction states in vivo. Science *137*, 499-508.

Chang, Y.F., Cheng, C.M., Chang, L.K., Jong, Y.J., and Yuo, C.Y. (2006). The F-box protein Fbxo7 interacts with human inhibitor of apoptosis protein cIAP1 and promotes cIAP1 ubiquitination. Biochem Biophys Res Commun *342*, 1022-1026.

Chartier-Harlin, M.C., Kachergus, J., Roumier, C., Mouroux, V., Douay, X., Lincoln, S., Levecque, C., Larvor, L., Andrieux, J., Hulihan, M.*, et al.* (2004). Alpha-synuclein locus duplication as a cause of familial Parkinson's disease. Lancet *364*, 1167-1169.

Chen, D., Gao, F., Li, B., Wang, H., Xu, Y., Zhu, C., and Wang, G. (2010). Parkin mono-ubiquitinates Bcl-2 and regulates autophagy. J Biol Chem *285*, 38214-38223.

Chen, H., Chomyn, A., and Chan, D.C. (2005). Disruption of fusion results in mitochondrial heterogeneity and dysfunction. J Biol Chem *280*, 26185-26192.

Chen, Q., Vazquez, E.J., Moghaddas, S., Hoppel, C.L., and Lesnefsky, E.J. (2003). Production of reactive oxygen species by mitochondria: central role of complex III. J Biol Chem *278*, 36027-36031.

Chinopoulos, C., and Adam-Vizi, V. (2012). Modulation of the mitochondrial permeability transition by cyclophilin D: moving closer to F(0)-F(1) ATP synthase? Mitochondrion *12*, 41-45.

Choe, M., Jackson, C., and Yu, B.P. (1995). Lipid peroxidation contributes to age-related membrane rigidity. Free Radic Biol Med *18*, 977-984.

Cipolat, S., Rudka, T., Hartmann, D., Costa, V., Serneels, L., Craessaerts, K., Metzger, K., Frezza, C., Annaert, W., D'Adamio, L.*, et al.* (2006). Mitochondrial rhomboid PARL regulates cytochrome c release during apoptosis via OPA1-dependent cristae remodeling. Cell *126*, 163-175.

Clark, I.E., Dodson, M.W., Jiang, C., Cao, J.H., Huh, J.R., Seol, J.H., Yoo, S.J., Hay, B.A., and Guo, M. (2006). Drosophila pink1 is required for mitochondrial function and interacts genetically with parkin. Nature *441*, 1162-1166.

Claros, M.G., and Vincens, P. (1996). Computational method to predict mitochondrially imported proteins and their targeting sequences. Eur J Biochem *241*, 779-786.

Cohen, G., and Hochstein, P. (1961). Glucose-6-phosphate dehydrogenase and detoxification of hydrogen peroxide in human erythrocytes. Science *134*, 1756-1757.

Cohen, M.M., Amiott, E.A., Day, A.R., Leboucher, G.P., Pryce, E.N., Glickman, M.H., McCaffery, J.M., Shaw, J.M., and Weissman, A.M. (2011). Sequential requirements for the GTPase domain of the mitofusin Fzo1 and the ubiquitin ligase SCFMdm30 in mitochondrial outer membrane fusion. J Cell Sci *124*, 1403-1410.

Cohen, M.M., Leboucher, G.P., Livnat-Levanon, N., Glickman, M.H., and Weissman, A.M. (2008). Ubiquitin-proteasome-dependent degradation of a mitofusin, a critical regulator of mitochondrial fusion. Mol Biol Cell *19*, 2457-2464.

Cookson, M.R. (2010). DJ-1, PINK1, and their effects on mitochondrial pathways. Mov Disord *25 Suppl 1*, S44-48.

Cotzias, G.C., Papavasiliou, P.S., and Gellene, R. (1968). Experimental treatment of parkinsonism with L-Dopa. Neurology *18*, 276-277.

Crompton, M. (1999). The mitochondrial permeability transition pore and its role in cell death. Biochem J *341 (Pt 2)*, 233-249.

Cuadrado, A., Moreno-Murciano, P., and Pedraza-Chaverri, J. (2009). The transcription factor Nrf2 as a new therapeutic target in Parkinson's disease. Expert Opin Ther Targets *13*, 319-329.

Cuadrado, A., and Nebreda, A.R. (2010). Mechanisms and functions of p38 MAPK signalling. Biochem J *429*, 403-417.

Dagda, R.K., and Chu, C.T. (2009). Mitochondrial quality control: insights on how Parkinson's disease related genes PINK1, parkin, and Omi/HtrA2 interact to maintain mitochondrial homeostasis. J Bioenerg Biomembr *41*, 473-479.

Dauer, W., and Przedborski, S. (2003). Parkinson's disease: mechanisms and models. Neuron *39*, 889-909.

Davis, H.E., Morgan, J.R., and Yarmush, M.L. (2002). Polybrene increases retrovirus gene transfer efficiency by enhancing receptor-independent virus adsorption on target cell membranes. Biophys Chem *97*, 159-172.

De Mena, L., Coto, E., Sanchez-Ferrero, E., Ribacoba, R., Guisasola, L.M., Salvador, C., Blazquez, M., and Alvarez, V. (2009). Mutational screening of the mortalin gene (HSPA9) in Parkinson's disease. J Neural Transm *116*, 1289-1293.

Deas, E., Plun-Favreau, H., Gandhi, S., Desmond, H., Kjaer, S., Loh, S.H., Renton, A.E., Harvey, R.J., Whitworth, A.J., Martins, L.M.*, et al.* (2011). PINK1 cleavage at position A103 by the mitochondrial protease PARL. Hum Mol Genet *20*, 867-879.

Deas, E., Plun-Favreau, H., and Wood, N.W. (2009). PINK1 function in health and disease. EMBO Mol Med *1*, 152-165.

DelleDonne, A., Klos, K.J., Fujishiro, H., Ahmed, Z., Parisi, J.E., Josephs, K.A., Frigerio, R., Burnett, M., Wszolek, Z.K., Uitti, R.J.*, et al.* (2008). Incidental Lewy body disease and preclinical Parkinson disease. Arch Neurol *65*, 1074-1080.

Delmas, P.D., Gineyts, E., Bertholin, A., Garnero, P., and Marchand, F. (1993). Immunoassay of pyridinoline crosslink excretion in normal adults and in Paget's disease. J Bone Miner Res *8*, 643-648.

Demple, B., and Harrison, L. (1994). Repair of oxidative damage to DNA: enzymology and biology. Annu Rev Biochem *63*, 915-948.

Deng, H., Dodson, M.W., Huang, H., and Guo, M. (2008). The Parkinson's disease genes pink1 and parkin promote mitochondrial fission and/or inhibit fusion in Drosophila. Proc Natl Acad Sci U S A *105*, 14503-14508.

Deng, H., Jankovic, J., Guo, Y., Xie, W., and Le, W. (2005). Small interfering RNA targeting the PINK1 induces apoptosis in dopaminergic cells SH-SY5Y. Biochem Biophys Res Commun *337*, 1133-1138.

Dennig, J., and Duncan, E. (2002). Gene transfer into eukaryotic cells using activated polyamidoamine dendrimers. J Biotechnol *90*, 339-347.

Denton, R.M., McCormack, J.G., and Edgell, N.J. (1980). Role of calcium ions in the regulation of intramitochondrial metabolism. Effects of Na+, Mg2+ and ruthenium red on the Ca2+-stimulated oxidation of oxoglutarate and on pyruvate dehydrogenase activity in intact rat heart mitochondria. Biochem J *190*, 107-117.

Desideri, E., and Martins, L.M. (2012). Mitochondrial Stress Signalling: HTRA2 and Parkinson's Disease. Int J Cell Biol *2012*, 607929.

Devi, L., Raghavendran, V., Prabhu, B.M., Avadhani, N.G., and Anandatheerthavarada, H.K. (2008). Mitochondrial import and accumulation of alpha-synuclein impair complex I in human dopaminergic neuronal cultures and Parkinson disease brain. J Biol Chem *283*, 9089-9100.

Devine, M.J., Plun-Favreau, H., and Wood, N.W. (2011). Parkinson's disease and cancer: two wars, one front. Nat Rev Cancer *11*, 812-823.

Di Bella, D., Lazzaro, F., Brusco, A., Plumari, M., Battaglia, G., Pastore, A., Finardi, A., Cagnoli, C., Tempia, F., Frontali, M.*, et al.* (2010). Mutations in the mitochondrial protease gene AFG3L2 cause dominant hereditary ataxia SCA28. Nat Genet *42*, 313-321.

Di Fonzo, A., Dekker, M.C., Montagna, P., Baruzzi, A., Yonova, E.H., Correia Guedes, L., Szczerbinska, A., Zhao, T., Dubbel-Hulsman, L.O., Wouters, C.H., *et al.* (2009a). FBXO7 mutations cause autosomal recessive, early-onset parkinsonian-pyramidal syndrome. Neurology *72*, 240-245.

Di Fonzo, A., Fabrizio, E., Thomas, A., Fincati, E., Marconi, R., Tinazzi, M., Breedveld, G.J., Simons, E.J., Chien, H.F., Ferreira, J.J., *et al.* (2009b). GIGYF2 mutations are not a frequent cause of familial Parkinson's disease. Parkinsonism Relat Disord *15*, 703-705.

Diez, M., Zimmermann, B., Borsch, M., Konig, M., Schweinberger, E., Steigmiller, S., Reuter, R., Felekyan, S., Kudryavtsev, V., Seidel, C.A., *et al.* (2004). Proton-powered subunit rotation in single membrane-bound F0F1-ATP synthase. Nat Struct Mol Biol *11*, 135-141.

Ding, W.X., Ni, H.M., Li, M., Liao, Y., Chen, X., Stolz, D.B., Dorn, G.W., 2nd, and Yin, X.M. (2010). Nix is critical to two distinct phases of mitophagy, reactive oxygen species-mediated autophagy induction and Parkin-ubiquitin-p62-mediated mitochondrial priming. J Biol Chem *285*, 27879-27890.

DiPolo, R. (1974). Effect of ATP on the calcium efflux in dialyzed squid giant axons. J Gen Physiol *64*, 503-517.

Dragunow, M. (2008). High-content analysis in neuroscience. Nat Rev Neurosci *9*, 779-788.

Draviam, V.M., Stegmeier, F., Nalepa, G., Sowa, M.E., Chen, J., Liang, A., Hannon, G.J., Sorger, P.K., Harper, J.W., and Elledge, S.J. (2007). A functional genomic screen identifies a role for TAO1 kinase in spindle-checkpoint signalling. Nat Cell Biol *9*, 556-564.

Drummond, A.J., Ashton, B., Buxton, S., Cheung, M., Cooper, A., Duran, C., Field, M., Heled, J., Kearse, M., Markowitz, S., *et al.* (2011). Geneious v5.4.

Du, C., Fang, M., Li, Y., Li, L., and Wang, X. (2000). Smac, a mitochondrial protein that promotes cytochrome c-dependent caspase activation by eliminating IAP inhibition. Cell *102*, 33-42.

Duchen, M.R., and Biscoe, T.J. (1992). Mitochondrial function in type I cells isolated from rabbit arterial chemoreceptors. J Physiol *450*, 13-31.

Duchen, M.R., Verkhratsky, A., and Muallem, S. (2008). Mitochondria and calcium in health and disease. Cell Calcium *44*, 1-5.

Echtay, K.S., Esteves, T.C., Pakay, J.L., Jekabsons, M.B., Lambert, A.J., Portero-Otin, M., Pamplona, R., Vidal-Puig, A.J., Wang, S., Roebuck, S.J.*, et al.* (2003). A signalling role for 4-hydroxy-2-nonenal in regulation of mitochondrial uncoupling. EMBO J *22*, 4103-4110.

Echtay, K.S., Murphy, M.P., Smith, R.A., Talbot, D.A., and Brand, M.D. (2002). Superoxide activates mitochondrial uncoupling protein 2 from the matrix side. Studies using targeted antioxidants. J Biol Chem *277*, 47129-47135.

Edwards, T.L., Scott, W.K., Almonte, C., Burt, A., Powell, E.H., Beecham, G.W., Wang, L., Zuchner, S., Konidari, I., Wang, G.*, et al.* (2010). Genome-wide association study confirms SNPs in SNCA and the MAPT region as common risk factors for Parkinson disease. Ann Hum Genet *74*, 97-109.

El-Agnaf, O.M., Salem, S.A., Paleologou, K.E., Cooper, L.J., Fullwood, N.J., Gibson, M.J., Curran, M.D., Court, J.A., Mann, D.M., Ikeda, S.*, et al.* (2003). Alpha-synuclein implicated in Parkinson's disease is present in extracellular biological fluids, including human plasma. FASEB J *17*, 1945-1947.

Elmer, L.W., and Bertoni, J.M. (2008). The increasing role of monoamine oxidase type B inhibitors in Parkinson's disease therapy. Expert Opin Pharmacother *9*, 2759-2772.

Elmore, S.P., Qian, T., Grissom, S.F., and Lemasters, J.J. (2001). The mitochondrial permeability transition initiates autophagy in rat hepatocytes. FASEB J *15*, 2286-2287.

Emanuelsson, O., Nielsen, H., Brunak, S., and von Heijne, G. (2000). Predicting subcellular localization of proteins based on their N-terminal amino acid sequence. J Mol Biol *300*, 1005-1016.

Emmanouilidou, E., Melachroinou, K., Roumeliotis, T., Garbis, S.D., Ntzouni, M., Margaritis, L.H., Stefanis, L., and Vekrellis, K. (2010). Cell-produced alpha-synuclein is secreted in a calcium-dependent manner by exosomes and impacts neuronal survival. J Neurosci *30*, 6838-6851.

Emre, M. (2003). Dementia associated with Parkinson's disease. Lancet Neurol *2*, 229-237.

Escobar-Henriques, M., Westermann, B., and Langer, T. (2006). Regulation of mitochondrial fusion by the F-box protein Mdm30 involves proteasome-independent turnover of Fzo1. J Cell Biol *173*, 645-650.

Eskelinen, E.L. (2005). Maturation of autophagic vacuoles in Mammalian cells. Autophagy *1*, 1-10.

Evans, C.A. (1907). On the Catalytic Decomposition of Hydrogen Peroxide by the Catalase of Blood. Biochem J *2*, 133-155.

Exner, N., Treske, B., Paquet, D., Holmstrom, K., Schiesling, C., Gispert, S., Carballo-Carbajal, I., Berg, D., Hoepken, H.H., Gasser, T.*, et al.* (2007). Loss-of-function of human PINK1 results in mitochondrial pathology and can be rescued by parkin. J Neurosci *27*, 12413-12418.

Fahn, S. (1991). An open trial of high-dosage antioxidants in early Parkinson's disease. Am J Clin Nutr *53*, 380S-382S.

Fahn, S. (2003). Description of Parkinson's disease as a clinical syndrome. Ann N Y Acad Sci *991*, 1-14.

Farrer, M.J. (2006). Genetics of Parkinson disease: paradigm shifts and future prospects. Nat Rev Genet *7*, 306-318.

Fasano, A., Daniele, A., and Albanese, A. (2012). Treatment of motor and non-motor features of Parkinson's disease with deep brain stimulation. Lancet Neurol *11*, 429-442.

Feldmann, G., Haouzi, D., Moreau, A., Durand-Schneider, A.M., Bringuier, A., Berson, A., Mansouri, A., Fau, D., and Pessayre, D. (2000). Opening of the mitochondrial permeability transition pore causes matrix expansion and outer membrane rupture in Fas-mediated hepatic apoptosis in mice. Hepatology *31*, 674-683.

Felgner, P.L., Gadek, T.R., Holm, M., Roman, R., Chan, H.W., Wenz, M., Northrop, J.P., Ringold, G.M., and Danielsen, M. (1987). Lipofection: a highly efficient, lipid-mediated DNA-transfection procedure. Proc Natl Acad Sci U S A *84*, 7413-7417.

Fernandez, H.H. (2012). Updates in the medical management of Parkinson disease. Cleve Clin J Med *79*, 28-35.

Filosto, M., Scarpelli, M., Cotelli, M.S., Vielmi, V., Todeschini, A., Gregorelli, V., Tonin, P., Tomelleri, G., and Padovani, A. (2011). The role of mitochondria in neurodegenerative diseases. J Neurol *258*, 1763-1774.

Fitzgerald, J.C., Camprubi, M.D., Dunn, L., Wu, H.C., Ip, N.Y., Kruger, R., Martins, L.M., Wood, N.W., and Plun-Favreau, H. (2012). Phosphorylation of HtrA2 by cyclin-dependent kinase-5 is important for mitochondrial function. Cell Death Differ *19*, 257-266.

Fleury, C., Neverova, M., Collins, S., Raimbault, S., Champigny, O., Levi-Meyrueis, C., Bouillaud, F., Seldin, M.F., Surwit, R.S., Ricquier, D*., et al.* (1997). Uncoupling protein-2: a novel gene linked to obesity and hyperinsulinemia. Nat Genet *15*, 269-272.

Fong, K.L., McCay, P.B., and Poyer, J.L. (1976). Evidence for superoxide-dependent reduction of Fe3+ and its role in enzyme-generated hydroxyl radical formation. Chem Biol Interact *15*, 77-89.

Forster, M.J., Dubey, A., Dawson, K.M., Stutts, W.A., Lal, H., and Sohal, R.S. (1996). Age-related losses of cognitive function and motor skills in mice are associated with oxidative protein damage in the brain. Proc Natl Acad Sci U S A *93*, 4765-4769.

Franco, R., DeHaven, W.I., Sifre, M.I., Bortner, C.D., and Cidlowski, J.A. (2008). Glutathione depletion and disruption of intracellular ionic homeostasis regulate lymphoid cell apoptosis. J Biol Chem *283*, 36071-36087.

Frezza, C., Cipolat, S., Martins de Brito, O., Micaroni, M., Beznoussenko, G.V., Rudka, T., Bartoli, D., Polishuck, R.S., Danial, N.N., De Strooper, B*., et al.* (2006). OPA1 controls apoptotic cristae remodeling independently from mitochondrial fusion. Cell *126*, 177-189.

Gandhi, S., Wood-Kaczmar, A., Yao, Z., Plun-Favreau, H., Deas, E., Klupsch, K., Downward, J., Latchman, D.S., Tabrizi, S.J., Wood, N.W*., et al.* (2009). PINK1-associated Parkinson's disease is caused by neuronal vulnerability to calcium-induced cell death. Mol Cell *33*, 627-638.

Gargini, R., Garcia-Escudero, V., and Izquierdo, M. (2011). Therapy mediated by mitophagy abrogates tumor progression. Autophagy *7*, 466-476.

Garnier, J., Osguthorpe, D.J., and Robson, B. (1978). Analysis of the accuracy and implications of simple methods for predicting the secondary structure of globular proteins. J Mol Biol *120*, 97-120.

Gasser, T., Muller-Myhsok, B., Wszolek, Z.K., Oehlmann, R., Calne, D.B., Bonifati, V., Bereznai, B., Fabrizio, E., Vieregge, P., and Horstmann, R.D. (1998). A susceptibility locus for Parkinson's disease maps to chromosome 2p13. Nat Genet *18*, 262-265.

Gautier, C.A., Kitada, T., and Shen, J. (2008). Loss of PINK1 causes mitochondrial functional defects and increased sensitivity to oxidative stress. Proc Natl Acad Sci U S A *105*, 11364-11369.

Gegg, M.E., Cooper, J.M., Chau, K.Y., Rojo, M., Schapira, A.H., and Taanman, J.W. (2010). Mitofusin 1 and mitofusin 2 are ubiquitinated in a PINK1/parkin-dependent manner upon induction of mitophagy. Hum Mol Genet *19*, 4861-4870.

Gegg, M.E., Cooper, J.M., Schapira, A.H., and Taanman, J.W. (2009). Silencing of PINK1 expression affects mitochondrial DNA and oxidative phosphorylation in dopaminergic cells. PLoS One *4*, e4756.

Geisler, S., Holmstrom, K.M., Skujat, D., Fiesel, F.C., Rothfuss, O.C., Kahle, P.J., and Springer, W. (2010a). PINK1/Parkin-mediated mitophagy is dependent on VDAC1 and p62/SQSTM1. Nat Cell Biol *12*, 119-131.

Geisler, S., Holmstrom, K.M., Treis, A., Skujat, D., Weber, S.S., Fiesel, F.C., Kahle, P.J., and Springer, W. (2010b). The PINK1/Parkin-mediated mitophagy is compromised by PD-associated mutations. Autophagy *6*, 871-878.

Gilks, W.P., Abou-Sleiman, P.M., Gandhi, S., Jain, S., Singleton, A., Lees, A.J., Shaw, K., Bhatia, K.P., Bonifati, V., Quinn, N.P.*, et al.* (2005). A common LRRK2 mutation in idiopathic Parkinson's disease. Lancet *365*, 415-416.

Giorgio, V., Bisetto, E., Soriano, M.E., Dabbeni-Sala, F., Basso, E., Petronilli, V., Forte, M.A., Bernardi, P., and Lippe, G. (2009). Cyclophilin D modulates mitochondrial F0F1-ATP synthase by interacting with the lateral stalk of the complex. J Biol Chem *284*, 33982-33988.

Gispert, S., Ricciardi, F., Kurz, A., Azizov, M., Hoepken, H.H., Becker, D., Voos, W., Leuner, K., Muller, W.E., Kudin, A.P.*, et al.* (2009). Parkinson phenotype in aged PINK1-deficient mice is accompanied by progressive mitochondrial dysfunction in absence of neurodegeneration. PLoS One *4*, e5777.

Gledhill, J.R., and Walker, J.E. (2006). Inhibitors of the catalytic domain of mitochondrial ATP synthase. Biochem Soc Trans *34*, 989-992.

Goldman, S.J., Taylor, R., Zhang, Y., and Jin, S. (2010). Autophagy and the degradation of mitochondria. Mitochondrion *10*, 309-315.

Golstein, P., and Kroemer, G. (2007). Cell death by necrosis: towards a molecular definition. Trends Biochem Sci *32*, 37-43.

Grandinetti, G., Ingle, N.P., and Reineke, T.M. (2011). Interaction of poly(ethylenimine)-DNA polyplexes with mitochondria: implications for a mechanism of cytotoxicity. Mol Pharm *8*, 1709-1719.

Gray, C.W., Ward, R.V., Karran, E., Turconi, S., Rowles, A., Viglienghi, D., Southan, C., Barton, A., Fantom, K.G., West, A.*, et al.* (2000). Characterization of human HtrA2, a novel serine protease involved in the mammalian cellular stress response. Eur J Biochem *267*, 5699-5710.

Green, D.R. (2000). Apoptotic pathways: paper wraps stone blunts scissors. Cell *102*, 1-4.

Green, D.R., Galluzzi, L., and Kroemer, G. (2011). Mitochondria and the autophagy-inflammation-cell death axis in organismal aging. Science *333*, 1109-1112.

Greene, J.C., Whitworth, A.J., Kuo, I., Andrews, L.A., Feany, M.B., and Pallanck, L.J. (2003). Mitochondrial pathology and apoptotic muscle degeneration in Drosophila parkin mutants. Proc Natl Acad Sci U S A *100*, 4078-4083.

Greenfield, J.G., and Bosanquet, F.D. (1953). The brain-stem lesions in Parkinsonism. J Neurol Neurosurg Psychiatry *16*, 213-226.

Gu, M., Gash, M.T., Mann, V.M., Javoy-Agid, F., Cooper, J.M., and Schapira, A.H. (1996). Mitochondrial defect in Huntington's disease caudate nucleus. Ann Neurol *39*, 385-389.

Gusdon, A.M., Zhu, J., Van Houten, B., and Chu, C.T. (2012). ATP13A2 regulates mitochondrial bioenergetics through macroautophagy. Neurobiol Dis *45*, 962-972.

Gutierrez, M.G., Munafo, D.B., Beron, W., and Colombo, M.I. (2004). Rab7 is required for the normal progression of the autophagic pathway in mammalian cells. J Cell Sci *117*, 2687-2697.

Guzman, J.N., Sanchez-Padilla, J., Wokosin, D., Kondapalli, J., Ilijic, E., Schumacker, P.T., and Surmeier, D.J. (2010). Oxidant stress evoked by pacemaking in dopaminergic neurons is attenuated by DJ-1. Nature *468*, 696-700.

Halliday, G.M., Holton, J.L., Revesz, T., and Dickson, D.W. (2011). Neuropathology underlying clinical variability in patients with synucleinopathies. Acta Neuropathol *122*, 187-204.

Hamza, T.H., Zabetian, C.P., Tenesa, A., Laederach, A., Montimurro, J., Yearout, D., Kay, D.M., Doheny, K.F., Paschall, J., Pugh, E.*, et al.* (2010). Common genetic variation in the HLA region is associated with late-onset sporadic Parkinson's disease. Nat Genet *42*, 781-785.

Hannon, G.J., and Rossi, J.J. (2004). Unlocking the potential of the human genome with RNA interference. Nature *431*, 371-378.

Hao, L.Y., Giasson, B.I., and Bonini, N.M. (2010). DJ-1 is critical for mitochondrial function and rescues PINK1 loss of function. Proc Natl Acad Sci U S A *107*, 9747-9752.

Haque, M.E., Mount, M.P., Safarpour, F., Abdel-Messih, E., Callaghan, S., Mazerolle, C., Kitada, T., Slack, R.S., Wallace, V., Shen, J.*, et al.* (2012). Inactivation of Pink1 in vivo sensitizes dopamine producing neurons to 1-methyl-4-phenyl-1,2,3,6-tetrahydropyridine (MPTP) and can be rescued by autosomal recessive PD genes, Parkin or DJ-1. J Biol Chem.

Haque, M.E., Thomas, K.J., D'Souza, C., Callaghan, S., Kitada, T., Slack, R.S., Fraser, P., Cookson, M.R., Tandon, A., and Park, D.S. (2008). Cytoplasmic Pink1 activity protects neurons from dopaminergic neurotoxin MPTP. Proc Natl Acad Sci U S A *105*, 1716-1721.

Hardy, J., Lewis, P., Revesz, T., Lees, A., and Paisan-Ruiz, C. (2009). The genetics of Parkinson's syndromes: a critical review. Curr Opin Genet Dev *19*, 254-265.

Hargreaves, I.P., Lane, A., and Sleiman, P.M. (2008). The coenzyme Q10 status of the brain regions of Parkinson's disease patients. Neurosci Lett *447*, 17-19.

Harman, D. (1965). The Free Radical Theory of Aging: Effect of Age on Serum Copper Levels. J Gerontol *20*, 151-153.

Harris, H., and Rubinsztein, D.C. (2012). Control of autophagy as a therapy for neurodegenerative disease. Nat Rev Neurol *8*, 108-117.

Hayashi-Takagi, A., Takaki, M., Graziane, N., Seshadri, S., Murdoch, H., Dunlop, A.J., Makino, Y., Seshadri, A.J., Ishizuka, K., Srivastava, D.P.*, et al.* (2010). Disrupted-in-Schizophrenia 1 (DISC1) regulates spines of the glutamate synapse via Rac1. Nat Neurosci *13*, 327-332.

He, C., and Levine, B. (2010). The Beclin 1 interactome. Curr Opin Cell Biol *22*, 140-149.

Healy, D.G., Abou-Sleiman, P.M., Casas, J.P., Ahmadi, K.R., Lynch, T., Gandhi, S., Muqit, M.M., Foltynie, T., Barker, R., Bhatia, K.P.*, et al.* (2006). UCHL-1 is not a Parkinson's disease susceptibility gene. Ann Neurol *59*, 627-633.

Hegde, R., Srinivasula, S.M., Zhang, Z., Wassell, R., Mukattash, R., Cilenti, L., DuBois, G., Lazebnik, Y., Zervos, A.S., Fernandes-Alnemri, T.*, et al.* (2002). Identification of Omi/HtrA2 as a mitochondrial apoptotic serine protease that disrupts inhibitor of apoptosis protein-caspase interaction. J Biol Chem *277*, 432-438.

Henchcliffe, C., Dodel, R., and Beal, M.F. (2011). Biomarkers of Parkinson's disease and Dementia with Lewy bodies. Prog Neurobiol *95*, 601-613.

Hernan, M.A., Takkouche, B., Caamano-Isorna, F., and Gestal-Otero, J.J. (2002). A meta-analysis of coffee drinking, cigarette smoking, and the risk of Parkinson's disease. Ann Neurol *52*, 276-284.

Herrero-Mendez, A., Almeida, A., Fernandez, E., Maestre, C., Moncada, S., and Bolanos, J.P. (2009). The bioenergetic and antioxidant status of neurons is controlled by continuous degradation of a key glycolytic enzyme by APC/C-Cdh1. Nat Cell Biol *11*, 747-752.

Hirsch, A.J. (2010). The use of RNAi-based screens to identify host proteins involved in viral replication. Future Microbiol *5*, 303-311.

Hirtz, D., Thurman, D.J., Gwinn-Hardy, K., Mohamed, M., Chaudhuri, A.R., and Zalutsky, R. (2007). How common are the "common" neurologic disorders? Neurology *68*, 326-337.

Holmgren, A. (1979). Thioredoxin catalyzes the reduction of insulin disulfides by dithiothreitol and dihydrolipoamide. J Biol Chem *254*, 9627-9632.

Hsu, J.M., Lee, Y.C., Yu, C.T., and Huang, C.Y. (2004). Fbx7 functions in the SCF complex regulating Cdk1-cyclin B-phosphorylated hepatoma up-regulated protein (HURP) proteolysis by a proline-rich region. J Biol Chem *279*, 32592-32602.

Hughes, A.J., Ben-Shlomo, Y., Daniel, S.E., and Lees, A.J. (1992). What features improve the accuracy of clinical diagnosis in Parkinson's disease: a clinicopathologic study. Neurology *42*, 1142-1146.

Hughson, L.R., Poon, V.I., Spowart, J.E., and Lum, J.J. (2012). Implications of therapy-induced selective autophagy on tumor metabolism and survival. Int J Cell Biol *2012*, 872091.

Huser, J., and Blatter, L.A. (1999). Fluctuations in mitochondrial membrane potential caused by repetitive gating of the permeability transition pore. Biochem J *343 Pt 2*, 311-317.

Hwang, L.H., and Gilboa, E. (1984). Expression of genes introduced into cells by retroviral infection is more efficient than that of genes introduced into cells by DNA transfection. J Virol *50*, 417-424.

Ibanez, P., Bonnet, A.M., Debarges, B., Lohmann, E., Tison, F., Pollak, P., Agid, Y., Durr, A., and Brice, A. (2004). Causal relation between alpha-synuclein gene duplication and familial Parkinson's disease. Lancet *364*, 1169-1171.

Imai, Y., and Lu, B. (2011). Mitochondrial dynamics and mitophagy in Parkinson's disease: disordered cellular power plant becomes a big deal in a major movement disorder. Curr Opin Neurobiol *21*, 935-941.

Imai, Y., Soda, M., Inoue, H., Hattori, N., Mizuno, Y., and Takahashi, R. (2001). An unfolded putative transmembrane polypeptide, which can lead to endoplasmic reticulum stress, is a substrate of Parkin. Cell *105*, 891-902.

Ingerman, E., Perkins, E.M., Marino, M., Mears, J.A., McCaffery, J.M., Hinshaw, J.E., and Nunnari, J. (2005). Dnm1 forms spirals that are structurally tailored to fit mitochondria. J Cell Biol *170*, 1021-1027.

International Parkinson's Disease Genomics Consortium, and Wellcome Trust Case Control Consortium 2 (2011). A two-stage meta-analysis identifies several new loci for Parkinson's disease. PLoS Genet *7*, e1002142.

Irrcher, I., Aleyasin, H., Seifert, E.L., Hewitt, S.J., Chhabra, S., Phillips, M., Lutz, A.K., Rousseaux, M.W., Bevilacqua, L., Jahani-Asl, A.*, et al.* (2010). Loss of the Parkinson's disease-linked gene DJ-1 perturbs mitochondrial dynamics. Hum Mol Genet *19*, 3734-3746.

Ishihara, N., Eura, Y., and Mihara, K. (2004). Mitofusin 1 and 2 play distinct roles in mitochondrial fusion reactions via GTPase activity. J Cell Sci *117*, 6535-6546.

Jager, S., Bucci, C., Tanida, I., Ueno, T., Kominami, E., Saftig, P., and Eskelinen, E.L. (2004). Role for Rab7 in maturation of late autophagic vacuoles. J Cell Sci *117*, 4837-4848.

Jaiswal, M.K., Zech, W.D., Goos, M., Leutbecher, C., Ferri, A., Zippelius, A., Carri, M.T., Nau, R., and Keller, B.U. (2009). Impairment of mitochondrial calcium handling in a mtSOD1 cell culture model of motoneuron disease. BMC Neurosci *10*, 64.

Jenner, P. (2003). Oxidative stress in Parkinson's disease. Ann Neurol *53 Suppl 3*, S26-36; discussion S36-28.

Jiang, H., Jiang, Q., Liu, W., and Feng, J. (2006). Parkin suppresses the expression of monoamine oxidases. J Biol Chem *281*, 8591-8599.

Jiang, H., Ren, Y., Zhao, J., and Feng, J. (2004a). Parkin protects human dopaminergic neuroblastoma cells against dopamine-induced apoptosis. Hum Mol Genet *13*, 1745-1754.

Jiang, M., Deng, L., and Chen, G. (2004b). High Ca(2+)-phosphate transfection efficiency enables single neuron gene analysis. Gene Ther *11*, 1303-1311.

Jin, J., Li, G.J., Davis, J., Zhu, D., Wang, Y., Pan, C., and Zhang, J. (2007). Identification of novel proteins associated with both alpha-synuclein and DJ-1. Mol Cell Proteomics *6*, 845-859.

Jin, S.M., Lazarou, M., Wang, C., Kane, L.A., Narendra, D.P., and Youle, R.J. (2010). Mitochondrial membrane potential regulates PINK1 import and proteolytic destabilization by PARL. J Cell Biol *191*, 933-942.

Joch, M., Ase, A.R., Chen, C.X., MacDonald, P.A., Kontogiannea, M., Corera, A.T., Brice, A., Seguela, P., and Fon, E.A. (2007). Parkin-mediated monoubiquitination of the PDZ protein PICK1 regulates the activity of acid-sensing ion channels. Mol Biol Cell *18*, 3105-3118.

Johnson, F., and Kaplitt, M.G. (2009). Novel mitochondrial substrates of omi indicate a new regulatory role in neurodegenerative disorders. PLoS One *4*, e7100.

Johnson, J.A., and Ogbi, M. (2011). Targeting the F1Fo ATP Synthase: modulation of the body's powerhouse and its implications for human disease. Curr Med Chem *18*, 4684-4714.

Jones, J.M., Datta, P., Srinivasula, S.M., Ji, W., Gupta, S., Zhang, Z., Davies, E., Hajnoczky, G., Saunders, T.L., Van Keuren, M.L.*, et al.* (2003). Loss of Omi mitochondrial protease activity causes the neuromuscular disorder of mnd2 mutant mice. Nature *425*, 721-727.

Jordan, E.T., Collins, M., Terefe, J., Ugozzoli, L., and Rubio, T. (2008). Optimizing electroporation conditions in primary and other difficult-to-transfect cells. J Biomol Tech *19*, 328-334.

Jouaville, L.S., Pinton, P., Bastianutto, C., Rutter, G.A., and Rizzuto, R. (1999). Regulation of mitochondrial ATP synthesis by calcium: evidence for a long-term metabolic priming. Proc Natl Acad Sci U S A *96*, 13807-13812.

Kabeya, Y., Mizushima, N., Ueno, T., Yamamoto, A., Kirisako, T., Noda, T., Kominami, E., Ohsumi, Y., and Yoshimori, T. (2000). LC3, a mammalian homologue of yeast Apg8p, is localized in autophagosome membranes after processing. EMBO J *19*, 5720-5728.

Kamp, F., Exner, N., Lutz, A.K., Wender, N., Hegermann, J., Brunner, B., Nuscher, B., Bartels, T., Giese, A., Beyer, K.*, et al.* (2010). Inhibition of mitochondrial fusion by alpha-synuclein is rescued by PINK1, Parkin and DJ-1. EMBO J *29*, 3571-3589.

Karbowski, M., and Neutzner, A. (2012). Neurodegeneration as a consequence of failed mitochondrial maintenance. Acta Neuropathol *123*, 157-171.

Karbowski, M., and Youle, R.J. (2011). Regulating mitochondrial outer membrane proteins by ubiquitination and proteasomal degradation. Curr Opin Cell Biol *23*, 476-482.

Kassner, P.D. (2008). Discovery of novel targets with high throughput RNA interference screening. Comb Chem High Throughput Screen *11*, 175-184.

Kawajiri, S., Saiki, S., Sato, S., Sato, F., Hatano, T., Eguchi, H., and Hattori, N. (2010). PINK1 is recruited to mitochondria with parkin and associates with LC3 in mitophagy. FEBS Lett *584*, 1073-1079.

Keeney, P.M., Xie, J., Capaldi, R.A., and Bennett, J.P., Jr. (2006). Parkinson's disease brain mitochondrial complex I has oxidatively damaged subunits and is functionally impaired and misassembled. J Neurosci *26*, 5256-5264.

Kelso, G.F., Porteous, C.M., Coulter, C.V., Hughes, G., Porteous, W.K., Ledgerwood, E.C., Smith, R.A., and Murphy, M.P. (2001). Selective targeting of a redox-active ubiquinone to mitochondria within cells: antioxidant and antiapoptotic properties. J Biol Chem *276*, 4588-4596.

Kennedy, K.A., Sandiford, S.D., Skerjanc, I.S., and Li, S.S. (2012). Reactive oxygen species and the neuronal fate. Cell Mol Life Sci *69*, 215-221.

Kerr, J.F., Wyllie, A.H., and Currie, A.R. (1972). Apoptosis: a basic biological phenomenon with wide-ranging implications in tissue kinetics. Br J Cancer *26*, 239-257.

Kieper, N., Holmstrom, K.M., Ciceri, D., Fiesel, F.C., Wolburg, H., Ziviani, E., Whitworth, A.J., Martins, L.M., Kahle, P.J., and Kruger, R. (2010). Modulation of mitochondrial function and morphology by interaction of Omi/HtrA2 with the mitochondrial fusion factor OPA1. Exp Cell Res *316*, 1213-1224.

Kim, I., Rodriguez-Enriquez, S., and Lemasters, J.J. (2007). Selective degradation of mitochondria by mitophagy. Arch Biochem Biophys *462*, 245-253.

Kim, K., Kim, I.H., Lee, K.Y., Rhee, S.G., and Stadtman, E.R. (1988). The isolation and purification of a specific "protector" protein which inhibits enzyme inactivation by a thiol/Fe(III)/O2 mixed-function oxidation system. J Biol Chem *263*, 4704-4711.

Kipreos, E.T., and Pagano, M. (2000). The F-box protein family. Genome Biol *1*, REVIEWS3002.

Kirk, R., Laman, H., Knowles, P.P., Murray-Rust, J., Lomonosov, M., Meziane el, K., and McDonald, N.Q. (2008). Structure of a conserved dimerization domain within the F-box protein Fbxo7 and the PI31 proteasome inhibitor. J Biol Chem *283*, 22325-22335.

Kitada, T., Asakawa, S., Hattori, N., Matsumine, H., Yamamura, Y., Minoshima, S., Yokochi, M., Mizuno, Y., and Shimizu, N. (1998). Mutations in the parkin gene cause autosomal recessive juvenile parkinsonism. Nature *392*, 605-608.

Klionsky, D.J. (2007). Autophagy: from phenomenology to molecular understanding in less than a decade. Nat Rev Mol Cell Biol *8*, 931-937.

Kluck, R.M., Bossy-Wetzel, E., Green, D.R., and Newmeyer, D.D. (1997). The release of cytochrome c from mitochondria: a primary site for Bcl-2 regulation of apoptosis. Science *275*, 1132-1136.

Kok, K.H., Lei, T., and Jin, D.Y. (2009). siRNA and shRNA screens advance key understanding of host factors required for HIV-1 replication. Retrovirology *6*, 78.

Kokoszka, J.E., Waymire, K.G., Levy, S.E., Sligh, J.E., Cai, J., Jones, D.P., MacGregor, G.R., and Wallace, D.C. (2004). The ADP/ATP translocator is not essential for the mitochondrial permeability transition pore. Nature *427*, 461-465.

Kooistra, J., Milojevic, J., Melacini, G., and Ortega, J. (2009). A new function of human HtrA2 as an amyloid-beta oligomerization inhibitor. J Alzheimers Dis *17*, 281-294.

Kordower, J.H., Chu, Y., Hauser, R.A., Freeman, T.B., and Olanow, C.W. (2008). Lewy body-like pathology in long-term embryonic nigral transplants in Parkinson's disease. Nat Med *14*, 504-506.

Korshunov, S.S., Skulachev, V.P., and Starkov, A.A. (1997). High protonic potential actuates a mechanism of production of reactive oxygen species in mitochondria. FEBS Lett *416*, 15-18.

Koshiba, T., Detmer, S.A., Kaiser, J.T., Chen, H., McCaffery, J.M., and Chan, D.C. (2004). Structural basis of mitochondrial tethering by mitofusin complexes. Science *305*, 858-862.

Krause, M., Fogel, W., Heck, A., Hacke, W., Bonsanto, M., Trenkwalder, C., and Tronnier, V. (2001). Deep brain stimulation for the treatment of Parkinson's disease: subthalamic nucleus versus globus pallidus internus. J Neurol Neurosurg Psychiatry *70*, 464-470.

Krebiehl, G., Ruckerbauer, S., Burbulla, L.F., Kieper, N., Maurer, B., Waak, J., Wolburg, H., Gizatullina, Z., Gellerich, F.N., Woitalla, D.*, et al.* (2010). Reduced basal autophagy and impaired mitochondrial dynamics due to loss of Parkinson's disease-associated protein DJ-1. PLoS One *5*, e9367.

Kruger, R., Sharma, M., Riess, O., Gasser, T., Van Broeckhoven, C., Theuns, J., Aasly, J., Annesi, G., Bentivoglio, A.R., Brice, A.*, et al.* (2011). A large-scale genetic association study to evaluate the contribution of Omi/HtrA2 (PARK13) to Parkinson's disease. Neurobiol Aging *32*, 548 e549-518.

Kuan, W.L., Poole, E., Fletcher, M., Karniely, S., Tyers, P., Wills, M., Barker, R.A., and Sinclair, J.H. (2012). A novel neuroprotective therapy for Parkinson's disease using a viral noncoding RNA that protects mitochondrial complex I activity. J Exp Med *209*, 1-10.

Kushnareva, Y., Murphy, A.N., and Andreyev, A. (2002). Complex I-mediated reactive oxygen species generation: modulation by cytochrome c and NAD(P)+ oxidation-reduction state. Biochem J *368*, 545-553.

Kuwana, T., Bouchier-Hayes, L., Chipuk, J.E., Bonzon, C., Sullivan, B.A., Green, D.R., and Newmeyer, D.D. (2005). BH3 domains of BH3-only proteins differentially regulate Bax-mediated mitochondrial membrane permeabilization both directly and indirectly. Mol Cell *17*, 525-535.

Lagos-Quintana, M., Rauhut, R., Lendeckel, W., and Tuschl, T. (2001). Identification of novel genes coding for small expressed RNAs. Science *294*, 853-858.

Laman, H., Funes, J.M., Ye, H., Henderson, S., Galinanes-Garcia, L., Hara, E., Knowles, P., McDonald, N., and Boshoff, C. (2005). Transforming activity of Fbxo7 is mediated specifically through regulation of cyclin D/cdk6. EMBO J *24*, 3104-3116.

Langston, J.W., Ballard, P., Tetrud, J.W., and Irwin, I. (1983). Chronic Parkinsonism in humans due to a product of meperidine-analog synthesis. Science *219*, 979-980.

Langston, J.W., Irwin, I., Langston, E.B., and Forno, L.S. (1984). 1-Methyl-4-phenylpyridinium ion (MPP+): identification of a metabolite of MPTP, a toxin selective to the substantia nigra. Neurosci Lett *48*, 87-92.

Lautier, C., Goldwurm, S., Durr, A., Giovannone, B., Tsiaras, W.G., Pezzoli, G., Brice, A., and Smith, R.J. (2008). Mutations in the GIGYF2 (TNRC15) gene at the PARK11 locus in familial Parkinson disease. Am J Hum Genet *82*, 822-833.

Lazarou, M., Jin, S.M., Kane, L.A., and Youle, R.J. (2012). Role of PINK1 binding to the TOM complex and alternate intracellular membranes in recruitment and activation of the E3 ligase Parkin. Dev Cell *22*, 320-333.

Lee, J.A. (2012). Neuronal autophagy: a housekeeper or a fighter in neuronal cell survival? Exp Neurobiol *21*, 1-8.

Lee, J.K., Belogrudov, G.I., and Stroud, R.M. (2008). Crystal structure of bovine mitochondrial factor B at 0.96-A resolution. Proc Natl Acad Sci U S A *105*, 13379-13384.

Lee, J.Y., Nagano, Y., Taylor, J.P., Lim, K.L., and Yao, T.P. (2010). Disease-causing mutations in parkin impair mitochondrial ubiquitination, aggregation, and HDAC6-dependent mitophagy. J Cell Biol *189*, 671-679.

Lees, A. (2007). Secondary Parkinsonism. In Parkinson's Disease & Movement Disorders, J. Jankovic, and E. Tolosa, eds., pp. 213-223.

Legros, F., Lombes, A., Frachon, P., and Rojo, M. (2002). Mitochondrial fusion in human cells is efficient, requires the inner membrane potential, and is mediated by mitofusins. Mol Biol Cell *13*, 4343-4354.

Lemasters, J.J., Nieminen, A.L., Qian, T., Trost, L.C., Elmore, S.P., Nishimura, Y., Crowe, R.A., Cascio, W.E., Bradham, C.A., Brenner, D.A.*, et al.* (1998). The mitochondrial permeability transition in cell death: a common mechanism in necrosis, apoptosis and autophagy. Biochim Biophys Acta *1366*, 177-196.

Leroy, E., Boyer, R., Auburger, G., Leube, B., Ulm, G., Mezey, E., Harta, G., Brownstein, M.J., Jonnalagada, S., Chernova, T.*, et al.* (1998). The ubiquitin pathway in Parkinson's disease. Nature *395*, 451-452.

Lesage, S., and Brice, A. (2012). Role of Mendelian genes in "sporadic" Parkinson's disease. Parkinsonism Relat Disord *18 Suppl 1*, S66-70.

LeWitt, P.A. (1991). Deprenyl's effect at slowing progression of parkinsonian disability: the DATATOP study. The Parkinson Study Group. Acta Neurol Scand Suppl *136*, 79-86.

Leyssens, A., Nowicky, A.V., Patterson, L., Crompton, M., and Duchen, M.R. (1996). The relationship between mitochondrial state, ATP hydrolysis, [Mg2+]i and [Ca2+]i studied in isolated rat cardiomyocytes. J Physiol *496 (Pt 1)*, 111-128.

Li, B., Hu, Q., Wang, H., Man, N., Ren, H., Wen, L., Nukina, N., Fei, E., and Wang, G. (2010). Omi/HtrA2 is a positive regulator of autophagy that facilitates the degradation of mutant proteins involved in neurodegenerative diseases. Cell Death Differ.

Li, J.Y., Englund, E., Holton, J.L., Soulet, D., Hagell, P., Lees, A.J., Lashley, T., Quinn, N.P., Rehncrona, S., Bjorklund, A*., et al.* (2008). Lewy bodies in grafted neurons in subjects with Parkinson's disease suggest host-to-graft disease propagation. Nat Med *14*, 501-503.

Li, W., Srinivasula, S.M., Chai, J., Li, P., Wu, J.W., Zhang, Z., Alnemri, E.S., and Shi, Y. (2002a). Structural insights into the pro-apoptotic function of mitochondrial serine protease HtrA2/Omi. Nat Struct Biol *9*, 436-441.

Li, W.W., Yang, R., Guo, J.C., Ren, H.M., Zha, X.L., Cheng, J.S., and Cai, D.F. (2007). Localization of alpha-synuclein to mitochondria within midbrain of mice. Neuroreport *18*, 1543-1546.

Li, Y.J., Scott, W.K., Hedges, D.J., Zhang, F., Gaskell, P.C., Nance, M.A., Watts, R.L., Hubble, J.P., Koller, W.C., Pahwa, R*., et al.* (2002b). Age at onset in two common neurodegenerative diseases is genetically controlled. Am J Hum Genet *70*, 985-993.

Lill, C.M., and Bertram, L. (2011). Towards unveiling the genetics of neurodegenerative diseases. Semin Neurol *31*, 531-541.

Lim, K.L., Chew, K.C., Tan, J.M., Wang, C., Chung, K.K., Zhang, Y., Tanaka, Y., Smith, W., Engelender, S., Ross, C.A*., et al.* (2005). Parkin mediates nonclassical, proteasomal-independent ubiquitination of synphilin-1: implications for Lewy body formation. J Neurosci *25*, 2002-2009.

Lin, C.H., Chen, M.L., Chen, G.S., Tai, C.H., and Wu, R.M. (2011). Novel variant Pro143Ala in HTRA2 contributes to Parkinson's disease by inducing hyperphosphorylation of HTRA2 protein in mitochondria. Hum Genet *130*, 817-827.

Lin, W., and Kang, U.J. (2008). Characterization of PINK1 processing, stability, and subcellular localization. J Neurochem *106*, 464-474.

Liu, S., Sawada, T., Lee, S., Yu, W., Silverio, G., Alapatt, P., Millan, I., Shen, A., Saxton, W., Kanao, T.*, et al.* (2012). Parkinson's disease-associated kinase PINK1 regulates Miro protein level and axonal transport of mitochondria. PLoS Genet *8*, e1002537.

Liu, W., Vives-Bauza, C., Acin-Perez, R., Yamamoto, A., Tan, Y., Li, Y., Magrane, J., Stavarache, M.A., Shaffer, S., Chang, S.*, et al.* (2009). PINK1 defect causes mitochondrial dysfunction, proteasomal deficit and alpha-synuclein aggregation in cell culture models of Parkinson's disease. PLoS One *4*, e4597.

Livak, K.J., and Schmittgen, T.D. (2001). Analysis of relative gene expression data using real-time quantitative PCR and the 2(-Delta Delta C(T)) Method. Methods *25*, 402-408.

Luk, K.C., Song, C., O'Brien, P., Stieber, A., Branch, J.R., Brunden, K.R., Trojanowski, J.Q., and Lee, V.M. (2009). Exogenous alpha-synuclein fibrils seed the formation of Lewy body-like intracellular inclusions in cultured cells. Proc Natl Acad Sci U S A *106*, 20051-20056.

Lwin, A., Orvisky, E., Goker-Alpan, O., LaMarca, M.E., and Sidransky, E. (2004). Glucocerebrosidase mutations in subjects with parkinsonism. Mol Genet Metab *81*, 70-73.

Lynch, R.E., and Fridovich, I. (1978). Permeation of the erythrocyte stroma by superoxide radical. J Biol Chem *253*, 4697-4699.

Majander, A., Lamminen, T., Juvonen, V., Aula, P., Nikoskelainen, E., Savontaus, M.L., and Wikstrom, M. (1997). Mutations in subunit 6 of the F1F0-ATP synthase cause two entirely different diseases. FEBS Lett *412*, 351-354.

Malo, N., Hanley, J.A., Cerquozzi, S., Pelletier, J., and Nadon, R. (2006). Statistical practice in high-throughput screening data analysis. Nat Biotechnol *24*, 167-175.

Mann, P.J. (1932). The reduction of glutathione by a liver system. Biochem J *26*, 785-790.

Marchetti, P., Decaudin, D., Macho, A., Zamzami, N., Hirsch, T., Susin, S.A., and Kroemer, G. (1997). Redox regulation of apoptosis: impact of thiol oxidation status on mitochondrial function. Eur J Immunol *27*, 289-296.

Marongiu, R., Spencer, B., Crews, L., Adame, A., Patrick, C., Trejo, M., Dallapiccola, B., Valente, E.M., and Masliah, E. (2009). Mutant Pink1 induces mitochondrial dysfunction in a neuronal cell model of Parkinson's disease by disturbing calcium flux. J Neurochem *108*, 1561-1574.

Martin, I., Dawson, V.L., and Dawson, T.M. (2011). Recent advances in the genetics of Parkinson's disease. Annu Rev Genomics Hum Genet *12*, 301-325.

Martins, L.M., Iaccarino, I., Tenev, T., Gschmeissner, S., Totty, N.F., Lemoine, N.R., Savopoulos, J., Gray, C.W., Creasy, C.L., Dingwall, C.*, et al.* (2002). The serine protease Omi/HtrA2 regulates apoptosis by binding XIAP through a reaper-like motif. J Biol Chem *277*, 439-444.

Martins, L.M., Morrison, A., Klupsch, K., Fedele, V., Moisoi, N., Teismann, P., Abuin, A., Grau, E., Geppert, M., Livi, G.P.*, et al.* (2004). Neuroprotective role of the Reaper-related serine protease HtrA2/Omi revealed by targeted deletion in mice. Mol Cell Biol *24*, 9848-9862.

Marzo, I., Brenner, C., Zamzami, N., Jurgensmeier, J.M., Susin, S.A., Vieira, H.L., Prevost, M.C., Xie, Z., Matsuyama, S., Reed, J.C.*, et al.* (1998). Bax and adenine nucleotide translocator cooperate in the mitochondrial control of apoptosis. Science *281*, 2027-2031.

Masaike, T., Koyama-Horibe, F., Oiwa, K., Yoshida, M., and Nishizaka, T. (2008). Cooperative three-step motions in catalytic subunits of F(1)-ATPase correlate with 80 degrees and 40 degrees substep rotations. Nat Struct Mol Biol *15*, 1326-1333.

McCormack, J.G., Bromidge, E.S., and Dawes, N.J. (1988). Characterization of the effects of Ca2+ on the intramitochondrial Ca2+-sensitive dehydrogenases within intact rat-kidney mitochondria. Biochim Biophys Acta *934*, 282-292.

Mears, J.A., Lackner, L.L., Fang, S., Ingerman, E., Nunnari, J., and Hinshaw, J.E. (2011). Conformational changes in Dnm1 support a contractile mechanism for mitochondrial fission. Nat Struct Mol Biol *18*, 20-26.

Meeusen, S., DeVay, R., Block, J., Cassidy-Stone, A., Wayson, S., McCaffery, J.M., and Nunnari, J. (2006). Mitochondrial inner-membrane fusion and crista maintenance requires the dynamin-related GTPase Mgm1. Cell *127*, 383-395.

Mills, G.C. (1960). Glutathione peroxidase and the destruction of hydrogen peroxide in animal tissues. Arch Biochem Biophys *86*, 1-5.

Misaka, T., Miyashita, T., and Kubo, Y. (2002). Primary structure of a dynamin-related mouse mitochondrial GTPase and its distribution in brain, subcellular localization, and effect on mitochondrial morphology. J Biol Chem *277*, 15834-15842.

Mitra, K., Wunder, C., Roysam, B., Lin, G., and Lippincott-Schwartz, J. (2009). A hyperfused mitochondrial state achieved at G1-S regulates cyclin E buildup and entry into S phase. Proc Natl Acad Sci U S A *106*, 11960-11965.

Mizuno, Y., Matuda, S., Yoshino, H., Mori, H., Hattori, N., and Ikebe, S. (1994). An immunohistochemical study on alpha-ketoglutarate dehydrogenase complex in Parkinson's disease. Ann Neurol *35*, 204-210.

Mizuno, Y., Suzuki, K., Sone, N., and Saitoh, T. (1988). Inhibition of mitochondrial respiration by 1-methyl-4-phenyl-1,2,3,6-tetrahydropyridine (MPTP) in mouse brain in vivo. Neurosci Lett *91*, 349-353.

Moffat, J., Grueneberg, D.A., Yang, X., Kim, S.Y., Kloepfer, A.M., Hinkle, G., Piqani, B., Eisenhaure, T.M., Luo, B., Grenier, J.K.*, et al.* (2006). A lentiviral RNAi library for human and mouse genes applied to an arrayed viral high-content screen. Cell *124*, 1283-1298.

Moisoi, N., Klupsch, K., Fedele, V., East, P., Sharma, S., Renton, A., Plun-Favreau, H., Edwards, R.E., Teismann, P., Esposti, M.D.*, et al.* (2009). Mitochondrial dysfunction triggered by loss of HtrA2 results in the activation of a brain-specific transcriptional stress response. Cell Death Differ *16*, 449-464.

Mones, R.J., Elizan, T.S., and Siegel, G.J. (1970). An analysis of L-dopa-induced dyskinesias in 152 cases of Parkinson's disease. Neurology *20*, 405-406.

Morais, V.A., Verstreken, P., Roethig, A., Smet, J., Snellinx, A., Vanbrabant, M., Haddad, D., Frezza, C., Mandemakers, W., Vogt-Weisenhorn, D.*, et al.* (2009). Parkinson's disease

mutations in PINK1 result in decreased Complex I activity and deficient synaptic function. EMBO Mol Med *1*, 99-111.

Moriwaki, Y., Kim, Y.J., Ido, Y., Misawa, H., Kawashima, K., Endo, S., and Takahashi, R. (2008). L347P PINK1 mutant that fails to bind to Hsp90/Cdc37 chaperones is rapidly degraded in a proteasome-dependent manner. Neurosci Res *61*, 43-48.

Mortiboys, H., Johansen, K.K., Aasly, J.O., and Bandmann, O. (2010). Mitochondrial impairment in patients with Parkinson disease with the G2019S mutation in LRRK2. Neurology *75*, 2017-2020.

Mukhopadhyay, P., Rajesh, M., Hasko, G., Hawkins, B.J., Madesh, M., and Pacher, P. (2007). Simultaneous detection of apoptosis and mitochondrial superoxide production in live cells by flow cytometry and confocal microscopy. Nat Protoc *2*, 2295-2301.

Muqit, M.M., Abou-Sleiman, P.M., Saurin, A.T., Harvey, K., Gandhi, S., Deas, E., Eaton, S., Payne Smith, M.D., Venner, K., Matilla, A.*, et al.* (2006). Altered cleavage and localization of PINK1 to aggresomes in the presence of proteasomal stress. J Neurochem *98*, 156-169.

Muratani, M., Kung, C., Shokat, K.M., and Tansey, W.P. (2005). The F box protein Dsg1/Mdm30 is a transcriptional coactivator that stimulates Gal4 turnover and cotranscriptional mRNA processing. Cell *120*, 887-899.

Nakagawa, T., Shimizu, S., Watanabe, T., Yamaguchi, O., Otsu, K., Yamagata, H., Inohara, H., Kubo, T., and Tsujimoto, Y. (2005). Cyclophilin D-dependent mitochondrial permeability transition regulates some necrotic but not apoptotic cell death. Nature *434*, 652-658.

Nakai, K., and Kanehisa, M. (1992). A knowledge base for predicting protein localization sites in eukaryotic cells. Genomics *14*, 897-911.

Nakamura, K., Nemani, V.M., Azarbal, F., Skibinski, G., Levy, J.M., Egami, K., Munishkina, L., Zhang, J., Gardner, B., Wakabayashi, J.*, et al.* (2011). Direct membrane association drives mitochondrial fission by the Parkinson disease-associated protein alpha-synuclein. J Biol Chem *286*, 20710-20726.

Nakamura, K., Nemani, V.M., Wallender, E.K., Kaehlcke, K., Ott, M., and Edwards, R.H. (2008). Optical reporters for the conformation of alpha-synuclein reveal a specific interaction with mitochondria. J Neurosci *28*, 12305-12317.

Naldini, L., Blomer, U., Gallay, P., Ory, D., Mulligan, R., Gage, F.H., Verma, I.M., and Trono, D. (1996). In vivo gene delivery and stable transduction of nondividing cells by a lentiviral vector. Science *272*, 263-267.

Narendra, D., Tanaka, A., Suen, D.F., and Youle, R.J. (2008). Parkin is recruited selectively to impaired mitochondria and promotes their autophagy. J Cell Biol *183*, 795-803.

Narendra, D.P., Jin, S.M., Tanaka, A., Suen, D.F., Gautier, C.A., Shen, J., Cookson, M.R., and Youle, R.J. (2010). PINK1 is selectively stabilized on impaired mitochondria to activate Parkin. PLoS Biol *8*, e1000298.

Negre-Salvayre, A., Hirtz, C., Carrera, G., Cazenave, R., Troly, M., Salvayre, R., Penicaud, L., and Casteilla, L. (1997). A role for uncoupling protein-2 as a regulator of mitochondrial hydrogen peroxide generation. FASEB J *11*, 809-815.

Nelson, D.E., and Laman, H. (2011). A competitive binding mechanism between SKP1 and exportin 1 (CRM1) controls the localization of a subset of F-box proteins. J Biol Chem.

Neufeld, H.A., Towner, R.D., and Pace, J. (1975). A rapid method for determining ATP by the firefly luciferin-luciferase system. Experientia *31*, 391-392.

Nichols, W.C., Kissell, D.K., Pankratz, N., Pauciulo, M.W., Elsaesser, V.E., Clark, K.A., Halter, C.A., Rudolph, A., Wojcieszek, J., Pfeiffer, R.F.*, et al.* (2009). Variation in GIGYF2 is not associated with Parkinson disease. Neurology *72*, 1886-1892.

Ono, T., Isobe, K., Nakada, K., and Hayashi, J.I. (2001). Human cells are protected from mitochondrial dysfunction by complementation of DNA products in fused mitochondria. Nat Genet *28*, 272-275.

Orvedahl, A., Sumpter, R., Jr., Xiao, G., Ng, A., Zou, Z., Tang, Y., Narimatsu, M., Gilpin, C., Sun, Q., Roth, M.*, et al.* (2011). Image-based genome-wide siRNA screen identifies selective autophagy factors. Nature *480*, 113-117.

Osman, C., Wilmes, C., Tatsuta, T., and Langer, T. (2007). Prohibitins interact genetically with Atp23, a novel processing peptidase and chaperone for the F1Fo-ATP synthase. Mol Biol Cell *18*, 627-635.

Paddison, P.J., Caudy, A.A., Bernstein, E., Hannon, G.J., and Conklin, D.S. (2002a). Short hairpin RNAs (shRNAs) induce sequence-specific silencing in mammalian cells. Genes Dev *16*, 948-958.

Paddison, P.J., Caudy, A.A., and Hannon, G.J. (2002b). Stable suppression of gene expression by RNAi in mammalian cells. Proc Natl Acad Sci U S A *99*, 1443-1448.

Paisan-Ruiz, C., Bhatia, K.P., Li, A., Hernandez, D., Davis, M., Wood, N.W., Hardy, J., Houlden, H., Singleton, A., and Schneider, S.A. (2009). Characterization of PLA2G6 as a locus for dystonia-parkinsonism. Ann Neurol *65*, 19-23.

Paisan-Ruiz, C., Guevara, R., Federoff, M., Hanagasi, H., Sina, F., Elahi, E., Schneider, S.A., Schwingenschuh, P., Bajaj, N., Emre, M.*, et al.* (2010). Early-onset L-dopa-responsive parkinsonism with pyramidal signs due to ATP13A2, PLA2G6, FBXO7 and spatacsin mutations. Mov Disord *25*, 1791-1800.

Paisan-Ruiz, C., Jain, S., Evans, E.W., Gilks, W.P., Simon, J., van der Brug, M., Lopez de Munain, A., Aparicio, S., Gil, A.M., Khan, N.*, et al.* (2004). Cloning of the gene containing mutations that cause PARK8-linked Parkinson's disease. Neuron *44*, 595-600.

Palacino, J.J., Sagi, D., Goldberg, M.S., Krauss, S., Motz, C., Wacker, M., Klose, J., and Shen, J. (2004). Mitochondrial dysfunction and oxidative damage in parkin-deficient mice. J Biol Chem *279*, 18614-18622.

Pallanck, L.J. (2010). Culling sick mitochondria from the herd. J Cell Biol *191*, 1225-1227.

Pankratz, N., Nichols, W.C., Uniacke, S.K., Halter, C., Rudolph, A., Shults, C., Conneally, P.M., and Foroud, T. (2002). Genome screen to identify susceptibility genes for Parkinson disease in a sample without parkin mutations. Am J Hum Genet *71*, 124-135.

Papa, L., and Germain, D. (2011). Estrogen receptor mediates a distinct mitochondrial unfolded protein response. J Cell Sci *124*, 1396-1402.

Papkovskaia, T.D., Chau, K.Y., Inesta-Vaquera, F., Papkovsky, D.B., Healy, D.G., Nishio, K., Staddon, J., Duchen, M.R., Hardy, J., Schapira, A.H.*, et al.* (2012). G2019S Leucine Rich Repeat Kinase 2 causes uncoupling protein mediated mitochondrial depolarisation. Hum Mol Genet.

Park, J., Lee, S.B., Lee, S., Kim, Y., Song, S., Kim, S., Bae, E., Kim, J., Shong, M., Kim, J.M., *et al.* (2006). Mitochondrial dysfunction in Drosophila PINK1 mutants is complemented by parkin. Nature *441*, 1157-1161.

Parker, W.D., Jr., Filley, C.M., and Parks, J.K. (1990). Cytochrome oxidase deficiency in Alzheimer's disease. Neurology *40*, 1302-1303.

Parkinson Study Group (2003). A controlled trial of rotigotine monotherapy in early Parkinson's disease. Arch Neurol *60*, 1721-1728.

Parsons, B.D., Schindler, A., Evans, D.H., and Foley, E. (2009). A direct phenotypic comparison of siRNA pools and multiple individual duplexes in a functional assay. PLoS One *4*, e8471.

Patton, E.E., Willems, A.R., and Tyers, M. (1998). Combinatorial control in ubiquitin-dependent proteolysis: don't Skp the F-box hypothesis. Trends Genet *14*, 236-243.

Pavlov, E.V., Priault, M., Pietkiewicz, D., Cheng, E.H., Antonsson, B., Manon, S., Korsmeyer, S.J., Mannella, C.A., and Kinnally, K.W. (2001). A novel, high conductance channel of mitochondria linked to apoptosis in mammalian cells and Bax expression in yeast. J Cell Biol *155*, 725-731.

Petit, A., Kawarai, T., Paitel, E., Sanjo, N., Maj, M., Scheid, M., Chen, F., Gu, Y., Hasegawa, H., Salehi-Rad, S., *et al.* (2005). Wild-type PINK1 prevents basal and induced neuronal apoptosis, a protective effect abrogated by Parkinson disease-related mutations. J Biol Chem *280*, 34025-34032.

Petronilli, V., Miotto, G., Canton, M., Brini, M., Colonna, R., Bernardi, P., and Di Lisa, F. (1999). Transient and long-lasting openings of the mitochondrial permeability transition pore can be monitored directly in intact cells by changes in mitochondrial calcein fluorescence. Biophys J *76*, 725-734.

Piccoli, C., Sardanelli, A., Scrima, R., Ripoli, M., Quarato, G., D'Aprile, A., Bellomo, F., Scacco, S., De Michele, G., Filla, A., *et al.* (2008). Mitochondrial respiratory dysfunction in familiar parkinsonism associated with PINK1 mutation. Neurochem Res *33*, 2565-2574.

Plun-Favreau, H., Klupsch, K., Moisoi, N., Gandhi, S., Kjaer, S., Frith, D., Harvey, K., Deas, E., Harvey, R.J., McDonald, N.*, et al.* (2007). The mitochondrial protease HtrA2 is regulated by Parkinson's disease-associated kinase PINK1. Nat Cell Biol *9*, 1243-1252.

Plun-Favreau, H., Lewis, P.A., Hardy, J., Martins, L.M., and Wood, N.W. (2010). Cancer and neurodegeneration: between the devil and the deep blue sea. PLoS Genet *6*, e1001257.

Poletti, M., De Rosa, A., and Bonuccelli, U. (2012). Affective symptoms and cognitive functions in Parkinson's disease. J Neurol Sci *317*, 97-102.

Polymeropoulos, M.H., Lavedan, C., Leroy, E., Ide, S.E., Dehejia, A., Dutra, A., Pike, B., Root, H., Rubenstein, J., Boyer, R.*, et al.* (1997). Mutation in the alpha-synuclein gene identified in families with Parkinson's disease. Science *276*, 2045-2047.

Poole, A.C., Thomas, R.E., Andrews, L.A., McBride, H.M., Whitworth, A.J., and Pallanck, L.J. (2008). The PINK1/Parkin pathway regulates mitochondrial morphology. Proc Natl Acad Sci U S A *105*, 1638-1643.

Poole, A.C., Thomas, R.E., Yu, S., Vincow, E.S., and Pallanck, L. (2010). The mitochondrial fusion-promoting factor mitofusin is a substrate of the PINK1/parkin pathway. PLoS One *5*, e10054.

Pridgeon, J.W., Olzmann, J.A., Chin, L.S., and Li, L. (2007). PINK1 protects against oxidative stress by phosphorylating mitochondrial chaperone TRAP1. PLoS Biol *5*, e172.

Rabilloud, T., Heller, M., Rigobello, M.P., Bindoli, A., Aebersold, R., and Lunardi, J. (2001). The mitochondrial antioxidant defence system and its response to oxidative stress. Proteomics *1*, 1105-1110.

Racay, P., Kaplan, P., Mezesova, V., and Lehotsky, J. (1997). Lipid peroxidation both inhibits Ca(2+)-ATPase and increases Ca2+ permeability of endoplasmic reticulum membrane. Biochem Mol Biol Int *41*, 647-655.

Radke, S., Chander, H., Schafer, P., Meiss, G., Kruger, R., Schulz, J.B., and Germain, D. (2008). Mitochondrial protein quality control by the proteasome involves ubiquitination and the protease Omi. J Biol Chem *283*, 12681-12685.

Raess, B.U., Keenan, C.E., and McConnell, E.J. (1997). Effects of 4-OH-2,3-trans-nonenal on human erythrocyte plasma membrane Ca2+ pump and passive Ca2+ permeability. Biochem Biophys Res Commun *235*, 451-454.

Rakovic, A., Grunewald, A., Kottwitz, J., Bruggemann, N., Pramstaller, P.P., Lohmann, K., and Klein, C. (2011). Mutations in PINK1 and Parkin impair ubiquitination of Mitofusins in human fibroblasts. PLoS One *6*, e16746.

Ramirez, A., Heimbach, A., Grundemann, J., Stiller, B., Hampshire, D., Cid, L.P., Goebel, I., Mubaidin, A.F., Wriekat, A.L., Roeper, J.*, et al.* (2006). Hereditary parkinsonism with dementia is caused by mutations in ATP13A2, encoding a lysosomal type 5 P-type ATPase. Nat Genet *38*, 1184-1191.

Rang, H., Dale, M., Ritter, J., and Moore, P. (2003). Pharmacology, 5th edn.

Rao, D.D., Vorhies, J.S., Senzer, N., and Nemunaitis, J. (2009). siRNA vs. shRNA: similarities and differences. Adv Drug Deliv Rev *61*, 746-759.

Rascol, O., Brooks, D.J., Korczyn, A.D., De Deyn, P.P., Clarke, C.E., and Lang, A.E. (2000). A five-year study of the incidence of dyskinesia in patients with early Parkinson's disease who were treated with ropinirole or levodopa. 056 Study Group. N Engl J Med *342*, 1484-1491.

Rasola, A., and Bernardi, P. (2007). The mitochondrial permeability transition pore and its involvement in cell death and in disease pathogenesis. Apoptosis *12*, 815-833.

Rasola, A., and Bernardi, P. (2011). Mitochondrial permeability transition in Ca(2+)-dependent apoptosis and necrosis. Cell Calcium *50*, 222-233.

Rausch, O. (2006). High content cellular screening. Curr Opin Chem Biol *10*, 316-320.

Ravikumar, B., Sarkar, S., Davies, J.E., Futter, M., Garcia-Arencibia, M., Green-Thompson, Z.W., Jimenez-Sanchez, M., Korolchuk, V.I., Lichtenberg, M., Luo, S.*, et al.* (2010). Regulation of mammalian autophagy in physiology and pathophysiology. Physiol Rev *90*, 1383-1435.

Reavie, L., Della Gatta, G., Crusio, K., Aranda-Orgilles, B., Buckley, S.M., Thompson, B., Lee, E., Gao, J., Bredemeyer, A.L., Helmink, B.A.*, et al.* (2010). Regulation of hematopoietic stem

cell differentiation by a single ubiquitin ligase-substrate complex. Nat Immunol *11*, 207-215.

Regnstrom, K., Ragnarsson, E.G., Koping-Hoggard, M., Torstensson, E., Nyblom, H., and Artursson, P. (2003). PEI - a potent, but not harmless, mucosal immuno-stimulator of mixed T-helper cell response and FasL-mediated cell death in mice. Gene Ther *10*, 1575-1583.

Rego, A.C., Ward, M.W., and Nicholls, D.G. (2001). Mitochondria control ampa/kainate receptor-induced cytoplasmic calcium deregulation in rat cerebellar granule cells. J Neurosci *21*, 1893-1901.

Reis, Y., Bernardo-Faura, M., Richter, D., Wolf, T., Brors, B., Hamacher-Brady, A., Eils, R., and Brady, N.R. (2012). Multi-parametric analysis and modeling of relationships between mitochondrial morphology and apoptosis. PLoS One *7*, e28694.

Rodriguez-Enriquez, S., Kim, I., Currin, R.T., and Lemasters, J.J. (2006). Tracker dyes to probe mitochondrial autophagy (mitophagy) in rat hepatocytes. Autophagy *2*, 39-46.

Ross, O.A., Soto, A.I., Vilarino-Guell, C., Heckman, M.G., Diehl, N.N., Hulihan, M.M., Aasly, J.O., Sando, S., Gibson, J.M., Lynch, T.*, et al.* (2008). Genetic variation of Omi/HtrA2 and Parkinson's disease. Parkinsonism Relat Disord *14*, 539-543.

Rottenberg, H., and Wu, S. (1998). Quantitative assay by flow cytometry of the mitochondrial membrane potential in intact cells. Biochim Biophys Acta *1404*, 393-404.

Saad, M., Lesage, S., Saint-Pierre, A., Corvol, J.C., Zelenika, D., Lambert, J.C., Vidailhet, M., Mellick, G.D., Lohmann, E., Durif, F.*, et al.* (2011). Genome-wide association study confirms BST1 and suggests a locus on 12q24 as the risk loci for Parkinson's disease in the European population. Hum Mol Genet *20*, 615-627.

Saftig, P., Beertsen, W., and Eskelinen, E.L. (2008). LAMP-2: a control step for phagosome and autophagosome maturation. Autophagy *4*, 510-512.

Saha, S., Guillily, M.D., Ferree, A., Lanceta, J., Chan, D., Ghosh, J., Hsu, C.H., Segal, L., Raghavan, K., Matsumoto, K.*, et al.* (2009). LRRK2 modulates vulnerability to mitochondrial dysfunction in Caenorhabditis elegans. J Neurosci *29*, 9210-9218.

Saito, Y., Suzuki, K., Hulette, C.M., and Murayama, S. (2004). Aberrant phosphorylation of alpha-synuclein in human Niemann-Pick type C1 disease. J Neuropathol Exp Neurol *63*, 323-328.

Samali, A., Cai, J., Zhivotovsky, B., Jones, D.P., and Orrenius, S. (1999). Presence of a pre-apoptotic complex of pro-caspase-3, Hsp60 and Hsp10 in the mitochondrial fraction of jurkat cells. EMBO J *18*, 2040-2048.

Sandebring, A., Thomas, K.J., Beilina, A., van der Brug, M., Cleland, M.M., Ahmad, R., Miller, D.W., Zambrano, I., Cowburn, R.F., Behbahani, H.*, et al.* (2009). Mitochondrial alterations in PINK1 deficient cells are influenced by calcineurin-dependent dephosphorylation of dynamin-related protein 1. PLoS One *4*, e5701.

Sarkar, S., Floto, R.A., Berger, Z., Imarisio, S., Cordenier, A., Pasco, M., Cook, L.J., and Rubinsztein, D.C. (2005). Lithium induces autophagy by inhibiting inositol monophosphatase. J Cell Biol *170*, 1101-1111.

Satake, W., Nakabayashi, Y., Mizuta, I., Hirota, Y., Ito, C., Kubo, M., Kawaguchi, T., Tsunoda, T., Watanabe, M., Takeda, A.*, et al.* (2009). Genome-wide association study identifies common variants at four loci as genetic risk factors for Parkinson's disease. Nat Genet *41*, 1303-1307.

Scaduto, R.C., Jr., and Grotyohann, L.W. (1999). Measurement of mitochondrial membrane potential using fluorescent rhodamine derivatives. Biophys J *76*, 469-477.

Schapira, A.H. (1993). Mitochondrial complex I deficiency in Parkinson's disease. Adv Neurol *60*, 288-291.

Schapira, A.H. (1999). Mitochondria in the aetiology and pathogenesis of Parkinson's disease. Parkinsonism Relat Disord *5*, 139-143.

Schapira, A.H., Cooper, J.M., Dexter, D., Jenner, P., Clark, J.B., and Marsden, C.D. (1989). Mitochondrial complex I deficiency in Parkinson's disease. Lancet *1*, 1269.

Schapira, A.H., and Tolosa, E. (2010). Molecular and clinical prodrome of Parkinson disease: implications for treatment. Nat Rev Neurol *6*, 309-317.

Scheffler, I. (1999). Mitochondria (Wiley-Blackwell).

Schleyer, M., Schmidt, B., and Neupert, W. (1982). Requirement of a membrane potential for the posttranslational transfer of proteins into mitochondria. Eur J Biochem *125*, 109-116.

Schon, E.A., Bonilla, E., and DiMauro, S. (1997). Mitochondrial DNA mutations and pathogenesis. J Bioenerg Biomembr *29*, 131-149.

Scott, M.D., and Frydman, J. (2003). Aberrant protein folding as the molecular basis of cancer. Methods Mol Biol *232*, 67-76.

Seglen, P.O., and Gordon, P.B. (1982). 3-Methyladenine: specific inhibitor of autophagic/lysosomal protein degradation in isolated rat hepatocytes. Proc Natl Acad Sci U S A *79*, 1889-1892.

Senior, A.E., Nadanaciva, S., and Weber, J. (2002). The molecular mechanism of ATP synthesis by F1F0-ATP synthase. Biochim Biophys Acta *1553*, 188-211.

Seol, W. (2010). Biochemical and molecular features of LRRK2 and its pathophysiological roles in Parkinson's disease. BMB Rep *43*, 233-244.

Seong, Y.M., Choi, J.Y., Park, H.J., Kim, K.J., Ahn, S.G., Seong, G.H., Kim, I.K., Kang, S., and Rhim, H. (2004). Autocatalytic processing of HtrA2/Omi is essential for induction of caspase-dependent cell death through antagonizing XIAP. J Biol Chem *279*, 37588-37596.

Sherer, T.B., Betarbet, R., Testa, C.M., Seo, B.B., Richardson, J.R., Kim, J.H., Miller, G.W., Yagi, T., Matsuno-Yagi, A., and Greenamyre, J.T. (2003). Mechanism of toxicity in rotenone models of Parkinson's disease. J Neurosci *23*, 10756-10764.

Shimura, H., Schlossmacher, M.G., Hattori, N., Frosch, M.P., Trockenbacher, A., Schneider, R., Mizuno, Y., Kosik, K.S., and Selkoe, D.J. (2001). Ubiquitination of a new form of alpha-synuclein by parkin from human brain: implications for Parkinson's disease. Science *293*, 263-269.

Shin, K., Nakamoto, R.K., Maeda, M., and Futai, M. (1992). F0F1-ATPase gamma subunit mutations perturb the coupling between catalysis and transport. J Biol Chem *267*, 20835-20839.

Shojaee, S., Sina, F., Banihosseini, S.S., Kazemi, M.H., Kalhor, R., Shahidi, G.A., Fakhrai-Rad, H., Ronaghi, M., and Elahi, E. (2008). Genome-wide linkage analysis of a Parkinsonian-pyramidal syndrome pedigree by 500 K SNP arrays. Am J Hum Genet *82*, 1375-1384.

Shoulson, I. (1989). Deprenyl and tocopherol antioxidative therapy of parkinsonism (DATATOP). Parkinson Study Group. Acta Neurol Scand Suppl *126*, 171-175.

Shukla, A., Durairaj, G., Schneider, J., Duan, Z., Shadle, T., and Bhaumik, S.R. (2009). Stimulation of mRNA export by an F-box protein, Mdm30p, in vivo. J Mol Biol *389*, 238-247.

Shults, C.W., Oakes, D., Kieburtz, K., Beal, M.F., Haas, R., Plumb, S., Juncos, J.L., Nutt, J., Shoulson, I., Carter, J.*, et al.* (2002). Effects of coenzyme Q10 in early Parkinson disease: evidence of slowing of the functional decline. Arch Neurol *59*, 1541-1550.

Siegfried, J., and Lippitz, B. (1994). Bilateral chronic electrostimulation of ventroposterolateral pallidum: a new therapeutic approach for alleviating all parkinsonian symptoms. Neurosurgery *35*, 1126-1129; discussion 1129-1130.

Silvestri, L., Caputo, V., Bellacchio, E., Atorino, L., Dallapiccola, B., Valente, E.M., and Casari, G. (2005). Mitochondrial import and enzymatic activity of PINK1 mutants associated to recessive parkinsonism. Hum Mol Genet *14*, 3477-3492.

Simon-Sanchez, J., Schulte, C., Bras, J.M., Sharma, M., Gibbs, J.R., Berg, D., Paisan-Ruiz, C., Lichtner, P., Scholz, S.W., Hernandez, D.G.*, et al.* (2009). Genome-wide association study reveals genetic risk underlying Parkinson's disease. Nat Genet *41*, 1308-1312.

Simon-Sanchez, J., and Singleton, A.B. (2008). Sequencing analysis of OMI/HTRA2 shows previously reported pathogenic mutations in neurologically normal controls. Hum Mol Genet *17*, 1988-1993.

Singleton, A.B., Farrer, M., Johnson, J., Singleton, A., Hague, S., Kachergus, J., Hulihan, M., Peuralinna, T., Dutra, A., Nussbaum, R.*, et al.* (2003). alpha-Synuclein locus triplication causes Parkinson's disease. Science *302*, 841.

Skowyra, D., Craig, K.L., Tyers, M., Elledge, S.J., and Harper, J.W. (1997). F-box proteins are receptors that recruit phosphorylated substrates to the SCF ubiquitin-ligase complex. Cell *91*, 209-219.

Skulachev, V.P. (1996). Why are mitochondria involved in apoptosis? Permeability transition pores and apoptosis as selective mechanisms to eliminate superoxide-producing mitochondria and cell. FEBS Lett *397*, 7-10.

Small, I., Peeters, N., Legeai, F., and Lurin, C. (2004). Predotar: A tool for rapidly screening proteomes for N-terminal targeting sequences. Proteomics *4*, 1581-1590.

Smirnova, E., Griparic, L., Shurland, D.L., and van der Bliek, A.M. (2001). Dynamin-related protein Drp1 is required for mitochondrial division in mammalian cells. Mol Biol Cell *12*, 2245-2256.

Snow, B.J., Rolfe, F.L., Lockhart, M.M., Frampton, C.M., O'Sullivan, J.D., Fung, V., Smith, R.A., Murphy, M.P., and Taylor, K.M. (2010). A double-blind, placebo-controlled study to assess the mitochondria-targeted antioxidant MitoQ as a disease-modifying therapy in Parkinson's disease. Mov Disord *25*, 1670-1674.

Solaini, G., Sgarbi, G., Lenaz, G., and Baracca, A. (2007). Evaluating mitochondrial membrane potential in cells. Biosci Rep *27*, 11-21.

Spiess, C., Beil, A., and Ehrmann, M. (1999). A temperature-dependent switch from chaperone to protease in a widely conserved heat shock protein. Cell *97*, 339-347.

Stacy, M., and Jankovic, J. (1992). Differential diagnosis of Parkinson's disease and the parkinsonism plus syndromes. Neurol Clin *10*, 341-359.

Staropoli, J.F., McDermott, C., Martinat, C., Schulman, B., Demireva, E., and Abeliovich, A. (2003). Parkin is a component of an SCF-like ubiquitin ligase complex and protects postmitotic neurons from kainate excitotoxicity. Neuron *37*, 735-749.

Storch, A., Jost, W.H., Vieregge, P., Spiegel, J., Greulich, W., Durner, J., Muller, T., Kupsch, A., Henningsen, H., Oertel, W.H.*, et al.* (2007). Randomized, double-blind, placebo-controlled trial on symptomatic effects of coenzyme Q(10) in Parkinson disease. Arch Neurol *64*, 938-944.

Strauss, K.M., Martins, L.M., Plun-Favreau, H., Marx, F.P., Kautzmann, S., Berg, D., Gasser, T., Wszolek, Z., Muller, T., Bornemann, A.*, et al.* (2005). Loss of function mutations in the gene encoding Omi/HtrA2 in Parkinson's disease. Hum Mol Genet *14*, 2099-2111.

Suzuki, Y., Imai, Y., Nakayama, H., Takahashi, K., Takio, K., and Takahashi, R. (2001). A serine protease, HtrA2, is released from the mitochondria and interacts with XIAP, inducing cell death. Mol Cell *8*, 613-621.

Swerdlow, R.H., Parks, J.K., Miller, S.W., Tuttle, J.B., Trimmer, P.A., Sheehan, J.P., Bennett, J.P., Jr., Davis, R.E., and Parker, W.D., Jr. (1996). Origin and functional consequences of the complex I defect in Parkinson's disease. Ann Neurol *40*, 663-671.

Szabo, I., De Pinto, V., and Zoratti, M. (1993). The mitochondrial permeability transition pore may comprise VDAC molecules. II. The electrophysiological properties of VDAC are compatible with those of the mitochondrial megachannel. FEBS Lett *330*, 206-210.

Szabo, I., and Zoratti, M. (1993). The mitochondrial permeability transition pore may comprise VDAC molecules. I. Binary structure and voltage dependence of the pore. FEBS Lett *330*, 201-205.

Szyrach, G., Ott, M., Bonnefoy, N., Neupert, W., and Herrmann, J.M. (2003). Ribosome binding to the Oxa1 complex facilitates co-translational protein insertion in mitochondria. EMBO J *22*, 6448-6457.

Tain, L.S., Chowdhury, R.B., Tao, R.N., Plun-Favreau, H., Moisoi, N., Martins, L.M., Downward, J., Whitworth, A.J., and Tapon, N. (2009). Drosophila HtrA2 is dispensable for apoptosis but acts downstream of PINK1 independently from Parkin. Cell Death Differ *16*, 1118-1125.

Takatori, S., Ito, G., and Iwatsubo, T. (2008). Cytoplasmic localization and proteasomal degradation of N-terminally cleaved form of PINK1. Neurosci Lett *430*, 13-17.

Tanaka, A. (2010). Parkin-mediated selective mitochondrial autophagy, mitophagy: Parkin purges damaged organelles from the vital mitochondrial network. FEBS Lett *584*, 1386-1392.

Tanaka, A., Cleland, M.M., Xu, S., Narendra, D.P., Suen, D.F., Karbowski, M., and Youle, R.J. (2010). Proteasome and p97 mediate mitophagy and degradation of mitofusins induced by Parkin. J Cell Biol *191*, 1367-1380.

Tanida, I., Ueno, T., and Kominami, E. (2004). LC3 conjugation system in mammalian autophagy. Int J Biochem Cell Biol *36*, 2503-2518.

Tanner, C.M. (1992). Occupational and environmental causes of parkinsonism. Occup Med *7*, 503-513.

Tatsuta, T., and Langer, T. (2008). Quality control of mitochondria: protection against neurodegeneration and ageing. EMBO J *27*, 306-314.

Thomas, K.J., McCoy, M.K., Blackinton, J., Beilina, A., van der Brug, M., Sandebring, A., Miller, D., Maric, D., Cedazo-Minguez, A., and Cookson, M.R. (2011). DJ-1 acts in parallel to the PINK1/parkin pathway to control mitochondrial function and autophagy. Hum Mol Genet *20*, 40-50.

Trempe, J.F. (2011). Reading the ubiquitin postal code. Curr Opin Struct Biol *21*, 792-801.

Trimmer, P.A., Swerdlow, R.H., Parks, J.K., Keeney, P., Bennett, J.P., Jr., Miller, S.W., Davis, R.E., and Parker, W.D., Jr. (2000). Abnormal mitochondrial morphology in sporadic Parkinson's and Alzheimer's disease cybrid cell lines. Exp Neurol *162*, 37-50.

Tsou, A.P., Yang, C.W., Huang, C.Y., Yu, R.C., Lee, Y.C., Chang, C.W., Chen, B.R., Chung, Y.F., Fann, M.J., Chi, C.W.*, et al.* (2003). Identification of a novel cell cycle regulated gene, HURP, overexpressed in human hepatocellular carcinoma. Oncogene *22*, 298-307.

Twig, G., Elorza, A., Molina, A.J., Mohamed, H., Wikstrom, J.D., Walzer, G., Stiles, L., Haigh, S.E., Katz, S., Las, G.*, et al.* (2008). Fission and selective fusion govern mitochondrial segregation and elimination by autophagy. EMBO J *27*, 433-446.

Valente, E.M., Abou-Sleiman, P.M., Caputo, V., Muqit, M.M., Harvey, K., Gispert, S., Ali, Z., Del Turco, D., Bentivoglio, A.R., Healy, D.G.*, et al.* (2004). Hereditary early-onset Parkinson's disease caused by mutations in PINK1. Science *304*, 1158-1160.

Valko, M., Leibfritz, D., Moncol, J., Cronin, M.T., Mazur, M., and Telser, J. (2007). Free radicals and antioxidants in normal physiological functions and human disease. Int J Biochem Cell Biol *39*, 44-84.

Van Remmen, H., and Richardson, A. (2001). Oxidative damage to mitochondria and aging. Exp Gerontol *36*, 957-968.

Vander Heiden, M.G., Cantley, L.C., and Thompson, C.B. (2009). Understanding the Warburg effect: the metabolic requirements of cell proliferation. Science *324*, 1029-1033.

Vekrellis, K., Xilouri, M., Emmanouilidou, E., Rideout, H.J., and Stefanis, L. (2011). Pathological roles of alpha-synuclein in neurological disorders. Lancet Neurol *10*, 1015-1025.

Verhagen, A.M., Silke, J., Ekert, P.G., Pakusch, M., Kaufmann, H., Connolly, L.M., Day, C.L., Tikoo, A., Burke, R., Wrobel, C.*, et al.* (2002). HtrA2 promotes cell death through its serine protease activity and its ability to antagonize inhibitor of apoptosis proteins. J Biol Chem *277*, 445-454.

Vidal-Puig, A.J., Grujic, D., Zhang, C.Y., Hagen, T., Boss, O., Ido, Y., Szczepanik, A., Wade, J., Mootha, V., Cortright, R.*, et al.* (2000). Energy metabolism in uncoupling protein 3 gene knockout mice. J Biol Chem *275*, 16258-16266.

Vilain, S., Esposito, G., Haddad, D., Schaap, O., Dobreva, M.P., Vos, M., Van Meensel, S., Morais, V.A., De Strooper, B., and Verstreken, P. (2012). The yeast complex I equivalent NADH dehydrogenase rescues pink1 mutants. PLoS Genet *8*, e1002456.

Vilarino-Guell, C., Ross, O.A., Soto, A.I., Farrer, M.J., Haugarvoll, K., Aasly, J.O., Uitti, R.J., and Wszolek, Z.K. (2009). Reported mutations in GIGYF2 are not a common cause of Parkinson's disease. Mov Disord *24*, 619-620.

Vives-Bauza, C., Zhou, C., Huang, Y., Cui, M., de Vries, R.L., Kim, J., May, J., Tocilescu, M.A., Liu, W., Ko, H.S.*, et al.* (2010). PINK1-dependent recruitment of Parkin to mitochondria in mitophagy. Proc Natl Acad Sci U S A *107*, 378-383.

von der Lehr, N., Johansson, S., Wu, S., Bahram, F., Castell, A., Cetinkaya, C., Hydbring, P., Weidung, I., Nakayama, K., Nakayama, K.I.*, et al.* (2003). The F-box protein Skp2 participates in c-Myc proteosomal degradation and acts as a cofactor for c-Myc-regulated transcription. Mol Cell *11*, 1189-1200.

Voos, W. (2012). Chaperone-protease networks in mitochondrial protein homeostasis. Biochim Biophys Acta.

Votyakova, T.V., and Reynolds, I.J. (2001). DeltaPsi(m)-Dependent and -independent production of reactive oxygen species by rat brain mitochondria. J Neurochem *79*, 266-277.

Wang, C.Y., Xu, Q., Weng, L., Zhang, Q., Zhang, H.N., Guo, J.F., Tan, L.M., Tang, J.G., Yan, X.X., and Tang, B.S. (2011a). Genetic variations of Omi/HTRA2 in Chinese patients with Parkinson's disease. Brain Res *1385*, 293-297.

Wang, H., and Oster, G. (1998). Energy transduction in the F1 motor of ATP synthase. Nature *396*, 279-282.

Wang, X., Winter, D., Ashrafi, G., Schlehe, J., Wong, Y.L., Selkoe, D., Rice, S., Steen, J., LaVoie, M.J., and Schwarz, T.L. (2011b). PINK1 and Parkin target Miro for phosphorylation and degradation to arrest mitochondrial motility. Cell *147*, 893-906.

Warburg, O. (1956). On the origin of cancer cells. Science *123*, 309-314.

Ward, M.W., Rego, A.C., Frenguelli, B.G., and Nicholls, D.G. (2000). Mitochondrial membrane potential and glutamate excitotoxicity in cultured cerebellar granule cells. J Neurosci *20*, 7208-7219.

Waterham, H.R., Koster, J., van Roermund, C.W., Mooyer, P.A., Wanders, R.J., and Leonard, J.V. (2007). A lethal defect of mitochondrial and peroxisomal fission. N Engl J Med *356*, 1736-1741.

Weihofen, A., Ostaszewski, B., Minami, Y., and Selkoe, D.J. (2008). Pink1 Parkinson mutations, the Cdc37/Hsp90 chaperones and Parkin all influence the maturation or subcellular distribution of Pink1. Hum Mol Genet *17*, 602-616.

Weihofen, A., Thomas, K.J., Ostaszewski, B.L., Cookson, M.R., and Selkoe, D.J. (2009). Pink1 forms a multiprotein complex with Miro and Milton, linking Pink1 function to mitochondrial trafficking. Biochemistry *48*, 2045-2052.

Weintraub, D., Comella, C.L., and Horn, S. (2008). Parkinson's disease--Part 1: Pathophysiology, symptoms, burden, diagnosis, and assessment. Am J Manag Care *14*, S40-48.

Weisiger, R.A., and Fridovich, I. (1973). Superoxide dismutase. Organelle specificity. J Biol Chem *248*, 3582-3592.

Werth, J.L., and Thayer, S.A. (1994). Mitochondria buffer physiological calcium loads in cultured rat dorsal root ganglion neurons. J Neurosci *14*, 348-356.

Weydt, P., and La Spada, A.R. (2006). Targeting protein aggregation in neurodegeneration--lessons from polyglutamine disorders. Expert Opin Ther Targets *10*, 505-513.

Williams, A., Sarkar, S., Cuddon, P., Ttofi, E.K., Saiki, S., Siddiqi, F.H., Jahreiss, L., Fleming, A., Pask, D., Goldsmith, P.*, et al.* (2008). Novel targets for Huntington's disease in an mTOR-independent autophagy pathway. Nat Chem Biol *4*, 295-305.

Woelk, T., Sigismund, S., Penengo, L., and Polo, S. (2007). The ubiquitination code: a signalling problem. Cell Div *2*, 11.

Wolters, N.M., and MacKeigan, J.P. (2008). From sequence to function: using RNAi to elucidate mechanisms of human disease. Cell Death Differ *15*, 809-819.

Wood-Kaczmar, A., Gandhi, S., Yao, Z., Abramov, A.Y., Miljan, E.A., Keen, G., Stanyer, L., Hargreaves, I., Klupsch, K., Deas, E.*, et al.* (2008). PINK1 is necessary for long term survival and mitochondrial function in human dopaminergic neurons. PLoS One *3*, e2455.

Wrogemann, K., and Pena, S.D. (1976). Mitochondrial calcium overload: A general mechanism for cell-necrosis in muscle diseases. Lancet *1*, 672-674.

Wu, X., Wakefield, J.K., Liu, H., Xiao, H., Kralovics, R., Prchal, J.T., and Kappes, J.C. (2000). Development of a novel trans-lentiviral vector that affords predictable safety. Mol Ther *2*, 47-55.

Xie, W., and Chung, K.K. (2012). Alpha-synuclein impairs normal dynamics of mitochondria in cell and animal models of Parkinson's disease. J Neurochem.

Yang, Y., Gehrke, S., Imai, Y., Huang, Z., Ouyang, Y., Wang, J.W., Yang, L., Beal, M.F., Vogel, H., and Lu, B. (2006). Mitochondrial pathology and muscle and dopaminergic neuron degeneration caused by inactivation of Drosophila Pink1 is rescued by Parkin. Proc Natl Acad Sci U S A *103*, 10793-10798.

Yang, Y., Ouyang, Y., Yang, L., Beal, M.F., McQuibban, A., Vogel, H., and Lu, B. (2008). Pink1 regulates mitochondrial dynamics through interaction with the fission/fusion machinery. Proc Natl Acad Sci U S A *105*, 7070-7075.

Yang, Z., and Klionsky, D.J. (2010). Eaten alive: a history of macroautophagy. Nat Cell Biol *12*, 814-822.

Youle, R.J., and Narendra, D.P. (2011). Mechanisms of mitophagy. Nat Rev Mol Cell Biol *12*, 9-14.

Yu, W., Sun, Y., Guo, S., and Lu, B. (2011). The PINK1/Parkin pathway regulates mitochondrial dynamics and function in mammalian hippocampal and dopaminergic neurons. Hum Mol Genet *20*, 3227-3240.

Zanella, F., Lorens, J.B., and Link, W. (2010). High content screening: seeing is believing. Trends Biotechnol *28*, 237-245.

Zeng, X., Neupert, W., and Tzagoloff, A. (2007). The metalloprotease encoded by ATP23 has a dual function in processing and assembly of subunit 6 of mitochondrial ATPase. Mol Biol Cell *18*, 617-626.

Zent, R., Ailenberg, M., Waddell, T.K., Downey, G.P., and Silverman, M. (1995). Puromycin aminonucleoside inhibits mesangial cell-induced contraction of collagen gels by stimulating production of reactive oxygen species. Kidney Int *47*, 811-817.

Zhang, D.X., and Gutterman, D.D. (2007). Mitochondrial reactive oxygen species-mediated signaling in endothelial cells. Am J Physiol Heart Circ Physiol *292*, H2023-2031.

Zhang, J., Perry, G., Smith, M.A., Robertson, D., Olson, S.J., Graham, D.G., and Montine, T.J. (1999). Parkinson's disease is associated with oxidative damage to cytoplasmic DNA and RNA in substantia nigra neurons. Am J Pathol *154*, 1423-1429.

Zhang, Y., Oldenburg, M., and Fillingame, R.H. (1994). Suppressor mutations in F1 subunit epsilon recouple ATP-driven H+ translocation in uncoupled Q42E subunit c mutant of Escherichia coli F1F0 ATP synthase. J Biol Chem *269*, 10221-10224.

Zhao, T., De Graaff, E., Breedveld, G.J., Loda, A., Severijnen, L.A., Wouters, C.H., Verheijen, F.W., Dekker, M.C., Montagna, P., Willemsen, R.*, et al.* (2011). Loss of nuclear activity of the FBXO7 protein in patients with parkinsonian-pyramidal syndrome (PARK15). PLoS One *6*, e16983.

Zhou, C., Huang, Y., Shao, Y., May, J., Prou, D., Perier, C., Dauer, W., Schon, E.A., and Przedborski, S. (2008). The kinase domain of mitochondrial PINK1 faces the cytoplasm. Proc Natl Acad Sci U S A *105*, 12022-12027.

Zimprich, A., Biskup, S., Leitner, P., Lichtner, P., Farrer, M., Lincoln, S., Kachergus, J., Hulihan, M., Uitti, R.J., Calne, D.B., *et al.* (2004). Mutations in LRRK2 cause autosomal-dominant parkinsonism with pleomorphic pathology. Neuron *44*, 601-607.

Ziviani, E., Tao, R.N., and Whitworth, A.J. (2010). Drosophila parkin requires PINK1 for mitochondrial translocation and ubiquitinates mitofusin. Proc Natl Acad Sci U S A *107*, 5018-5023.

Ziviani, E., and Whitworth, A.J. (2010). How could Parkin-mediated ubiquitination of mitofusin promote mitophagy? Autophagy *6*, 660-662.

Zuchner, S., Mersiyanova, I.V., Muglia, M., Bissar-Tadmouri, N., Rochelle, J., Dadali, E.L., Zappia, M., Nelis, E., Patitucci, A., Senderek, J., *et al.* (2004). Mutations in the mitochondrial GTPase mitofusin 2 cause Charcot-Marie-Tooth neuropathy type 2A. Nat Genet *36*, 449-451.